JOSÉ HELBER VINCO

Obtenção de vanádio de alta pureza para aplicação em baterias de fluxo redox de vanádio

São Paulo

2022

JOSÉ HELBER VINCO

Obtenção de vanádio de alta pureza para aplicação em baterias de fluxo redox de vanádio

Versão Corrigida

Dissertação apresentado à Escola Politécnica da Universidade de São Paulo para obtenção do título de Mestre em Ciências.

Área de concentração: Engenharia Química

Orientador: Prof. Dr. Jorge Alberto Soares Tenório

São Paulo

2022

JOSÉ HELBER VINCO

Obtaining high purity vanadium for application in vanadium redox flow batteries

São Paulo

2022

JOSÉ HELBER VINCO

Obtaining high purity vanadium for application in vanadium redox flow batteries

Corrected version

Master's thesis presented to the Polytechnic School of the University of São Paulo to obtain the title of Master of Science.

Area of concentration: Chemical Engineering

Supervisor: Prof. Dr. Jorge Alberto Soares Tenório

São Paulo

2022

Este exemplar foi revisado e corrigido em relação à versão original, sobresponsabilidade única do autor e com a anuência de seu orientador.

São Paulo, 25 de abril de 2022

Assinatura do autor: José Helber Vinco

Assinatura do orientador:

Catalogação-na-publicação

Vinco, José Helber
Obtenção de vanádio de alta pureza para aplicação em baterias de fluxo redox de vanádio / J. H. Vinco, J. A. S. Tenório -- versão corr. -- São Paulo, 2022.
200 p.

Dissertação (Mestrado) - Escola Politécnica da Universidade de São Paulo. Departamento de Engenharia Química.

1.Resinas de troca iônica 2.Resinas quelantes 3.Adsorção 4.Recuperação de vanádio 5.Bateria de fluxo redox de vanádio I.Universidade de São Paulo. Escola Politécnica. Departamento de Engenharia Química II.t. III.Tenório, Jorge Alberto Soares

ACKNOWLEDGMENTS

To God, for everything.

To my supervisor, Prof. Dr. Jorge Alberto Soares Tenório: for believing in me and for accepting me as part of our research group, and for encouraging me to excel as a researcher constantly.

To Prof. Drª. Denise Crocce Romano Espinosa, for sharing knowledge and valuable experiences.

To Dr. Amilton Barbosa Botelho Junior, who from the beginning was very helpful. Thank you for the teachings and for contributing to the realization of this research.

To Ualisson Bellon, for all the support, companionship and friendship. I will be forever grateful for encouraging me to be a researcher and having the courage to fly higher.

To my friends Ana Eluiza Esther da Cunha Domingos – who, despite being physically distant, was an important foundation – and Franco Garjulli, for having welcomed me very well in the laboratory and in life.

To my friends from LAREX: Jonathan Tenório Vinhal, Thamiris Auxiliadora Gonçalves Martins, Juliana Mendes de Oliveira, Rafael Giuga Borba de Melo, Nayara Gomes, Isabela Falconi Brandolis Alves and Rafael Piumatti de Oliveira, for making the days lighter, helping me to take care of my infinite column experiments, for the laughter, for the complicity and partnership. Thank you for being much more than co-workers, but friends for life.

To the other students and members of LAREX, for the incentives, daily exchanges of knowledge, moments of relaxation and joy.

To the technician Ana Carolina Fadel Dalsin, for always being willing to help and contribute to the solution of research problems

To my family, especially my parents, José dos Santos Vinco and Maria da Penha Avanci Vinco and my brother, Eduardo Vinco, for being my foundation of much love and for always showing pride in my achievements.

To the Conselho Nacional de Desenvolvimento Científico e Tecnológico (CNPq) for funding my Masters scholarship (process 130978/2020-5).

To FAPESP/CAPES - Foundation for Research Support of the State of São Paulo (process number 2012/51871-9, 2019/11866-5), for the funding.

To the company Largo Resources, represented by Eng. Heitor Augusto Duarte, for having contributed to the motivation of this work and for providing the V_2O_5 to carry out the experiments.

To all, my most sincere thanks!

RESUMO

O vanádio é um metal de importância estratégica que, dentre suas aplicações industriais, desempenha um papel crítico na produção de ligas metálicas de alta performance. Uma aplicação para o vanádio que vem se destacando no setor energético é na produção de eletrólitos para Baterias de Fluxo Redox de Vanádio (BFRV). Essas baterias empregam o vanádio em seus quatro estados de oxidação como espécies ativas dos seus eletrólitos para armazenarem energia de fontes renováveis de produção em ampla escala. Vanádio – comumente V_2O_5 – com um alto grau de pureza (99.8%) é requerido como matéria-prima. Nessa vertente, o objetivo deste trabalho foi empregar as resinas de troca iônica como técnica de purificação de uma solução ácida de vanádio contaminada com ferro, tendo em vista que as principais ocorrências naturais do vanádio são associadas a esse elemento. Foram avaliadas três resinas quelantes de troca iônica (Lewatit® MonoPlus TP 209 XL, Lewatit® TP 207, Dowex™ M4195) e uma resina de troca catiônica forte (Lewatit® MonoPlus S 200H). O estudo da adsorção se deu pela avaliação da influência de parâmetros nos ensaios em batelada e em colunas de leito fixo. O pH, a relação massa de resina/volume de solução, a temperatura e o tempo de contato foram investigados. Os resultados mostraram que o aumento do pH de 0,5 para 2,0 favoreceu a adsorção de ambos os metais pelas resinas testadas, mas que as quelantes foram mais seletivas para vanádio. A adsorção de vanádio foi melhor ajustada pela isoterma de Langmuir nas TP 209 XL, TP 207 e S 200 H e pela isoterma de Temkin para a M4195. Já o mecanismo de adsorção de ferro variou entre os modelos de Langmuir, Freundlich e Temkin. A adsorção de vanádio pelas resinas quelantes, assim como a de ferro por todas, é de natureza endotérmica ($\Delta H^0 > 0$). Além disso, ambos os metais se adsorvem nas resinas de forma espontânea ($\Delta G^0 < 0$). Em relação à cinética, o modelo de pseudo-segunda ordem foi o que melhor se ajustou à adsorção de ambos os metais pelas resinas, indicando que o processo é controlado por quimissorção. Com a variação da vazão de 2 para 3 volumes de leito/hora nos ensaios em coluna com as resinas quelantes, os resultados das curvas de ruptura foram similares. Na etapa de eluição, vanádio foi eficientemente recuperado empregando-se solução de H_2SO_4 (1 mol.L^{-1}). Utilizando um sistema de 5 colunas em série, foi possível recuperar ao final 94 e 98% de todo o vanádio, respectivamente, pelas resinas TP 209 XL e TP 207. A eluição obtida até a terceira coluna da resina TP 207, assim como da

primeira coluna da resina TP 209 XL continha vanádio com pureza de 99.8%, chegando a 99.9% na primeira coluna com a resina TP 207. As soluções purificadas foram então submetidas à precipitação pela adição de $(NH_4)_2SO_4$, gerando $(NH_4)_2V_6O_{16}$, que foi então calcinado à V_2O_5 (99.9% puro), sendo as fases confirmadas por DRX e TG-DTG.

Palavras-chave: resinas de troca iônica; resinas quelantes; adsorção; recuperação de vanádio; bateria de fluxo redox de vanádio.

ABSTRACT

Vanadium is a strategically important metal that, among its industrial applications, plays a critical role in the production of high-performance alloys. An application for vanadium that stands out in the energy sector is in the production of electrolytes for Vanadium Redox Flow Batteries (VRFBs). These batteries use vanadium in its four oxidation states as active species in their electrolytes to store energy from renewable sources of large-scale production. Vanadium – commonly V_2O_5 – with a high degree of purity (99.8%) is required as raw material. The objective of this research was to use ion exchange resins as a purification technique for an acid solution of vanadium contaminated with iron, given that the main natural occurrences of vanadium are associated with this element. Three ion exchange chelating resins (Lewatit® MonoPlus TP 209 XL, Lewatit® TP 207 and Dowex™ M4195) and a strong cation exchange resin (Lewatit® MonoPlus S 200H) were evaluated. The study of adsorption was carried out by investigating the influence of parameters in the batch and fixed bed column tests. The pH, resin mass/solution volume ratio, temperature and contact time were investigated. The results showed that the increase in pH from 0.5 to 2.0 favored the adsorption of both metals by the tested resins, but that chelating ones were more selective for vanadium. Vanadium adsorption was better adjusted by the Langmuir isotherm for TP 209 XL, TP 207 and S 200 H and by the Temkin isotherm for M4195. The iron adsorption mechanism varied between the Langmuir, Freundlich and Temkin models. Vanadium adsorption by chelating resins, as well as iron adsorption by all of them, is endothermic in nature ($\Delta H^0 > 0$). Furthermore, both metals adsorb onto resins spontaneously ($\Delta G^0 < 0$). Regarding the kinetics, the pseudo-second order model was the one that best fitted the adsorption of both metals by the resins, indicating that the process is controlled by chemisorption. Breakthrough curves of chelating resins were similar changing the flow from 2 to 3 bed volumes/hour in the column experiments. In the elution step, vanadium was efficiently recovered using a H_2SO_4 (1 $mol.L^{-1}$) solution. Using a system of 5 columns in series, it was possible to recover, at the end, 94 and 98% of all the vanadium by the resins TP 209 XL and TP 207 (respectively). The elution obtained up to the third column of the TP 207 resin, as well as the first column of the TP 209 XL resin, contained 99.8% pure vanadium, reaching 99.9% in the first column with the TP 207 resin. The purified solutions were then subjected to precipitation by

the addition of $(NH_4)_2SO_4$, producing $(NH_4)_2V_6O_{16}$, which was then calcined to V_2O_5 (99.9% pure), phases that were confirmed by XRD and TG-DTG.

Palavras-chave: ion exchange resins; chelating resins; adsorption; vanadium recovery; vanadium redox flow battery.

LIST OF FIGURES

LIST OF TABLES

CONTENTS

1. INTRODUCTION

Metals are present in many products consumed by society, proving to be increasingly essential to modern technological development. Industries seek to deal with social demands, which constantly request more advanced technologies, which leads them to investments that increase the quantity, diversity and quality of the metals applied in their products [1]. According to the European Commission (EC), access to a stable supply of many minerals, metals needed by industry and other raw materials is a factor that strongly affects a country's economy [2].

The EC has issued a list of 30 critical raw materials, which include a selection of metals of great importance to the European Union (EU) economy, but which add a high risk to their supply [2]. Vanadium, in addition to being included in the list, is also among the critical metals in the United States [3] and Brazil [4], which shows its strategic importance [5].

Estimates of the global mine production of vanadium in the year 2020 was approximately 86,000 tons [6]. China is the main producer of vanadium in mines (53,000 tonnes), followed by Russia (18,000 tonnes), South Africa (8,200 tonnes) and Brazil (6,600 tonnes) [6]. Brazil only entered the market in 2014, producing around 1,030 tons of vanadium [7]. The Brazilian production of the metal in mine varied, between 2015 and 2019, from 5,800 [8] to 5,940 tons [6], showing a peak in production in 2016 of 8,000 tonnes [9].

In 2019, 71% of the entire global supply of vanadium was in the form of a co-product of iron processing for steel production, while 18% of the recovery as a main product from magnetite and titanomagnetite ores. The remaining (11%) was represented by recovery as a by-product of petroleum residues, fly ash, alumina slag and recycling of catalysts used in petroleum refining [10].

Preliminary data from the Brazilian National Mining Agency (ANM) show that in 2020, Brazil processed 412,661 tons of ore through the mining company Vanádio de Maracás S.A., which holds 100% of the country’s vanadium exploitation. This production resulted in an amount of approximately R$150 million [11].

In economic concentrations, vanadium is present in a variety of mineral deposits, in addition to being obtained from sources such as fossil fuels [5]. In Brazil,

minable reserves of vanadium are estimated at 94 thousand tons of V_2O_5, corresponding to 0.5% of world reserves, which in 2017 were 19.7 million tons [12]. The municipality of Maracás (BA) has the largest vanadium reserve in the country. In this ore, vanadium is associated with iron and titanium. Data from Largo Resources, a Canadian mining company that owns Vanádio de Maracás, indicate that the average content of vanadium ore located in Maracás-BA is 1.34% in V_2O_5, above the 0.4% found in mines of South Africa (considered until then as the highest amounts ever found in the world) [12,13]. The occurrence of vanadiniferous ore from Campo Alegre de Lourdes-BA was characterized by Alcântara *et al.* [14] with contents of vanadium V_2O_3 and V_2O_4 between 0.88-0.89% (in the magnetic concentrate). Cassa *et al.* [15], associated vanadium in solid solution with iron in the form of $Fe_3O_4.VO_4$ and $FeO.V_2O_3$, in contents between 0.7-0.8%, mainly in the mineral phases of hematite-martite (alteration of magnetite to hematite) and altered ilmenite.

Vanadium plays a critical role in many industrial applications, particularly in steel production [1]. The majority applicability of vanadium is in the production of metal alloys, giving them better properties (tensile strength, hardness and fatigue resistance), and increasing their performance [16]. In addition, vanadium is widely applied in catalysts in the chemical industry and in the production of batteries with high storage capacity [5].

Steel alloys account for 90% of all vanadium consumption, with the other 10% made up of titanium alloys, chemicals and others (mainly batteries) [17]. The addition of vanadium to iron and steel promotes hardening of the alloy, encouraging its use in the production of tools and automobiles as it adds strength and reliability to the material. In addition, it makes the material susceptible to being used in extremely low and high temperatures [18].

As reported by EC [19], the difficulty in substituting a material can be evaluated through the Substitution Index, which weights all applications, assigning a value between 0 and 1, with 0 being the most replaceable. Data released by the EU in 2017 indicate vanadium substitution indices for supply risk and economic importance, respectively, equal to 0.94 and 0.91 [19], which reinforces the difficult replacement of this metal in most of its applications. Titanium alloys, for example, which use high-purity vanadium, are applied in the aerospace industry and cannot be substituted [20].

Another promising use for high purity vanadium is in Vanadium Redox Flow Batteries (VRFB). Redox flow batteries (RFB) are mainly used in large-scale stationary energy storage [21] and consist of a device that converts, in a reversible way, electrical and chemical energy through two redox reactions that occur simultaneously in half-cells separated by a membrane, which acts by preventing the crossing between the two electrolytes, in order to maintain charge neutrality between the solutions of the two half-cells, allowing the exchange of ions [22,23]. The two half-cells together make up the electrochemical flow cell, which corresponds to the fundamental unit of a RFB [24].

First proposed by Skyllas-Kazacos and colleagues and patented in 1986, the VRFB employs the same chemical element (vanadium) in both half-cells [25]. As a result, having anolyte and catholyte made up of redox active pairs of the same element, the battery life is extended because eventual contamination between the electrolytes during operation is attenuated [24,26]. In VRFB the vanadium is present in its four oxidation states: in the negative half-cell there is the pair V^{2+}/V^{3+} and in the positive half-cell there is the pair V^{4+}(or VO^{2+})/V^{5+}(or VO_2^{+}) [27,28].

Until April 2019, there were 113 VRFBs installed worldwide, with China and the US having 17 of them in each country. China, however, is the country with the highest installed power, equal to 15,825 kW, which represents approximately 40% of the total global power (39,664 kW) [29].

V_2O_5 is the preferred raw material in the preparation of vanadium electrolyte due to the best cost-benefit ratio among vanadium sources [30]. Currently, high purity V_2O_5 (99.8%) is preferably adopted as starting material in VRFBs [31]. However, since there are many sources available for the recovery of V_2O_5 [16,32], several contaminating elements can normally be included in the final product. Thus, it is essential that efficient and low-cost processes are studied for vanadium purification mostly due to a growing demand for cost reduction of vanadium electrolytes. Still, industrially, the increase in the final purity of V_2O_5 is still associated with a large increase in the final value of this material [31,33].

Among the possible methods for solution purification, there is ion exchange, which has received increasing attention in several industrial sectors, being defined as a reversible exchange of ions between a solid phase and a solution phase [34]. This reaction allows not only the removal of all ions from a solution, but also, in many cases,

selective separation [35,36]. Among the materials capable of ion exchange and which have adequate properties are synthetic resins. These resins fulfill requirements demanded by ion exchange technology because they have characteristics such as: (i) high number of exchangeable ions per unit mass; (ii) structure that guarantees good accessibility of functional groups and better diffusion rate of ions through the resin particles; (iii) good chemical and mechanical resistance; (iv) non-dissolution; (v) maintenance of capacity even after many uses and (vi) fast operation [37].

In the present study, it is proposed to use ion exchange resins as a purification technique for a solution of vanadium contaminated with iron, aiming to obtain high purity vanadium aiming its application in VRFBs. The work contemplates the results involving four different commercial ion exchange resins, three of them chelating and one of strong cation exchange. Batch tests were approached to study: (i) the adsorption mechanisms; (ii) the adsorption isotherms that best describe the process; (iii) the thermodynamic parameters involved in the adsorption; and, also, (iv) the kinetic models to which the adsorption is conditioned. In addition, tests were also carried out in a continuous system in view of its greater relevance for practical applications, since they reproduce industrial conditions on a laboratory scale.

This document presents four manuscripts submitted to scientific journals. The first is a review article and is part of the literature review section (subsection 2.2). It was published in the Journal of Energy Storage [38] and aimed to provide a detailed review of the main components of VRFBs, providing insights into the fundamentals, mechanism, optimization and evolution of the technology. The preparation of electrolytes for these batteries and the influence of impurities on the performance of the system were discussed.

The second manuscript, presented in subsection 5.1, was published in the journal Minerals Engineering [39]. The objective of this article was to evaluate the ion exchange of the four resins, evaluating the effect of pH, the adsorption mechanism through three models of adsorption isotherms (Langmuir, Freundlich and Temkin) and also to determine the effect of temperature through a thermodynamic study.

The third manuscript is presented in subsection 5.2 and was accepted in the journal Transactions of Nonferrous Metals Society of China. In this article, a study of the kinetics of metal adsorption processes was carried out. Four kinetic models were

evaluated (pseudo-first order, pseudo-second order, intraparticle diffusion and Elovich). Furthermore, the adsorption was also characterized by means of Scanning Electron Microscopy with Energy Dispersive Spectroscopy (SEM-EDS) and Fourier Transform Infrared Spectroscopy (FT-IR).

The fourth manuscript is presented in subsection 5.3 and contains the results of studies in a continuous system. The results for loading and elution of the resins in column were presented, as well as a mass balance for a system of columns in series. Lastly, a pure vanadium solution was obtained which, after undergoing precipitation and calcination, produced highly pure V_2O_5.

Finally, in section 6, the conclusions of the three manuscripts of section 5 are presented.

1.1 Scientific contribution

Natural vanadium occurrences are normally associated with iron mainly because, in their +3 oxidation state, they have almost identical ionic radius and behave chemically in a similar way [40]. Thus, acid leaching of these ferrous ore occurrences (which are the main ore sources [41]) to obtain vanadium produce solutions normally contaminated with iron. Although separating vanadium through ion exchange resins is a well-developed matter [42–48], most of the literature explore the separation of this element as an anionic species.

This research brings new advances on batch and column experiments on separating vanadium from iron (both being cationic species) in acid solutions. Experiments elucidate the adsorption mechanisms of each of both metals by the different resins, as well as explore the thermodynamics involved in the process. Kinetics on the adsorption of iron and vanadium is investigated to determinate the limiting step. The interaction between the functional groups of these resins and the adsorbed metals is discussed by means of FTIR data. These discussions bring new data about these resins, which can work as guides to further scientific advances on separating vanadium and iron from other solutions.

1.2 Technological contribution

As previously discussed, ultrapure vanadium (≥ 99.8%) is required for application in the production of electrolytes for VRFBs. Ding et al. [49] showed that the presence of Fe^{3+} in the electrolyte negatively interfered with the overall performance of the battery by: (i) impairing the thermal stability of the positive electrolyte; (ii) decreasing the diffusion coefficient of vanadium ions; (iii) increasing system load transfer resistance; and (iv) competing with vanadium ions for the reaction between the redox pairs.

In view of the appeal for cost reduction in obtaining vanadium with high purity, this dissertation deals with separation of vanadium and iron by using ion exchange resins. These, in addition to being widely used in industrial processing [50], demonstrate advantages such as low energy consumption, kinetically fast reaction,

simplicity in operation and low operating cost [51], which justifies its use as the purification method used in this research.

Experiments in a continuous system at optimized conditions of pH, temperature and flow rate here explored show that is possible to separate vanadium from iron with ion exchange resins. The results described here could be scaled to industrial operations to produce high purity vanadium solutions, that once precipitated and calcinated, result in V_2O_5 99.8% pure. This could be an important route for the final purification of vanadium pentoxide obtained from the processing of Brazilian titanomagnetite ores.

2. LITERATURE REVIEW

2.1 Unfolding the Vanadium Redox Flow Batteries: an indeep perspective on its components and current operation challenges

José Helber Vinco; Ana Eluiza Esther da Cunha Domingos; Denise Crocce Romano Espinosa; Jorge Alberto Soares Tenório; Marcela dos Passos Galluzzi Baltazar.

Department of Chemical Engineering, Polytechnic School of the University of Sao Paulo (USP).

Abstract

The trend of increasing energy production from renewable sources has awakened great interest in the use of Vanadium Redox Flow Batteries (VRFB) in large-scale energy storage. The VRFB correspond to emerging technology, in continuous improvement and with high application potential. In this review, several evolutionary aspects of the battery are addressed. An in-depth survey of the main components of the battery, such as electrolytes, electrodes and membrane. Design and sizing issues are also approached, providing the reader, in addition to knowledge about the operating principles, a detailed perspective how technology has improved since its inception. A perspective upon inherent limitations and hindrances, together with recent developments to circumvent these was brought, highlighting both the economic and operational views aiming its transposition to real systems. Therefore, this review opportunely summarizes the fundamental technologies involved in VRFBs and encourages continuous research for their improvement.

Keywords: Redox flow batteries; Vanadium redox flow batteries; Energy storage; Fundamentals of vanadium redox flow batteries; Operating principles.

Symbols and abbreviations

AEM = anion exchange membranes;

AEIM = amphoteric ion exchange membranes;
AOS = average oxidation state;
BP = bipolar plates;
BPFB = Bromine-polysulfide flow batteries;
CAPEX = capital expenditure;
CEM = cation exchange membranes;
CNF = carbon nanofibers;
EES = electrochemical energy storage;
ESS = energy storage system;
E/P = energy to power ratio;
GF = graphite felt;
ICFB = Iron-Chromium flow batteries;
IEM = ion exchange membranes;
LAB = Lead-acid batteries;
LIB = Lithium-ion batteries;
NaSB = Sodium-Sulphur batteries;
NCB = Nickel-Cadmium batteries;
NMHB = Nickel-metal hydride batteries;
RFBs = redox flow batteries;
SEI = Sumitomo Electric Industries;
SHE = standard hydrogen electrode;
SOC = state of charge;
SOH = state of health;
OCV = open circuit voltage;
VRFB = Vanadium redox flow batteries;
ZBFB = Zinc-Bromine flow batteries;
ZCFB = Zinc-Cerium flow batteries;
λ = Darcy friction factor;
L = pipe length;
d = pipe diameter;
ρ = electrolyte density;
v = electrolyte velocity;
Re = Reynolds number;
μ = viscosity of electrolyte;
A = pipe area;
f_c = summation coefficient of loss coefficients;
l = length of porous electrode;
A' = cross-sectional area in the flow direction in the electrode;
k = permeability of the porous electrode;
$Q_{h\text{-}cel}$ = volume flow rate in each half-cell;
d_f = fiber diameter;
K = Kozenye-Carman constant;
ε = porosity of electrode.

2.1.1 Introduction

Climate changes have already been proven to be associated with greenhouse gas emissions, mainly due to fossil fuel burning due to energy production [52]. In addition to the recognized role that renewable energies play in decarbonizing the global energy sector [53]. In this scenario, energy sources such as wind and solar are presented as important allies in building a more sustainable future. Although these two energy sources' consumption increased by around 370% per decade, fuel

consumption such as gas, oil, and coal for power generation was still 28 times higher in 2018 [52,54]. However, according to the International Energy Agency [55], it is estimated that by 2040, a 60% increase in the global demand for energy reserved for renewable sources, especially solar photovoltaic and wind energy, which correspond to half of that fraction.

On the other hand, renewable energy sources do not usually have a consistent and immediate supply, given their inherently fluctuating nature; leads to a destabilization of the electricity grid [56]. Thus, the implementation of an efficient promising energy storage system (ESS) is essential. This system aims to allow intermittent renewable sources to be applied to electrical since they store the energy generated and release it under demand conditions, also oscillating and variable [31]. Thus, it becomes possible to produce energy in low demand times, when the associated cost is lower, and to use it in periods when demand exceeds production capacity [57].

There are several characteristics to be considered when designing an ESS. The technology must meet requirements such as energy efficiency, reliability, economy, long life, scalability, high storage capacity, low response time, security and low cost [57–60]. In this context, among the technologies for energy storage, electrochemical systems are superior, mainly due to the required parameters' performance and suitability [27]. In this respect, redox flow batteries (RFBs) have received great attention for ESS application, demonstrating flexible design, high efficiency, and long service life [61]. RFBs consist of secondary (rechargeable) batteries [22], in which energy conversions based on reversible electrochemical reactions of two redox pairs occur. This type of battery consists of two main parts connected via pumps: stacked cells where electrochemical reactions occur and external tanks where electrolytes are stored [21]. Among the available RFB’s technologies, VRFBs are the most promising for large-scale energy storage [62]. They bring together four different oxidation states of vanadium ions to form two separate redox pairs, anolyte and catholyte, thus having only vanadium as an active element on both sides [63]. The use of vanadium as the only active species is mainly linked to the mitigation of contamination problems between the electrolytes, which causes an extension of the battery life, in addition to keeping the species soluble without the phase change in the electrodes [24].

In view of this, numerous researches have been developed over the past few years, as the feasibility of applying VRFBs also increases. Recent studies direct their experimental results to the prospects for improving the system, based on the original mechanism proposed by the Skyllas-Kazacos group in the late 1980s [25,64]. Since then, for at least three decades, research has been carried out extensively, aiming to contribute to the battery's technological evolution. Many of these studies have been reviewed recently, both from the point of view of the battery mechanism as a whole [59,60,65–67], as well as specific technologies related to VRFB system components [31,32,68–71].

However, in view of the fact that there is a deficit of deepening on the general issues of composition, mechanism and optimization of VRFBs, it is proposed with the present study a detailed review on the subject, bringing a view on the fundamentals and the evolution of technology. Therefore, the work's objective is to serve as a basis for new studies and research based on an intensive and diversified review regarding structural components of design, fundamental principles of the electrochemical mechanism, including their favoring and limitations. Finally, it is also discussed what has been suggested in the segment as a way to optimize these limitations through critical areas of research, contributing to the future improvement of VRFBs.

2.1.2 VRFB mechanism, structure and sizing

2.1.2.1 Fundamental characteristics and operating principle

RFBs differ from conventional solid-state batteries, mainly because they do not contain the energy of the active-redox materials inside the electrodes, but because they use an electrolyte pumping system contained in external tanks, sized for a specific application requirement, as a way of storing energy, which is converted as the electrolytes react into the battery stack [21,22]. This working mechanism, in which there is a reaction between two electrolytes, also contributes to the prolongation of the battery's life, since complex redox reactions with electrodeposition or loss of electroactive compounds, structural changes and, also, that these suffer mechanical deformations every time the battery is cycled [21,72]. Besides, the spatial separation between the electrolyte tanks and the electrodes is responsible for dissociating the

energy and power of the RFBs, since the volume of the electrolyte determines the total energy stored by the battery, the concentration of active species, the voltage of each cell and the number of stacks contained. The power is then dependent on the active species' kinetic behavior and the electrode's total area [65].

The four oxidation states of vanadium are present in VRFBs [73]: the pair V^{2+}/V^{3+} in the negative half-cell and the pair V^{4+}(or VO^{2+})/V^{5+}(or VO_2^{+}) in the positive half-cell [27,28]. There are two external tanks in the system for the storage of redox electrolytic pairs. From these tanks, the electrolytes are pumped to circulate separately through the corresponding half-cells, where the reaction occurs in inert electrodes [23,74]. The two half-cells, composed of an electrode and a bipolar plate, are separated by an ion exchange membrane that prevents cross-mixing between the two electrolytes and allows ion exchange, maintaining the charge neutrality between the solutions [23,74,75]. Together, the two half-cells form an electrochemical flow cell, the fundamental unit of an RFB system [24], represented schematically by a VRFB in Figure 1.

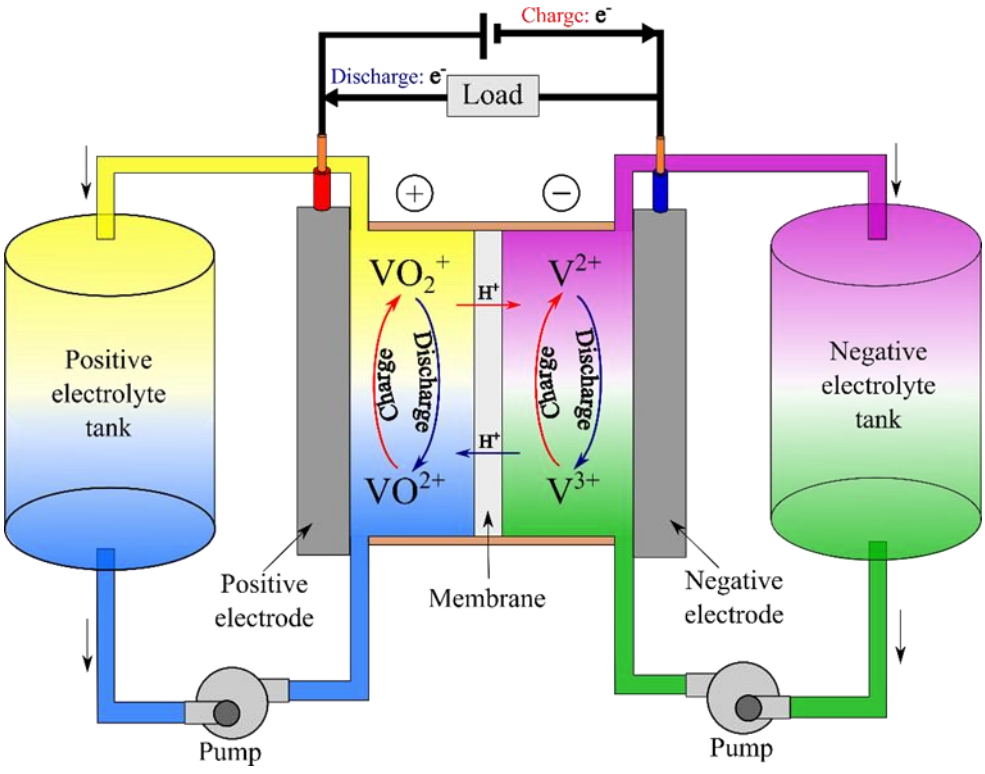

Figure 1. Representative diagram of a vanadium redox flow battery. (Based on [31,66,76]).

In a charging operation, on the positive side, tetravalent vanadium ions oxidize to pentavalent ions, with the release of H^+ ions and electrons, while on the negative side there is a reduction of trivalent ions to bivalent ions, as react with electrons that arrive through of the external circuit [74]. Their coloring identifies these different vanadium ions that occur in the cell: the oxidation states V^{2+}, V^{3+}, VO^{2+} and VO_2^+ present, in that order, the violet, green, blue and light-yellow colorings [62].

The combination of several individual cells forms a cell stack assembly [77]. The cells connect to increase the system's potential in a bipolar design configuration, the basic module of an RFB system. In this module, the negative electrode of a cell and the adjacent cell's negative electrode are electrically connected, maintaining the reagents physically separated [78]. The sum of each cell's individual potential is equal to the value of the potential difference developed and, in view of the purpose of using the VRFBs, several stacks are organized, in turn, to form matrices that allow larger applications [24,76].

The design of the VRFBs is directly related to battery operation issues, such as the performance and efficiency of the system, to meet the purpose for which it was designed: the energy storage [79]. This justifies the spatial separation between the main components of the battery, the storage tanks and the stack, which are intentionally designed so that the sizing of the power (kW or MW) and the stored energy capacity (kWh) occur independently [80].

2.1.2.2 Hydraulic subsystem

The hydraulic subsystem can be mainly responsible for the flow and storage of electrolytes since the electrical energy, after conversion into chemical energy, is stored in the external tanks in the form of an electrolyte solution [24,81]. The electrolyte transport occurs through pipes, with its flow facilitated by the aid of pumps [32]. The flow rate of the pumps is entirely related to the efficiency of battery operation, a relationship due mainly, according to Tang et al. [79], dependence on factors such as excess potential and pump head losses associated with the flow. The study proves that the efficiency of VRFB is higher with a flow variation when compared to pumps that work with constant flow rates.

On the other hand, a high increase in pump flow can lead to high energy consumption during loading, resulting in a reduction in the energy efficiency of VRFB [82]. Pump head losses are among the problems associated with bypass currents. The currents can be avoided by controlling the pump's flow, together with the ideal sizing of the battery. This can reduce energy costs that reach a consumption of up to 3% of the energy stored by the battery [59].

Regarding pressure losses, these can be defined mainly by the loss of resistance by friction in the pipes (Eq. (1)); congestion loss due to curves, valves, tank inlets, and outlets (Eq. (4)); pressure losses in the flow structure (Eq. (5)) and on the porous electrodes (Eq. (6)), so that the sum of these provides the total pressure drop [83].

$$P_{pipe} = \lambda \frac{L}{d} \frac{\rho v^2}{2}, \text{ in which} \quad (1)$$

$$\lambda = \frac{64}{Re} \quad (2)$$

$$Re = \frac{\rho d Q}{\mu A} \quad (3)$$

$$P_{cong} = f_c \frac{\rho v^2}{2} \quad (4)$$

$$P_{ff} = 157116Q + 0{,}8 \quad (5)$$

$$P_{felt} = \frac{\mu l Q_{h-cel}}{kA'}, \text{ in which} \quad (6)$$

$$k = \frac{d_f^2}{16K} \frac{\varepsilon^3}{(1-\varepsilon)^2} \quad (7)$$

Control strategies based on the mass transfer flow are also being developed recently, strengthening the pump flow control ratio [82]. Wang et al. [84] propose a dynamic flow control strategy based on a transient model to determine an ideal flow rate applicable to the conditions of variation of charge and discharge of energy in the battery, ensuring system efficiency, through simulation results, above 87%. However, there is still a need to improve the model developed, as well as experimental tests of the proposed control strategy to prove the efficiency obtained in simulation.

In practice, peristaltic pumps are used for the VRFB system as they have a simple operating mechanism and continuous suction. This through flexible tubes pressed by rollers, which provides a constant flow of electrolytic solution in different directions (from the battery to the battery and vice versa), just alternating the rotation of the pump, this favors the electrolyte current change during loading and discharging the battery [76,80,85]. This recirculation mode is considered the most simple, economical and efficient method in the construction and operation of VRFBs, as it stores the solution in only two external tanks, one for the catholyte and the other for the storage of anolyte [60].

The tank system must be designed according to the need for electrolyte storage, associated with the energy and operating capacity of the plant, knowing that the energy capacity is directly related to the volume of electrolyte contained in the tanks, so that the increase in electrolyte concentration implies reducing the size of the storage tanks [65]. Thus, an over-dimensioning leads to cost problems due to the expense of construction and expansion of territorial occupation, going against the environmental issues that support the growth prospects of VRFBs in the sustainable energy storage market [60].

Within the environmental panorama, the optimization of the dimensioning of the system is also linked to the emissions generated, especially in its construction, evidenced by the work of Arbabzadeh et al. [86], which evaluated the emissions generated by the materials used in the projection of an oversized system, taking into account the life cycle and the total energy cost. Cao et al. [32] also highlight the manufacturing costs of tanks due to the concentration of vanadium in the electrolytes, due to their influence on energy density.

Based on this particularity, that of having vanadium as the only active element in the electrolyte, contamination in the system is undesirable and should be avoided so that the tanks' projection guarantees the least possible interaction with the electrolyte [60]. The internal waterproofing of tanks by means of sealing is a proactive alternative in this sense [87,88].

The tanks' ideal design should also be free of any air intakes, avoiding the reaction between the electrolyte and oxygen, causing an early discharge of the battery, for example, by the oxidation of the V^{2+} species. However, there are already quite

applicable methods to combat the problem, such as purging with nitrogen gas [85,87,89].

2.1.2.3 Electrical subsystem: cells and stacks

The energy conversion mechanism is the principle of the electrical subsystem. This conversion occurs inside the pile, which is considered a fundamental part of the VRFB since energy is converted through oxidation reactions and reduction of vanadium species [24]. The stack consists of a set of cells pressed in a series configuration. The number of interconnected cells determines the total battery voltage, as well as the battery capacity [59].

The cells' design includes two half-cells, one positive and one negative, separated by an ion exchange membrane that is responsible for preventing cross-contamination of the electrolytes [90,91]. The cells are further structured by a set of components distributed in sandwich layers, including bipolar plates (BP), joints and electrodes [92], as shown in Figure 2.

The electrodes do not participate in redox reactions. Therefore, under properly controlled operating conditions, they have long durability, acting only as a place for the occurrence of electrochemical reactions [31]. Therefore, its geometry must be considered during the design, aiming at an expansive surface area for greater contact with the flow of electrolytes [93].

Generally, the electrodes are connected to the bipolar plates through joints that establish the necessary compression for the electrode's ideal contact with the bipolar plate and the ion exchange membrane. The joints are also used to connect the other parts of the stack [60]. Among the most used materials to structure the joints, polyvinyl chloride (PVC) and silicone stand out for being acid-resistant insulators, highly flexible and durable due to the high mechanical stability when compacted, providing greater safety to the pile and preventing leakage of solution through of a good cell seal [59,94]. In addition, the plates facilitate the conduction of the electrolyte through channels dug in its walls, generating an electrical connection between the adjacent cells, hence the need for high electrical conductivity and low acid permeability through BP [95]. Conventionally, carbon plates are used to compose BP. However, oxidation problems

were detected with oxidation potentials of up to 2.0 V, although oxidation can be avoided by replacing graphite plates with carbon-polyethylene plates [92].

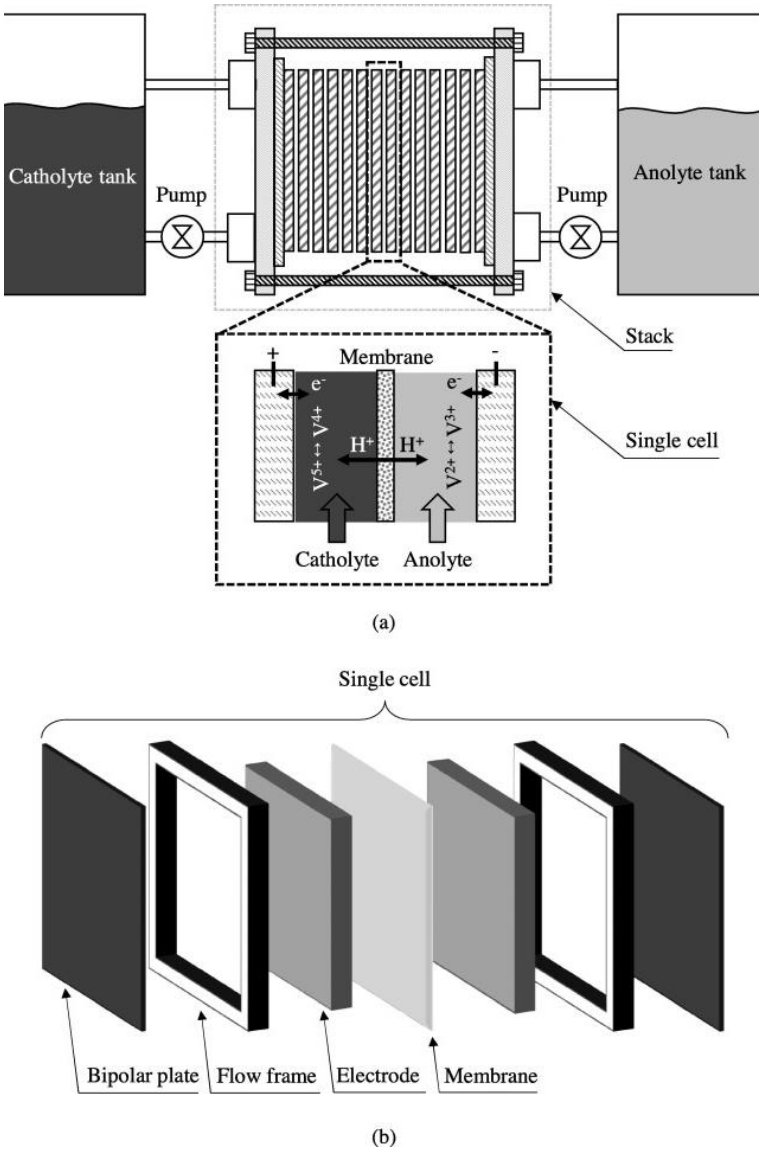

Figure 2. Scheme of a VRFB system, illustrating (a) a stack and (b) a single cell (Reproduced with permission by [95] Copyright 2015, Elsevier).

Another important factor that significantly influences batteries' performance is the flow fields in BP that contribute to electrolytes' uniform transport [96]. Ma [97] claims that energy efficiency, working current and battery life as a whole are influenced by the uniformity of electrolyte distribution across the cells that make up the stack.

In this sense, the design of the internal flow of a stack, that is, through the unit cells, may involve feeding the cells by electrolytes in parallel or in series, but the parallel method is more recommended, in view of the range of same volumetric flow in each unit cell, unlike the series flow that promotes disparities in the supply of each individual cell and promotes a change in the concentration of electrolytes [24,98]. For serial feeding, also called cascade, there are still two ways of circulating electrolytes through the stack: equicurrent and the countercurrent modes. In the first one, the positive and negative electrolytes enter and exit from the same side, while in the countercurrent mode, the positive electrolyte enters the exit side of the negative electrolyte and vice versa. The countercurrent configuration offers advantages such as reducing the voltage variation of the cells that make up the stack and reducing the water imbalance across the membranes that make up each battery cell, a phenomenon discussed in topic 3.3.1) [74,98].

The sizing of the channels must be performed by analyzing the implanted VRFB system, as they can decrease the pressure drop of the cell. With this, it is possible to increase the battery performance, considering the channels commonly applied to VRFBs, such as conventional, parallel, interdigitated and serpentine fields [60]. Many studies associate the increase in battery performance with the adoption of serpentine flow channels. They justify the lower pressure drop established by applying this type of field, as the work of Kumar and Jayanti [94], which also highlights an increase in the energy efficiency of 80%.

Generally, Arenas et al. [24] reiterate that the most critical aspect involved in stack design is precisely the design of cell structures coupled to the structures responsible for collecting and distributing the flow of electrolytes. Aiming to reduce the number of cells that have common current collectors and thus allow not only the optimization of the construction of the modules, but also the reduction of shunt currents, the stack design has also involved the grouping of cells in separate subsacks by intermediate collector plates joined to the compressor end plates [24,99–101].

A new framework for VRFBs, however, was developed by Al-Yasiri & Park [102], eliminating endplates and joints with the incorporation of serpentine flow channels, ensuring safety improvements and increased cell durability, in addition to minimizing the costs of assembling the stack. However, the transfer of electrons for the occurrence

of redox reactions and respective energy conversions occurs through the current collectors next to the external circuit due to electronic mobility [40].

Houser et al. [103], on the other hand, demonstrated that parasitic pumping losses have no significant influence on the net battery power and proposed two new designs for RFBs (Equal Path Length (EPL) and Aspect Ratio (AR)), which demonstrate superiority to standard serpentine and interdigitated designs in mass transit. By the EPL architecture, although energetically less favorable, the results pointed to a system with higher maximum power density, while the AR design was related to an improvement of the benefits already obtained in the EPL to achieve an operation with good electrochemical performance and of high energy efficiency [103].

During charging, the battery receives an external electrical stimulus making the level of electronic energy in the electrode higher than in the electrolyte, favoring the direction of electron flow from the electrode to the electrolyte, transferring them from the positive electrode to the negative electrode through the current collector and the external circuit, oxidizing the species of VO^{2+} to VO_2^{+} and reducing V^{3+} to V^{2+} by the supply of electrons [60]. In the case of unloading, the reverse occurs because the electrolyte, in this case, has a higher energy level than the electrode, so the electrons are transferred from the negative to the positive electrode, and oxidation from V^{2+} to V^{3+} releases the electron needed to reduce VO_2^{+} to VO^{2+} [82].

Current collectors are usually copper plates, given the high conductivity required for electron transport [24,80]. Kim et al. [87] even covered the copper plates with tin to increase the electronic conduction capacity, already Maurya et al. [104] used gold-plated collector plates, despite the cost of this type of coating is high.

2.1.2.4 Control subsystem

The control and monitoring of the battery are provided by means of sensors and software necessary to control the flow of electrolytes, energy conditioning, as well as by monitoring temperature parameters, pH, gas release, current measurement and battery potential [24].

Barelli et al. [80] adopted in their VRFB experimental control and monitoring system thermocouples for online measurement and battery voltage monitoring. While

Han & Tan [88] established a subsystem restricted only to the temperature profile, due to the limited temperature range to keep the active species soluble considering the heat generated by the pile during the operation.

2.1.3 Fundamental principles of the main cellular constituents of a VRFB system

2.1.3.1 Electrolytes

2.1.3.1.1 General characteristics

In a VRFB, the electrolyte is used as a medium for energy storage, so that its volume and concentration directly affect the battery's capacity and energy density [105–107]. In these batteries, active redox soluble vanadium species supported by electrolyte liquids [108] are implemented, providing ionic conductivity and allowing electrochemical reactions.

The electrolyte corresponds to one of the most important components of a VRFB [109] and also one of the most costly factors [62]. In view of its influence on its performance, the selection of the supporting electrolyte to be employed must comprise requirements such as high solubility and stability, low cost, good electrochemical performance and ample potential for operation [107,110]. Therefore, it is essential to ensure the electrolyte's stability and solubility to improve the performance and the overall life cycle of the battery [111].

Liu & Zou [105] state that different types of acids can be used as supporting electrolytes in VRFBs, such as sulfuric acid [112], hydrochloric acid [113], methanesulfonic acid [109], a mixture between these [73], or some organic electrolyte, such as vanadium acetylacetonate studied by Liu et al. [114]. Vanadium compounds such as vanadium trichloride (VCl_3), vanadium pentoxide (V_2O_5) and vanadyl sulfate ($VOSO_4$) were initially evaluated in supporting electrolytes under different concentrations, such as hydrochloric acid (HCl), sodium hydroxide (NaOH) and sulfuric acid (H_2SO_4) [64]. The combination of VCl_3 and HCl, however, was considered inadequate due to the generation of chlorine gas and, associated with low solubility of V_2O_5 in acids, the vanadyl sulfate solution with sulfuric acid as the supporting electrolyte was selected for use in both electrolytes [64]. Later, however, methods for obtaining electrolytes from V_2O_5 were developed [31].

Thus, VRFBs' electrolytes commonly use sulfuric acid as a supporting electrolyte for vanadium ions [67,115]. The VRFB technology was even patented with sulfuric acid as a support in the anolyte and catholyte [25], which acts both in increasing these electrolytes' ionic conductivity well as in the supply of hydrogen ions to the positive half-cell electrode reaction [107].

2.1.3.1.2 Electrochemical reactions

Initially, the positive electrolyte reservoir is filled with a V(IV) solution, and a V(III) solution is added to the negative electrolyte tank, as shown in Figure 1. As the electricity to be stored is applied to the electrodes of the positive and negative half-cells, the V(IV) ions of the positive electrolyte are then oxidized to the V(V) ions. At the same time, the V(III) ions are reduced to the V(II) ions in the negative electrolyte [116]. Studies have even shown that the reaction involving species V(III) and V(II) in the negative electrolyte is the limiting factor for VRFBs [117–119]. Eqs. (8), (9) and (10) show the reactions during battery charging, respectively, on the positive electrode, the negative electrode, and the cell's general reaction, accompanied by their corresponding redox potential [27,70,120,121].

Positive electrode reaction:

$$VO^{2+} + H_2O \rightarrow VO_2{}^{+} + 2H^{+} + e^{-} \quad E^0 = +1.004V \text{ vs. SHE} \qquad (8)$$

Negative electrode reaction:

$$V^{3+} + e^{-} \rightarrow V^{2+} \quad E^0 = -0.255V \text{ vs. SHE} \qquad (9)$$

General cell reaction:

$$VO^{2+} + H_2O + V^{3+} \rightarrow VO_2{}^{+} + V^{2+} + 2H^{+} \quad E^0 = +1.259V \text{ vs. SHE} \qquad (10)$$

The change in the oxidation states of vanadium species after the charging process, from +4 to +5 and from +3 to +2 in the positive and negative electrolytes, respectively, causes the difference in oxidation number between the electrolytes of the tanks before and after loading increase from +1 to +3. Conceptually, this change can be interpreted by the energy storage that started to occur in the increased bivalent oxidation number [116]. The standard open circuit voltage (OCV) of a cell, as shown in

Eq. (10), is approximately 1.26V. However, in real cell conditions, at a state of charge (SOC) of 50%, the cell's OCV is 1.4V [71] because, according to Knehr & Kumbur [122], proton activities should be considered, as well as Donnan's potential. Pavelka et al. [123] still complement that anionic species are sometimes neglected in the Nernst equation.

Many commercial electrolytes for VRFBs are currently being prepared to contain species V(III) and V(IV) in their 1:1 molar ratio (see section 3.1.5), which are subjected to a process pre-loading that aims to convert the mixture to its negative and positive forms in their respective reservoirs [68]. Eq. (11) contains the reaction representing this process, which is sometimes called the cross-contamination reaction, since it also represents the process caused when vanadium ions cross the membrane that separates the two half-cells [116].

$$VO^{2+} + 2H^{+} + e^{-} \leftrightarrow V^{3+} + H_2O \qquad E^0 = +0.337V \text{ vs. SHE} \qquad (11)$$

The reaction that occurs between species V(III) and V(IV) (Eq. (11)) has high activation energy and requires negative potentials to be processed, being likely that the formation of V(IV) in the catholyte will also proceed with the formation of V(V) followed by the reaction of this species with V(III) [124].

2.1.3.1.2.1 Side reactions

The use of all active redox species based on the same base compound has the advantage of not implying a permanent loss of the battery's storage capacity when species of an electrolyte cross the membrane and are incorporated into the electrolyte the adjacent half-cell [125]. Bearing in mind that, occasionally, vanadium ions in an electrolyte permeate through the membrane that separates the two half cells, Table 1 summarizes the self-discharge reactions that can occur in the electrolytes of the positive and negative half cells.

Table 1. Self-discharging reactions caused by the vanadium ions permeated into the counter electrolytes (Adapted from [116,126]).

	Vanadium Ions Permeated	Self-discharging Reactions
Negative Electrode	VO^{2+}	$VO^{2+} + V^{2+} + 2H^{+} \rightarrow 2V^{3+} + H_2O$
	$VO_2{}^{+}$	$VO_2{}^{+} + 2V^{2+} + 4H^{+} \rightarrow 3V^{2+} + 2H_2O$
	$VO_2{}^{+}$	$VO_2{}^{+} + V^{3+} \rightarrow 2VO^{2+}$
Positive Electrode	V^{2+}	$V^{2+} + 2VO_2{}^{+} + 2H^{+} \rightarrow 3VO^{2+} + H_2O$
	V^{2+}	$V^{2+} + VO^{2+} + 2H^{+} \rightarrow 2V^{3+} + H_2O$
	V^{3+}	$V^{3+} + VO_2{}^{+} \rightarrow 2VO^{2+}$

Yuan et al. [66] state that the catholyte may present a mixture between ions V(IV) and V(V), as well as anolyte a mixture of ions V(II) and V(III), depending on the SOC of the battery, the which promotes the creation of ion concentration gradients and this, in turn, is linked to the crossing of species between half-cells. Sun et al. [127] reported that the difference in concentration that forms between the vanadium ions of the positive and negative electrolytes is, in fact, the main motivator for the permeation of these ions through the membrane.

Sun et al. [128] observed through the results of their experiments that the self-discharge reactions are stimulated by the increase in the flow of electrolyte through half-cells, leading to a higher rate of crossing vanadium ions through the membrane. The authors further state that the process as a whole is related to the diffusion coefficient of vanadium ions that, in 1 M of V in 4 M of SO_4^{2-} solution and through a Nafion 115 membrane, increase in the following order: $V^{3+} < VO_2{}^{+} < VO^{2+} < V^{2+}$ [128]. In another study involving the Nafion 115 membrane, Sun et al. [129] reaffirmed that, in a 1.7 M V solution in 3 M H_2SO_4, the V^{2+} species has the highest diffusion coefficient among the different valences of vanadium. Cao et al. [130] showed with their experiments that, in an anion exchange membrane (FAP450), the diffusivity coefficient of the different oxidation states of vanadium follows another order: $V^{3+} < V^{2+} < VO_2{}^{+} < VO^{2+}$, the behavior being explained by the presence of positive functional groups in the membrane that more strongly repel the V^{3+} cation. The results also showed that for the two tested negatively charged membranes (F930 and VB2), the VO_2^{+} and V^{2+}ions had diffusion coefficients up to an order of magnitude lower than those of the V^{3+} e VO^{2+} ions, a result considered essential by the authors to reduce the

temperature increase of the stack in periods with high SOCs [130]. Agar et al. [126], with their studies, pointed out that, as well as the diffusion properties inherent to vanadium ions, characteristics related to the membrane used in the battery, such as hydraulic permeability and electrokinetics, are also significant factors that must be taken into account in studies that aim to minimize the occurrence of this phenomenon.

In this sense, Nguyen et al. [131] evaluated the difference in the permeability behavior of vanadium ions in relation to the type of functional group present in the membrane and the influence of the battery equilibrium condition. The results obtained showed that the positively functionalized membrane (Nafion 117), in equilibrium condition, absorbed all the vanadium in all its oxidation states. Still, in the +2 oxidation state, it was more strongly absorbed in relation to the others. On the other hand, the negatively functionalized membrane (FAP 450) demonstrated a large absorption of V (V) ions and that, therefore, there was a large increase in area-specific resistivity [131]. Sun et al. [129], in turn, investigated, in battery operating conditions, the permeability of various ions through the Nafion 115 and VX-20 membranes (which have, respectively, negative and positive groups on their surface). The authors showed after charge/recharge cycles that, in the case of using the Nafion 115 membrane, there was an accumulation of V^{2+} ions in the negative half-cell due to the difference in the permeability of vanadium in its different oxidation states, resulting in a weakening of the capacity of the battery [129]. In the case of the VX-20 membrane, there was an accumulation of VO_2^+ ions in the positive half-cell from side reactions in the positive and negative electrodes, also causing loss of battery capacity [129].

In the work of Wiedemann et al. [132] the diffusion coefficient of vanadium ions in their four oxidation states through different cation exchange membranes was determined. The results revealed that one of the evaluated membranes (CMX) the coefficients are higher for all, but that the CMS membrane had the lowest values, especially for the V^{2+} and V^{3+} cations, and that this membrane has a greater selectivity between the ions H_3O^+ and vanadium ions. According to the authors, this type of feature is especially desirable to avoid cross-contamination and prevent side discharge reactions [132]. Likewise, Chen et al. [133] determined the diffusion coefficient of VO^{2+} and VO_2^+ ions through three different membranes with negative functional groups. Unlike the work by Wiedemann et al. [132], in which diffusion was limited to electrolytes with a vanadium concentration around 0.1 $mol.L^{-1}$, the studies by Chen et al. [133] were

conducted using solutions containing up to 1.0 mol.L^{-1} of vanadium, where higher energy densities are considered. They showed that the lower diffusion coefficients of these ions associated with a high potential difference between the membrane prevent the unwanted crossing of vanadium ions.

Yang et al. [134] incorporated all possible ion crossing mechanisms into a model in order to investigate them and contribute to the understanding of the impacts on battery performance. When investigating the effect of the electric field on this phenomenon, the authors found that the difference in concentration between H+ ions in the positive and negative half-cells, even under an open circuit condition, causes migration of vanadium ions, with the transfer rate being strongly affected by the H^+ concentration gradient. Furthermore, the results reinforced that the discrepancy observed in the diffusion coefficients for ions in different vanadium oxidation states contributes to the creation of vanadium accumulations in the positive half-cell during the charge/discharge cycles, leading to a decline in the capacity of the battery [134].

Under operational conditions, especially when VRFBs are overloaded, other side reactions may occur. These involve the evolution of hydrogen gas (negative electrode), the evolution of oxygen gas and carbon dioxide generation by corrosion of the graphite plate that makes up the electrode (positive electrode). These reactions lead to loss of performance and compromising the battery structure itself [116,135,136]. Eqs. (12), (13) and (14) present, in this sequence and with their respective potentials, the reactions of formation of H_2, O_2 and CO_2 in the electrodes of a VRFB [137].

Hydrogen evolution:

$$2H^+ + 2e^- \rightarrow H_2 \uparrow \quad E^0 \leq 0.000V \text{ vs. SHE} \tag{12}$$

Oxygen evolution:

$$2H_2O \rightarrow O_2 \uparrow + 4H^+ + 4e^- \quad E^0 \geq 1.230V \text{ vs. SHE} \tag{13}$$

Carbon corrosion:

$$C + 2H_2O \rightarrow CO_2 \uparrow + 4H^+ + 4e^- \quad E^0 \geq 0.207V \text{ vs. SHE} \tag{14}$$

The degradation of the electrodes, either by corrosion or by the generation of hydrogen gas, represents an important reason for the loss of performance of a VRFB system [135]. Many studies that have been developed address the effects of hydrogen evolution [138–146]. In the negative electrode, the formation of H_2 bubbles is associated

not only with the reduction of the efficiency of the battery by consuming part of the electric current that reaches the electrode, competing directly with the reduction of V^{3+} to V^{2+} [147], but also because it affects performance by interfering with the flow of the electrolyte, reducing the area available for the occurrence of the redox reaction [139]. H_2 bubbles can also contribute to the degradation of the electrodes' surface made of carbon felt, oxidizing their surface [138]. However, if this evolution of hydrogen does not occur without control, which could lead to a complete failure of a VRFB [142,144,148], Piewk et al. [148] point to another configuration of conventional VRFBs in which a catalytic reactor is coupled to a secondary circuit on the negative side of the battery, responsible for producing hydrogen. This system is called double circuit vanadium redox flow battery and, in addition to energy storage by the traditional electrolyte, it allows the production of hydrogen through the reaction between vanadium ions (V(II)) with protons naturally present in the electrolyte, thus increasing the energy storage capacity of these systems [148–151].

Al-Fetlawi et al. [152] state that in the positive electrode, in turn, the evolution of O_2 and its consequent formation of bubbles affect the performance of the VRFBs by reducing the electrochemically active area of the electrode, as well as by reducing the diffusion coefficients of vanadium ions and effective ionic and thermal conductivities. The authors also point to a stimulus for the formation of O_2 bubbles by increasing the operating temperature and that, for this reaction to occur, part of the electrical current available to the electrode for oxidation of the V(IV) ion is consumed, reducing the efficiency of the system [152]. Zhang et al. [153] complement that not only the round-trip energy efficiency is impaired but also the Coulombic efficiency and the composition of the electrolytes, which becomes unbalanced and implies problems in the cycling of the battery, requiring control and monitoring as indicated by Corcuera & Skyllas-Kazacos [154].

The evolution of CO_2, in turn, may be associated with a process of intergranular corrosion of the surface of the graphite electrode [155]. According to the authors, the process is highly damaging to the battery, which can lead to failure and even leakage of electrolytes, in addition to, for example, the problems that infer the battery's electrochemical performance with issues related to the formation of bubbles. Liu et al. [155] also found that when functional groups such as COOH and C=O are present on the electrode surface, they can act as catalysts for the CO_2 evolution reaction, which leads to an increase in the corrosion rate.

2.1.3.1.3 The electrolyte imbalance and electrolyte regeneration

Another consequence of cross-contamination between electrolytes and side reactions is an electrolyte imbalance, which directly affects battery performance by reducing its capacity [156]. According to Roznyatovskaya et al. [157], this imbalance results from the inequality in the amount of oxidized and reduced vanadium species so that only one half-cell of the battery can reach a SOC of 100%, corresponding to that which has the limiting amount of species active. Jirabovornwisut & Arpornwichanop [158] highlight that, depending on the cause of the imbalance, both the positive and negative half-cells can be the limiting factor in the process. One way to verify this electrolyte imbalance in practice is through the measurement of the state of health (SOH). The SOH estimates the degree of battery weakening in the face of its deterioration over the charge and discharge cycles and, together with the SOC, represents the key variables in the system's energy management [159]. Generally speaking, the difference between the SOC of the positive and negative half-cells is the battery's SOH.

When you have an electrolyte imbalance, a change in the optimal initial average oxidation state (AOS) between the active species in the positive and negative half-cells is also verified. Initially, the AOS value is equal to +3.5, meaning that in positive and negative electrolytes there are, respectively, 50% of VO^{2+} and 50% of V^{3+} [160]. Determining the concentration of species in the anolyte using UV-vis spectroscopy has been discussed in the literature [157,161–163]. The strong colors and quite distinguishable from the different oxidation states of vanadium make the UV-vis technique a good candidate for determining the concentration of these species in solution and consequently the possible unbalance between the half-cells, since the species absorb light in different bands of the spectrum [162,163].

Two methods to attenuate the effects caused by electrolyte imbalance and to rebalance them were proposed by Corcuera & Skyllas-Kazacos [154]: (i) remixing the cell electrolytes and (ii) rebalancing by adding compounds to the catholyte. However, the cause of the imbalance must be known, as the first method applies to cases where there was only transfer of vanadium ions across the membrane, while the second is for cases where this transfer resulted in unwanted side reactions [154,158]. In addition to remixing resulting in energy losses as electrolytes are mixed and reset to an AOS of +3.5, it has demonstrated failures after some attempts to restore the initial battery's

capacity. Rudolph et al. [164] argue that the positive effect originating from remixing becomes quickly reversed after some restorations due to the decrease in the battery's internal resistance, mainly due to the change in the concentration of hydrogen in the electrolytes.

The method for chemical rebalancing proposed by Corcuera & Skyllas-Kazacos [154] consists of adding a chemical reductant or organic compounds such as oxalic acid, methanol and ethanol. These compounds are added to partially reduce VO_2^+ to VO^{2+}, which allows balancing the ratio between V^{2+} and VO_2^+, since the V^{2+} species becomes limiting due to the reactions of hydrogen evolution and oxidation by air [154,158]. Another method for rebalancing electrolytes was proposed by Whitehead & Harrer [143], which uses hydrogen. The proposal consists of reusing the hydrogen evolved by the side reaction in the anolyte, feeding it into the catholyte in order to, with the use of a catalyst, reduce the VO_2^+ as in the method using chemical compounds. However, the disadvantage of using hydrogen as a reducer is the low reaction rate between H_2 and VO_2^+ [143].

2.1.3.1.4 Influence of electrolyte on VRFB performance

For the various vanadium species used in VRFBs, sulfuric acid is, in fact, considered the best solvent [165]. On the other hand, this traditional VRFB system, based on the use of sulfuric acid, is significantly limited by the vanadium ion's solubility and stability, strongly dependent on the temperature and concentration of the acid [105]. As a result, there is a narrowing of the operating temperature range (10°C – 40°C), as well as the energy density of the battery, which is limited to 25 $Mh.L^{-1}$ for an active vanadium concentration below 2.0 $mol.L^{-1}$ [166,167]. The V(V) is the species that most restricts the battery's autonomy because in a solution that has a concentration ranging from 1.5 to 2.0 $mol.L^{-1}$, it undergoes thermal precipitation in the form of V_2O_5 at temperatures above 40°C and dissipation when below 10°C [107]. However, low temperatures are also related to the precipitation of species V(II), V(III) and V(IV) [168]. The use of additives for the thermal stabilization of electrolytes against temperature increase during the battery operation process will be addressed in subsection 7.1.

The efficient performance of the electrochemical cell is a critical factor for a VRFB since it depends on the reaction kinetics between the redox pairs [32] as well as

the energy density of the battery is influenced by the concentration of vanadium ions in the electrolytes. In this regard, over the years, much has been contributed to improving performance and reducing the cost of VRFBs, with high concentration electrolytes being developed [106,167–172].

In addition to the aforementioned factors, the power density and, therefore, the performance of the VRFBs, are also influenced by the flow and distribution of electrolytes in the electrodes [173] because of the relationship of these parameters with the supply of reagents and removal of formed products where reactions occur close to the electrode surface [174]. In addition, to achieve energy rates per power greater than 4, thus corresponding to a capacity to store energy for more than 4 hours, the economy of a VRFB becomes critical due to the electrolyte, which now includes an expressive percentage in cost with kWh[32]. This is motivated, for example, by the degree of purity required of the compounds traditionally used in the preparation of electrolytes, vanadium pentoxide and vanadyl sulfate, since the presence of impurities may be associated with a reduction in battery performance over the long term and, as a consequence of the increase in purity, there is also the price increase with the production of the electrolyte [32,175].

2.1.3.1.4.1 Influence of electrolyte flow-rate

The hydraulic subsystem of a VRFB system was discussed in section 2.2, where issues about the sizing of pumps and electrolyte storage tanks were addressed, as well as the influence of pump flow on battery operating efficiency. Ulaganathan et al. [59] point to the importance of the flow rate of electrolytes in determining energy efficiency and cell capacity. A higher electrolyte flow rate implies an increase in overall performance (especially capacity) of the VRFB; however, it will imply a reduction in system efficiency by increasing pump consumption [176]. Thus, it is essential to determine an ideal electrolyte flow rate in order to balance the system capacity gain with its efficiency loss.

Skyllas-Kazacos et al. [177] state that it is necessary to provide a flow considered to be a minimum (stoichiometric flow) to each half-cell and with a necessary rate so that the concentration does not reach zero before the electrolyte leaves the cell. This flow rate is a function of the reaction stoichiometry, the current applied to the system and the SOC of each cell so that each cell must receive a flow at the same

rate, although small variations occur as a result of pressure drops [177]. In this way, keeping the electrolyte concentration fixed, the minimum necessary flow rate varies with the SOC of the system. Even, to minimize the loss of concentration potentials, VRFB systems typically operate with a flow rate greater than the stoichiometric, which is linked to the geometry and design of the cell [177].

In the work by Khazaeli et al. [178], the authors argue that the high flow rate of the electrolyte can lead to a lower mass transfer bias, which would be desirable, but that this leads to a large pressure drop across the stack. Thus, the authors investigate these two phenomena as a function of the electrolyte's flow rate and associate this with the battery's SOC. The results obtained by simulation show that, at higher flow rates, there are gains associated with a shorter residence time and a more uniform profile of electroactive substances through the battery electrodes. In addition to the increase in cellular voltage, the increase in the flow rate implied the possibility of battery operation at low SOC during discharge, making the electrochemical energy conversion in the VRFBs longer, which, in turn, is related to a relief of electrode deterioration problems [178].

2.1.3.1.5 Preparation of the electrolytes of a VRFB

Building a VRFB has crucial steps for its proper functioning, which correspond to the processes of initial preparation and electrolyte loading [60]. Since the electrolytes store the active redox species that carry energy, the prepared solutions' physical-chemical properties represent critical factors for the technology's proper functioning [179].

Vanadium electrolytes are mainly obtained from $VOSO_4$ or V_2O_5 [31]. Skyllas-Kazacos & Grossmith [120] used different concentrations of $VOSO_4$ in a fixed concentration (2 $mol.L^{-1}$) of H_2SO_4 in the preparation of cathodic and anodic solutions. Using a basic charging system, the authors loaded three equal volumes of V (IV) solution, two of them in the positive electrolyte composition and one for the negative. During the initial charge, V (IV) oxidizes to V (V) on the positive electrode and reduces to V (II) on the negative electrode. The additional volume of positive electrolyte was discarded after complete loading, aiming to obtain equal volumes in each half-cell [120]. Li et al. [180] also prepared electrolytes from $VOSO_4$, but used equal volumes of

solutions on both the positive and negative sides. For this, an initial charge was given to reduce V (IV) to V (III) in the negative electrolyte and oxidation from V (IV) to V (V) in the positive electrolyte, followed by the addition of oxalic acid (reducing agent) in the V (V) solution to reduce it back to V (IV). Finally, Li et al. [180] recharged both sides, thus obtaining V (II) and V (V), respectively, in the negative and positive half-cells.

Skyllas-Kazacos [181] has patented a method for preparing electrolytes that consist of using a mixture of V_2O_5 and powdered V_2O_3 as vanadium sources, simultaneously dissolved in sulfuric acid. According to the author, with the powders' particle size and surface area, an equimolar mixture between V^{3+} and VO^{2+}, called $V^{3.5+}$, is obtained with the technique. The $V^{3.5+}$ electrolyte is, in a special way, preferred by the industry to be used as a positive and negative electrolyte because, with that, the VRFB system can operate without requiring an initial rebalancing of positive and negative capacities [30].

Methods for obtaining electrolytes for VRFB are also found in the literature, with V_2O_5 as a source, using electrolytic dissolution [182–186]. Through this preparation technique, each half-cell is filled with support electrolytes in the same concentration and, on the negative side, a suspension of powdered V_2O_5 is added. While at the positive pole there is an evolution of oxygen, at the negative pole V_2O_5 is reduced to $V^{3,5+}$, as shown by Eq. (15) [184].

$$V_2O_5(s) + 8H^+ + 3e^- \rightarrow V^{3+} + VO^{2+} + 4H_2O \quad (15)$$

Regardless of the vanadium source and preparation method adopted, the electrolytes must go through a pre-charging process for the VRFB system to operate. In cases where VO^{2+} is used as an electrolyte, the preload is responsible for generating V^{2+} and VO_2^+ as negative and positive electrolytes, respectively, representing a SOC of 100% [25]. In cases where $V^{3,5+}$ is used as a starting electrolyte, the negative and positive half-cells after preload are obtained, respectively, the V^{3+} and VO^{2+} electrolytes, which corresponds to a SOC of 0% [184].

It is important to highlight two factors related to the electrolytes of a VRFB that still represent a limitation to its potential for use: the low energy density due to the electrolyte's low solubility and its susceptibility oxidation to the air of the species V^{2+}

[76]. In addition to representing a challenge, Skyllas-Kazacos et al. [187] state that the relatively low energy density of VRFB electrolytes (generally in the range of 20 to 33 $Wh.L^{-1}$) limits applications for the technology, mainly in terms of physical space or weight. Regarding the stability of the V(II) species in solution against exposure to oxygen, the acidic state in which electrolytic solutions are commonly found, associated with the presence of oxygen, favor immediate oxidation of V(II) ions (Eq. (16)) [188], causing an electrolyte imbalance between the redox pairs and, consequently, reducing the battery capacity [189].

$$O_2(g) + 4H^+(aq) + 4V^{2+}(aq) \longleftrightarrow 4V^{3+}(aq) + 2H_2O(l) \quad (16)$$

Ngamsai & Arpornwichanop [188] investigated the reaction kinetics presented in Eq. (16) and concluded that the oxidation reaction of V^{2+} ions is faster when these ions are in lower concentration in the electrolyte and there is excess oxygen in the system. The authors also pointed out that the increase in the interfacial area between air and electrolyte is associated with high oxidation of V(II). Thus, the battery's projection should seek to reduce the contact area between the electrolytes and the air to minimize this process's occurrence.

2.1.3.1.5.1 Optimized electrolyte preparation

Ideal functioning might be provided by combining the effects of viscosity, activity and electrochemical conductivity. Jing et al. [190] have tested distinct concentrations of $VOSO_4$ in H_2SO_4 to evaluate the behavior of the electrolyte in charge/discharge processes and achieved the best electrochemical performance with 1.6 $mol.L^{-1}$ of $VOSO_4$ and 2.8 $mol.L^{-1}$ of H_2SO_4. Their results pointed that an increase of $VOSO_4$ concentration caused a decrease in conductivity while an increase in H_2SO_4 concentration improved it.

Mohamed et al. [191] have performed similar tests, but experimenting with an equimolar mixing of V(III) and V(IV) (1.6 $mol.L^{-1}$) in H_2SO_4 (4.0 $mol.L^{-1}$). Dilution of vanadium concentration in the solution for 0.8 $mol.L^{-1}$, fixing the initial concentration of H_2SO_4 resulted in a slight decrease in the cellular tension, although a solution with

highest concentration of vanadium was associated to a greater electrolytic resistance to ion movement. A decrease in H_2SO_4 concentration (3.0 mol.L^{-1}), but fixing the initial concentration of vanadium, however, was caused a charging time twice as long the more concentrated electrolyte, as well as a lower charge acceptance.

Shah et al. [192] developed a model for simulating the performance of a VRFB. The study obtained that a mixture of electrolytes of V (III) and V (IV) with an initial concentration of vanadium ions of 1.080 mol.L^{-1} demonstrated a coulombic efficiency lower than that developed by the electrolyte with a concentration of 1.440 mol.L^{-1}. Both electrolytes were supported in 4.000 mol.L^{-1} of H_2SO_4 and the result of the model was validated by data obtained experimentally by the authors themselves [192].

Kazacos et al. [193] examined V(V) precipitation to optimize the electrolyte concentration for VRFBs. They found that, in fact, the electrolyte present in the positive half-cell is susceptible to V(V) precipitation, but that the such phenomenon is mainly observed when the solutions are fully charged, at high temperatures and go through long periods without cycling. Thus, according to the authors, the composition of 2 mol.L^{-1} V(V) in 3-4 mol.L^{-1} H_2SO_4 can be safely used in systems that will not be subjected to high temperatures and that will undergo continuous loading and unloading cycles. Still, otherwise, the most appropriate preparation would be to reduce the concentration of V(V) to 1.5 mol.L^{-1}, maintaining that of H_2SO_4 in 3-4 mol.L^{-1}. However, in the concentration of 2 mol.L^{-1} of V(V) and 3 mol.L^{-1} H_2SO_4, the electrolyte, maintained at 40°C and under a 90% SOC, did not show precipitation [193] .

Intriguing results were found for V(V) solutions with concentrations greater than 3 mol.L^{-1} in H_2SO_4 with concentrations greater than 4.5 mol.L^{-1} in experiments of Skyllas-Kazacos et al. [106]. The authors did not verify precipitation in the analyzed solutions, even after 30 days and with the system subjected to 40°C. The study also shows that the increase from 1.5 to 2 mol.L^{-1} in the concentration of V(V) at 30°C favors the thermal precipitation in the positive electrolyte, but that, possibly, vanadium concentrations above 3 mol.L^{-1} can be used in VRFBs, in order to improve the energy density provided [106]. Rahman & Skyllas-Kazacos [168] showed that electrolytes with a V(V) concentration varying between 3.0 and 3.5 mol.L^{-1} in a sulfate concentration equal to 6 mol.L^{-1} are stable up to 30°C. They also proved that in higher concentrations, in addition to the loss of stability at these temperatures, the electrolyte greatly increases its viscosity, making hydraulic flow impractical [168].

Wen et al. [194] state that the electrolyte stability is most strongly affected by the relationship between the concentration of vanadium and H_2SO_4 and that an increase in the concentration of H_2SO_4 attenuates the precipitation of the V(V) ions but that a very high concentration impacts on the precipitation of the ions. V(III) ions in the negative electrolyte. Thus, the authors found that a preferred electrolyte to be used in VRFBs, from the point of view of stability, must have between 1.5 and 1.6 $mol.L^{-1}$ of vanadium in 4 to 5 $mol.L^{-1}$ of H_2SO_4, operating above -10°C [194].

The effect of the H_2SO_4 concentration used in a VRFB was evaluated by Islam et al. [195] regarding the impact on the transfer of vanadium ions and water across the ion exchange membrane separates the two half-cells. The experiments showed that the V(III) electrolyte synthesized by researchers from $VOSO_4$ at a concentration of 2 $mol.L^{-1}$, when the concentration of its supporting electrolyte increased from 2 to 6 $mol.L^{-1}$, implied a decrease in the transport of vanadium and ions of water from the negative to the positive half-cell, this improved the overall battery energy storage capacity by 50% [195].

2.1.3.1.6 Effect of the presence of impurities on the electrolytes

Although $VOSO_4$ is used in the preparation of electrolytes, the best cost-benefit ratio of V_2O_5 makes it the most required raw material [30], which is predominantly applied with high purity (99.8%) [31]. However, the diversity of sources available for recovery of V_2O_5, comprising ores, concentrates, metallurgical slags, oil residues and fly ash [16,32] may be associated with the incorporation of elements such as Fe, Na, Si, K, Ca, Mg, Cr, Zn, Cu, Mn and Ni to vanadium pentoxide, which in turn stimulates the need for tests to use a product of less purity (98%) in obtaining the electrolytes [31,32,194]. Among these metals, for example, Cu, Cr, Mn and Ni, as well as Sn and Mo, can harm the cycles of VRFBs because they act as catalysts for the evolution of H_2 that occurs in the negative electrode [71].

While some impurities may not be detrimental to the smooth functioning of the VRFB system, the presence of some can cause operational and performance problems, as is the case with Ni and Cu which, according to Cao et al. [32], are deposited on the negative half-cell electrode and contribute to the evolution of hydrogen as the battery is charged. In addition, Ding et al. [61] state that redox

reactions can also be negatively influenced, considering the impact that these impurities can affect the system in terms of stability and diffusion of vanadium ions through the electrolyte.

The ferric ion had its effect on the positive electrolyte of a VRFB evaluated by Ding et al. [49], who added different concentrations of Fe(III) in vanadium electrolytes composed of 1.6 mol.L^{-1} of V(IV) and 2.8 mol.L^{-1} of H_2SO_4 which, according to studies by Jing et al. [190], provide an ideal operating condition for VRFB. The presence of the Fe(III) ion in the electrolytic medium has been shown to contribute beneficially to the battery's reaction rate, favoring, for example, the diffusion of V(IV) ions through the electrolyte, up to a concentration of 0.0196 mol.L^{-1}. Above this concentration, the authors state that the V(IV) electrolyte lost thermal stability, resistance to charge transfer increased and, despite this, there was competition from ferric ions for the battery's redox reaction.

In obtaining vanadium from ores or concentrates leached, silicon is sometimes dissolved together with vanadium, often remaining in some content in the final product [196]. Thus, some literature reported the effect of silicates on the composition of the electrolytes [197–199]. Soluble silicates should have their concentration reduced to less than 1000ppm, preferably less than 500 ppm, say Nakajima et al. [197], because according to the authors, soluble silicates such as Na_2SiO_3, when in higher concentrations, can react with the sulfuric acid commonly used as a supporting electrolyte and produce H_2SiO_3, causing gelation of the acidic solution. Kubata et al. [198], in turn, used a relationship for the concentration of a contaminant with which they relate an increase in this to the decrease in battery performance. The authors then concluded that, for Si, the ratio is less than 5 ppm.m^3/m^2 (concentration of impurity x volume of electrolytes / total electrode area). Above this value, the impurity begins to influence the good performance of the system VRFB [198].

Nakajima et al. [197] and Kubata et al. [198] also evaluated in their patents the presence of the ammonium ion (NH_4^+) in the electrolyte, in which the authors reported that: NH_4^+ ions can cause instability in the electrolyte solution since they are associated with precipitation of vanadium, but can be removed from the system by heating in an inert gas atmosphere (400 to 690°C for 1 to 4 hours) [197]; deposition of vanadium-ammonium compounds can occur on carbon electrodes and, therefore, the concentration of NH_4^+ in the electrolyte must be below 20 ppm, as it is possible to nullify such phenomenon [198].

In addition to the NH_4^+ ion, Wen et al. [194] also evaluated the influence of the variation in the concentration of K^+ and Na^+ ions in a V(IV) electrolyte prepared with $VOSO_4$ with H_2SO_4 as a supporting electrolyte. In a concentration of H_2SO_4 equal to 5 $mol.L^{-1}$ and V(IV) equal to 2 $mol.L^{-1}$, the authors state that the three studied ions' presence contributed to the decrease in the number of vanadium ions kept in solution presenting a detrimental effect for the good battery operation. When changing the acid concentration to 4 $mol.L^{-1}$, however, Wen et al. [194] found that the ions V(IV) had their stability slightly increased by increasing 0.05 mol% in the ratio K^+/V(IV), in contrast to the verified with NH_4^+ and Na^+, that the increase remained responsible for the increase in precipitation ions V(IV).

The presence of the K^+ ion was also evaluated in vanadium electrolytes in which the metal was in other oxidation states (+3, +3.5 and +5) by Ding et al. [61]. The authors were able to verify that, for the three electrolytes studied, the addition of K^+ was associated with an increase in the electrolyte viscosity and a decrease in its conductivity. Regarding stability, Ding et al. [61] state that the K^+ ion had little effect on the V(III) electrolyte but that it negatively interfered with the others' stability. The authors also found a concentration that they considered to be an acceptable maximum limit for the presence of K^+ in solution, equal to $8.0.10^{-3}$ $mol.L^{-1}$. According to the results obtained by the researchers, below this concentration, a VRFB could fully act in a temperature range between -10 and 40°C, so that, in higher concentrations, the presence of K^+ was associated with a considerable increase in resistance to charge transfer, which in turn implies a decrease in electrochemical performance of electrolytes [61].

The effect of Cr^{+3} as an impurity in the positive electrolyte influences the reaction activity, ion diffusivity of vanadium and causes interface film and electrode reaction impedances, prejudicing the electrochemical performance of the V(V)/V(IV) redox par [200]. Huang et al. [200] found that in concentrations of up to 0.10 $g.L^{-1}$, Cr^{+3} has little effect in the battery electrode reaction, but up to the maximum concentration of to 0.30 $g.L^{-1}$ it favors the V(V)/V(IV) reaction by increasing its reversibility and decreasing ion diffusion resistance. The presence of Mn^{2+} in the positive electrolyte also has important reactional interferences, as studied by Huang et al. [201]. They showed that an increase in Mn^{2+} (from 0.04 to 0.13 $g.L^{-1}$) amplified the vanadium ion diffusion coefficient in 60%, improving both reaction activity and reversibility. However, Mn^{2+} in a concentration of 0.07 $g.L^{-1}$ the resistance to the reaction in the electrode and the

interfacial resistance grow 25% higher, implying that such impurity might have adverse effects in the VRFBs functioning [201].

In^{3+} ions also had their influence on the electrochemical performance of a positive electrolyte for a VRFB studied by He et al. [202], who found that the addition of In^{3+} to the electrolyte that comprises the redox pair V(V)/V(IV) increases not only the electrochemical activity but also the reaction kinetics. According to the results obtained by the authors, this condition is achieved when the ions of In^{3+} are in a concentration of 10.10^{-3} $mol.L^{-1}$, with which the researchers obtained an increase of 1.9% in the energy efficiency of the cell in relation to a cell whose electrolyte was not added from the impurity. In this case, the presence of In^{3+} assumed an additive role, because it directly contributed to battery improvement by affecting the hydration status of vanadium ions in the electrolyte and thereby increasing the charge transfer process that occurs at the interface between the electrode and the electrolyte [202].

2.1.3.2 Electrodes

2.1.3.2.1 General features

The electrode corresponds to one of the main components of VRFBs [66], performing the function of providing a surface that is electrochemically active so that redox reactions occur between the vanadium ion pairs of the electrolytes [21,203]. Electrolytes, such as the electrodes, are related to the determination of the system's energy storage capacity, whereas the area of the electrodes - associated with the number of cells contained in the battery cell - determines the power of the VRFBs [204]. Mehboob et al. [85] and Wang et al. [21] explain that precisely because the redox reactions between the VO^{2+}/VO_2^{+} and V^{3+}/V^{2+} pairs are processed in the electrodes while charging and discharging the battery, these are a vital part of the system, this because the catalytic effect they have on reactions directly implies an efficient use of vanadium electrolytes. This can significantly increase battery power. In this context, for Shen et al. [205], a bad electrochemical activity and kinetics represent a major problem for VRFBs and, therefore, as stated by Wang et al. [63], the electrodes must be highly catalytic for redox reactions to take place and charge the electrolyte effectively.

When selecting an electrode, some requirements must be met, such as: have a three-dimensional porous structure that facilitates the flow of electrolyte through its

surface, whose active area is as large as possible; demonstrate high electrochemical activity in the face of redox reactions; present low electronic resistance [21]; not participating in reactions, being, therefore, inert both mechanically and chemically to the active redox species and the supporting electrolyte that will flow through its surface; demonstrate electrochemical stability across the potential window to which the system will be subjected, and chemistry in environments subject to very low pH values; have high hydrogen and oxygen overvoltage and high and efficient electrical conductivity to respond quickly to charge transfer processes [66,203]. Ulaganathan et al. [59] explain how some of these specifications for the electrode composition material can affect the performance of VRFBs. According to the authors, the electrical resistance is related to the ohmic losses that can happen during the process of passing electric current. This directly affects device voltage and battery energy efficiency; overvoltage losses are influenced by the electrochemical activity of the material, which also implies the tension that will develop in the loading and unloading processes; the porosity of the material is related to the pressure drop in the flow of the electrolyte through the cell stack, which can lead to energy losses by pumping.

Since the first studies regarding VRFBs, when the system was being proposed and developed by Skyllas-Kazacos and collaborators, the tests were carried out using carbon, or graphite, as the production base material of the electrodes [25,64,120,206–211]. The first research specifically on electrodes for VRFBs was published by Rychcik & Skyllas-Kazacos [209]. With this study, the authors concluded that, under various forms analyzed, graphite and carbon performed well as a negative electrode.

Electrodes are currently mainly found with carbon fiber as the base material in the constitution, commonly as carbon felt, graphite felt (GF), and carbon paper [116,137]. GF are the most used because, among the requirements pointed out as essential to the electrodes, they present high conductivity, good chemical stability, high surface area, a large window of operation potential, in addition to the low cost of the material [116,205,212–215].

Shen et al. [205] state, however, that a limitation to the use of this material in the production of the electrodes consists of its weak kinetic reversibility. Ulaganathan et al. [59] and Kim et al. [203] complement stating that an adaptation of the fuel cells of the “zero-gap” reactors is being carried out on the batteries of the VRFBs. The goal is

to improve performance and achieve high power densities, which confronts most commercial graphite papers' somewhat low electrochemical activity [216–227].

2.1.3.2.2 Reaction mechanism of vanadium species and electrodes

The definition of the electrode geometry, associated with its shape and surface morphology, as well as the electrolyte flow, correspond to primordial factors in the projection of the VRFBs, because they are related to mass transport and the electrode kinetics in general [93]. Understanding the reaction mechanism that is involved in the redox reactions that take place in the electrodes is extremely important because it allows developing strategies to improve the behavior of active species, as well as designing materials that optimize reaction rates. As shown by Fan et al. [228], at least four general steps can be verified in the reaction processes in electrodes: the electrochemical step, in which electron transfers occur; the stage of diffusion of reagents and products through the electrolyte-electrode interface (mass transfer); this interface where the charge-discharge process of the double electric layer (non-Faradaic process) is also verified; and finally, the migration processes of both the released electrons, which follow the collector, and the other species through the electrolyte.

The reactions that occur between the vanadium ions in the positive and negative electrodes were presented, respectively, by Eqs. (8) and (9). The mechanisms for these reactions were proposed by Sun and Skyllas-Kazacos in two works. They report how the functional oxygen groups on the graphite electrode surface interfere with the reaction activity of the VO^{2+}/ VO_2^{+} and V^{2+}/V^{3+} pairs [216,229]. According to the authors, when thermally activating graphite electrodes, redox cells' energy efficiency increased by 10%. They attributed this increase to the formation of functional groups C–O–H and C=O on the electrode surface, which would act as active sites for vanadium ions, thus catalyzing the reactions.

In a charging operation, the reaction at the cathode starts by transporting the VO^{2+} ions from the catholyte to the electrode surface, then ion exchange of these with the H^{+} ions of the phenolic groups present, with the VO^{2+} ions remaining on the electrode surface, as represented by Figure 3a. Of these ions, an electron is transferred to the electrode along the C–O–V bond, one of the atoms of the functional

group C–O being transferred to VO^{2+} ions, which is responsible for forming VO_2^+ on the electrode surface (Figure 3b). In the last step (Figure 3c), there is an exchange of ions between the H^+ ions in the solution with the VO_2^+ ion formed on the electrode surface. Then the oxidation reaction with the VO_2^+ ions is completed, diffusing through the electrolyte [216]. In the unloading process, these reaction steps are inversely related to the loading process.

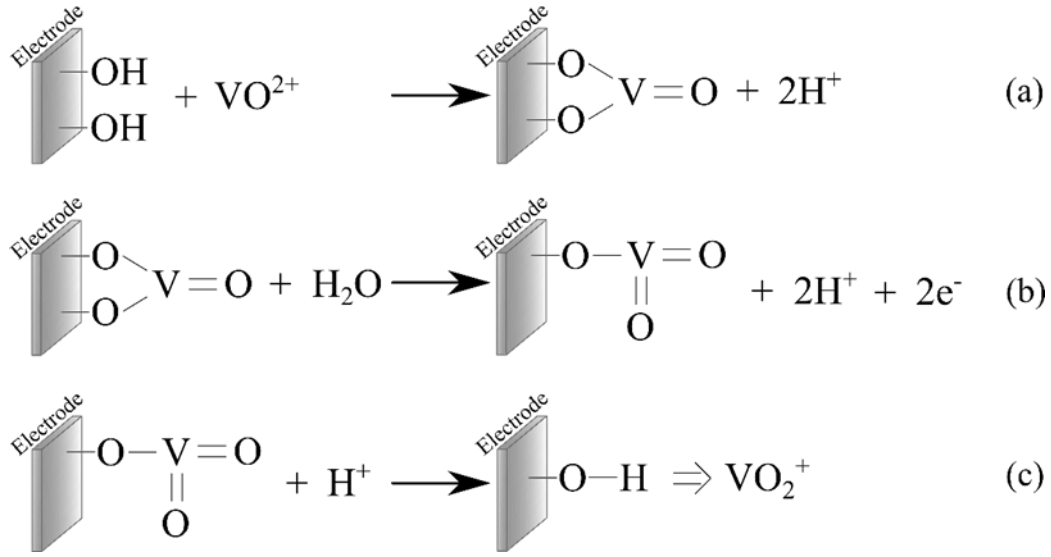

Figure 3. Reaction mechanism of the positive electrode during the charging process (Based on [216]).

In the anode, during the system loading, the V^{3+} ions initially diffuse from the anolyte to the electrode surface, where there is an exchange between one of these ions with an H^+ ion from a phenol group, as shown in Figure 4a. This process is followed by the transfer of electrons from the electrode surface to the V^{3+} ion, through the C–O–V bond, in order to form V^{2+} (Figure 4b). Finally, the reduction reaction is completed with the ion exchange between the formed ions and H^+ ions in the solution, with the release and diffusion of the V^{2+} ions in the electrolyte (Figure 4c) [229]. During battery discharge, the oxidation mechanism from V^{2+} to V^{3+} occurs in the opposite direction.

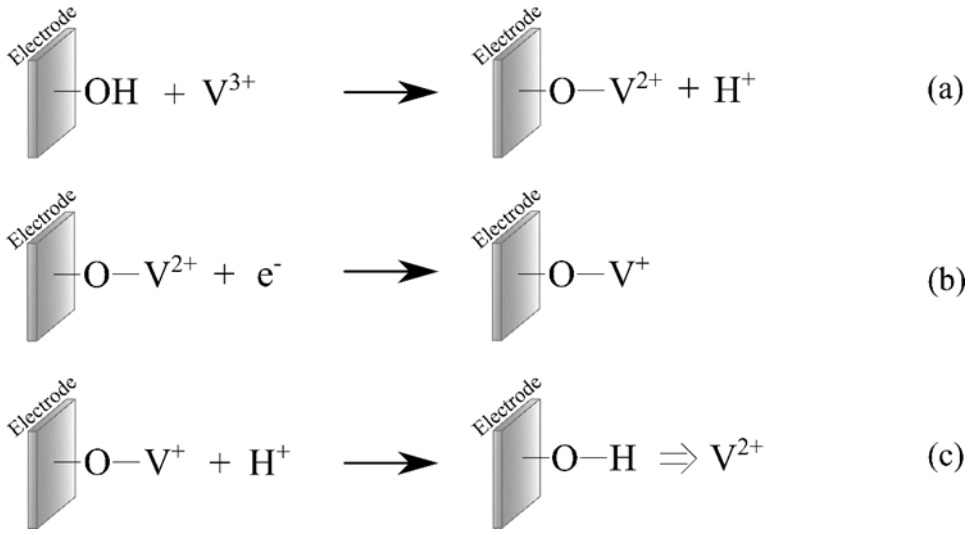

Figure 4. Reaction mechanism of the negative electrode during the charging process. (Based on [229]).

Zhong & Skyllas-Kazacos [210] investigated the VO^{2+}/VO_2^{+} redox couple's reaction kinetics for different carbon and graphite electrodes. They reported that they obtained a charge transfer coefficient and an equilibrium exchange current density, respectively, 0.71 and $2.47.10^{-4}$ $A.cm^{-2}$ for a graphite disc electrode, with 3 $mol.L^{-1}$ H_2SO_4 as the supporting electrolyte. In addition, values of the order of 10^{-2} $A.cm^{-2}$ were achieved for the exchange current density when using GF and crosslinked glass carbon electrodes, attributed by the authors to the greater surface area that these electrodes offer.

Gattrell and collaborators [135,230] also studied the reaction kinetics of the VO^{2+}/VO_2^{+} redox couple and they reported that, using a graphite electrode, a low symmetry factor was found in the curves polarization of this redox reaction. For the authors, the phenomenon is best explained as due to a layer of adsorbed intermediates that takes time to desorb from the electrode surface and by which the transfer of electrons to reactive species occurs, which leads to loss of the potential applied to conduct the stage reaction effectively. In this way, it is possible to assign a kinetic limitation to the reaction between VO^{2+} and VO_2^{+} species because, in this case, there is also the transfer of an oxygen atom preceding or following an electron transfer step, thus representing the probable limiting reaction of general mechanism. The reaction between V^{3+} and V^{2+} is faster, it has a much higher exchange current and its high

symmetry implies that simple electron transfers occur during the reaction [135,210,230,231].

Contrary to the results of Gattrel et al. [230], Aaron et al. [232] used dynamic hydrogen electrodes in the two half-cells of a VRFB to study the kinetics of the redox pairs in the positive and negative electrolytes and, interestingly, obtained an exchange current density for the redox pair VO^{2+}/VO_2^{+} approximately 44 times higher than for the V^{3+}/V^{2+} pair.

With this, it is understood that kinetically the reaction involved in the negative electrode is limiting to the battery's performance because it is the slowest reaction. This result, in turn, is not easily understood because of the observation of the reactions between each of the redox pairs (Eqs. (8) and (9)), which explains the greater complexity involved in the reaction of the positive electrode. The result obtained by Aaron et al. [232], in turn, is supported by the study by Choi et al. [233], in which the authors measured and compared the polarization of the positive and negative electrodes using a dynamic hydrogen electrode and found that the polarization of the positive electrode is superior to the polarization of the negative electrode. In this sense, Agar et al. [145] studied the configurations of crude carbon felt electrodes and treated thermally and chemically, aiming to determine which half-cell reaction limits the performance of a VRFB. The better performance provided by the heat-treated electrode implied its use in both half-cells as a base case. From the analysis of voltage efficiencies and cyclic voltammetry, the authors found that hydrogen evolution occurs in a potential very close to the reduction potential for V^{3+}. With this, Agar et al. [145] also suggested that the reaction limiting the performance of VRFBs is that which occurs in the negative electrode, but that this is not due to a slow reaction kinetics, but due to the formation of H_2 bubbles, which would be responsible for blocking the active sites of the reaction between the pair V^{3+}/V^{2+}. In addition, as the investigations of Choi et al. [234], the reaction on the negative electrode is highly dependent on the heat treatment of the electrode and the reaction temperature, in contrast to the pair VO^{2+}/VO_2^{+} on the positive electrode, which is quite indifferent to these variables. Thus, it is essential to carry out studies covering the most diverse materials of electrode composition, as well as functional groups present on the surface of these electrodes, in order to electrochemically evaluate not only the kinetics of redox reactions but the reaction set as a whole of the positive and negative electrodes of the VRFBs.

Wu et al. [235] investigated the kinetic behavior of the VO^{2+}/VO_2^{+} and V^{3+}/V^{2+} redox pairs on carbon paper electrodes. The authors proposed a reaction mechanism based on an internal sphere that takes place on the electrode's surface and that, similarly to that presented by Sun & Skyllas-Kazacos [216,229], is catalyzed by functional oxygen groups introduced by surface treatment. Yue et al. [236] also studied the use of electrodes composed of highly hydroxylated carbon fibers through the results obtained with the kinetics of redox pairs. The researchers also presented a mechanism similar to that of Sun & Skyllas-Kazacos [216,229]. They showed that the presence of the hydroxyl functional group on the surface of the electrodes implied a great increase in electrochemical activity. The experimental results also revealed that the redox reactions between V^{3+}/V^{2+} are more strongly dependent on the presence of OH groups in the carbon fibers, because, as attributed by the authors, vanadium ions are found in different forms in the sulfuric solution and, differently of the V(IV) and V(IV) forms, the absence of oxygen in the V(II) and V(III) ions hinders their ion exchange with the hydrogen of the OH groups.

The presence of phosphate groups on the electrode surface is also promising in the catalysis of the reactions between the VRFB redox pairs. The pair of solitary electrons in the phosphorus atom's 3p orbitals induces the local charge density and the vague 3d orbitals, in turn, allow to form bonds with carbon and oxygen atoms which provides more active sites to the vanadium molecules [237,238]. Kim et al. [239] studied the kinetics of carbon felter electrodes embedded in phosphorus on their surface. According to the authors, the phosphorus formed functional groups of phosphate and some chemical portions of –OH, which guaranteed the surface good hydrophilicity. With this, the redox reactions of the catholyte and anolyte's active species were improved because the phosphate groups are rich in oxygen. According to the reaction mechanism proposed by Kim et al. [239], the electronic transfer between the species of the VO^{2+}/VO_2^{+} and V^{3+}/V^{2+} pairs occurs through the P–O–C bond, which facilitates the electron transfer, since the phosphorus acts as an electron donor.

Porosity in a carbon-cloth electrode has also been reported by Zhou et al. [240]. The researchers developed a porous structure in macro-scale responsible for inferring to the system properties such as high hydraulic permeability and high effective ionic conductivity. In addition, Zhou et al. [240] also activated the electrodes with KOH, which created a nanoporous surface structure that increased the area of the electrode

available to redox reactions by at least 13 $m^2.g^{-1}$. This electrode provided the battery with energy efficiency of 80.1%, at a current density of 400 $mA.cm^{-2}$, with an electrolyte utilization of 74.6%, as opposed to the 61.1% electrolyte utilization observed when used a conventional carbon-paper electrode, demonstrating that this type of electrode is promising for use in VRFBs [240].

Graphite electrodes have also been studied in terms of reaction kinetics on their surface. An electrochemical activation on a GF electrode was performed by Zhang et al. [241] to study the catalytic effect that different functional oxygen groups have on the oxidation reaction of the VO^{2+}/VO_2^+ redox pair. The authors proposed a mechanism for the C–OH groups, as well as Sun & Skyllas-Kazacos [216] and another for the COOH groups, emphasizing that both serve as an active site in GF electrodes to catalyze the oxidation reaction of VO^{2+} to VO_2^+. In addition, Zhang et al. [241] reported that the COOH group provided H^+ ions more easily to the reaction compared to the COH group. Li et al. [242] prepared a graphite-graphite oxide electrode and studied the redox reactions for the V^{3+}/V^{2+} and VO^{2+}/VO_2^+ pairs. Applying an oxidation treatment, the authors reported that at least three functional oxygen groups were introduced at the basal planes and at the edges of the graphite oxide sheets: carbonyl group, ether group and ester group. These functional groups were responsible for improving the composite electrode's hydrophilic capacity, and both redox pairs demonstrated catalyzed reactions. Li et al. [242] also assumed the catalytic reaction mechanisms for the reactions. They showed that these functional oxygen groups' presence facilitated the adsorption of more reactive ions and catalyzing electron transfers and oxygen. In general, the graphite oxide electrode demonstrated better electrochemical performance compared to a graphite electrode, with almost twice the increase in the peak redox currents of the two redox pairs, in addition to the resistance to reduced charge transfer.

In order to achieve high performance VRFBs, a topic of great importance is the design of electrodes. Through this, it is possible to improve the polarization of the system as a whole, through interference in ohmic, activation and concentration polarizations [243]. Multiscale-pore electrodes have been reported to increase current density flow. Zhou et al. [243] presented a method to form a porous dual-scale electrode through activation of carbon paper – the large pores (formed between carbon fibers) worked as high-flow-paths for electrolytes, small pores (in the surface of the

carbon fibers) provided area for fast electrochemical reactions – both resulting in high energy efficiency (82-88%) at current densities of 200-400 $mA.cm^{-2}$. Linking natural multiscale-pore-networks to the mass transport and exchange functions necessary to the VRFB electrodes, Wu et al. [244] produced a multiscale-pore-network structured carbon felt electrode by a carbonthermic reduction of a ZnO layer formed onto the carbon layer. The hierarchically porous network occurred similarly to the reports of Zhou et al. [243], once electrolytes flowed through larger pores and redox reactions, together with ion diffusion, occurred in the submicron and nano-scale pores. Zhang et al. [245] have also worked in the process of creating a hierarchically porous network binding carbon nanofibers to carbon felt – also optimizing the surface composition by co-doping sulfur and nitrogen to catalyze vanadium redox reactions – reporting high energy efficiency (82.4%) to a current density of 320 $mA.cm^{-2}$.

2.1.3.3 Membranes

2.1.3.3.1 General characteristics

Another important component of a redox flow cell is the ion exchange membrane [23], which works by separating the active species from the positive and negative half-cells and allowing the passage, for example, of H^+, SO_4^{2-} and HSO_4^- ions [21,66,246]. This process is responsible for completing the electronic circuit while the current is flowing [23,247]. For this reason, the membrane, specifically the resistance it offers, is one of the factors that limits the power density of a VRFB [59], proving to be crucial in maintaining the high efficiency of the system for several cycles [248]. Membranes can represent about 40% of the total cost of a VRFB cell stack [249] and, therefore, it is necessary to develop advanced structures that link quality at a lower cost, which is an important requirement to be observed in the selection of the material used [250].

According to Wang et al. [63], the membranes need to demonstrate stability against the electrolyte in the entire SOC range to which the battery will be subjected, considering the acid character of the electrolytes and the presence of highly oxidizing species in them. An ideal membrane must also have good ionic conductivity, precisely to complete the circuit, minimize ohmic losses and, thus, not compromise the cell's voltage efficiency [66]. Another essential characteristic of membranes for VRFBs is

their high ion selectivity, so that they are permeable to the ions that are related to the load balancing that complete the circuit, but act as a barrier to the active species of vanadium, to prevent the reactions of self-discharge and contribute to the maximization of coulombic efficiency [248]. In this sense, an antagonism can be established between high ion selectivity and good ion conductivity since the increase in one is commonly linked to the decrease in the other. Thus, Wang et al. [21] reiterate that a balance between these two properties must be found. And yet, Ulaganathan et al. [59] complement by stating that, in fact, the increase in ionic conductivity critically implies a reduction in cell resistance, but that the use of a thinner membrane can also compromise the mechanical stability of the cell. This further demonstrates the need to use a membrane that can offer high performance with good ionic conductivity.

The membrane's chemical composition and properties correspond to the main interferences in the transport of species across the membrane [126]. Among the transport phenomena that occur in a VRFB, the permeation of vanadium ions and water through the membrane deserves great prominence due to its impact on the performance and the stability of the cycles [31,251,252]. The crossing of vanadium ions from one half-cell to another through the membrane and consequent reaction with other vanadium ions causes a phenomenon of self-discharge (Table 1), depicted in topic 3.1.2.1 of this article. In that topic, the effects of the crossover of vanadium ions on the battery's efficiency and capacity as a whole were discussed, which addressed the role that the membrane plays in preventing this process, precisely because of its permeability properties. Regarding water transfer, Sukkar & Skyllas-Kazacos [184] state that the process can generate preferential volumetric transfer and that at least three phenomena cause water transport: the movement of ions due to concentration gradients, migration of the species involved in battery charge balancing, and the osmotic pressure differential that is created between the positive and negative electrolytes. Thus, an essential requirement in selecting a membrane for application in VRFBs concerns its ability to prevent excessive water transfer between the two half cells [184]. This is because, positively, it is possible to avoid precipitation of vanadium salts in the cells by adopting membranes with ideal water transfer properties [66]. However, if there is the preferential transfer of water from one electrolyte to the other through the membrane, one of them will become concentrated in vanadium as the other will be diluted, varying according to the specifications of the adopted membrane and the charge state of the system [246,253].

2.1.3.3.2 Classification of membranes for VRFB

Numerous types of membranes have been developed over the years seeking to meet the properties required by VRFBs [254–268]. Commonly, these membranes can be classified into porous membranes and ion exchange membranes (IEM), the latter being subdivided according to the type of functional groups present on the surface in cation exchange membranes (CEM), anion exchange membranes (AEM) and membranes that conduct cations and anions, known as amphoteric ion exchange membranes (AIEM), which can be synthesized to contain a selective layer of cations and another for anions [65,66]. Table 2 gathers the characteristics VRFBs systems when applying different membranes from recent works.

Table 2. Different types of membranes and their influence in the VRFBs performance.

Polymer/Membrane name	Type	Thickness (μm)	Ionic conductivity (mS cm^{-1})	Water uptake (wt.%)	Diffusion coefficient ($cm^2\ min^{-1}$)	Current density (mA cm^{-2})	Coulomb efficiency (%)	Energy efficiency (%)	Voltage efficiency (%)	Reference
PVDF/HA–45	CEM	–	69	46	2.5×10^{-7}	100	95	80	84	[269]
0.7 μm PB	AEM	30	2	–	–	120	98	83	85	[270]
SPES (IL–30)	CEM	–	15	–	1.4×10^{-8}	140	99	79	80	[271]
$M_{D2.0-10}$	AIEM	–	–	–	1.7×10^{-7}	80	99	82	83	[272]
PE/PBI	CEM	25	6	21	5.0×10^{-7}	200	99	80	81	[273]
SPEEK/TPAM-1%	AIEM	108	70	39	3.0×10^{-7}	60	98	84	87	[274]
PSU/SPSF-62	CEM	76	40*	25	2.9×10^{-6}	100	99	87	86	[275]
SPEEK/ZC-GO-2	AIEM	75	33	37	12.7×10^{-7}	50	99	91	93	[276]
SPEKS/sGO (0.5%)	CEM	50	51	31	5×10^{-8}	40	99	83	83	[277]
SPAEK/$Ce_2Zr_2O_7$ (2%)	CEM	45	87	52	1.3×10^{-9}	40	100	82	83	[278]
PSU/PSf-c-PTA-1.4	AEM	125	20	37	2.6×10^{-7}	120	98	84	86	[279]
SPPO-2%GO	CEM	40	16	16	1.1×10^{-8}	40	98	69	71	[280]

Note: ***** Estimated average values for distinct temperatures.

2.1.3.3.2.1 Cation exchange membranes

Cation exchange membranes refer to those with negatively charged functional groups in their structure, such as $–SO_3^–$, $–COO^–$, $–PO_3^{2–}$, $–PO_3H^–$, and $–C_6H_4O^–$ [66,281]. The carboxylic acid group, for example, promotes a weak exchange capacity in the polymer that constitutes the membrane and is therefore not feasible to apply. The functional groups made up of sulfonic or phosphonic acids, in turn, are considered strong cation exchangers, as they easily dissociate the mobile cation from the group and are therefore more widely used in the composition of CEM for VRFBs [65]. One of the major obstacles to using this type of membrane as a half-cell separator in a VRFB is its impact on the battery's energy capacity. This is due to the probable cross contamination between vanadium ions that pass through its structure [184,282]. The diffusion process of vanadium ion by CEMs has been studied by some authors [127,133,282]. Historically, a CEM has been the most popular and employed membrane in redox flow systems due to a better performance: DuPont's Nafion. It is a copolymer of sulfonated tetrafluoroethylene, proton transporter, especially used as a membrane in a VRFB to support strong acid electrolytes and highly oxidative ions such as VO_2^+ [21,248,249,283].

In addition to their greater chemical stability, Nafion membranes also demonstrate high proton conductivity [284–286]. These membranes, on the other hand, have as main disadvantages their high cost, in addition to low ion selectivity, having a relatively high permeability to vanadium ions [111,246,248,253,287], impairing not only the energy and coulombic efficiency of the system but also limiting a wide practical application of this material in commercial batteries. This crossover effect of vanadium ions is attenuated when the battery is in operation, especially when there are high current densities. On these occasions, the protons show greater diffusivity than metal ions [65].

However, Nafion membranes are the most proven to have long-term chemical stability [288] and, for this reason, are still among the most used membranes for VRFBs. Thus, many studies have been developed to circumvent the problem of permeability of vanadium ions and their high cost, making changes in their surface, using a hybrid system of membranes and, still, using membranes with thinner thicknesses [253,285,286,289–296].

Several models have been proposed to help understand the structure and consequent mechanism of operation of the Nafion CEMs [297–305]. Schmidt-Rohr &

Chen [306] even reported the difficulty encountered during the first studies in proposing a convincing model, which contributed to understanding the set of information released about the membrane. However, the model proposed in the work of Gierke et al. [307], called the cluster-network model and later reaffirmed by Hsu & Gierke [308], is shown to be the most popular and the one that best explains the transport of ions through the polymer that constitutes the membrane, even in the case of a semi-phenomenological model and therefore of little predictive value, as stated by Mauritz & Moore [284].

In general, CEMs have two regions with different hydrophilicity [284], which is responsible for the functioning mechanism of these membranes. Normally, as is the case with Nafion membranes where the difference in behavior is more pronounced between the two regions, there is an electrically neutral, hydrophobic, and flexible skeleton and the SO_3^- functional groups, highly hydrophilic and commonly associated with H^+ ions, forming a side chain [111,309–311], schematically introduced in Figure 5.

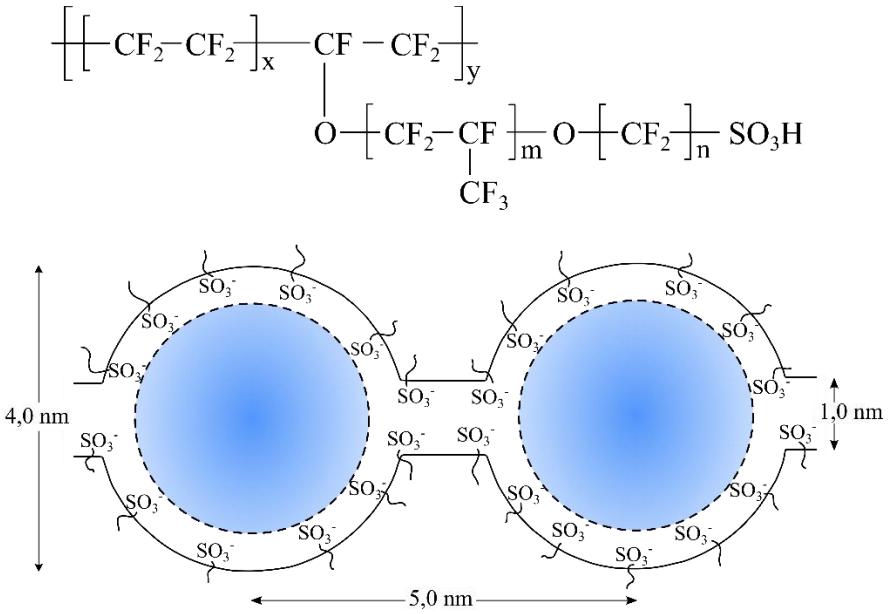

Figure 5. Nafion structure and the cluster-network model (based on [65,284,308]).

According to Karimi et al. [312], Nafion membranes' properties will be significantly impacted by their morphology. The natural phase separation between the skeleton of the membrane and the functional groups results from the difference in the nature of the regions, being intensified by the solvation process [311], which, in the case of VRFBs, is caused by the water from the electrolytes. The diameters presented by the cluster in a state of hydration and balance are due to a minimization of total free

energy between the terms compose it [308]. As shown in Figure 5, the sulfonated ion clusters of 4nm are connected to water channels of 1 nm in diameter, which are interconnected and dispersed inside the skeleton [313], exactly in which the transport occurs of protons across the membrane [314,315]. The configuration proposed by the model is responsible for attenuating the hydrophobic interaction of water with the skeleton and the electrostatic repulsion of nearby sulfonate groups [308]. This hydrophobic structure acts mainly in providing mechanical integrity and chemical stability, while the hydrophilic domains, results of the aggregate of the sulfonated groups, are responsible for providing the membrane conductivity [65,111].

Besides, mainly due to the high cost of Nafion membranes, others have also been tested for use in VRFBs. Among these, it highlight those that use sulfonated functional groups, which were inserted, for example, in poly (phenylsulfone) [316], poly(fluorenyl ether ketone sulfone) [265], poly(phthalazinone ether ketone) and tungstophosphoric acid composite [257], poly(ether ether ketone) composite, polypropylene and perfluorosulfonic acid [317], poly(ether sulfone) and sulfonated poly(ether ether ketone) composite [318], poly(arylene ether) [319], poly(phenylene) [320], poly(ether ether ketone) and poly(1,4-phenylene ether ether sulfone) [321]. The results obtained were predominantly compared to Nafion membranes and, in general, the use of these membranes in VRFBs was linked to high ion selectivity, low vanadium ion permeability, high coulombic efficiency and good chemical stability, thus showing promise.

2.1.3.3.2.2 Anion exchange membranes

Despite efforts aimed at solving the problem of vanadium ion permeability in EMFs, due to their nature, this remains an evident limitation, even if in an attenuated way. In this sense, AEMs have been used in systems such as those of VRFBs, in which the active species are cations [322]. These membranes, in turn, contain positively charged groups in their structure, such as $–NH_3^+$, $–NRH_2^+$, $–NR_2H^+$, $–NR_3^+$, $–PR_3^+$, $–SR_2^+$ [66,281], which electrostatically repel cations (a phenomenon known as Donnan exclusion) [323] and, consequently, inhibit the permeation of vanadium ions between the two half-cells [65]. Unlike CEMs, which have strong cation-exchange groups attached in their structure, the most common anion exchangers in AEMs are not strong [322], but which, according to Chen et al. [324], both protons and sulfate anions are effectively transported.

Different AEMs have already been tested as IEM in VRFBs, with very promising results being obtained: significant reduction in water transport [325]; improvement of energy, voltage and total system efficiencies [326]; decreased area resistance, low vanadium ion permeability and open circuit voltage stability for a long period of time [327] and greater vanadium selectivity and energy efficiency [328]. Besides, the use of this type of membrane in VRFB systems, due to the low permeability of the vanadium species that make up the electrolytes, was associated with high current efficiency, high coulombic efficiency, and good operational stability of the battery over the cycles [324,329,330]. According to the dynamic simulations performed by Tang et al. [331], the use of Selemion AMV anion exchange membrane reduced the diffusion coefficients of vanadium ions, except for the V^{3+} species, by at least one order of magnitude in relation to the values obtained for the Selemion CMV cation exchange membrane. The authors attributed the repulsion that the membrane exerts in the vanadium cations to the lower diffusion rate. However, they reported that, in the long run, the AEM presented a tendency of decrease in the capacity superior to that verified for the CEM. Mohammadi & Skyllas-Kazacos [332] investigated the chemical stability of Selemion AMV and CMV membranes. For this, the authors used sulfuric acid solutions at 0.1 $mol.L^{-1}$ and 0.2 $mol.L^{-1}$ of V(V), immersed samples of the membranes, and evaluated their degradation by quantifying the concentration of V(IV), resulting from the reduction of V(V). The results showed that CMV was much more oxidized than AMV. The mass loss of CMV was 45.2%, while that of AMV 6.3%, which implied, respectively, 66 and 23% reduction from V(V) to V(IV) in each of the membranes.

Sun et al. [262] studied three AEMs, with different ion exchange capacities, of poly (phenylene) and functionalized by quaternary ammonium groups, comparing the results with those of a standard Nafion membrane in terms of cycling efficiency, specific sand resistance, permeation of vanadium ions and durability. The experiments showed that the AEM with the lowest ion exchange capacity was the one that resulted in the highest specific sand resistance. This, however, was linked to its better coulombic efficiency (99%) compared to the others, mainly due to the lower crossing of VO^{2+} ions, but also to the lowest cell voltage observed. In terms of stability, the membrane with the highest coulombic efficiency proved to be intact, just like the analyzed Nafion membrane, commonly known and used for its high stability [262]. Similar results were obtained by Zhang et al. [333], who also inserted quaternary ammonium groups in poly (phthalazinone ether ketone ketone) for use as AEM in a VRFB. According to the

authors, the permeability of ions V(III) and V(IV) was much lower for AEM compared to a Nafion membrane tested under the same conditions. However, both the charging capacity and the discharge capacity of the battery with the AEM as a separator of the positive and negative half-cells were lower than those obtained with the Nafion membrane, mainly due to the greater area resistance of the AEM. In addition, greater coulombic efficiency was achieved by the system containing the AEM and a comparable general energy efficiency was obtained in relation to the Nafion membrane. With that, Zhang et al. [333] attributed to the presence of quaternary ammonium groups in the membrane the low permeability of vanadium ions, which was directly related to the good performance of the membrane during the cycles performed. In subsequent studies, Zhang et al. [334] synthesized an adamantane-containing poly (aryl ether ketone) membrane functionalized with quaternary ammonium groups as anion exchangers. The data obtained, in general, agreed with those of Sun et al. [262] and Zhang et al. [333], which pointed to low permeability of vanadium ions, which resulted in high coulombic and energetic efficiencies, higher than those obtained for Nafion membranes. However, in ex situ tests, the results showed that in a 0.15 $mol.L^{-1}$ solution of VO_2^+, the analyzed AEM demonstrated less chemical stability in relation to the Nafion membrane, which remained practically stable throughout the test. Chen et al. [324] confirmed the effectiveness of quaternary ammonium groups as substitutes for poly (fluorenyl ether) AEMs by obtaining a very low permeability of VO^{2+} ions through the membrane and a coulombic efficiency of 100%. The authors also reiterated that the promising results of the analyzed membranes are for applications in VRFB that operate intermittently or at moderate current densities.

It is important to highlight that the membrane preparation process parameters have a considerable influence on the properties they present when exposed to VRFBs systems. Xing et al. [328] prepared AEMs of quaternized poly (phthalazinone ether sulfone) and investigated the influence of time, temperature and concentration of the amination process. The authors showed that the increase in the three parameters was associated with an increase in the ion exchange capacity of the membrane, as well as in the water content, as well as in the decrease in area resistance. Finally, they concluded that the assessed AEM exhibited not only greater selectivity for vanadium ions but also greater energy efficiency compared to two Nafion membranes tested.

AEMs functionalized with pyridinium groups also offer good results in relation to their use in VRFBs. This can be seen in the work of Zhang et al. [335], in which the

authors prepared a poly (phenyl sulfone) membrane and investigated its application as an IEM in VRFB. The results showed that, in addition to the lower permeability of vanadium ions concerning a Nafion membrane, the tested AEM showed stability and high performance, with the battery showing greater efficiency. Equally promising results were obtained by Zeng et al. [336]. The authors used the bromomethylated poly (2,6-dimethyl-1,4-phenylene oxide) membrane and resulted in a VRFB with stable operational capacity over several cycles due to the good performance of the membrane.

2.1.3.3.2.3 Porous membranes

Although the use of membrane porosity for application in RFBs was initially limited and resulted in low coulombic efficiency of batteries [65], porous membranes have now consolidated themselves as separator technology. The use of porous separators in VRFBs was demonstrated by Chieng et al. [337]. The authors used a modified Daramic microporous separator due to the low cost and chemical stability demonstrated by Daramic in vanadium electrolytes. Originally, this membrane provided the system with a coulombic efficiency of 77%. However, by modifying the structure through treatment with polyelectrolyte/ion exchange resin, coulombic efficiency exceeded 90%. Besides, even after 1650 cycles of a VRFB, the membrane showed stability [337]. Later, two studies by Mohammadi & Skyllas-Kazacos [332,338] showed that the Daramic membrane shows low stability, which, in fact, is increased in composite Daramic membranes. Currently, in addition to microfiltration separators, ultra and nanofiltration separators are also available [339]. Among these, nanofiltration membranes are the ones that have shown the most promising results in VRFBs. They are made up of many small pores and use a pressure difference of 5 to 20 bar between the two sides as a force to guide the permeation of ions through it [340].

Nanofiltration membranes have a different functioning mechanism than IEM, based on the principle of adjusting selectivity between vanadium ions and H^+ protons by excluding pore size [341]. They can efficiently separate vanadium ions (in their four oxidation states) from protons due to the difference in radius and charge density because Stokes' rays and charge density of vanadium species are much greater than that of H^+ ions [341,342]. Therefore, the membrane's pores must be designed to allow H+ ions' passage but small enough to prevent vanadium ions' cross-contamination. For this idea, nanofiltration membranes not only demonstrate a solution to one of the

major problems of IEM, related to the permeability of vanadium ions but also exhibit an alternative for the application of VRFB separators with high operational performance.

As reported by Zhang et al. [341], a high selectivity V/H nanofiltration membrane, composed of polyacrylonitrile, was responsible for providing a coulombic efficiency of up to 95% and an energy efficiency of 77% to a VRFB. Both were obtained when the smallest pore size distribution of the membranes was evaluated. Later, Zhang et al. [255] modified these membranes with silica and reported a significant increase in V/H selectivity, as well as an increase in battery coulombic efficiency to 98% and energy efficiency to 79%. Silica was also used to modify poly (ether sulfone) nanofiltration membranes in the studies by Xi et al. [343]. The results showed that the silica membranes' modification increases the coulombic efficiency by more than 10% and the energy efficiency of the VRFB by 7% compared to the efficiencies presented with the original nanoporous separator. Wei et al. [288] incorporated silica into a polytetrafluoroethylene matrix and reported that, in addition to the low cost of the material, the use of this material as a separator in a VRFB was associated with excellent electrochemical performance, with high energy and coulombic efficiency (respectively 80% and 93%). The silica particles contribute to the increased performance of VRFBs because they are submicron size, forming nanoporous channels when incorporated into these membranes [288].

A polybenzimidazole membrane, which is also based on the principle of nanofiltration, was evaluated in VRFBs by Zhou et al. [344]. The researchers claim that the polymer's structure is chemically stable and that its pores reach a maximum of 2 nm in diameter, at least half of that seen in Nafion membranes. A VRFB employing the polybenzimidazole membrane, as presented by the authors, presents coulombic efficiency close to 100% when submitted to a current density between 20 and 80 $mA.cm^{-2}$. In addition, given its low permeability to vanadium ions, the membrane was also related to a low decay of battery capacity per cycle, around 0.3% [344].

In general, not only the composition of the membrane, but also the morphology presents itself as an important parameter to be controlled in maximizing performance. Li et al. [345] showed with their studies that the energy and coulombic efficiencies of a VRFB operating with nanoporous membranes of optimized morphology were similar to those obtained with standard Nafion membranes. According to the authors, the size distribution and the interconnection between the pores influence the area resistance

and ion permeability, which directly implies battery performance. Research by Cao et al. [346] and Cao et al. [347] with poly (vinylidene fluoride) membranes also showed how VRFB performance could be optimized by controlling the morphology of the material that makes up the porous membranes.

2.1.4 Modelling of VRFBs

As shown, VRFB systems still have several critical challenges that require optimizations to make the technology more applicable in practical fields. The improvement, which is sometimes related to materials, structure design, and even battery operating conditions, can be efficiently implemented through modeling, which intrinsically is more accessible due to its cost-saving and of time, when related, for example, to exhaustive laboratory tests [348]. Zheng et al. [348] state that, from the perspective of optimization, the creation of simulation models must include in its objective the development of a system that combines increased performance at a lower cost.

An essential parameter to be considered when modeling VRFB systems is their SOC. This represents the amount of energy the battery is storing in relation to its total capacity, and it also estimates the concentration of active vanadium species, as a reactant or product, at a given point in time. Thus, in models that assess the battery's electrical potential, it is a variable that must be inserted since it is SOC-dependent [349,350].

Several models have been documented, which aim to optimize various aspects of the battery, such as cost, pump power, thermo-hydraulic effects, the electrical system, and management and control. Zhang et al. [350] evaluated the costs associated with the construction and scalability of a VRFB, incorporating vanadium, electrode, and membrane costs into the model. The authors showed that the high price associated with vanadium was especially important in the final cost of the system, evidencing the need to purchase vanadium with high levels of purity, but at lower prices. Another point demonstrated was that, for VRFB projects, a system with lower power capacity and longer cycle time is more economically viable, given the sensitivity of the cost of capital to SOC limits [350]. On the other hand, Noack et al. [351] developed a model to investigate the impact of the materials that make up the

components on the cost of the system, allowing for targeted optimization. According to the authors, the model satisfactorily considered the bipolar plates, the membrane transport properties, and the voltage of each cell in the total energy supplied by the battery. It showed that the biggest influences on the cost of the system are about the cost of the battery, mainly the gasket, bipolar plates, and electrode felts [351].

As discussed in section 3.1.3, the stability of vanadium ions is highly dependent on the system temperature. Although they have a mechanism for cooling the system temperature, VRFBs can suffer from heat build-up mainly due to self-discharge reactions. Thus, it is crucial to know the temperature of the electrolytes during battery operation and, therefore, thermal models are documented in the literature. In the study developed by Wei et al. [352] were incorporated into the linearized dynamic electro-thermal model the heat generation model, the Foster network, and the electrical model. Thus, the authors demonstrated that the refrigerant flow rate has a great impact on the temperature of the electrolytes, and the flow of these, in turn, has a significant effect on the pressure drop and battery efficiency. Similar conclusions were reached by Tang et al. [353], who created a model for electrolyte temperature control, to which the authors incorporated the effect of self-discharge reactions and were based on mass and energy balance equations.

Additionally, Tang et al. [353] also showed with the simulation results the importance of membrane permeability in VRFB systems and also the need to replace the Nafion membrane for large-scale applications, given its permeability to vanadium ions. However, in this study, the effects of energy loss by the pump and on thermal modeling were neglected. So, Xiong et al. [354] developed a model in which they included the effect of an auxiliary pump. The study demonstrated that pump power is sensitive to both hydraulic design and electrolyte flow rates. Therefore, according to the developed model, the authors proposed conditions that provide better overall battery performance in terms of energy efficiency. Turker et al. [355] modeled a VRFB system already aimed at large-scale applications in the same vein. In addition to showing the high correlation between SOC parameters, power and general efficiency, the results were promising in evaluating operational strategies aimed at achieving greater operating efficiencies in scaled systems. The model by Gu et al. [356] also included the electrolyte concentration to relate it to the battery potential and SOC. The results obtained by the simulation presented the dynamic response of the VRFB in its

loading and unloading cycles. They demonstrated the possibility of simulating it as a function of essential parameters of the system.

Electrical modeling and for control purposes of VRFBs have also been widely explored. Bhattacharjee & Saha [357] developed a generalized electrical model for the VRFB system in which important physical parameters such as self-discharge reactions, flow rate and charge-discharge current profiles were considered. It was possible to estimate the stack terminal voltage and SOC as a function of different battery charge and discharge conditions. According to the researchers, it is essential to design an optimal rate controller for the electrolyte flow and allow its interface with real renewable energy production systems [357]. Electrical models that were later associated with control and management systems of VRFB systems are found in the works by Wei et al. [358–360]. The authors developed a model whose parameters as a function of time are accurately adapted online, which allowed to estimate the battery's terminal voltage, OCV and SOC with speed and accuracy. Therefore, the studies offered a robust way to control a VRFB system, with fast convergence, low computational cost and which also includes variations in the operating condition due to battery degradation over time. This effect from the fluctuating nature of wind power generation was mitigated in the model developed by Ontiveros et al. [361], who coupled an energy conditioning system to a VRFB. The results obtained by the simulations carried out showed similarity with the data collected from real devices. Therefore, a potentialization of the incorporation of wind energy in the electric network was provided.

The use of modeling in VRFB systems can also be useful in alleviating the problems caused by electrolyte imbalance, as shown in the study by Jienkulsawad et al. [362]. A dynamic model was developed based on the mass transport equation to which the authors incorporated the electrochemical kinetics and the diffusion processes of vanadium ions. Thus, the model results contributed to the online optimization of the system because, by estimating the concentration of vanadium ions throughout the operational process, which can change as degradation occurs due to electrolyte imbalance, it was possible to determine the rate of optimal electrolyte flow, which increased the energy efficiency of the battery [362].

2.1.5 VRFBs compared to other electrochemical energy storage (EES) technologies and its utilization field

2.1.5.1 VRFBs against other EES technologies

EES through involve a wide range of small-scale and large-scale applications [363]. EES uses chemical species to extract energy through chemical/physical sorption, chemical transformation or chemical intercalation [364]. Various types of EES are available in the market, so the main commercial types will be shortly discussed.

Lead-acid batteries (LAB) have been applied in many fields of the industry over a century [365]. Negative electrodes of LAB are composed majorly of metallic lead while the positive ones are composed of lead oxides in a range of compositions [366]. The electrolyte is an aqueous sulphuric acid solution that acts in the discharge processes [367]. In the negative electrode, sulphuric acid dissolves the Pb leaving free electrons, while (Pb^{2+}) in solution associate to (SO_4^{2-}) forming ($PbSO_4$) [368]. In the positive electrode, H^+ from the acid takes the oxygen from the lead oxide forming hydroxyls that later combine to other free H^+ to form water, while the (Pb^{2+}) in solution also combine to form lead sulfate [369]. Such discharge reaction produces around 2V [367]. LAB do operate in a wide range of temperatures (between freezing and boiling points of H_2SO_4), which is a great advantage [370]. An obvious disadvantage is its dependence of hazardous lead, additionally to a low volumetric energy density [371].

Nickel-Cadmium batteries (NCB) are a well consolidated technology used for industrial purposes [372]. The cathode in NCB is composed of cadmium while the anode is NiOOH [373,374], while the electrolyte is an aqueous solution of KOH. The cadmium is converted to $Cd(OH)_2$ while the anode transforms to $Ni(OH)_2$. $Cd(OH)_2$ gains two electrons to reduce into Cd and $2OH^-$, while $2Ni(OH)_2$ combines with 2OH to form NiOOH, water and $2e^-$ [375,376]. The charge/discharge reactions produces around 1.3 V . Some advantages of NCB are their applicability in low temperatures (-20°C) and their natural high conductive nature that allows quick charge/discharge (which can also be disadvantageous once they are susceptible to self-discharge), although a clear hindrance is the use of cadmium, a toxic metal [377].

Nickel-metal-hydride batteries (NMHB) are similar to NCB, but the negative electrode is made of metal alloys (such nickel and lanthanum alloys) with hydrogen-absorbing material [363]. The electrolyte is also aqueous potassium hydroxide solution

with lithium hydroxide as an additive that helps improving charging efficiency [378]. The positive electrode reaction is the same as for the NCBs, but in the negative electrode water reacts with the metal alloys (M) and a free electron generating OH- and MH [379]. NMHB have an energy density 40% superior to NCB [380] with an open circuit voltage of 1.2 V at half of its state of charge and, even though the performance decreases, cells are still can work in temperatures below -30°C and up past 100°C [368]. Besides, NMHB are environmentally safer than NCB once it does not use cadmium, but they also have a high discharge rate that makes them unsuitable to long-term storage necessities [381].

Lithium-ion batteries (LIB) are a family of batteries used in many kinds of technologies due to its high effectivity and properties, such as high energy density and low-self-discharge rates [382]. Graphite is the anode material, while the cathode may vary depending on the kind of LIB ($LiCoO_2$, $LiMn_2O_4$, $LiFePO_4$, $LiNiCoAl_2O$ and $LiNiMnCoO_2$) and the electrolyte is a non-aqueous component [383]. The electrolyte is composed of a mixture of organic solvents (to improve ion mobility) and lithium salts (LiPF6, LiClO4 and LiAsF6) [384]. The charging reaction involves the movement of lithium ion from the cathode to the anode through the electrolyte, returning to the cathode in the discharge [384], producing a typical voltage of ≈ 3.7 V [385]. Some disadvantages of LIB are: (i) sensibility to high temperatures, suffering fast degradation; (ii) due to the production of oxygen in the cathode, an intrinsic danger is imparted to LIB, since lithium is pyrophoric; and (iii) deep discharge cycles can severely damage the battery, requiring an expensive onboard circuit [386].

Sodium-Sulphur batteries (NaSB) are a high-temperature kind of batteries (work at a temperature of 300°C) and was brought out by FORD Motor Co in the 1960s and modernly developed to a commercial technology by Tokyo Electric Power and NGK insulators [387]. The positive and negative electrodes of NaSB are molten sulphur and molten sodium (respectively), separated by a solid electrolyte of ceramic alumina [388]. Sodium (2Na) goes through the electrolyte and combine with sulfur (4S) producing polysulfides (Na_2S_4) during the charging process, while in the discharge the sodium ions return to the electrolyte and the electrons flow in an external circuit, producing ≈ 2 V [389]. NaSB have high power density, high efficiency and long lifetime, but the fact it works with high temperatures require a system of thermal control to avoid risks, and

there is as well an imparted danger to sodium that reacts to water if it they come in contact under the atmosphere [390].

Table 3 compares a few information of EES systems. Energy efficiency of VRFBs are among the highest between EES technologies, but bellow LIB (as well as for capital expenditure – CAPEX). VRFBs have the greatest cycle lifetime among the EES, with extremely low self-discharging rates [391], which makes than the most promising ones for stationary purposes. A major advantage of VRFBs is that using the same elements in half-cells avoid problems of cross-contamination in long-term application [392]. They also have low maintenance cost and can deep charge not damaging their efficiency and life cycle [363].

Distinguishing from conventional batteries, RFBs are the most promising ones for storing energy from national grids [393]. RFBs have excellency features, such as excellent scalabilities and long-life cycling with moderate costs due to their three main components architecture [394]: a stack of electrochemical cells, an energy storage tank and a flow system. Apart from VRFBs (the utmost successful ones among the RFBs), some examples of other redox flow batteries are: (i) Iron-Chromium, (ii) Zinc-Bromine, (iii) Bromide-Polysulfide and (iv) Zinc-Cerium.

Iron-Chromium flow batteries (ICFB) are among the first RFBs technologies, in which at the positive electrode an aqueous solution of ferric/ferrous (Fe^{2+}/Fe^{3+}) redox couple is present, while the negative electrolyte is a mixture of Cr^{2+}/Cr^{3+} ions [395]. Although ICFB have characteristics of proper RFBs, they have a considerably low energy density (around 15 $Wh \cdot kg^{-1}$) and a short lifetime of 730 cycles [396] together with problems that are difficult to overcome [397], such as: the (i) poor reversibility, (i) low reaction kinetics of the chromium couple, (iii) electrocatalyst poisoning easily occurs due to impurities in the electrolyte and (iv) cross contamination tends to occur with the extension of cycle time.

In Zinc-Bromine flow batteries (ZBFB), the catholyte is liquid and the anode is solid plated zinc [391]. According to Abdin & Khalilpour [380] and references therein, ZBFB have good reversibility, high energy density (30-80 $Wh \cdot kg^{-1}$) but much shorter lifetime cycles when compared to VRFBs (1500-2000). Other disadvantages includes the formation of dendrites and material corrosion (due to the bromine) [398]. In the Bromide-Polysulfide flow batteries (BPFB), the negative electrolyte is sodium

polysulfide while the positive is sodium bromide, which are abundant, low-cost highly soluble in aqueous electrolytes [395] with an energy efficiency around 60-65% [399]. The system is, however, susceptible to cross-contamination and precipitation of phases which – together with a potential environmental risk caused by bromine – is an important disadvantage of the BPFB [400].

Zinc-Cerium flow batteries (ZCFB) have the highest theoretical voltage (≈ 2.5 V) among the RFBs [401]. However, Weber et al. [395] and references therein reported that it drops (<2 V) during the discharge. The reaction of charge/discharge is led by two redox couples, in the negative side of the battery by Zn/Zn^{2+} and at the positive side by Ce^{3+}/Ce^{4+} [402]. Emmett & Roberts [403] and references therein show that ZCFB have an energy density of a maximum of 11 ($Wh\ L^{-1}$), and due the fact that these are at their early stages of development there are still issues to overcome [74,401].

EES technologies are attractive when their functionality is reliable and effective – with relatively high cost-benefice – to a given utility. Renewable sources usually have an intermittent/seasonal timescale that demand a system that can operate in variable time-arrays in a grid scale plant [404]. Although the VRFBs still have improvements to be acquired, they are in a prominent position among the EES, since they demonstrate to be a multimegawatt and megawatt-hour energy storage system for renewable sources [363].

Table 3. A few characteristics of electrochemical energy storage technologies.

EES	Electrodes	Electrolyte	E. density ($Wh \cdot kg^{-1}$)	E. efficiency (%)	Lifetime (cycles)	CAPEX ($€ \cdot kWh^{-1}$)
VRFB	Carbon felter (I)	V in H_2SO_4 (aqueous) (II)	15-50 (III)	70-85 (IV)	20000 (IV)	500-650 (IV)
LAB	Metallic lead and lead oxides (V)	H_2SO_4 (aqueous) (VI)	30-45 (III)	75-90 (IV)	300-2000 (IV)	300-600 (IV)
NCB	Cd and NiOOH (VII)	KOH (aqueous) (VII)	15-40 (III)	60-65 (IV)	1000 (IV)	-
NMHB	NiOOH and hydrogen-absorbing metal alloys (III)	KOH with lithium hydroxide (aqueous) (VIII)	40-80 (III)	70 (IV)	1400 (IV)	400-700 (IX)
LIB	Graphite and lithium composts (X)	Li salts and organic solvents (non-aqueous) (XI)	60-200 (III)	90-95 (IV)	500-15000 (IV)	1000-1500 (IV)
NaSB	Molten sulfur and molten sodium (XII)	Ceramic alumina (solid) (XIII)	100-250 (III)	70-85 (IV)	3000-7000 (IV)	130-230 (IV)

Note: (I) and (II) revisit sections (3.2 and 3.1, respectively); (III) [363]; (IV) [391] and references therein; (V) [366]; (VI) [367]; (VII) [405]; (VIII) [378]; (IX) [406]; (X) [383]; (XI) [384]; (XII) [387]; and (XIII) [407].

2.1.5.2 The practical field of utilization of VRFBs

VRFBs are applied in several stationary electrical storage systems, specifically in those that do not require a high power/energy ratio [74]. According to Skyllas-Kazacos et al. [187], a wide range of applications has already been contemplated with the installed systems, which, according to Sánchez-Díez et al. [408], benefit from their individual capacity for independence between nominal power and stored energy, a benefit that, associated with its economic scalability, will probably make the limitation of its energy density minimal. RFBs, in general, are very promising for all fast and bulk applications. Among these, the following stand out: time shift, renewable integration, network investment deferral, primary control power, secondary control power, tertiary control power [409].

As already discussed, one of the most prominent applications for VRFBs concerns their integration with wind and photovoltaic generating systems. Several studies have been published discussing using these batteries in the storage of these renewable energies [410–414]. The Tomamae wind farm on Hokkaido Island (Japan), for example, stores the energy produced in a 4 MW VRFB, whose main purpose is to smooth the energy peaks caused by the intermittence of the wind. The United States also has an installed VRFB with 0.6 MW of power, which is used to store the energy produced in a waste plant [409,415].

The fast response time associated with the outstanding high-rate output performance in short periods of time characteristic of VRFBs are crucial properties for the effective use of these batteries in charge leveling and momentary voltage drop compensation, in addition to the aforementioned stabilization of fluctuations arising from of wind and photovoltaic power plants [416].

Mitsubishi Chemicals, still in 1997, installed in Kashima-Kita, Japan, a plant based on VRFB technology, applied in load leveling, with a nominal power of 200 kW and a capacity of 800 kWh [417]. In 2001, Sumitomo Electric Industries (SEI) built a VRFB in Tottori Sanyo Electric (Japan) to compensate for momentary voltage drops in a semiconductor plant. The system operated at 1.5 MW/1.5 MWh, reaching up to 3.0 MW with 1.5 seconds and without delay in cases of voltage drop [416]. According to Johnson et al. [418], in these industries with brief periods of very high demand, installing these batteries with high power is common. With this, energy savings are

achieved, considering that the batteries work briefly during peak periods and consume nighttime energy that has a lower cost to charge. Later, in 2015, SEI, together with Hokkaido Electric Power Company, installed the Minami Hayakita substation, which operates at 15 MW/60 MWh [419]. In Germany, a large 2 MW/8 MWh energy storage VRFB station, commissioned in 2019, is also installed [408]. Furthermore, according to Aramendia et al. [419], the largest project involving a VRFB to date refers to the one conceived by Rongke Power and UniEnergy for a plant in northern China, which should operate with 200 MW and 800 MWh, certainly the largest energy storage plant electrochemistry in the world.

Cunha et al. [74] point to another possible application for VRFB systems: fast charging of electric vehicles at existing gas stations. According to the authors, deactivated stations could store electrolytes in their tanks and electric vehicles could refuel using the energy stored in these VRFBs. The practice, in addition to being an alternative to electrical consumption in periods of grid blackouts and allowing the storage of energy produced at times of lower cost, is shown as a way to integrate electric vehicles to redox flow technology, which still is limited for installation in electric vehicles due to its low energy density [74].

2.1.6 System costs

Although the VRFB technology is already commercialized and several installations are verified globally, a major challenge for the generalization of its installation in large ESS is linked to the reduction of system costs [420]. Cunha et al. [74] point out that the economic feasibility assessment of a project involving installing these batteries needs to be cautious considering that the technology is recent in the market and the costs incurred with the purchase vary significantly between the manufacturers. In general, VRFBs are complex from a technical point of view and the different configurations for the system that aim to meet the specifications of installed power and available energy capacity (associated, respectively, with the cell size and the amount of stored vanadium electrolyte) are defined by several important parameters, such as cell voltage, current density, area of each cell, materials used in construction, concentration of vanadium in the electrolytes etc. [74,421].

In addition to having advantages such as longer lifespan in relation to LIBs and a more flexible energy/power ratio [74], VRFBs stand out as one of the most promising technologies for a possible price reduction until 2030, reaching up to 66 % cheaper [422].

Cost estimates have already been made based on price patterns obtained from comparisons in commercial catalogs for VFRB, with which it was concluded that three components make up the final price of the installation: the capacity-dependent one (about 300 € · kWh^{-1}), the one dependent on the installed power (560 € · kW^{-1}) and the fixed cost (750 €, 6,000 € or 11,250 € per unit, respectively, referring to the acquisition of 10, 100 or 1000 units), being these values refer to the installation of a small system with 4–8 kW / 20–40 kWh [74].

In the work of Viswanathan et al. [423] a cost model was developed for a VRFB based on different operating conditions and with information from various suppliers. It was shown that energy to power ratio (E/P) is an important parameter that contributes to the minimization of the total costs of implementing the system, since in higher E/P ratios there is a domain of energy component costs, while that at lower E/P ratios, power component costs stand out [423]. For a VRFB, increasing the E/P ratio from 0.25 to 4 h increased by 35 percentage points the cost share of V_2O_5 for electrolyte production in the total cost of the system, which became the highest cost component, while the separators dropped 17 percentage points and became the second component with the largest share of the total cost [423]. According to Zhang et al. [350], a factor that helps to understand the great sensitivity of the cost of the battery kWh as a function of the electrolyte is the increase in the price of vanadium due to the purity of the material. This can increase up to 100 times the cost with the electrolytes when comparing industrial-grade vanadium with laboratory-grade vanadium, which can increase the price of kWh from around 300 to up to $12000.

Minke and collaborators performed an economic evaluation of electrodes [424] and membranes [425] with applications in RFB systems and later published a cost model for VRFBs in megawatt scale [420]. The authors divided the system into the energy and power subsystems and showed that, for a power subsystem with 250 kW, the battery costs reached €219000, with the membrane being the component that represents the highest cost and has the potential to reduce by up to 42% this amount, reaching 128000 €. In the cost function for the total system, the power subsystem

shows a cost of 1080 € · kW^{-1} while the energy subsystem has a contribution of 385 € · kW^{-1}. Electrolyte again accounted for about half the cost of the system (43 and 55% for systems with E/P equal to 4 and 8 h, respectively) [420]. A cost performance model for an optimized VRFB system, on the other hand, was developed by Crawford et al. [426], which reached a cost estimate of less than 350 $ · kWh^{-1} in a 4 h E/P, with the expectation of reaching up to 160 $ · kWh^{-1} for the same E/P, for performance improvement and anticipated cost savings. In line with this result, in the work by Zeng et al. [427], the capital cost with 1 MW–8 h energy storage VRFB system was estimated at 229 $ · kWh^{-1}.

Recently, Rodby et al. [125] evaluated the levelized cost of storage for VRFB systems and, unlike previous studies, incorporated capacity losses and recovery through electrolyte rebalancing in the analysis. The authors concluded with the developed techno-economic model that measures can be taken to reduce costs, such as: the adoption of a rebalancing schedule, as an operational strategy; reduction of loss rates over cycles, such as improved performance; battery sizing, such as design strategies; and electrolyte leasing, as an investment opportunity with reduced initial cost capital [125]. Still on cost reduction strategies, Zheng et al. [428] report that an improvement in the technical-economic performance of RFBs can be achieved by prioritizing parameters such as high current density and low pump power required, and that the manufacture of electrodes and membranes must be improved with the incorporation of materials with reduced costs and that offer the same performance.

2.1.7 Optimization of VRFBs: recent research

In recent years, numerous studies have been driven by the need to mitigate the limitations of VRFBs. They seek an increase in energy efficiency and density, and this also mitigates precipitation problems of active vanadium species, or even working on optimizing the process with the addition of substances with catalytic action to accelerate redox reactions and enhance the performance of VRFBs.

In this sense, the main studies have focused mainly on the preparation of electrolytes, one of the battery's primary components, optimization of electrodes and ion exchange membranes.

2.1.7.1 Additives for electrolytes

The idea of electrolyte as a significant part of VRFB is reinforced because in addition to determining energy density, it also delimits battery operational issues (such as temperature). With this, recurrent problems of the limitations of vanadium species can be minimized, mainly avoided, in the presence of stabilizing agents as initially proposed by the group coordinated by Skyllas-Kasacos in the late 1990s. However, these agents cannot negatively influence electrolytes, resulting in battery inefficiency [32].

Thus, the type of substance used as an additive needs to be favorable to all oxidation states of V, on the contrary, while one species is favored in the electrolyte, another can be destabilized. This is what happens with the addition of K_2SO_4, considered an excellent stabilizer of the V^{4+} species, it can cause an increase in the precipitation rate of V^{5+} [60].

Cao et al. [32] suggest for the mitigation of precipitation problems the use of mixed acids as inhibitory agents. While reducing additives are more efficient as thermal stabilizers, covering the solubility temperature ranges of vanadium oxidation species.

In the work of Jin et al. [429], organophosphate compounds in the thermal stabilization of V(V) ions were also reported. The authors demonstrated that the use of 3-aminopropylphosphonic acid (3APPA) and sodium 3-phosphonopropionate (3PPA-Na) as additives in the positive electrolyte of a VRFB inhibits the precipitation of V_2O_5. The experiments proved that the –OH, =O and $–NH_2$ groups present in 3APPA control the growth of hydrated penta-coordinated vanadate ions, while 3PPA-Na, with alkali metal ions, inhibited precipitation by being absorbed on the surface of the vanadate particle. In addition to the stabilizing effect, the 3APPA additive, by helping to prevent precipitation, was also responsible for improving the retention of the battery's discharge capacity, increasing it by more than 16 percentage points compared to an electrolyte without stabilizing additives [429].

Li et al. [430] dedicated their studies to using organic additives in positive electrolytes to control and improve VO_2^+ solubility. Analyzing the efficiency of fructose, mannitol, glucose, and D-sorbitol, Li and collaborators [430]' results pointed out D-sorbitol as the additive that shows the best electrochemical activity, reaching an energy efficiency of 81.8% [430]. These results are linked to the increase in available hydroxyl

groups (–OH) that react with species V (IV), favoring the increase of active sites conducive to the occurrence of redox reactions of pair V(IV)/V(V) [31,430].

Besides –OH, others organic additives have a stabilizing effect due to functional groups such as CHO and C=O, which, when adsorbed on the initial V_2O_5 nuclei formed, act by repelling the other V(V) ions in solution and preventing precipitation [431,432]. However, organic compounds functionalized by these groups are not stable in V(V) solution, demonstrated by stability tests carried out by Zhang et al. [433], in which the authors noted the color change from yellow to blue, indicating the reduction from V(V) to V(IV). Furthermore, the effect of oxidation of stabilizing organic compounds on the positive electrolyte of VRFBs was carefully evaluated in work by Nguyen et al. [434]. The authors state that the stability provided by some organic additives may be a function of the partial reduction from V(V) to V(IV) and not effectively of the non-precipitation of V(V) species. For this, in the study conducted by Nguyen et al. [434], several organic additives classified into carboxylic, alcohol and multifunctional groups were included. Through titration and UV-Vis spectroscopy, it was shown that these additives reduced the SOC of the charged electrolyte and decreased the battery capacity, explained by reduction of the oxidation state of V(V) species in the positive electrolyte.

On the other hand, Rahman & Skyllas-Kasacos [435] emphasize that inorganic additives perform better than organic ones, based on the results obtained in experimental studies. The researchers developed the additive KS11, which consists of a mixture of 1% by weight of K_3PO_4 and 1% by weight of SHMP ($NaPO_3$), achieving a stable solubility for species V(IV) in a temperature range of 5°C to 20°C, avoiding the precipitation of V(V) concentrated in 4 $mol.L^{-1}$ at 50°C [435].

Tetrabasic sodium pyrophosphate (SPT) can also be another option for introducing phosphate ions to the catholyte. It acts by slowing the precipitation of the V species and increasing the electrochemical performance of the battery. This was done by Park et al. [436], which added SPT in a concentration of 0.05 $mol.L^{-1}$ to 2 $mol.L^{-1}$ vanadium and 4 $mol.L^{-1}$ sulfate, attesting to energy efficiency of 74.6%, corresponding to an increase of 2.8% in relation to white.

Tian et al. [437] justify phosphate additives' influence on reducing the precipitation rate of V (V). When the temperature is increased, the activation energy of

the hydrating compound of V becomes lower than that of dehydration. Roznyatovskaya et al. [438] also observed the delay in V (V) precipitation rate with the use of phosphoric acid in the catholyte when the temperature was raised to 50°C. They set the maximum phosphate concentration as an additive at 0.15 $mol.L^{-1}$; otherwise, exceeding the additive concentration, $VOPO_4$ precipitation is likely to occur [438].

However, according to Nguyen et al. [439], the precipitation of the compound $VOPO_4$ can be effectively avoided by the insertion of ammonium ions as stabilizing additives in the proportion of 1:1 with phosphate ions, since ammonium alone does not provide a good synergistic effect as in the presence of phosphate.

The use of a mixed acid solution of sulfate and chloride salts was proposed by Yang et al. [440] based on favoring the stability of species V(II) and V(V) by chloride ions. The study adopted an ideal electrolytic composition for the stability of the four active species of V in the electrolyte with a concentration of 2.4 $mol.L^{-1}$ vanadium, 6.2 $mol.L^{-1}$ chloride ion and 2.5 $mol.L^{-1}$ sulfate ion, meeting the solubility in a wide range of temperature from -20ºC to 50°C [440].

The same temperature range was maintained by a further study by Yang et al. [441] changing the optimal electrolytic composition, varying the concentration of V to 2.2 $mol.L^{-1}$, increasing the concentration of sulfate ions to 2.75 $mol.L^{-1}$ and decreasing the chloride ions to 5.8 $mol.L^{-1}$. The group concludes that the new study shows a better electrochemical performance due to the common effect of physicochemical properties such as viscosity, conductivity and vanadium concentration [441].

A more recent study by Yang et al. [442] excluded the need for chloride ions, especially for, according to Nguyen et al. [439], to avoid the generation of toxic halogen gases produced by the action of chlorine. However, due to this elimination, the temperature range was reduced to a new scale that meets from -10°C to 40°C. In addition, a control of the concentration of compositions is required along with their charge status, indicating a concentration of vanadium of 2 $mol.L^{-1}$ and 5.5 $mol.L^{-1}$ of sulfate as ideal to maintain an energy efficiency around 80% [442].

The control of the total concentration of vanadium and sulfuric acid as a supporting electrolyte for the expansion of the VRFB operating temperature range was also the basis of study for Wang et al. [443] from previous work by the group. Analyzing the different concentrations of the species (0.44-2.2 $mol.L^{-1}$ for V and 1.5-3.0 $mol.L^{-1}$

for H_2SO_4), they attested the static stability of vanadium ions in their four valence states to a concentration of 1.5 mol.L^{-1} in 2.0 mol.L^{-1} H_2SO_4 solution operating in a wide temperature range from -25°C to 60°C in the absence of additives. This result makes the study's application more economically viable by minimizing cost issues with the addition of substances with an electrolytic stabilizing effect [443].

Other research refers to the addition of stabilizing and catalytic substances to the anolyte, such as that of Shen et al. [205] in which the authors used antimony ions (Sb^{3+}) in the negative electrolyte and noticed an increase of 9.6% from the initial energy efficiency of 57.5%, that is, reaching an efficiency of 67.1%. The study of the group delimits an ideal concentration of Sb^{3+} in 5.10^{-3} mol.L^{-1} so that the system is favored with the improvement of the reaction kinetics of the redox pair V(II)/V(III), commonly slow, as well as its electrochemical activity [205].

Tin ions have also been tested by Mehbood et al. [85] as homogeneous electrocatalysts, in order to improve the reaction kinetics of redox pairs. As these ions have a greater catalytic action under the anolyte's reactions in relation to those of the catholyte, the study was based on the addition of Sn^{2+} ions to a concentration of 0.01 mol.L^{-1} in the negative electrolytes, accelerating the reactions of the pair V^{3+}/V^{2+} [85]. Still, according to Mehbood et al. [85], this behavior is mainly due to the electrodeposition of Sn^{2+} ions on the electrodes tested in the study, favoring the occurrence of reactions during loading and unloading.

In this perspective, other works bring new alternatives of catalyst ions, such as the one carried out by Duan et al. [444], who, in addition to adopting the pair VO^{2+}/V^{3+} aiming to increase the volumetric capacity for a new vanadium battery named VRFB, analyzed the efficiency of using copper (Cu^{+}) and bismuth (Bi^{3+}) nanocatalysts in anolytes. The authors observed that copper ions were more effective than Bi^{3+} in increasing the performance of VRFBs, also increasing energy efficiency by more than 70%.

Park et al. [445], in turn, suggest an even more daring study using Ti and Mn ions as additives to meet a high concentration of V in positive and negative electrolytes, and consequently to achieve an even higher energy density. The addition of the new elements was carried out by the researchers using the V/Mn pair in the positive electrolyte and V/Ti in the negative electrolyte. The V-Mn-Ti/V-Mn-Ti system obtained

an optimal condition for the ratio of the concentrations of 1.1 mol.L^{-1} of V, 1.5 mol.L^{-1} of Mn and 1.5 mol.L^{-1} of Ti to 1.6 mol.L^{-1} of H_2SO_4 electrolyte supporting, reaching at the end an energy density of 39.4 Wh/L.

2.1.7.2 Electrode optimizations

The most recent research on performance optimization of the electrodes mainly consider design factors and treatments (thermal, chemical and surface) associated with their purposes in VRFB, that is, to improve the electrochemical behavior, decrease the ohmic resistance and increase the locations reaction assets, since this is one of the greatest functionalities of the electrode, act as a propitious place for the occurrence of redox reactions [60].

Small structural modifications to the design can also improve the electrodes' performance and a consequent increase in the efficiency of the VRFB system. The application of mesoporous graphene is one of these alternatives and was used by Opar et al. [446] in the three-dimensional form of electrocatalyst synthesized to the carbon felt electrode for presenting a wrinkled configuration capable of providing the electrode with an increase in the areas of active surfaces for the kinetic improvement of the cell's redox reactions, reaching an energy efficiency of loading and unloading 76.5% at an current density of 10 mA·cm^{-2}.

The projections of flow channels on the electrodes are also improved, seeking the appropriate dimensioning to benefit the increase of the active surface areas as favorable places for redox reactions, decreasing the flow resistance and energy consumption of the pumps, and achieving energy improvements up to 2.7% [447].

In this sense, the lack of contact between the electrode and the electrolyte due to a bad sizing of the flow channels affects the kinetics of redox reactions, as well as the battery performance. This is because uniform cellular compression aided by joints favors the contact between the cell constituents, essential to increase the contact between the electrode, current collector, and electrolyte [93]. Cellular organization by uniformly compressing its components can increase the efficiency of the electrode, as well as the entire battery.

A recent study was based on the use of efficient performance electrodes based on design modifications. Gautam & Verma [448] developed their own activated GF

electrode, applicable as cathode and anode. The electrode had surface nanofissures that were pretreated with nitrogen doping, facilitating the electrolyte flows in the electrode by increasing the surface areas of active contact. These contribute to the electrode's hydrophilic behavior during the redox reactions of VO^{2+}/VO_2^{+} and V^{3+}/V^{2+} [448]. The occurrence of these mechanisms provided the study of Gautam and Verma [448] with excellent results in terms of improving the energy efficiency achieved, up to 89%, and current density around 50 $mA \cdot cm^{-2}$.

Because carbon felts and GF are the main materials used as VRFB electrodes, Mehbood et al. [85] based their research on the test based on these two types of electrodes. For this, they used carbon felt electrodes based on polyacrylonitrile (PAN-CF) and graphite felt based on rayon (Rayo-GF) and highlighted that those made of carbon felt PAN-CF performed better than Rayo- GF, demonstrating an improvement in the performance of the redox pair V^{3+}/V^{2+}, in addition to accelerating the reaction kinetics between V^{4+}/V^{5+}.

The aggregation of nanoparticles has been widely addressed by current research due to its electrocatalytic effects on the electrodes. The uniform aggregation of NiO nanoparticles to GF electrodes was developed by Yun et al. [449] through heat treatment converting the precursor $Ni(NO_3)_2 \cdot 6H_2O$ (nickel nitrate hexahydrate) into NiO at 300°C. Among the results achieved, the increase in energy efficiency stood out by 74.5% in addition to the improvement in the reaction kinetics of redox pairs due to the strong adsorption of vanadium ions to the electrode surface caused by the action of the functional oxygen groups provided by the NiO/GF system [449].

In a previous study, the group of Mehbood et al. [76] suggested the use of electrocatalysts added to carbon felt electrodes, such as SnO_2 nanocatalysts, achieving energy efficiency of 77.3% with a high current density of 150 $mA \cdot cm^{-2}$. In addition, they also achieved a 2.7-fold improvement in cycling stability. The study proved by means of cyclic voltammetry and electrochemical impedance spectrometry the acceleration of charge and discharge reaction rates due to the reduction of superpotentials caused by the electrocatalytic activity of SnO_2 nanoparticles [76].

A catalytic structure in the electrodes was also adopted by Wu et al. [450]. The authors report that, although thin-film electrodes are highly desirable for VRFBs, they have the problem of high resistance to mass transport. However, Wu et al. [450]

presented a thin-film dual-layer electrode, in which one layer has a structural function and the other catalytic function, which has pores that provide the active site for redox reactions. The researchers demonstrated that this electrode had an energy efficiency of 76.1% when the system operates with a current density of 240 $mA.cm^{-2}$, higher than the 61.9% found in conventional electrospun fiber mat electrodes. In general, a VRFB employing a thin-film dual-layer electrode operated for more than 800 cycles in a stable manner with 80.2% energy efficiency, under the same current density condition[450].

He et al. [451] used carbon nanofibers (CNF) as electrodes and, through electrospinning, uniformly incorporated high purity rutile (TiO_2) into them for the respective negative electrode application. The CNF/TiO_2 system has a synergistic effect of TiO_2 on CNF which, combined with CNF's high electrical conductivity, facilitates electron transport, increases the electrochemical activity of the V^{3+}/V^{2+} redox pair and causes, according to the study, a 7.8% increase in energy efficiency at a current density of 90 $mA \cdot cm^{-2}$.

High purity rutile was also added to carbon felt electrodes by Vázquez-Galván et al. [452]. In this case, however, the procedure was carried out employing ammonolysis, that is, a hydrothermal step for doping TiO_2 followed by nitriding at 900°C. The catalytic properties of the nitrogen groups associated with the TiO_2 effect provided the VRFB system with advantages such as improved catalytic kinetics of the redox reaction V^{3+}/V^{2+}, inhibition of hydrogen evolution, the high potential density of up to 700 $mW \cdot cm^{-2}$, high density of current (150$mA \cdot cm^{-2}$) and energy efficiency greater than 71% [452].

The improvement of energy efficiency and capacity is also favored by the electrocatalytic activity of cobalt deposition on positive GF electrodes. Xiang & Daoud [453] led the study by impregnating a thin layer of cobalt oxide from a solution of $Co(NO_3)_2 \cdot 6H_2O$ and ethanol in ultrasound and thermally treating the electrode at 400°C. The experimental results by cyclic voltammetry and electrochemical impedance spectroscopy demonstrated an improvement in energy, coulomb and voltage efficiencies, equivalent to 69.4%, 89.5% and 77.6%, respectively [453].

The use of different treatments, or even the combination of them, offers electrodes improvements both from an electrochemical point of view, as well as energy and voltage efficiencies. Eifert et al. [137], for example, identified the improvement in

the electrochemical activity of carbon felt electrodes through heat treatment, favoring positive and negative redox reactions.

Electrode heat treatments are most applied because they are more practical and economical [60]. However, this type of treatment favors the increase of side reactions (corrosion of carbon and evolution of hydrogen) and proves to be a negative point. However, Eifert et al. [137] believe that, even so, advantageous results prevail.

Side reactions can be avoided, for example, by the oxidative influence of sulfuric acid when the thermally treated carbon felt emerges in the solution. On the other hand, this mechanism can also reduce the electrode's electrochemical activity, negatively influencing the efficiency of the system. The recycling of aged cathodic carbon felts, however, appears as a mitigating alternative for future application in the form of anode electrodes, due to the chemical aging of the heat-treated electrodes decreasing the electrochemical performance of the reaction of the redox pair V^{4+}/V^{5+} by the oxidation of oxygen atmospheric, and in contrast increase the electrochemical activity of the redox pair V^{2+}/V^{3+} [85].

The combination of thermal and chemical treatments to improve battery performance includes the addition of functional groups, as performed in an experimental study by Shah et al. [454] in which the authors added S and N to positive and negative GF electrodes through hydrothermal treatment with ammonium persulfate solution at 180°C. They obtained an improvement in the voltaic efficiency to 95%, besides doubling the electrodes' electrochemical improvement factor in relation to those that are not submitted to the treatments. The treated electrodes are favored by increasing active sites of sulfate, nitrogen and oxygen groups attached to the carbon surface [454].

The combination of nitrogen and oxygen as kinetic enhancers of vanadium redox reactions on active electrode surfaces was also proven by Kim et al. [455] when performing a double atomic doping of N and O on GF electrodes by the thermolytic method of urea. The methodology based on the immersion of GF and the consequent impregnation of N and O by a solution based on urea and polyethylene glycol resulted in the double doping of nitrogen and oxygen atoms to the carbon network on the electrode surface, followed by a thermal treatment in tubular reactor purged with 2.5% O_2 up to 973K [455].

Although graphitic nitrogen, also called quaternary nitrogen, is considerably more stable in an acid medium, the increase in catalytic activity is mainly due to the pyrrolic N group, linked to the active hydroxyl sites due to the presence of oxygen groups [452]. In the study by Kim et al. [455], this process contributes to an improvement in the electrodes' reaction kinetics, especially the VO_2^+/VO^{2+} redox reaction, potentiated mainly by the action of nitrogen in relation to oxygen atoms. According to the analysis of the results, the identification of startling N peaks obeys a linear correlation (R^2 = 0.93) from the peak potential of the cyclic voltammogram (ΔE) together with the number of N atoms, being the thermal treatment oxidative. However, a facilitator of the process of doping the atomic content of N under the carbon felt. Pre-treatments of this type can contribute to an increase of up to 20% in the voltage efficiency of VRFBs, that is, reaching values around 86% and energy efficiency above 80%, also increasing the capacities of loads and discharges that reach be up to 2 times larger than VRFB using traditional GF electrodes [455].

2.1.7.3 Improvement of membranes

Considering that the biggest challenge of the ion exchange membrane is to maintain chemical stability and conductivity, recent studies work with the perspective of minimizing this problem that still does not present a perfectly solvable condition due to maintaining the balance between the crossing of protons and the crossover of vanadium ions, implying the achievement of maximum efficiency [60].

In this perspective, the incrustation of vanadium ions in the membrane can be a problem, mainly for the V^{5+} and V^{4+} species. The hydrophobic composition of the Nafion membranes [456] allows that there is no interaction of the same with the hydrated electrolyte, although the sulfonic groups located in the porous channels of the membrane have hydrophilic properties, blocking the passage of the proton flow and decreasing the conductivity of the membrane [60].

Nafion membranes, which are generally energy efficient in the order of 72% [457,458], can have their channels unblocked by their immersion in sulfuric acid, despite the process compromising conductivity protons at the same time that the V species are repelled [60].

Modifications to the membrane structure have been proposed, such as overlapping layers, for example, which consists of applying multiple layers of

polyelectrolytes to the surface of low-cost membranes, forming a barrier capable of reducing the permeability of the VO^{2+} species through repulsion by the presence of V ions. However, the disadvantage of the method is that this barrier decreases proton conductivity [459].

Changes in membrane design were also proposed by Wang et al. [460] from the deposition of hydrophobic nanofissures under the membrane surface, preventing vanadium species' permeability while proton conduction is maintained. The idealized cracks cover the membranes of poly(arylene ether sulfone) through plasma treatment, so that they are demonstrated as cheap optimization alternatives, despite the energy efficiency obtained in the experimental study of the group, about 85.37%, failing to be superior to the tests performed with the Nafion membrane, 85.11% [460].

Zeng et al. [81] suggest the application of anionic membranes in VRFBs as potential reducers of vanadium ions crossing as electroactive species, the feasibility of their application being assessed by Roh et al. [457], who developed a membrane from poly(phenylene oxide), proposing the favoring of proton transport due to the presence of the functional group –OH. Through the developed membrane, the researchers also ensure an increase in Donnan's exclusion effect as an exclusive advantage of the research, raising the coulombic efficiency to 99.5%, about 6% more than the Nafion membrane.

Che et al. [461] propose an increase in ion selectivity through the application of porous polybenzimidazole membranes, in which they use a modeling method based on SiO_2 and a NaOH-based attack solution. The results achieved with the membrane application increased coulombic efficiency, reaching a percentage of 99.5%, analogous to an energy efficiency of 87.9%.

In addition, the selectivity and conductivity of the membrane can be improved by the addition of special anionic and cationic groups, as well as the application of functional additives, such as sulfated zirconia, synthesized to the VRFBs membranes. The S-ZrO_2 particles have a high acidity, capable of providing a highly favorable medium for proton transport improvement. Parallel to this, the additive acts as a kind of barrier preventing the migration of vanadium species [462]. Zhang et al. [462] used the additive in experimental studies and achieved high coulomb and energy efficiency, about 98.89% and 86.78%, respectively. In comparison to the Nafion membrane, the

S-ZrO2 doped membrane demonstrates a viable application to the improvement of the VRFB system even by maintaining the cycling stability even after 70 charge and discharge cycles at a current density of 100 $mA \cdot cm^{-2}$.

The combination of different membrane properties can also favor the optimization of battery performance. The high proton conduction, typical property of poly(ether ether ketone) membranes, added to the low permeability to vanadium ions characteristic of poly(vinylidene fluoride) membranes through urethane acrylate, can increase the ionic selectivity of the membrane, increasing the coulombic and energetic efficiencies of VRFB [463].

Sulfonated poly(ether ether) membranes were also improved from the doping of WO_3 nanoparticles as a catalytic additive by the group of Sun et al. [456]. The researchers found a hybrid inorganic-organic membrane formed by sulfonated poly(ether ether ketone) with a concentration of up to 23.6% of the additive potential, demonstrating that the main advantage over the Nafion membrane is the ion selectivity at 30°C, about 3.2 times higher [456].

In a current study, Wang et al. [458] suggest a new class of anionic membranes based on poly (terphenylene) to maintain a high conductivity of protons associated with the low permeability of vanadium ions. The new membrane synthesized with polymers of terphenyl, biphenyl and alkyl groups of quaternary ammonium exceeded the selectivity of the Nafion membrane by 28 times with the increase of energy efficiency in the order of 93.64% and current density of 20 $mA \cdot cm^{-2}$, demonstrating a promising role in the application of VRFBs [458].

Sol gel-based methods are also widely discussed today in membrane synthesis. They aim to optimize cell performance and mainly reduce membranes' wear, since the sol gel coating acts to control corrosion and prevents interactions with the electrolyte from occurring [464,465].

The sol gel process, characterized by hydrolysis and condensation reactions, can provide the membrane with advantageous chemical and physical properties, improving battery performance [91,465]. The review by Balaji et al. [91] lists some of these characteristics comparing them with Nafion membranes not doped by the method, however, the study also reveals the flaws and limitations present in the application of the method, as well as the mechanical resistance of the membranes

influenced by the action of ethanol molecules formed as by-product of tetraethylorthosilicate hydrolysis, encompassing new research perspectives using, for example, nitrogen doped alkoxifluorosilanes.

2.1.8 Conclusions

VRFB technology has already proven to be highly promising and advanced for use in high capacity ESS. However, clearly some challenges still need to be solved for their full transposition to robust and real energy storage systems. In this review, the characteristics that underlie the VRFBs were addressed, providing the reader with an in-depth perspective on the main components of the system, presenting its technical principles and basic properties. An overview was taken from the creation to the development of current technologies that remarkably endeavor to mitigate or even eliminate the impasses inherent in the original battery configuration.

- In general, the need for spatial separation between the electrolyte storage tanks and the battery is of paramount importance for the VRFBs' operating dynamics. Its design is developed based on the questions of operation, performance and efficiency of the system, aiming at the end a high efficiency of energy storage. In this sense, the global system can be structured in subsystems such as hydraulic, electrical and control, ranging from the flow of electrolytes from the tanks to the battery for the respective transformation of chemical energy to electrical energy until the control of the systems.

- The technologies that involve the preparation of electrolytes have been remarkably improved, aiming at obtaining greater chemical stability, greater concentration and, thus, providing greater energy density of VRFB. The impact of the presence of impurities is also being evaluated, in order to make their preparation less costly. In addition, several additives have been suggested for incorporation into the electrolytes, in order to maximize the overall performance of the battery by improving its performance.

- Graphite-based electrodes stand out as the most common in VRFBs, despite their limitations regarding the functioning of the battery, such as the wear itself over the cycles. This suggests the introduction of new materials that can combine good catalytic activity, low cost and resistance, in addition, of course,

to the use of techniques that improve performance, such as the use of thermal, chemical and surface treatments. Changes in the design of the electrodes also appear as new proposals for optimization based on the adoption of nanofissures and the aggregation of nanoparticles in their structure, contributing to the expansion of the surface and enhancement of the catalysis.

- The permeability to vanadium ions is still the biggest problem in membranes, as well as their contribution to the total cost of batteries. Thus, one of the biggest challenges in the development of new membranes for VRFBs is to minimize cross-contamination, decrease its cost and, at the same time, maintain its chemical and electrochemical stability. Added to this, recent structural advances that include the introduction of multiple layers and nano-slits, acting to decrease the permeability of V ions.

3. OBJECTIVES

The research developed in this dissertation aims to purify an acidic vanadium solution using ion exchange resins; to study the parameters involved in the adsorption processes through batch tests; to evaluate the separation of vanadium from iron in continuous system tests and obtain high purity V_2O_5 for application in VRFBs.

4. MATERIALS AND METHODS

The Figure 6 shows the general flowchart of the experiments conducted in the present work.

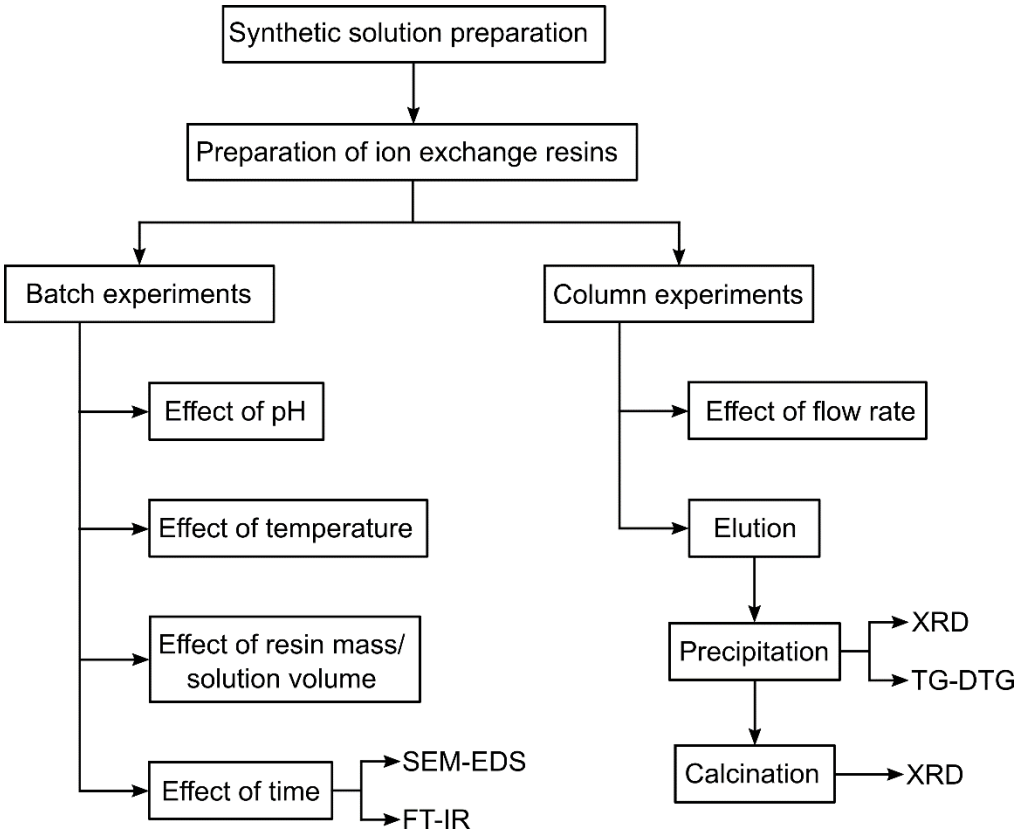

Figure 6. Schematic flowchart of the methodology used in the present work.

Firstly, the synthetic solution was prepared. Commercial V_2O_5 was used, which has about 0.5% of impurities (mostly entirely represented by iron). 10 g of this material were transferred to a 500 mL Erlenmeyer flask, in which 400 mL of aqua regia were added. The system was left under stirring for 24 hours and then 0.2 g of metallic iron was solubilized. Then, the liquid was filtered and transferred to a 2 L volumetric flask, so the volume was completed by the addition of ultrapure water.

Vanadium and iron of the obtained solution were then quantified and the result was used to construct a Pourbaix diagram, which was essential to determine the Eh x pH condition which the VO^{2+} and Fe^{2+} species would be predominant in the solution. This analysis was important because, for two of the tested resins, vanadium in its +4

oxidation state is among the metals for which the resin shows selectivity. Furthermore, that Fe^{3+} would be preferentially adsorbed over vanadium. Therefore, the redox potential and pH of the medium were adjusted, respectively, by adding a solution of sodium dithionite ($Na_2S_2O_4$, 1 mol.L^{-1}) and sodium hydroxide (NaOH, 10 mol.L^{-1}).

Four commercial resins were tested in the purification of the vanadium solution: Lewatit® MonoPlus TP 209 XL, Lewatit® TP 207, Dowex™ M4195 (ion exchange chelating resins) and Lewatit® MonoPlus S 200 H (strong cationic exchange resin). Before each experiment, these resins went through a preparation process. This procedure had two objectives: (i) to eliminate possible impurities and (ii) to charge the functional groups with exchangeable H^+ ions.

The resins were placed in 250 mL Erlenmeyer flasks and washings interspersed with hydrochloric acid solution (HCl, 4 mol.L^{-1}) and ultrapure water were performed three times each. The flasks were taken to an orbital shaker that operated with agitation of 200 rpm at 25 °C. Each washing step lasted 4 hours, the last one being carried out with water. At the end, the flasks went through an ultrasonic bath in order to release any solid impurity that could be adhered to the resins. For the batch experiments, resins were separated by vacuum filtration and taken to dry in an oven at 60 °C for 24 hours, while for the continuous system tests they remained conditioned in water until added to the columns.

Batch tests were performed first and the following parameters were investigated: pH, temperature, resin mass/solution volume ratio and contact time. All these experiments were performed in 250 mL Erlenmeyer flasks in an orbital shaker at 200 rpm. The adsorption efficiency was evaluated through the quantification of vanadium and iron in solution before and after each test (by means of absorption atomic spectroscopy), since the difference represents how much of each metal was adsorbed by the known mass of resin.

The first parameter analyzed was pH, for which the range between 0.5 and 2.0 was investigated, with a variation of 0.25 between each point. The pH adjustment of the medium for each point was performed by the adding an NaOH solution (10 mol.L^{-1}). For each analyzed pH value, 1 g of dry resin was weighed and 50 ml of solution was added. Flasks were left shaking for 2 hours at 25 °C.

The influence of temperature was investigated from 25 to 55 °C, with a variation of 10 °C between each point. For all these tests, a solution with a pH equal to 1.0 was used, adjusted to the temperature corresponding to which the solution would be tested. The resin mass/solution volume ratio was kept constant (1 g dry resin/50 ml solution) in a contact time of 120 min. With the data obtained from these experiments, a study was carried out on the thermodynamic parameters – enthalpy (ΔH^0), Gibbs free energy (ΔG^0) and entropy (ΔS^0) – related to the adsorption of metals by the resins. These parameters are important because they provide information about the spontaneity of adsorption reactions, as well as whether the processes are endothermic or exothermic.

The experiments varying the relationship between the resin mass and the solution volume were carried out in order to investigate the adsorption mechanism of metals in the active sites of the functional groups. The volume of solution was kept fixed at 50 mL and a mass variation from 0.055 g to 9.000 g was used. The solution pH was corrected to 1.0, the system temperature maintained at 25 °C and the contact time was equal to 120 min. The adsorption results obtained were studied based on three adsorption isotherm models: Langmuir, Freundlich and Temkin. These are equilibrium curves that provide information about the amount of each metal that is adsorbed per unit mass of resin as a function of equilibrium concentration.

The influence of contact time was used in the study of adsorption kinetics. The contact time between resin and solution was varied from 30 min to 1440 min. The resin mass/volume of solution ratio was equal to 1 g/50 mL, the pH was adjusted to 2.0 and tests were carried out at 25 °C. Four kinetic models were evaluated – pseudo-first order, pseudo-second order, Elovich and intraparticle diffusion – in order to obtain data related to the determinant mechanism of adsorption as well as the controlling step.

Then, resins from the Erlenmeyer flasks (after 1440 min of contact) were filtered, washed with water and dried in an oven at 60 °C for 24 hours. These were taken for analysis by scanning electron microscopy (SEM) coupled to an energy dispersive spectroscopy (EDS) and infrared spectroscopy by Fourier transform (FT-IR). The same resins were evaluated before the ion exchange experiments through SEM-EDS and FT-IR in order to better understand post-experiments changes and to further characterize the adsorption.

Studies in a continuous system were the next step after the batch experiments. Fixed bed glass columns 50 cm long and 1 cm inside diameter were used. The resins were wet packed to a bed height of 30 cm, resulting in a bed volume (BV) of approximately 23.6 cm^3. In the experiments in continuous system, only the ion exchange chelating resins were evaluated, because they were the ones that showed the best performance in batch experiments. Columns were loaded using two different operating flow rates: 2 and 3 BV/h (0.8 and 1.2 mL/min, respectively). Flow control was carried out through the use of peristaltic pumps at the inlet and outlet of the columns. These experiments were used to build the breakthrough curves for each resin at each operational flow. The initial pH of the solution was kept at 2.0 for all tests and the temperature at 25 ± 1 °C. After loading the column until exhaustion, it was eluted to obtain a pure vanadium solution. Elution was carried out by flowing a sulfuric acid solution (H_2SO_4, 1 $mol.L^{-1}$) at a flow rate of 3 BV/h.

The eluted purified vanadium solution was subsequently subjected to the ammonium sulfate precipitation process ($(NH_4)_2SO_4$). Initially, the solution was subjected to an oxidation process, to convert +4 vanadium species (VO^{2+}) to VO_2^+.The procedure was performed in a 250 mL beaker partially immersed in a thermal fluid. The set was placed on a hot plate with magnetic stirring. At 50 °C, hydrogen peroxide (H_2O_2, 29%) was added in a quantity 10 times greater than stoichiometric and left under stirring for 30 min. the temperature was raised to 90 °C and a solution of $(NH_4)_2SO_4$ (500 $g.L^{-1}$) was added until the pH of the solution reached 2.2. Stirring remained for 2 hours and the precipitate filtered off under vacuum and dried in an oven at 60 °C for 24 hours. To identify the crystalline phase in which vanadium precipitated, the solid was analyzed through X-Ray Diffraction (XRD) and thermogravimetric analysis (TG-DTG).

After characterization, the precipitate was calcined in a muffle furnace to obtain high-purity V_2O_5. The procedure was carried out at 550 °C for 2 hours under a synthetic air atmosphere. The identification of the expected product was also given by the analysis of the calcined solid through XRD.

The methodology described here is further detailed in subsections 5.1, 5.2 and 5.3. In these subsections are (respectively) manuscripts 02, 03 and 04, which contemplate the research of the present work (Figure 7).

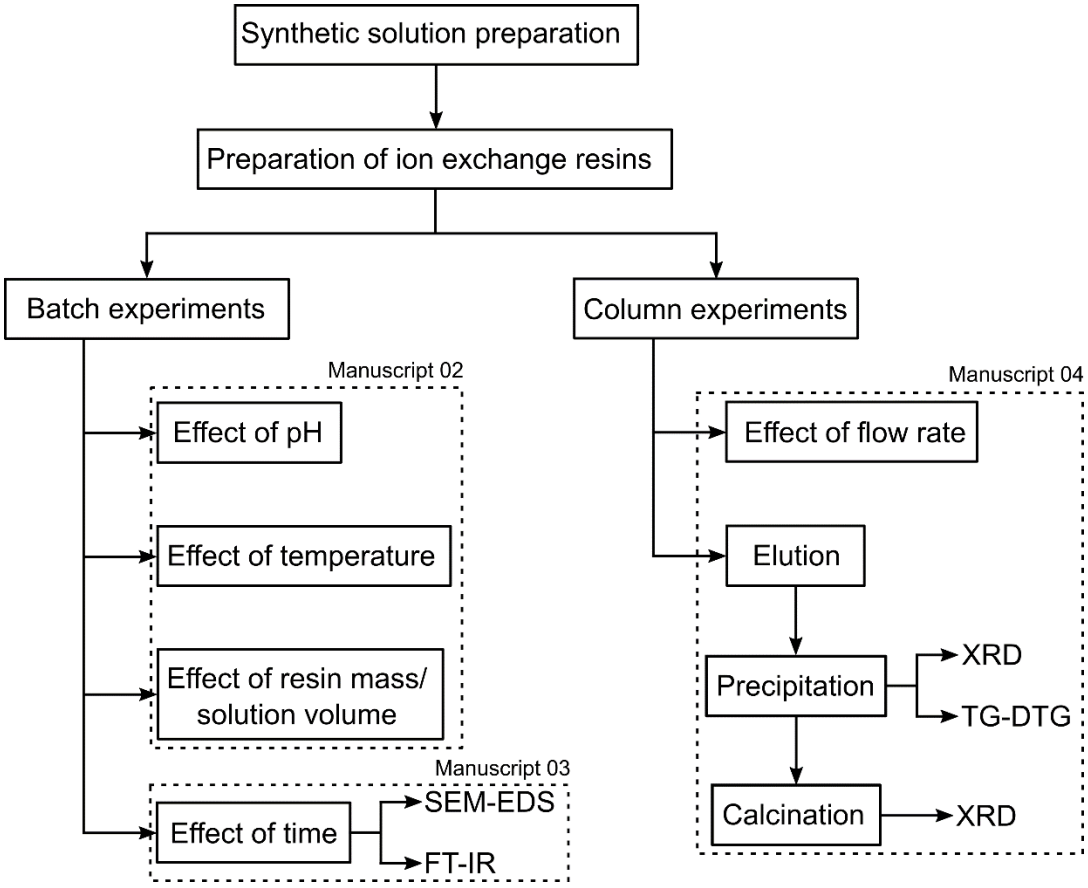

Figure 7. Flowchart segmenting the results of the methodology used in this work.

5. RESULTS AND DISCUSSION

This section presents three manuscripts produced during the research for scientific journals and that contemplate the results obtained with the experiments described in the methodology of section 4.

In subsection 5.1, results on the influence of pH variation (0.5 – 2.0), resin mass/solution volume ratio (0.055 – 9,000 g/50 mL) and temperature (25 – 55 °C) are shown. These data were used to investigate which of three adsorption isotherm models (Langmuir, Freundlich and Temkin) best describes the adsorption of metals to the functional groups of the resins. The thermodynamic parameters (ΔH^0, ΔG^0 e ΔS^0) for the adsorption vanadium and iron in the four evaluated resins are also calculated.

In subsection 5.2 are the results of the kinetic study carried out from the experiments varying the contact time between resin and solution (30 – 1440 min). The kinetic parameters were calculated for each of the four models (pseudo-first order, pseudo-second order, intraparticle diffusion and Elovich) to obtain the one that best describes the adsorption of both metals. SEM-EDS images and FT-IR spectra are also shown, performed for the resins before and after the experiments that evaluated the influence of the contact time.

Finally, subsection 5.3 shows the results obtained in experiments in continuous system, carried out in ion exchange columns. The breakthrough curves for vanadium and iron at two flow rates (2 and 3 BV/h) are presented, as well as the elution curves for both metals. Lastly, results on the precipitation of the pure vanadium solution, followed by the calcination of the precipitate to obtain V_2O_5 are shown.

5.1 Purification of an iron contaminated vanadium solution through ion exchange resins

Vinco, J. H.; Botelho Junior, A.B.; Duarte, H.A.; Espinosa, D.C.R., Tenório, J.A.S.

Department of Chemical Engineering, Polytechnic School of the University of São Paulo (USP).

Abstract

The present work aimed to study the behavior of four ion exchange resins: Lewatit® MonoPlus TP 209 XL, Lewatit® TP 207, Dowex™ M4195 (chelating resins) and Lewatit® MonoPlus S 200 H (strong cationic exchange resin) in the selective recovery of vanadium from an acid solution containing iron as an impurity. Batch experiments were carried out to evaluate the influence of parameters such as pH (0.50–2.00), resin mass (0.055–9.000 g) and temperature (293–328 K). Ion-adsorption mechanisms of the resins and thermodynamic parameters of adsorption reactions were evaluated. Increasing the pH from 0.50 to 2.00 favored the adsorption of both iron and vanadium by the resins. Chelating resins were more selective for vanadium than S 200 H resin. Vanadium adsorption better adjusted to the Langmuir isotherm for the TP 209 XL, TP 207 and S 200 H resins, while M4195 adjusted better to the Temkin isotherm. The iron adsorption mechanism, however, varied between the Langmuir, Freundlich and Temkin models. The positive values of ΔH^0 expressed the endothermic nature of the vanadium adsorption process for the three chelating resins and for iron in all of them. Furthermore, negative ΔG^0 values revealed a spontaneous character of the adsorption of both metals to all of the resins. In terms of mass of adsorbed ions, chelating resins showed good selectivity for vanadium compared to iron and these are, therefore, promising to obtain pure vanadium solutions in greater scale operations.

Keywords: Vanadium recovery; adsorption; chelating resins; cation exchange resins.

5.1.1 Introduction

Vanadium is a strategic metal, included in 2017 in the list of metals considered critical by the European Union [5,466], widely applied in the production of high-performance metal alloys, such as high-strength steel and alloys for the aerospace industry. About 85% of all of the vanadium production is consumed by steel industries as railroads, with an emphasis on the production of high strength low alloy (HSLA) steels [467]. One of the most recent and remarkable uses of vanadium is in large-scale energy storage systems, mainly for renewable sources [196]. The renewable sources global demand tend to increase up to 60% until 2040 [55], and given their intrinsically fluctuating nature production, robust storage systems are demanded [56]. Vanadium redox flow batteries represent one of the most promising technologies for this purpose [38]. These batteries have vanadium in four oxidation states: the pair V^{2+}/V^{3+} as the anode and the pair VO^{2+}/VO_2^{+} as the cathode, which are solubilized in the electrolytes responsible for effectively storing the energy of the system [107].

Highly pure vanadium (predominantly 99.8%) is required to prepare the electrolyte for these batteries [31]. In the sources of vanadium, such as: (i) ores, (ii) concentrates, (iii) metallurgical slag and (iv) oil residues [16], several impurities are normally associated. Iron deposits represent one of the main sources of vanadium [41] and, usually, liquors derived of leaching processes contain iron as a contaminant. This occurs because these metals, when in their oxidation state +3, have nearly identical ionic rays and behave chemically similarly [40].

Acid leaching of vanadium-bearing-stone-coal is an efficient process to solubilize vanadium [468–470]. For titanomagnetite ores – a chemical series of cubic minerals with an inverse spinels structure, where pure magnetite (Fe_3O_4) and ulvöspinel (Fe_2TiO_4) form the endmembers [471] – acid leaching has been reported using hydrofluoric [472], sulfuric [473,474], nitric [475] and hydrochloric acids [476]. In these experiments, the required hydrogenionic potential in these experiments might cause the leaching of iron as well.

Lee et al. [477] recently reviewed the literature and demonstrated the potential and importance of recovering vanadium from slag, aiming a more sustainable production that is increasingly linked to the circular economy. Through the last years, obtaining vanadium from secondary sources is a recurrent research interest. These secondary sources include vanadium-bearing steel slag [478], shale [479], slag [480] and spent catalyst [481]. These sources are usually leached in an acidic medium and

generate liquors containing many impurities. In such perspective, it is necessary a purification technique in order not only to concentrate the metal of interest in the leaching liquors, but also to obtain it with the necessary purity [196].

Ion exchange resins are widely used in industrial processing [50], mainly due to the large number of different types of commercially available resins, which are applied in the recovery of specific elements [482]. Furthermore, the technique also offers advantages, such as low energy consumption, fast reaction, simplicity in operation and low operating cost [51]. Chelating resins are among the ion exchange resins which, in terms of extraction, are more suitable because they also interact electrostatically with the metal, which makes them selective [51]. The selectivity of chelating resins depends on their functional groups – which contain one or more donor groups, such as nitrogen, sulfur, oxygen and phosphorus atoms – forming coordinated bonds with metallic ions [483,484].

Although ion exchange resins have been applied to recover vanadium [485–488], the knowledge of selective recovery of cationic species of vanadium from an acid medium containing Fe^{2+} is still scarce. Our paper brings new high quality experimental results using four ion exchange resins, opening a new path for industrial purposes. To accomplish that, the selectivity of these to adsorb vanadium in relation to iron was studied through the evaluation of: (i) the effect of pH; (ii) the adsorption isotherm models (Langmuir, Freundlich and Temkin) and (iii) the effect of temperature by a thermodynamic study.

5.1.2 Materials and methods

5.1.2.1 Ion exchange resins

The resins used in this study were: (i) Lewatit® MonoPlus TP 209 XL; (ii) Lewatit® TP 207; (iii) Dowex™ M4195 and; (iv) Lewatit® MonoPlus S 200 H. Details of each of them are exposed in Table 4 and the respective chemical structures of each functional group in Figure 8.

Table 4. Summary of the resins chosen for adsorption experiments of vanadium and iron.

Resin name	Class	Functional group	Matrix	Water content (delivery form) (%)	Structure	Selectivity order	Reference
MonoPlus TP 209 XL	Chelating/cation exchange	Iminodiacetic acid (IDA)	Styrene/ DVB	≈ 50	Macroporous	$Fe^{3+} > Cu^{2+} > VO^{2+} > UO^{2+} > Pb^{2+} > Ni^{2+} > Zn^{2+} > Cd^{2+} > Fe^{2+} > Mn^{2+} > Ca^{2+} > Mg^{2+} >> Na$	[489]
TP 207	Chelating/cation exchange	Iminodiacetic acid (IDA)	Styrene	48 – 56	Macroporous	$Cu > VO^{2+} > UO^{2+} > Pb > Ni > Zn > Cd > Fe^{2+} > Be > Mn > Ca > Mg > Sr > Ba >>> Na$	[490]
M4195	Chelating	Bis-Picolylamine	Styrene/ DVB	40 – 60	Macroporous	$Cu^{2+} >> Ni^{2+} > Fe^{3+} > Zn^{2+} > Co^{2+} > Cd^{2+} > Fe^{2+}$	[491]
MonoPlus S 200 H	Strong acidic cation exchange	Sulfonic acid	Styrene/ DVB	45 – 50	Gel	-	[492]

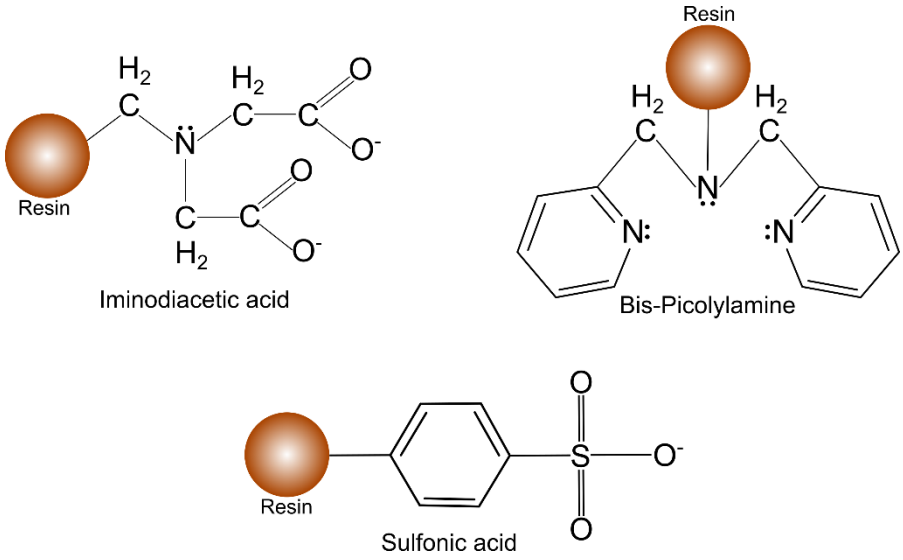

Figure 8. Functional groups (structural representation) of the resins used in this paper: iminodiacetic acid (TP 209 XL and TP 207 resins), bis-picolylamine (M4195 resin) and sulfonic acid (S 200 H resin).

Before experiments, the resins were washed with a hydrochloric acid solution (4 mol.L $^{-1}$ HCl) followed by deionized water thrice (lastly by ultrapure water). Each washing steps was performed for 4 hours in 250 mL Erlenmeyer flasks in an orbital shaker (200 rpm) at 298 K. After such process, flasks (containing water and resins) were submitted to an ultrasonic bath (35 W) for 10 minutes, to contribute with the removal of any physical impurity derived from their production. Finally, the resins were filtrated and dried at 333 K for 24 hours.

5.1.2.2 Synthetic solution

The synthetic solution was prepared by dissolving 10 g of commercial vanadium pentoxide (V_2O_5, 99.5% of purity) in 400 mL of aqua regia in agitation. After 24 hours, 1 g of iron sulfate (III) ($Fe_2(SO_4)_3$) was added to the solution, that was subsequently filtered and then filled with ultra-pure water to a final volume of 2 L.

A Pourbaix diagram was elaborated using the software FactSage (8.0 version) – applying the average final concentration of the solution (2.8 g.L^{-1} of vanadium and 0.08 g.L^{-1} of iron) – for vanadium (Figure 9a) and iron (Figure 9b), both in the presence of chlorine.

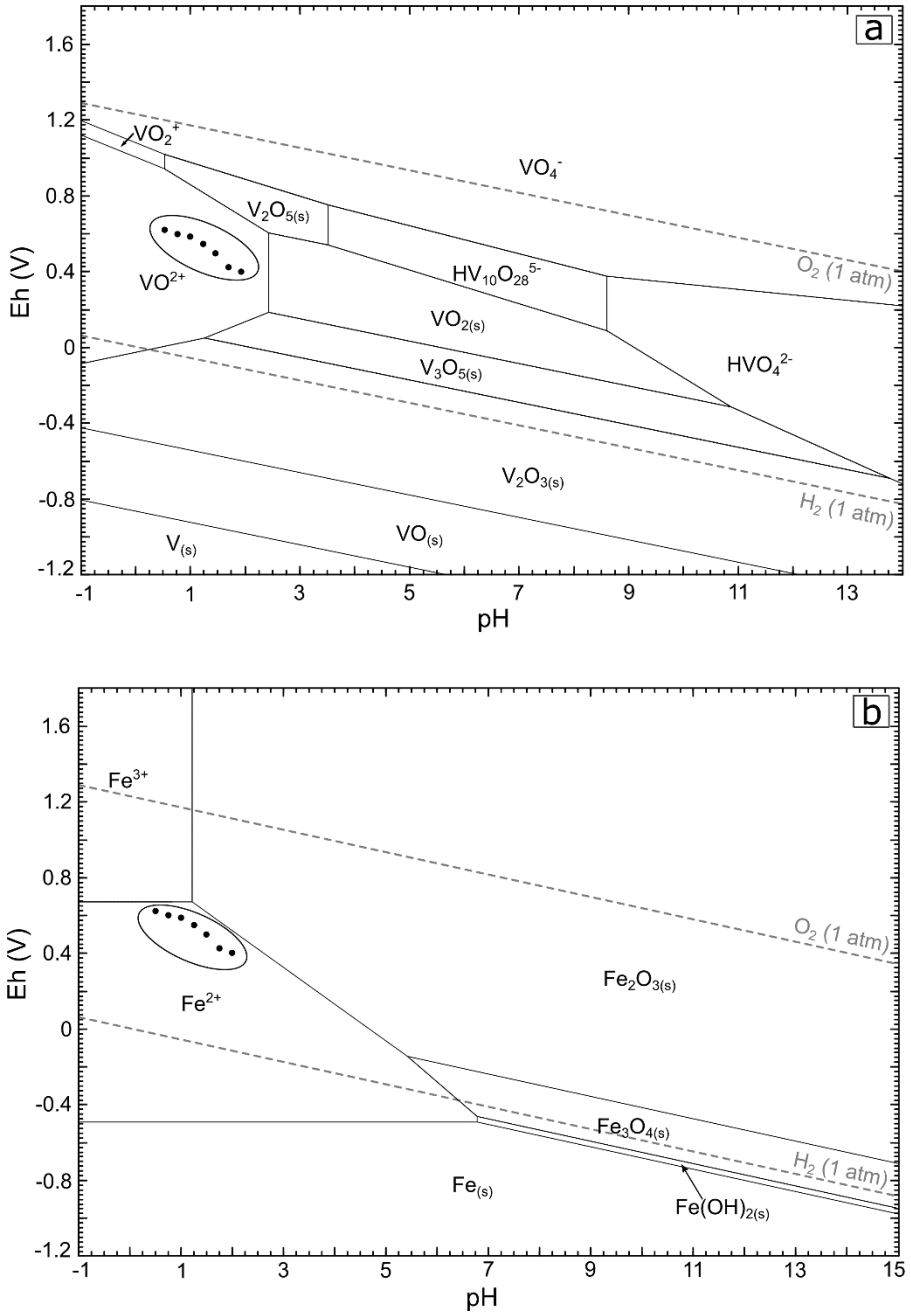

Figure 9. Pourbaix diagrams of V (a) and Fe (b), showing the predominance of species as a function of Eh x pH. Experimental points are represented in the stability field of Fe (II) and V (IV) involved in by an ellipse.

Considering the selectivity order of the chelating resins, which is directly related to its functional groups and its high extracting capacity of a given ion [482] (Table 4), Fe (III) is primarily recovered by chelating resins when compared to Fe (II). Botelho Junior et al. [493] showed that chelating resins functioned by iminodiacetate and bis-picolylamine groups preferably recover other metals than Fe (II) in multielement

solutions. Besides, V (IV) has a higher affinity to the IDA functional group in comparison to Fe (II). Therefore, pH and redox potential (Eh) were corrected to a stability region of both V (IV) and Fe (II) (see Figure 9), by adding, respectively, a solution of sodium hydroxide (NaOH) (10 mol.L^{-1}) and sodium dithionite ($Na_2S_2O_4$) (1 mol.L^{-1}).

5.1.2.3 Ion exchange experiments

Ion exchange experiments were performed in batch using Erlenmeyer flasks in an orbital shaker (200 rpm) at 298 K for 120 minutes. The ratio of 1 g of wet resin for 50 mL of solution was applied in all experiments, except for the mass influence of resins. Chemical analyses of the solutions (before and after every experiment) were performed through Atomic Absorption Spectrometry (AAS, SHIMADZU AA-7000). The parameters pH, mass influence of resins and temperature were evaluated as it follows:

a) The adsorption behavior was explored in a pH range of 0.50-2.00 with steps of 0.25. Eh values varied between 0.6 and 0.4 V. The superior range (2.00) was chosen to avoid iron precipitation [494–497] as well as vanadium. Such effect is verified in Figure 9, which shows that VO^{2+} and Fe^{2+} (in the range of the studied redox potential) precipitates if pH is increased to values beyond 2.00. Vanadium and iron initial concentrations were, respectively, 2.40±0.12 g.L^{-1} and 0.03±0.0004 g.L^{-1}.

b) Experiments varying the ratio between mass of resin (0.055 g to 9.000 g) and volume of solution (50 mL) were performed to understand the adsorption mechanism of metal ions in the resin's active sites. The results were used to study three adsorption models: Langmuir, Freundlich and Temkin. Equilibrium isotherms provide information about the amount of material that is adsorbed per unit mass of adsorbent, as a function of the equilibrium concentration of adsorbate [498].

The isotherm model of Langmuir (Eq. (17)) presumes that: (i) for each active site in the resin there is adsorption of a single ion, creating a saturated monolayer; (ii) there is no interaction between the adsorbed ions; and (iii) there is no migration of these in the superficial plane [499–501].

Freundlich isotherm (Eq. (18)), on the other hand, is based on an adsorption occurring in multilayers that interact with themselves. Furthermore, the amount of adsorbed ions is related to their concentration in solution, and energy decreases exponentially at the end of the adsorption process [499,501,502].

Temkin isotherm (Eq. (19)) opposes Freundlich's model by assuming that adsorption heat of the molecules in the adsorbent surface layer decreases linearly instead of logarithmically, and that bonding energies have a uniform distribution [502,503].

$$q_e = q_m \frac{b_L\, C_e}{1 + b_L\, C_e} \tag{17}$$

$$q_e = K_F C_e^{\frac{1}{n}} \tag{18}$$

$$q_e = B_T \ln A_T C_e \tag{19}$$

In which: $q_e\ (mg.g^{-1})$ is the amount of solute adsorbed in the equilibrium; $b_L\ (L.mg^{-1})$ is the Langmuir constant related to sorption energy and equilibrium constant; $q_m\ (mg.g^{-1})$ is the maximum saturated monolayer adsorption capacity of the adsorbent; $C_e\ (mg.L^{-1})$ is the final concentration of the metal ion in the liquid phase; $K_f\ ((mg.g^{-1})(mg.L^{-1})^{\frac{1}{n}})$ is the Freundlich constant related to the adsorption capacity; n (dimensionless) is the constant related to the adsorption intensity or the degree of adsorption favorability; $B_T = \frac{R\,T}{b_T}$ is related to the heat of adsorption, in which b_T $(J.mol^{-1})$ is the Temkin isotherm constant, R is the universal constant for gases (8.314 $J.mol^{-1}.K^{-1}$); T is the absolute temperature and $A_T\ (L.mg^{-1})$ is the binding equilibrium constant of the Temkin isotherm.

The adjustments of the data to the Langmuir, Freundlich and Temkin isotherm models and the obtaining of the parameters of each one occurred through linearization of the Eqs. (17), (18) and (19), respectively represented by Eqs. (20), (21) and (22).

$$\frac{1}{q_e} = \left(\frac{1}{b_L q_m}\right).\frac{1}{C_e} + \frac{1}{q_m} \tag{20}$$

$$\ln q_e = \ln K_f + \frac{1}{n} \ln C_e \tag{21}$$

$$q_e = B_T \ln A_T + B_T \ln C_e \tag{22}$$

c) For the thermodynamic analysis, the effect of temperature (between 298 and 328 K) was evaluated, aiming to understand the spontaneity of the adsorption process [504]. Vanadium and iron initial concentrations were, respectively, 2.53±0.38 $g.L^{-1}$ and 0.04±0.0018 $g.L^{-1}$. Through the Van't Hoff's equation (Eq. (23)) it is possible to calculate thermodynamic functions like enthalpy (ΔH), entropy (ΔS) and Gibbs free energy (ΔG) during the process of metal ions adsorption [499,505–507].

$$\frac{d(\ln K_{eq})}{dT} = \frac{\Delta H}{RT^2} \quad (23)$$

In which:

$$K_{eq} = \text{equilibrium constant}$$

$$K_{eq} = \frac{q_e}{C_e}$$

The change in Gibbs free energy can be expressed as a function of temperature and the equilibrium constant (Eq. (24)) and yet, be obtained in terms of enthalpy, entropy and temperature (Eq. (25)).

$$\Delta G^0 = -RT\ln K_{eq} \quad (24)$$

$$\Delta G^0 = \Delta H^0 - T\Delta S^0 \quad (25)$$

In Eq. (24), the calculated values of K_{eq} would be expressed in $L.g^{-1}$. However, this would represent an error in the calculation of the Gibbs free energy, since it has the unit $J.mol^{-1}$. This is a problem often neglected in adsorption studies and a correction is needed for the calculation of ΔG^0 [508]. As discussed by Milonjić [509], multiplying it by 10^3 makes K_{eq} (given in $L.g^{-1}$) dimensionless.

Combining the Eqs. (24) and (25), Eq (26) is obtained. Through Eq. (26), the aforementioned thermodynamic functions are obtained from the slope of the $\ln K_{eq}$ versus T^{-1} plot and its intercept on the ordinate axis.

$$\ln K_{eq} = -\frac{\Delta G^0}{RT} = \frac{\Delta S^0}{R} - \frac{\Delta H^0}{RT} \quad (26)$$

5.1.3 Results and discussion

5.1.3.1 Effect of pH

Figure 10 shows the results of the effect of pH on the adsorption of vanadium and iron. TP209XL resin exhibits greater metal adsorption as the pH increases (Figure 10a), being visually possible to verify an increase in the intensity of the coloring, which is related to metallic ions that gradually occupies active sites of the resins, providing blue color. The observed color is due to the presence of adsorbed VO^{2+} ions, considering that, in solution, vanadium in its +4 oxidation state is blue in color [62].

For all of the studied resins, the increase of the pH was associated with a greater adsorption of ions in solution (Figures 10b and 10c). The functional groups of the resins in acidic medium are protonated. Thus, at lower pH values there is a higher concentration of H^+ ions in solution which, in addition to acting on the functional groups of the resins, compete with the metal ions for the exchangeable sites [510].

As the solution's pH increases, there is a process of deprotonation of the active sites, which is associated with an increase in the density of negative charges on the surface of the resins and an electrostatic attraction between the positively charged ions and the surface [510,511]. Consequently, the greater availability of binding sites favored an increase in the adsorption of vanadium and iron ions in solution, easily noticed when the exchange capacities (q_e) of pH values equal to 0.50 and 2.00 are compared.

As shown in Figures 10b and 10c, all studied resins showed similar behavior in terms of extracting a greater amount of vanadium in relation to the amount of iron. At a pH equal to 2.00, the greatest extraction of both elements occurs. With the exception of the last pH value - in which the M4195 resin doubled the amount of vanadium ions adsorbed in relation to the slightly previous pH value and exceeded the extraction of the others (from 14 to 38 $mg.g^{-1}$) – the resins TP 207 and TP 209XL demonstrated a better and stable performance in the adsorption of vanadium over the entire analyzed range (Table 5), extracting about 25% of all vanadium in solution with a pH value of 1.50.

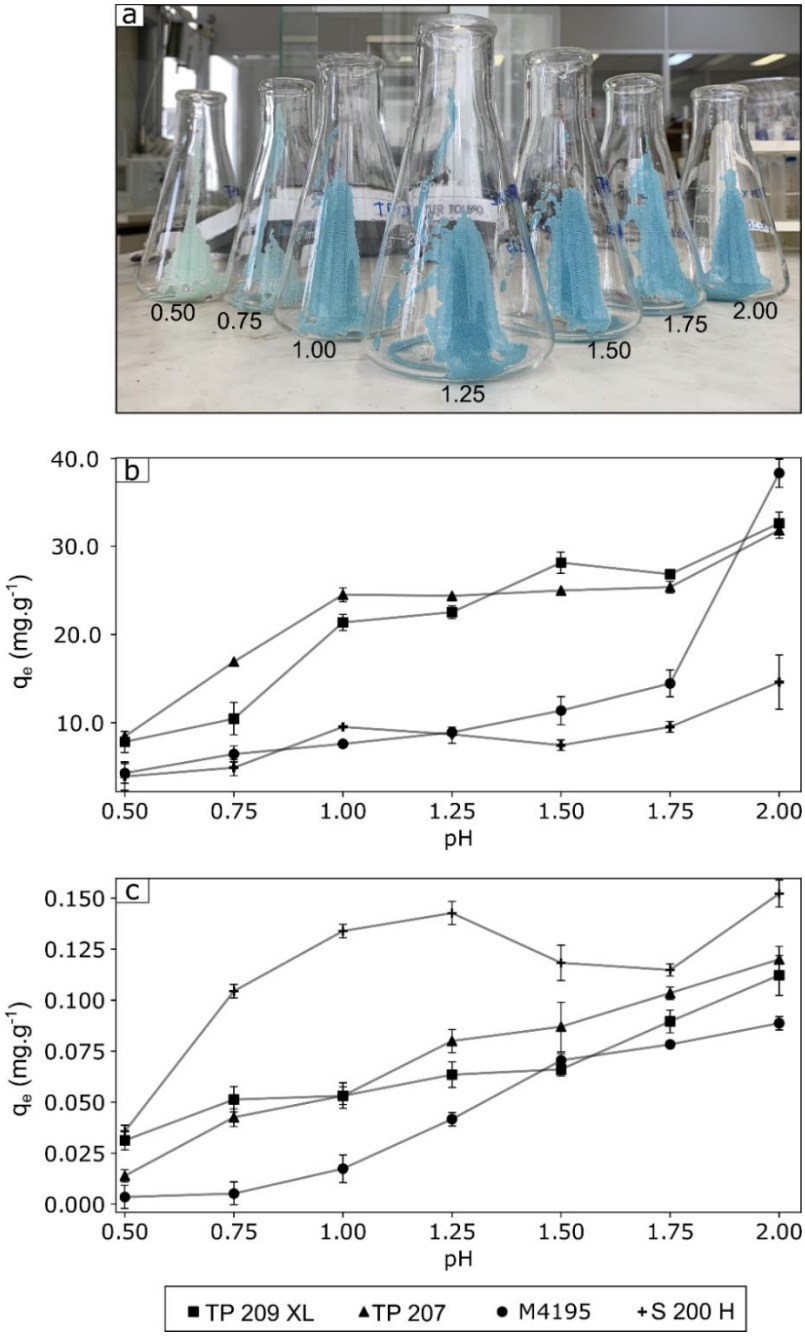

Figure 10. Effect of pH on the adsorption of vanadium and iron ions by TP 209 XL, TP 207, M4195 and S 200 H resins. In (a), visual result of the experiment performed with TP209XL resin. In (b) and (c), respectively, the mass of vanadium and iron ions adsorbed per gram of dry resin (q_e) as a function of the increase of pH. Time: 2 hours, dry resin mass: 1g, solution volume: 50mL, initial concentration: 2.40±0.12 g.L^{-1} of V and 0.030±0.0004 g.L^{-1} of Fe.

However, for the (1.00 – 1.75) pH range, the recovery of vanadium by TP 207 is practically constant (from 24.5 to 25.4 mg of vanadium recovered per gram of resin), while iron fold in the same range (from 0.05 to 0.10 mg.g^{-1}). The S 200 H resin, in turn,

proved to be the least efficient for vanadium adsorption, with a maximum extraction of the metal close to 11% at a pH equal to 2.00. At the same time, it surpassed the other resins in the recovery of iron over the entire pH range analyzed, obtaining a maximum extraction at pH 2.00, with 10.0% adsorption of all of the available metal.

Thus, chelating resins (TP 209 XL, TP 207 and M4195) were more selective in the separation of vanadium and reached higher percentage values in the recovery of this metal in when compared to iron, which was poorly adsorbed.

It is important to emphasize that vanadium extraction (Table 5) was obtained with batch tests containing a resin mass/solution volume ratio equal to 1g/50mL and, furthermore, that initial concentration of vanadium in the medium is high (≈ 3 $g.L^{-1}$). Other studies in the literature that obtained higher percentages of vanadium extraction with ion exchange resins in batch experiments worked with higher ratios (10g/150mL), which favors the adsorption due to a higher availability of active sites [44,46].

Table 5. Percentage of vanadium and iron ions adsorbed by resins as a function of the pH. (Time: 2 hours, dry resin mass: 1g, solution volume: 50mL, initial concentration: 2.40±0.12 $g.L^{-1}$ of V and 0.030±0.0004 $g.L^{-1}$ of Fe).

pH	Percentage (%) of adsorbed vanadium and iron ions							
	TP 209 XL		TP 207		M4195		S 200 H	
	V	Fe	V	Fe	V	Fe	V	Fe
0.50	6.5	2.1	7.0	0.9	3.5	0.2	3.2	2.3
0.75	8.7	3.4	14.1	2.9	5.4	0.4	4.1	7.0
1.00	17.0	3.6	19.5	3.6	6.1	1.2	7.6	9.0
1.25	19.4	4.1	21.0	5.2	7.7	2.7	7.5	9.2
1.50	23.7	4.3	21.1	5.6	9.6	4.6	6.3	7.6
1.75	24.4	5.9	23.0	6.8	13.1	5.1	8.7	7.5
2.00	25.3	7.4	24.8	7.9	29.8	5.8	11.4	10.0

Tsuboi et al. [512] studied the recovery of vanadium and gallium from a coal fly ash leaching liquor using an IDA functional group chelating resin containing, in addition to these, ferric, ferrous and aluminum ions. Batch tests were carried out to study the effect of the pH, and results showed that, with the exception of the ferrous ion, the increase in pH was also associated with a greater extraction of the other metal ions, with the greatest recovery of vanadium obtained at pH equal to 2.5, approximately 4 $mg.g^{-1}$. In addition, the authors stated that a reduction of the ferric ion to the ferrous

ion prevents the adsorption of iron by this functional group [512], given the selectivity order of chelating resins with the IDA functional group (Table 4).

Soldi et al. [486] reported similar results studying the recovery of vanadium by Chelex 100 chelating resin (IDA functional group). Their data showed an increasing recovery of vanadium from pH 0.5 to pH values close to 4, which they attributed to the complete deprotonation of the functional groups in the resin from the last pH value.

Fan et al. [513] selectively separated vanadium from a solution containing chromium using an anion exchange resin, which functional group was $N(CH_3)_2$. The data depicted that a decrease in pH from 6.5 to 2.5 increased the extraction of vanadium from about 23% to 33% (as the maximum recovery). Extraction, however, lowered abruptly from an additional decrease of pH from 2.5. According to the authors, the anionic species of adsorbed vanadium does not occur at lower pH values, since cationic species predominate in these, as shown in Figure 9.

Other studies aiming to recover vanadium through ion exchange resins are documented in the literature (Table 6). Most of these are focused in the recovering of anionic species of vanadium using, predominantly, anion exchange resins (chelating or not) since cationic species would not be adsorbed by these resins. However, as presented in this work, cationic species of vanadium (VO^{2+}) in a medium with Fe^{2+} are also selectively adsorbed, mainly due to the functional groups of the chelating resins. Therefore, chelation is the most plausible mechanism to explain the sorption of VO^{2+} by the resins TP 209 XL, TP 207 e M4195. Meanwhile, sorption probably occurs through ion exchange in the S 200 H resin, since it has demonstrated no selectivity among the different cations in the solution. The interaction among the ions and functional groups is proposed in Figure 11: for the iminodiacetic acid groups, VO^{2+} and Fe^{2+} might create a bond with oxygen of the deprotonated hydroxyl and electrostatically interact with nitrogen (from the donator group); for the bis-picolylamine functional group, chelation could occur with the interactions of these cations with the three nitrogen atoms present in their structure; and, lastly, for the sulfonic acid functionalized resin, it is proposed that two atoms of oxygen (from the deprotonated hydroxyl) are necessary to bound with either VO^{2+} or Fe^{2+} requiring, therefore, the interaction of two functional groups for each adsorbed ion.

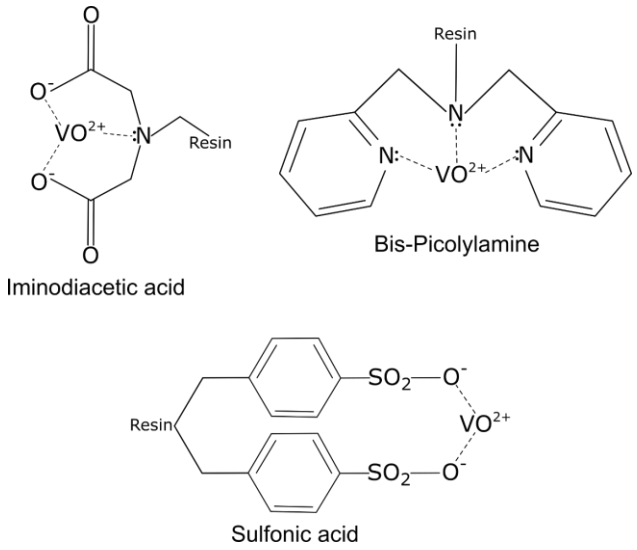

Figure 11. Proposed interaction among the ions and functional groups for the adsorption of VO^{2+} species by the resins' functional groups. Fe^{2+} would interact similarly with the resins, since it is bivalent too.

Table 6. Previous studies on recovery distinct vanadium species from contaminated solutions with ion exchange resins.

Resin	Class	Functional group	Recovered vanadium species	Main contaminating elements	pH	Temperature (K)	q_m	Reference
ZGA414	weak base	$–N(CH_3)_2.H_2O$	$H_2V_{10}O_{28}^{4–}$	Fe, Al, Mg	2.5	298	150 $\mathrm{mg\,V.mL^{-1}}$ wet resin	[42]
Amberlite® IRA-400	strong anion exchange	$–N^+R_3$	$HVO_4^{2–}$, $VO_4^{3–}$ and $V_2O_7^{4–}$	Al, Si, P, S, As, Ca	13.3	293	9.8 $\mathrm{mg\,V.g^{-1}}$	[44]
Amberlite® IRA-400	strong anion exchange	$–N^+R_3$	$HVO_4^{2–}$ (predominant)	Ca, Mg, Al, Si, S	11.5	293	27 $\mathrm{mg\,V.g^{-1}}$	[514]
D201	strong base	$N–(CH_3)_2)C_2H_4OH$	$H_2VO_4^-$	Ca, Al, Fe, Mg, Sc	1.8	–	–	[48]
T A–62(MP)	strong anion exchange	$–N^+R_3$	$HV_{10}O_{28}^{5–}$ (predominant)	–	6 – 7	303	36.9 $\mathrm{mg\,V.g^{-1}}$	[45]
OECH–VP	anion exchange	amine groups	VO_3^-	Cr	6.6	293	203.6 $\mathrm{mg\,V.g^{-1}}$	[43]
Dowex® 1X2	strong anion exchange	trimethylbenzyl ammonium	VO_3^-	K	8	303	–	[47]

5.1.3.2 Adsorption isotherms

The parameters obtained from the linearized models of Langmuir isotherms (Eq. (20) – $1/q_e$vs $1/C_e$), Freundlich (Eq. (21) – $\ln q_e$ vs $\ln C_e$) and Temkin (Eq. (22) – q_e vs $\ln C_e$), were used to calculate their respective graphic solutions and plotted together with the experimental data (q_e vs C_e). Table 7 contains the calculated values of each parameter for both iron and vanadium.

The given parameters in Table 7 showed that vanadium adsorption is better adjusted by the Langmuir isotherm model for resins TP 209 XL (Figure 12a), TP 207 (Figure 12c) and S 200 H (Figure 12g), considering the greatest determination coefficients (R^2) were obtained by linearizing this model. It indicates that vanadium adsorption in these resins forms a saturated monolayer, with no interaction between the adsorbed ions. On the other hand, the model that fits the adsorption of vanadium by the M4195 resin is the Temkin isotherm (Figure 12e), meaning that heat adsorption of the molecules in the surface layer of the resin decreases linearly until the end of the process. The positive parameter B_T, related to the ion adsorption heat in the resin, indicates that, under the conditions of the test, this process is endothermic [515,516].

Adsorption of iron by the TP 209 XL resin, as it happened for vanadium, is better explained by the Langmuir isotherm model (Figure 12b), indicating the formation of a monolayer. The experimental data of iron adsorption by TP 207 and M4195 resins adjusted to the Freundlich model (Figures 12d and 12f), suggesting that ions are adsorbed in multilayers and interact with each other. In addition, the value of n^{-1} is between 0 and 1, reaffirming the favorability of the adsorption process [517]. Iron adsorption by the M4195 resin was better adjusted by the Langmuir model (when comparing R^2 values), however, the parameters predicted by this model are negative. Palanivell et al. [518] and Kiurski et al. [519] justified that such behavior occurs when the adsorption of the metal in the resin does not follow the approach proposed by the model. Therefore, the Freundlich model is more suitable to explain iron adsorption for this resin. Iron adsorption by S 200 H resin is best explained by the Temkin isotherm model (Figure 12h). Under the experimental conditions, the adsorption is endothermic, given the positive parameter B_T [515,516].

Figure 12 displays the models adjusted to the experimental points. It is possible to verify that, although the graphic adjustment of the models is satisfactory, it is necessary to consider the value of the coefficient of determination (R^2), as well as the coherence of the parameters calculated in Table 7, for a better interpretation of the adsorption mechanism in each resin.

Table 7. Model parameters of the adsorption isotherms calculated from the linearization of the Langmuir, Freundlich and Temkin models for vanadium and iron of each studied resin.

		Langmuir model			**Freundlich model**			**Temkin model**		
		q_m (i)	b_L (ii)	R^2	K_f (iii)	n	R^2	A_T (iv)	B_T	R^2
TP 209 XL	V	33.29	0.0012	0.993	0.42	1.90	0.953	0.012	7.11	0.970
	Fe	0.55	0.0035	0.976	0.0020	1.03	0.975	0.10	0.0571	0.911
TP 207	V	28.34	0.0016	0.964	0.40	1.87	0.953	0.011	7.723	0.912
	Fe	0.46	0.0075	0.936	0.0038	1.10	0.945	0.13	0.0732	0.842
M4195	V	11.46	0.0020	0.997	0.50	2.63	0.981	0.019	2.508	0.998
	Fe	-2.65	-0.0011	0.994	0.0030	1.01	0.987	0.15	0.0590	0.974
S 200 H	V	12.69	0.0025	0.987	0.34	2.20	0.952	0.023	2.792	0.954
	Fe	1.05	0.14	0.960	0.22	2.57	0.958	1.16	0.242	0.974

(i) q_m $(mg.g^{-1})$, (ii) b_L $(L.mg^{-1})$, (iii) K_f $((mg.g^{-1})(mg.L^{-1})^{\frac{1}{n}})$, (iv) A_T $(L.mg^{-1})$

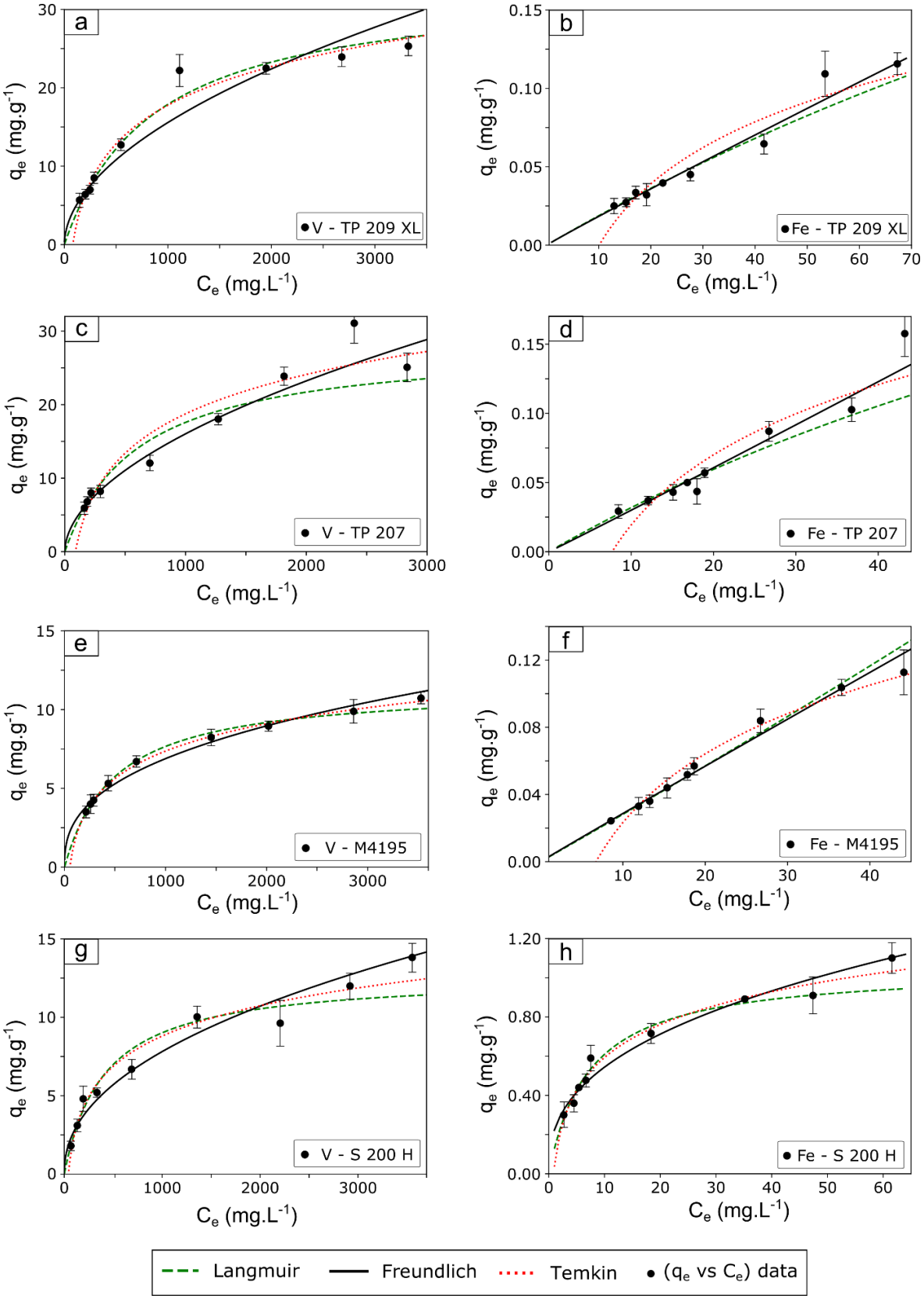

Figure 12. Models of adsorption isotherms for resins TP 209 XL, TP 207, M4195 and S200H. Adsorption isotherms for vanadium are shown in (a), (c), (e) and (g) and; (b), (d), (f) and (h) are the adsorption isotherms for iron. q_e is the mass of vanadium and iron ions adsorbed per gram of dry resin in the equilibrium.

5.1.3.3 Thermodynamic evaluation

The effect of temperature on the amount of vanadium and iron adsorbed by resins was evaluated by varying the temperature from 298 to 328 K, performing experiments with Erlenmeyer flasks containing 1 g of resin and 50 mL of solution for 120 min. The results are shown in Figure 13.

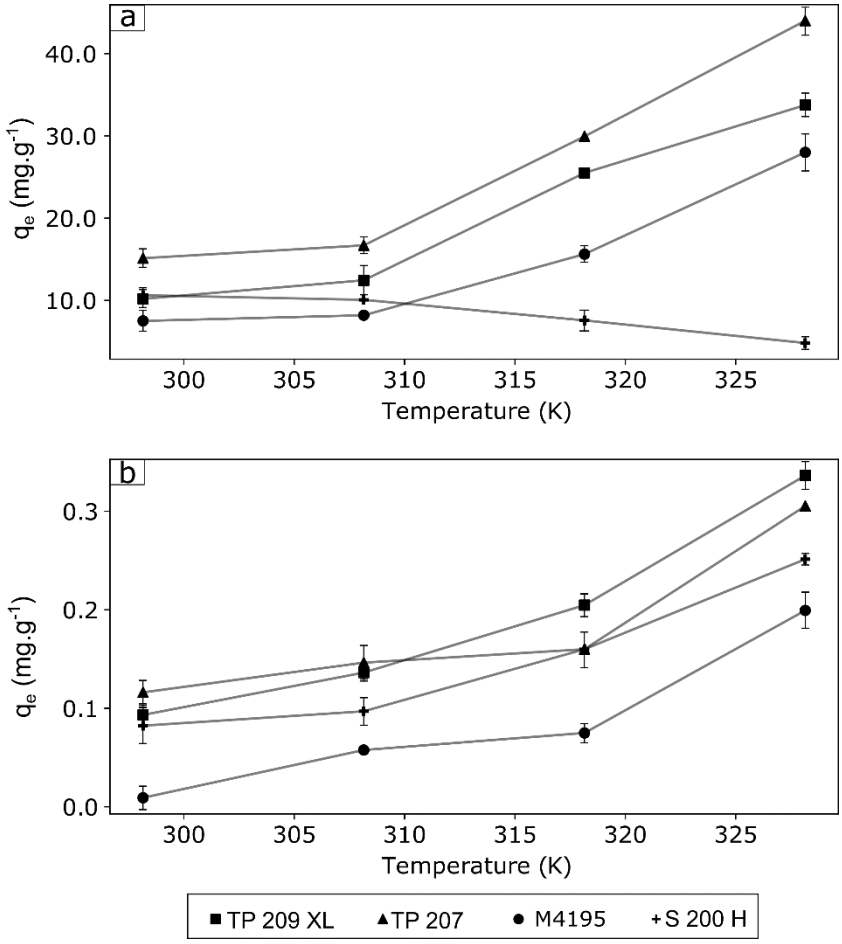

Figure 13. Effect of temperature variation and the amount of vanadium (a) and iron (b) ions adsorbed by resins TP 209 XL, TP 207, M4195 and S 200 H. (Time: 2 hours, dry resin mass: 1g, solution volume: 50mL, initial concentration: 2.53±0.39 g.L^{-1} of V and 0.044±0.0019 g.L^{-1} of Fe). q_e is the mass of vanadium and iron ions adsorbed per gram of dry resin in the equilibrium.

An increase in temperature from 298 to 308 K showed slightly effect on vanadium adsorption (Figure 13a). From 308 K up to 328 K there is an increase in the value of q_e for resins TP 207, TP 209 XL and M4195, which corresponds to 44.0, 33.7 and 28.0 mg of adsorbed vanadium per gram of resin, respectively. These results indicate a favorability of the adsorption process by increasing the temperature. The

adsorption of vanadium by the S 200 H resin, in turn, was not favored by an increase in temperature. At 298 K, 10.6 mg of vanadium per gram of resin was adsorbed, and at 328 K, only 4.8 mg of vanadium per gram of resin was adsorbed. This represents a drop in recovery efficiency from 9.4% to 3.1% (Table 8).

Table 8. Percentage of vanadium and iron ions adsorbed by resins as a function of the temperature variation. (Time: 2 hours, dry resin mass: 1g, solution volume: 50mL, initial concentration: 2.53±0.39 $g.L^{-1}$ of V and 0.044±0.0019 $g.L^{-1}$ of Fe).

Temperature (K)	**Percentage (%) of adsorbed vanadium and iron ions**							
	TP 209 XL		**TP 207**		**M4195**		**S 200 H**	
	V	**Fe**	**V**	**Fe**	**V**	**Fe**	**V**	**Fe**
298	9.0	4.5	13.4	5.6	6.6	0.4	9.4	3.9
308	11.0	6.5	14.7	7.0	7.2	2.7	8.9	4.6
318	20.3	9.2	23.8	7.2	12.4	3.4	6.0	7.2
328	21.9	14.8	28.5	13.4	18.2	8.8	3.1	11.1

Regarding the adsorption of iron, for all of resins, the increase in the temperature was associated with an increase in the amount of adsorbed iron ions (Figure 13b). The resins with greater and lesser iron recovery were, respectively, TP 209 XL (0.34 $mg.g^{-1}$ – 14.8%) and M4195 (0.20 $mg.g^{-1}$ – 8.8%). Although the increase in temperature is also associated with an increase in the extraction of iron, the recovery of vanadium is mostly favored by the chelating resins. This is evidenced comparing the mass of each of the metals adsorbed per gram of resin (q_e) as a function of the increase in temperature (Figure 13).

From the temperature tests, the data displayed in Table 9 were used to plot $\ln K_{eq}$ versus T^{-1} and to calculate the thermodynamic parameters of the vanadium and iron adsorption process by the studied resins.

Table 9. Variables used to graph Van't Hoff linearized equation and coefficients for determining the lines adjusted to the experimental data.

Resin	T (K)	C_e (g. L^{-1})		K_{eq}		R^2	
		V	Fe	V	Fe	V	Fe
TP 209 XL	298	2.06	0.0399	4.94	2.34	0.920	0.987
	308	2.02	0.0393	6.16	3.46		
	318	2.01	0.0407	12.69	5.03		
	328	2.41	0.0387	14.01	8.68		
TP 207	298	1.96	0.0395	7.71	2.94	0.934	0.807
	308	1.93	0.0391	8.64	3.74		
	318	1.92	0.0416	15.59	3.85		
	328	2.20	0.0394	19.97	7.76		
M4195	298	2.11	0.0416	3.55	1.12	0.927	0.827
	308	2.10	0.0409	3.89	1.41		
	318	2.21	0.0433	7.08	1.73		
	328	2.52	0.0415	11.09	4.80		
S 200 H	298	2.05	0.0401	5.18	2.05	0.869	0.950
	308	2.07	0.0401	4.87	2.41		
	318	2.37	0.0416	3.19	3.85		
	328	2.99	0.0404	1.61	6.22		

Based on the results obtained with the linear regressions of the data displayed in Table 9, thermodynamic parameters (Gibbs free energy, entropy and enthalpy) were calculated for the adsorption process of vanadium and iron ions, which are summarized in Table 10. The adsorption thermodynamics is necessary to interpret the spontaneity and behavior of the sorption of metal ions in the active sites of the functional groups of resins [520].

Table 10. Thermodynamic parameters obtained for the adsorption of vanadium and iron ions by TP209XL, TP207, M4195, S200H resins.

Resin	T (K)	ΔG^0 (kJ.mol^{-1})		ΔS^0 (J.K^{-1}.mol^{-1})		ΔH^0 (kJ.mol^{-1})	
		V	Fe	V	Fe	V	Fe
TP 209 XL	298	-3.96	-2.10	118.05	124.06	31.33	34.99
	308	-4.66	-3.18				
	318	-6.72	-4.27				
	328	-7.20	-5.90				
TP 207	298	-5.06	-2.68	109,96	87,64	27.93	23.64
	308	-5.52	-3.38				
	318	-7.26	-3.56				
	328	-8.17	-5.59				
M4195	298	-3.14	-0.278	118,36	123,08	32.48	36.82
	308	-3.48	-0.875				
	318	-5.18	-1.45				
	328	-6.56	-4.28				
S 200 H	298	-4.08	-1.78	-90,91	108,00	-31.59	30.67
	308	-4.06	-2.26				
	318	-3.07	-3.56				
	328	-1.30	-4.98				

ΔG^0 values are negative for both metals through the whole range of temperature (Table 10) for all evaluated resins, suggesting that the adsorption process is spontaneous or has favorable free energy [504,521]. In addition, with the exception of the adsorption of vanadium by the S 200 H resin, the increase in temperature was associated with a decrease in the value of Gibbs free energy, which indicates that the process of sorption of these metals by these resins is more favorable at higher temperatures [520].

ΔH^0 and ΔS^0 values are negative only in the case of adsorption of vanadium by S200H resin, indicating the exothermic nature of the process, confirmed by the increase in ΔG^0 and visualized by the decrease in the amount of adsorbed vanadium (Figure 13a) as the system temperature increased. ΔH^0 and ΔS^0 are positive for the other cases. Positive values of the enthalpy variation infers that an increase in temperature favors adsorption, which indicates an endothermic process. Therefore, an input of energy is necessary for a more advantageous sorption of ions [522]. Positive entropy variations indicate an increase in randomness at the time of adsorption [504]

and are associated with a spontaneous process, which is coherent with the calculates ΔG^0 positive values.

Polowczyk et al. [523] and Huang et al. [524] also obtained a positive variation of enthalpy in the removal of vanadium by ion exchange chelating resins, attributing the result to the endothermic behavior of the process. Cu^{2+} recovery by TP 207 resin was reported by Botelho Junior et al. [493]: an increase in temperature from 298 K to 333 K was associated with an increase in recovery from 62.39 to 68.50% of the metal, indicating the endothermic nature of the process. Gode & Pehlivan [525] showed that, for the same resin, a temperature increase from 298 K to 338 K demonstrated little effect on Cu^{3+} recovery, which was attributed to an exothermic character of the adsorption process.

5.2 Kinetic modeling of the adsorption of vanadium and iron from an acid solution through ion exchange resins

José Helber VINCO; Amilton Barbosa BOTELHO JUNIOR; Heitor Augusto DUARTE; Denise Crocce Romano ESPINOSA; Jorge Alberto Soares TENÓRIO.

Department of Chemical Engineering, Polytechnic School of the University of São Paulo (USP).

Abstract

This study assessed the adsorption process and the reaction kinetics involved in the selective recovery of vanadium from an acid solution containing iron as an impurity. Four commercial resins were studied: Lewatit® MonoPlus TP 209 XL, Lewatit® TP 207, Dowex™ M4195 (chelating resins) and Lewatit® MonoPlus S 200 H (strong cationic exchange resin). To investigate the effect of time on the adsorption process, batch experiments were carried out using the following initial conditions: pH 2.00, at 298.15 K, and a proportion of 1 g of resin to 50 mL of solution. The variation of pH over time was analyzed. Chelating resins released less H^+ ions as the adsorption occurs, resulting in a lower drop of pH when compared to S 200 H resin. Ions adsorption by the resins was also evaluated through FT-IR and SEM-EDS before and after the experiments. Among the evaluated kinetic models (pseudo-first order, pseudo-second order, Elovich, and intraparticle diffusion) the pseudo-second order best fits the experimental data of the adsorption of vanadium and iron by all of the four resins. M4195 resin showed the highest recovery of vanadium and the lowest adsorption of iron. Kinetic data, which are fundamental to industrial processes applications, are provided.

Keywords: Vanadium recovery; adsorption; chelating resins; metal ions; cation exchange resin; batch study.

5.2.1 Introduction

One of the main applications of vanadium is as an additive in steel alloys (e.g, ferrovanadium) which represents a consumption over 80% of the global production [16,467]. Vanadium have been standing out and getting more space for storage batteries on a large scale, especially from renewable sources, which you likely cause a grow on its demand in the coming years [196,526]. Vanadium consumption for electrolyte production is estimated to grow by as much as 44% by the year 2027 as these batteries gain more visibility [527].

Vanadium occurs predominantly in the form of V^{3+} replacing Fe^{3+} or Al^{3+} in several minerals in ore deposits and crude oil. In addition, metallurgical slags has become other important source for obtaining vanadium [196]. Regardless of the origin, impurities will be associated in the vanadium extraction, which reflect in a necessity for methods to purify and obtain products with high purity, especially for application in electrolytes of vanadium redox flow batteries. However, there is a lack in the literature of deep studies on about the influence of impurities in the battery's performance. Therefore, these applications still require a product with purity above 99.8%, greatly increasing its cost [31].

In the literature, there are several works aimed at the purification of solutions containing vanadium and other impurities using techniques such as solvent extraction [528–533], chemical precipitation [534–536] and ion exchange resins [537–541]. A comparison between these methods for recovering vanadium from leach liquors was also critically reviewed in the work by Zhang et al. [542].

In this context, ion exchange resins stand out, especially chelating resins, considering that the ion exchange technique applied to the recovery of strategic metals is among the fundamental technologies for the development and progress of society [543]. Ion exchange was linked to several modern technologies, being widely used in several industrial applications which include advanced separations, such as metal recovery, water treatment and removal of radioactive isotopes [544]. In addition to their extensive industrial use [50], ion exchange resins offer advantages such as low energy cost, simplicity in operation and fast kinetics, reflecting a low operating cost [51].

There are several commercial resins available designed to recover different metals [482]. Cationic, anionic and chelating resins are used in different purification

processes, and chelators in chelating resins have been developed to improve the selectivity of the process. The order of selectivity of these resins depends on their functional groups [51]. An electrostatic interaction between functional group and the adsorbed metal occurs by donor atoms present in their functional groups, such as nitrogen, sulfur, oxygen and phosphorus, which have pairs of unemployed electrons and act forming coordinated links with adsorbed metals [483,484].

The investigation of the adsorption process by kinetic modeling is crucial, owing to the (i) ideal conditions of operation in large-scale batch; (ii) mechanism of sorption between the metal and the resin and; and (iii) control of the reaction rate including mass transportation and chemical reaction processes [545,546]. Febrianto et al. [547] stated that, in projects of an adsorption system, the knowledge of the adsorption rate involved in the recovery of a metal by a certain resin figure among the most important steps, because, from such study, it is known the time of residence of the adsorbate.

Besides, the kinetic modeling is important to evaluate the separation rate between vanadium and contaminants. Therefore, this study is devoted to investigate the adsorption and model adsorption kinetics of iron and vanadium by ion exchange resins. Three chelating resins and one strong cationic resin were tested. The kinetic investigation was performed through the evaluation of four kinetic models (pseudo-first order, pseudo-second order, Elovich and intraparticle diffusion). FT-IR and SEM-EDS analyses were used as chemical characterization of the resins to enhance the interpretation of the process.

5.2.2 Methods

5.2.2.1 Ion exchange resins and synthetic solution

Four ion exchange resins were used: Lewatit® MonoPlus TP 209 XL, Lewatit® TP 207, Dowex™ M4195 and Lewatit® MonoPlus S 200 H. These resins are functionalized by the following functional groups: iminodiacetic acid, iminodiacetic acid, bis-picolylamine and sulfonic acid, respectively. In Figure 14 depicts the structure of each of these groups.

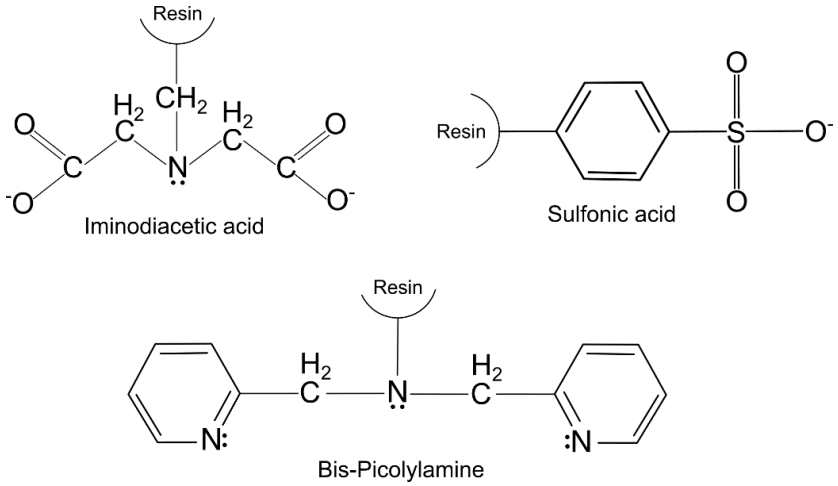

Figure 14. Functional groups of the resins: iminodiacetic acid (TP 209 XL and TP 207 resins), sulfonic acid (S 200 H resin) and bis-picolylamine (M4195 resin).

A pre-treatment step was performed previously to the experiments aiming to eliminate any possible remnant impurity of the resins manufacture and to obtain H^+ exchangeable ions. The pre-treatment consisted in washing the resins with hydrochloric acid solution (4 mol.L^{-1} HCl) interspersed with three-fold deionized water. The washing process was conducted in Erlenmeyer flasks (250 mL) in orbital shaker (200 rpm) under a temperature of 298.15K at intervals of 4 hours at each wash. After the last wash with water, flasks were taken to an ultrasonic bath for 10 minutes. Finally, the resins were separated by filtration and dried at 333.15K for 24 hours.

The synthetic solution was prepared by the dissolution of 10 g of commercial vanadium pentoxide (V_2O_5, 99.5% of purity) in 400 mL of aqua regia under stirring. After 24 hours, the obtained solution was filtered and 0.2 g of metallic iron (Fe) was added to the solution. After homogenization, ultra-pure water was added to a volume of 2 L. Thus, a solution with 2.7 g.L^{-1} of vanadium and 0.1 g.L^{-1} of iron was obtained. Subsequently, based on another study already carried out [39], the pH and the redox potential (Eh) were corrected to obtain V (IV) and Fe (II) by the addition of a sodium hydroxide (NaOH) solution (10 mol.L^{-1}) and sodium dithionite ($Na_2S_2O_4$) (1 mol.L^{-1}), respectively.

The purification of a solution of the same composition using the same resins tested in the present work was investigated by Vinco et al. [39]. In such work, the authors studied the influence of pH, resin mass/solution volume and system

temperature, evaluating the sorption process through adsorption isotherms and the thermodynamic parameters involved.

5.2.2.2 Ionic exchange experiments and kinetic study

The kinetic experiments for iron and vanadium adsorption were evaluated from 30min to 1440min. Tests were carried out Erlenmeyer flasks (250 mL) submitted to 200 rpm stirring in orbital shaker. A ratio of 1g of resin for 50 mL of solution at pH 2.0 was used.

The separation coefficient of V ($\beta_{V/Fe}$) for each evaluated adsorption time was calculated by the Eq. (27) [548,549]

$$\beta_{V/Fe} = \frac{C_{V,r}\, C_{Fe,s}}{C_{Fe,r}\, C_{V,s}} \quad (27)$$

In which: $C_{V,r}$ and $C_{Fe,r}$ are the concentrations of V and Fe in the resin, respectively, and $C_{V,s}$ and $C_{Fe,s}$ are the concentrations of V and Fe in solution, respectively.

Kinetic modeling was performed according to data obtained to investigate the adsorption mechanism, the rates control of mass transport and the chemical reaction process [547]. In the present study, it was evaluated four distinct kinetic models: pseudo-first order, pseudo-second order, Elovich and intraparticle diffusion.

The kinetic models of pseudo-first and pseudo-second order are the most employed in the kinetic metal adsorption study [499,547]. They are widely used in the description of the adsorption rate in liquid-solid type interactions, both being obtained from the integration of Eq. (28) [550].

$$\frac{dq_t}{dt} = k_n(q_e - q_t)^n \quad (28)$$

In which: q_e and q_t are the amount of solute adsorbed per mass of adsorbent $(mg.g^{-1})$ at equilibrium and time t (min), respectively; and k_n is the constant rate of the pseudo-n-th order kinetic model (min^{-1}).

Lagergren [551] showed that the obtained equation from the integration of Eq. (28), when n = 1 under boundary conditions of: t = 0, q_t = 0 e t = t, $q_e = q_t$, naming the model of pseudo-first order (Eq. (29)) [550]. It is assumed that the adsorption

processes that best fit this model have the adsorption driven by the mass concentration gradient [552]. Therefore, this model is more appropriate for the most initial steps in the adsorption process [553], since in more advanced stages the change in the concentration of metal ions in solution, in accordance with the fall in the number of active sites available in the resin, makes the model less applicable [554].

$$\ln(q_e - q_t) = \ln(q_e) - k_1 t \quad (29)$$

In which: k_1 is the equilibrium rate constant of the pseudo-first order equation $(\min^{-1})$.

A linear model (Eq. (29)) might be rearranged to a non-linear form (Eq. (30)).

$$q_t = q_e(1 - e^{-k_1 t}) \quad (30)$$

Ho & McKay [555] integrated Eq. (28) assuming n = 2 and using the same boundary conditions of Lagergren [551], thus obtaining an expression for the pseudo-second order model (Eq. (31)). According to the model, the rate of pseudo-second order reactions is predominantly related to the amount of metal ions that are on the surface of the adsorbent [552]. This model assumes that there is the occurrence of two reactions, being the (i) balance quickly reached by the first, and a second (ii) slower, which can extend for a long period of time, as chemisorption works as the determining step [554,556].

$$q_t = \frac{k_2 {q_e}^2 t}{k_2 q_e t + 1} \quad (31)$$

In which: k_2 is the equilibrium rate constant of the pseudo-second order equation $(\min^{-1})$.

The nonlinear expression of the pseudo-second order model (Eq. (31)) can then be rearranged to obtain a linearized model (Eq. (32)):

$$\frac{t}{q_t} = \frac{1}{k_2 {q_e}^2} + \frac{1}{q_e} t \quad (32)$$

In these two models, however, all stages of the adsorption process, such as diffusion in the film, adsorption and intraparticle diffusion, and thus, through them, the adsorption mechanism cannot be identified [499,557].

The kinetics rate of chemisorption of Elovich (Eq. (33)) distinguishes from previous models to deal with an exponential drop in the adsorption rate over time. [558].

$$\frac{dq_t}{dt} = \alpha\, e^{-\beta q_t} \quad (33)$$

In which: α is the constant of initial sorption rate ($mg.g^{-1}.min^{-1}$) e β is the constant of desorption ($g.mg^{-1}$), related to the extension of surface coverage and activation energy for chemisorption.

Chien & Clayton [559] integrated Eq. (33) using the following boundary conditions: t = 0, q_t = 0 and t = t, q_t = q_t. They assumed αβt >> 1, obtaining the linearized expression for the Elovich model (Eq. (34)).

$$q_t = \frac{1}{\beta}\ln(\alpha\beta) + \frac{1}{\beta}\ln(t) \quad (34)$$

Regarding the mechanism related to the adsorption process of metals in adsorbents, four primordial stages are involved: (i) diffusion of metal ions to the liquid film on the surface of the adsorbent solid material; (ii) diffusion of these metal ions through the superficial liquid film; (iii) adsorption of the ions at the active sites of the adsorbent surface, a process of physical or chemical nature; and (iv) diffusion of ions through the pores of the adsorbent particles [560]. The diffusion rate of intraparticular mass (Eq. (35)) proposed by Weber & Morris [561] predicts that the intraparticle diffusion stage is the limiting step of the adsorption process when the kinetic data is suitable for their model, i.e., when the amount of metal ions adsorbed by adsorbent mass plotted in function of the square root of the contact time results in a straight line.

$$q_t = k_p t^{1/2} + C \quad (35)$$

In which: k_p is the constant of the intraparticle diffusion rate ($g.mg^{-1}min^{-1}$) and C is a constant that reflects the effect of the limit layer, so that the greater its value, the greater is the contribution of surface adsorption in the rate limitation. [560].

5.2.2.3 Chemical analysis

Samples before and after experiments were analyzed by Atomic Absorption Spectrometry equipment (AAS) (SHIMADZU AA-7000). The characterization of the resins before and after experiments were carried out in scanning electron microscopy analyzes (SEM) coupled to an energy dispersive spectroscopy (EDS) (Phenom ProX equipment) and infrared spectroscopy by Fourier transform (FT-IR) (Bruker Tensor 27 spectrometer). For FT-IR analysis, the resins were grounded to make KBr tablets.

5.2.3 Results and discussion

5.2.3.1 Adsorption experiments

The effect of time on vanadium and iron adsorption was studied at pH 2.0, 1 g of resin and 50 mL of solution at 298.15 K. The use of pH 2.0 is in agreement with the study carried out previously, which demonstrated the influence of pH on the recovery of these metals. In this work, it was demonstrated within the range of pH evaluated (0.50 – 2.00) that pH 2.0 favored the adsorption of vanadium ions by the resins under study, providing the highest percentage of recovery. The data percentage of each metal adsorbed by the resins as a function of time are depicted in Table 11. In 60 min, the TP 209 XL resin recovered 6.67% of the solution vanadium. After 90 min, it increased to 25.8%, reaching a maximum in 180 min (31.4%). The resin TP 207 reached 22.5% of vanadium extraction in 30 min of contact and only in 420 min did it reach a maximum recovery value (31.8%). After these maximums, both maintained a behavior close to stability.

The resins TP 209 XL and TP 207 showed a similar vanadium recovery in 1440 min (30.4 and 30.5%, respectively). Iron extraction, however, was 41.5% by TP 209XL - up to 9% higher than TP 207 (32.5%). This was reflected in low vanadium-to-iron separation coefficients, especially after 420 min of contact between the resin and the solution (Table 11). It is also noted that, for the case of TP 207 resin, the best separation between the two metals occurred in the first 30 min, where the $\beta_{V/Fe}$was equal to 9.1 – the highest value obtained among all those calculated.

Although with the same functional group and the same matrix composition, it is possible to notice a difference in the amount of vanadium and iron ions adsorbed by TP 209 XL and TP 207 chelating resins. Zainol & Nicol [562] had also observed similar behavior, which compared five resins functionalized by iminodiacetic acid (Amberlite IRC 748, Lewatit TP 207, Lewatit TP 208, Purolite S 930 and Lewatit TP 207 Monoplus) in the recovery of nickel and cobalt. The authors demonstrated that, despite having the same functional group, the performance of each one was different. Probably it occurs due to oscillations in the synthesis that could result in variations in the matrix crosslinking, density of functional groups and even in the size of each particle.

In the case of M4195 and S 200 H resins, in contrast, the percentage of vanadium ions adsorbed achieved the equilibrium after 60 min of contact. These two

resins were more selective for vanadium than iron in comparison to TP 207 and TP 209 XL, as depicted in Table 11, where there are higher values of $\beta_{V/Fe}$ related to the TP 209 XL and TP 207 resins. The recovery of vanadium by the M4195 resin reached equilibrium with adsorption efficiency up to 45%, while the iron adsorption reached 14%. The adsorption of vanadium and iron by S 200H were 35.5% and 7.2%, respectively.

Table 11. Percentage (%) of V and Fe ions adsorbed by resins and separation coefficient ($\beta_{V/Fe}$) as a function of contact time.

Time	TP 209 XL			TP 207			M4195			S 200 H		
(min)	V	Fe	$\beta_{V/Fe}$	V	Fe	$\beta_{V/Fe}$	V	Fe	$\beta_{V/Fe}$	V	Fe	$\beta_{V/Fe}$
30	3.8	5.2	0.7	22.5	3.1	9.1	35.4	10.3	4.8	34.7	6.8	7.3
60	6.7	10.3	0.6	24.1	5.8	5.2	40.2	15.2	3.8	35.5	7.2	7.1
90	25.8	11.3	2.7	25.6	7.9	4.0	42.5	14.5	4.4	38.0	9.0	6.2
120	30.9	16.2	2.3	28.9	9.9	3.7	42.1	13.8	4.6	36.9	10.8	4.8
180	31.4	24.4	1.4	28.4	12.8	2.7	43.2	13.6	4.8	35.8	11.5	4.3
300	28.5	35.4	0.7	30.4	17.2	2.1	43.3	14.7	4.4	35.9	10.5	4.8
420	30.1	38.3	0.7	31.8	29.3	1.1	45.9	14.5	5.0	35.0	10.5	4.6
540	29.9	39.7	0.6	31.7	31.4	1.0	45.0	14.7	4.7	33.4	11.5	3.9
960	28.3	40.9	0.6	31.1	30.9	1.0	45.5	13.7	5.3	33.7	11.4	3.9
1440	30.4	41.5	0.6	30.5	32.5	0.9	41.7	14.2	4.3	36.9	10.3	5.1

The pH of the solution was monitored over time, which is presented in Figure 15. For all resins studied, it can be seen that there is an initial drop in the pH value, followed by a plateau. This behavior is explained by the H^+ ions initially occupied the functional groups of the resins and released into the solution due to the exchange with vanadium and iron ions. It makes the solution more acidic. Even, the stabilization of the pH after the fall over time is in accordance with the stabilization of metals adsorption.

According to data presented in Figure 15 and Table 11, although their behaviors are associated, the percentage of metals extraction by each resin is not proportional to how much the pH of the medium decreases, that is, how much of H^+ is released into the solution. It can be visualized by the data from the M4195 resin, which demonstrates that, even though the resin that presented the greatest extraction of vanadium from the

solution, it was the one that resulted in the lowest pH drop among the four resins analyzed.

The differences between the pH values among the resins are probably due to their exchange mechanism. For chelating resins (TP 209 XL, TP 207 and M4195), the decrease in pH was less pronounced in relation to the cation exchange resin S 200 H which, after 30min, a pH drop from 2.0 to 0.6 was observed (Figure 15). This phenomenon can be explained by the adsorption of the metallic ions exclusively by ion exchange with the H^+ ions. That is, since it is not a chelating resin, the only way to recover metals in solution is through the ion exchange process, with a greater release of H^+ ions. Among the chelating resins, TP 207 and TP 209 XL had similar pH values over time (pH 1.2) due to the same functional group. For M4195 chelating resin, the pH reached 1.4 as the reaction achieved the equilibrium.

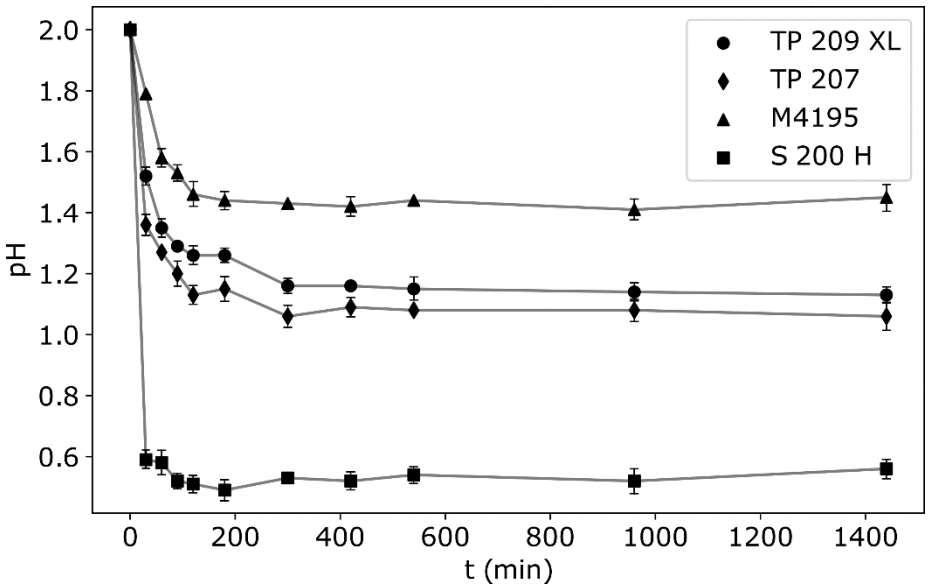

Figure 15. Variation of the pH of the medium as a function of the contact time for each of the resins for the followed experimental conditions: 298.15 K, 1 g of resin per 50 mL of sulution, at a initial pH of 2.

5.2.3.1.1 Kinetic modeling

Kinetic parameters were obtained through the plot of the linearized models of pseudo-first order (Eq. (29) – $\ln(q_e - q_t)$ vs t), pseudo-second order (Eq. (32) – t/q_t vs t), Elovich (Eq. (34) – q_t vs $\ln(t)$) and intraparticle diffusion (Eq. (35) –

q_t vs $t^{1/2}$). The data plotted for each kinetic model is presented in Figure 16 (q_t vs t). Table 12 shows the parameters for each kinetic model for all resins studied. The choice of which kinetic model best explains the adsorption behavior of vanadium and iron ions by resins must be based not only in the value of the determination coefficient obtained with the linearization of the models, but also how the models will be adjusted over time to all experimental points, and whether the calculated kinetic parameters are consistent.

Parameters depicted in Table 12 shows that the adsorption of vanadium by the four resins follows a pseudo-second order kinetics, in view of the higher values of the correlation coefficient (R^2) obtained by the linearization of this model. A best fit in this model indicates that the adsorption of vanadium ions in the functional groups of the resins has their rate controlled by the amount of the metallic ion that is on the surface of the resin and, also, by the valence forces that occur due to the sharing of electrons between the metal ions and the functional groups [563].

It indicates that in the first hours of contact of the solution with the resin there is a fast adsorption of vanadium ions. However, as the active sites become occupied by the metal, the large amount of ions results in a slower adsorption rate. This is also assumed by the model, which reiterates that the balance of the process is quickly achieved by a first ion exchange reaction that occurs in the system. Given the high correlation of the data to the model (all close to 1), the values for the calculated amount of ions adsorbed in the equilibrium per gram of resin (q_e) are in agreement with those verified experimentally. Figures 16a,c,e,g demonstrated that the pseudo-second order model exhibits a stability behavior when the adsorption of vanadium ions had reached equilibrium after 240 min for all resins.

The adsorption kinetics of iron is also explained by the pseudo-second order model for all four resins. For the TP 207 resin, although the correlation coefficients obtained for the pseudo-first and pseudo-second order kinetics are equal (0.992), the analysis in Figure 16d shows that the best fit of the pseudo-second order model to the experimental points when compared to the pseudo-first order. In addition, the system still seems has not reached equilibrium at 1440 min, since the adsorption rate is increasing. Therefore, although the q_e value calculated by the pseudo-first order model (0.60 $mg.g^{-1}$) is apparently the closest to the presented data, it does not represent the

actual amount of iron ions adsorbed in the equilibrium, which probably be better explained by the value obtained by the pseudo-second order model (0.82 $\mathrm{mg.g^{-1}}$). Fatima et al. [564] investigated the adsorption kinetics of some metals when using a cationic exchange resin functionalized by the sulfonic acid group. It was shown that, for Fe (II) recovery, the pseudo-second order model is also the one that best relates to the data obtained, indicating that chemical sorption may be the limiting step of the reaction rate.

Table 12. Kinetic parameters calculated from the pseudo-first order, pseudo-second order, Elovich and intraparticle diffusion models for the vanadium and iron elements of each of the studied resins.

		Pseudo-first order			Pseudo-second order			Elovich			Intraparticle diffusion		
		k_1 (i)	q_e (ii)	R^2	k_2 (i)	q_e (ii)	R^2	α (iii)	β (iv)	R^2	k_p (v)	C	R^2
TP 209 XL	V	3.13×10^{-2}	162.26	0.919	9.10×10^{-4}	54.35	0.997	1.76×10^{0}	0.040	0.965	6.44	-15.67	0.990
	Fe	4.47×10^{-3}	0.95	0.983	9.29×10^{-3}	0.91	0.998	9.41×10^{-3}	3.82	0.951	0.050	-0.21	0.977
TP 207	V	6.86×10^{-3}	20.07	0.982	7.99×10^{-4}	58.95	0.999	1.26×10^{2}	0.16	0.981	1.11	35.05	0.978
	Fe	2.33×10^{-3}	0.60	0.992	3.24×10^{-3}	0.82	0.992	5.44×10^{-3}	6.05	0.966	0.019	-0.0085	0.941
M4195	V	7.89×10^{-3}	20.95	0.916	1.24×10^{-3}	84.42	0.999	2.36×10^{8}	0.29	0.840	1.70	58.19	0.872
	Fe	2.29×10^{-3}	0.039	0.747	4.85×10^{-1}	0.27	0.999	9.02×10^{3}	73.37	0.768	0.0017	0.23	0.759
S 200 H	V	1.11×10^{-2}	9.19	0.888	3.21×10^{-3}	67.57	0.999	2.68×10^{4}	0.19	0.823	1.29	55.35	0.781
	Fe	1.58×10^{-2}	0.19	0.954	2.12×10^{-1}	0.21	0.993	7.63×10^{-3}	13.54	0.950	0.012	0.050	0.928

(i) k_1, k_2 (min^{-1}), (ii) q_e $(\mathrm{mg.g}^{-1})$, (iii) α $(\mathrm{mg.g}^{-1}.\mathrm{min}^{-1})$, (iv) β $(\mathrm{g.mg}^{-1})$, (v) k_p $(\mathrm{g.mg}^{-1}\mathrm{min}^{-1})$

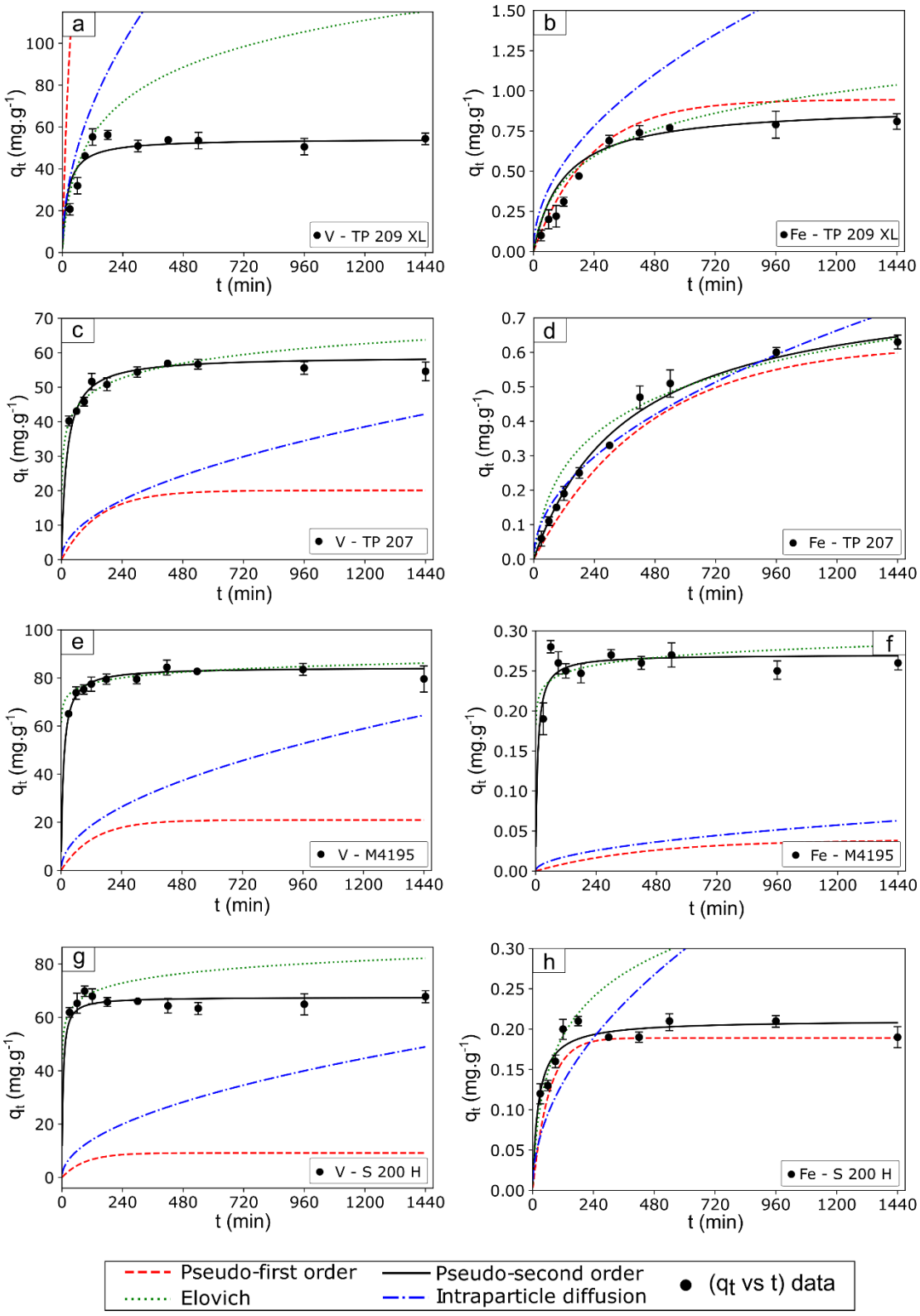

Figure 16. Kinetic models obtained for TP 209 XL, TP 207, M4195 and S 200 H resins. In (a), (c), (e) and (g) the kinetic models for vanadium and in (b), (d), (f) and (h) are the kinetic models for iron.

5.2.3.2 Characterization of resins in the adsorption

In order to understand the chemical bond connection that occurs between the metal ions and the resins, FT-IR (Figure 17) and SEM-EDS (Figure 18) analysis were performed before and after the adsorption experiments.

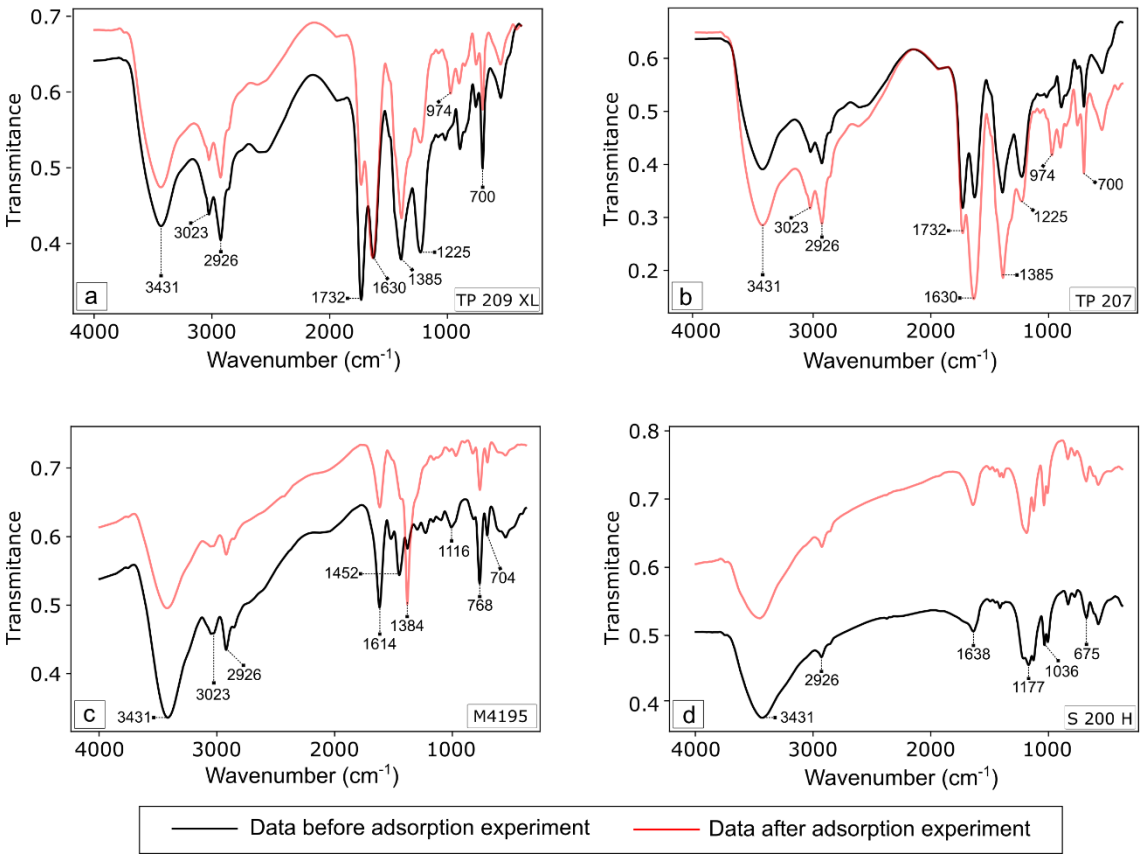

Figure 17. FT-IR spectrum before and after the adsorption experiments for the (a) TP 209 XL, (b) TP 207, (c) M4195 and (d) S 200 H resins.

FT-IR spectrum shows strong and wide bands at $3431\ \mathrm{cm}^{-1}$. These are related both to the vibrations of the hydroxyl groups (O–H) and the stretching vibrations of (N–H) [565,566]. The peaks at $3023\ \mathrm{cm}^{-1}$ come from the asymmetric stretching of the $\nu_{as}(\mathrm{C-H})$ from the (C–H) bonds present in the aromatic rings [566]. The hydrogen vibration band outside the plane of the aromatic ring $\delta(\mathrm{C-H})$, is responsible for the appearance of the observed peaks at $700\ \mathrm{cm}^{-1}$ (Figures 17a and 17b) and $704\ \mathrm{cm}^{-1}$ (Figure 17c) [567]. The peaks at $2926\ \mathrm{cm}^{-1}$ refer to $\nu_{as}(-\mathrm{CH_2})$, an antisymmetric stretching vibrations of the $-\mathrm{CH_2}$ groups [566,568]. Meanwhile, M4195

resin (Figure 17c) also presents a peak at $1452\ \mathrm{cm^{-1}}$, which is related to the asymmetric scissoring vibration band of $\delta_{as}(-CH_2)$ groups [565,569].

Peaks at $1630\ \mathrm{cm^{-1}}$ and $1732\ \mathrm{cm^{-1}}$ (Figures 17a and 17b) indicates the presence of hydrophilic groups $(C=O)$ at $1620-1640\ \mathrm{cm^{-1}}$ and $1710-1740\ \mathrm{cm^{-1}}$, being the second one characterizing the presence of $C=O$ of $COOH$ groups [570,571]. Besides, peaks at $1385\ \mathrm{cm^{-1}}$ are associated to the symmetric deformation of carboxylate ions - $\nu_s(-COO^-)$ [572]. The presence of bands of $(C=O)$ in the TP 209 XL and TP 207 resins is also confirmed by peaks at $1225\ \mathrm{cm^{-1}}$ [573].

In Figure 17d, the presence of the $(-SO_3H)$ in S 200 H resin can be identified by the specific peaks of this group that occurred in $1177\ \mathrm{cm^{-1}}$, $1036\ \mathrm{cm^{-1}}$ e $675\ \mathrm{cm^{-1}}$ [574]. The peak at $1177\ \mathrm{cm^{-1}}$ refers to the asymmetric stretching mode of the $(S=O)$ bond, while the $1036\ \mathrm{cm^{-1}}$ occurs due to the symmetric stretching mode in the same bond [575]. The $1638\ \mathrm{cm^{-1}}$ peak must be associated to the $(C=C)$ bonds [576].

Pyridine groups of M4195 resin (Figure 17c) were identified through the vibration at $1614\ \mathrm{cm^{-1}}$, reflecting the $(C=N)$ bond [569]. The peaks at $1116\ \mathrm{cm^{-1}}$ and $768\ \mathrm{cm^{-1}}$ are related, respectively, to $(C-N)$ and $(C-H)$ of the pyridine molecule [569]. The peak at $1384\ \mathrm{cm^{-1}}$ is also a $(C-N)$ stretching mode correspondent [577]. It becomes stronger and quite accentuated in the spectrum corresponding to the M4195 resin after the adsorption experiments, probably due to the adsorption and complexation of vanadium ions by the functional group.

The presence of peaks at $974\ \mathrm{cm^{-1}}$ shown in TP 209 XL e TP 207 resins (Figures 17a and 17b, respectively) after the adsorption process can be attributed to the deformation vibrations of the copolymer benzene ring (ST-DVB), which forms the matrix of both resins [566]. The spectra after contact with the solution (Figures 17a, 17b and 17c) was altered in several peaks, either by attenuation or by intensification. It corroborates the fact that, in the functional group of chelating resins, complexation with metals also occurs and not just an adsorption process.

TP 207 resin was studied for copper recovery with iron as an impurity in the work of Botelho Junior et al. [578]. The authors obtained FT-IR spectra with peaks at values very close to those shown in Figure 17b and also demonstrated that, when in

contact with the copper and iron ions, the resin undergoes a process of coordination between the functional group and the solution ions.

Sofińska-Chmiel & Kołodyńska [579] evaluated the spectrum of the M4195 resin before and after the sorption of metals such as copper and zinc and the behavior was analogous to that shown in Figure 17c. The change in peak intensity in the region between $1250\ \mathrm{cm}^{-1}$ and $1650\ \mathrm{cm}^{-1}$ was attributed by the authors to the formation of bands and coordination links of these functional groups with the adsorbed metals.

Wołowicz & Hubicki [580] studied the chelating resin TP 220 with bis-picolylamine functional group and compared its FTIR spectra with M4195. The authors also suggested that the peak attenuation in the region regarding the vibration of the atoms of the functional groups was due to their participation in the bond with the recovered metal (Pd).

These results corroborate with those presented in section 5.2.3.1, where it was shown that the recovery of metal ions by chelating resins occurred not only by ion exchange, but also by complexing these with the functional group.

In the present study, it was analyzed by SEM/EDS the resins before and after the experiments to investigate the adsorption process. None of the resins showed physical changes on their surfaces after the experiments. Although reported as macroporous resins [581], it was found a very smooth surface, most of them in a diameter range of 300-400 μm. As the SEM image and EDS spectra were similar among the resins studied, Figure 18 shows only the data obtained for TP 209 XL resin (the other ones are showed in the Supplementary file).

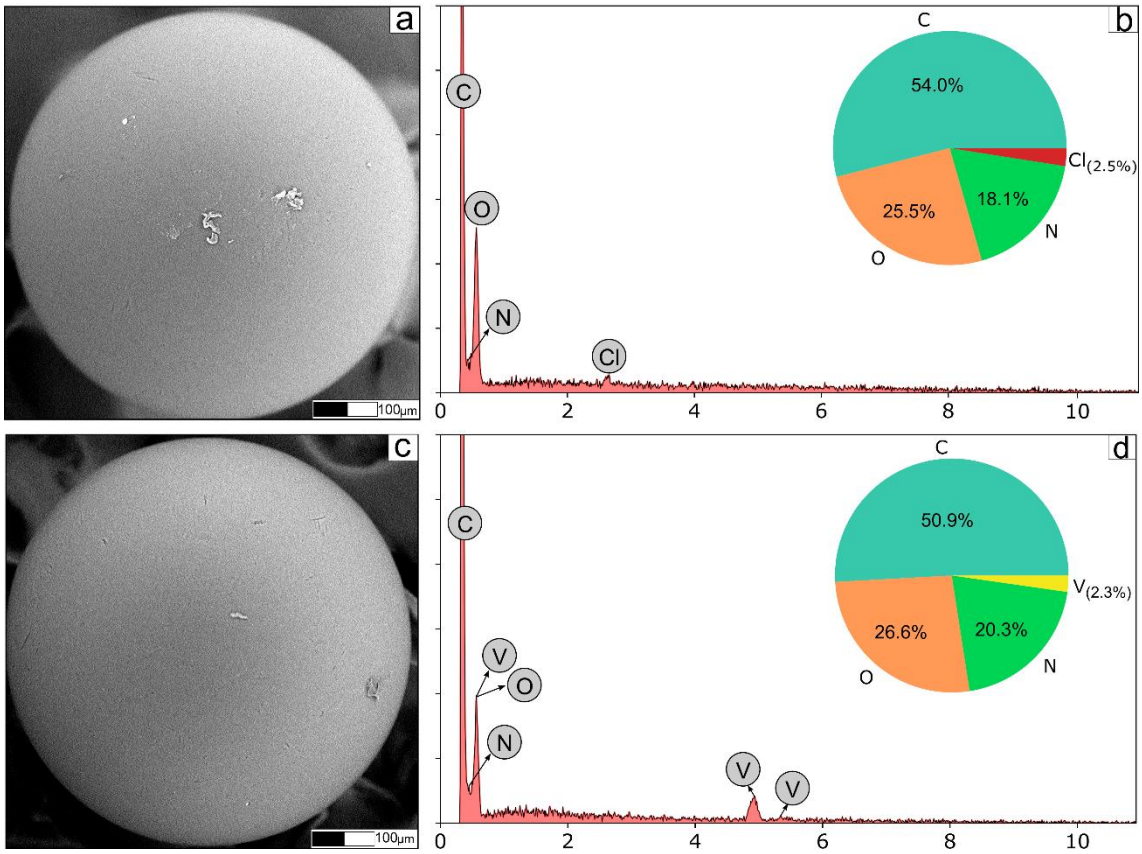

Figure 18. SEM image and its respective EDS spectra for TP 209 XL resin before (a, b) and after (c, d) the adsorption experiments.

TP 209 XL and TP 207 resins have quite similar EDS spectrum. Major elements are, respectively, carbon (54.0%, 45.7%), oxygen (25.5%, 30.2%) and nitrogen (18.1%, 18.0%), as expected, once these compose their functional groups (iminodiacetic acid – Figure 14). Carbon (50.5%), nitrogen (22.1%) and oxygen (23.7%) are also the major elements in the M4195 resin. Finally, major elements of the S 200 H resin are carbon (48.8%), oxygen (33.7%) and sulfur (17.5%), which are coherent with the sulfonic acid functional group. Chlorine is also present in the spectrum of TP 209XL, TP 207 and M4195 resins, and probably related to the washing process with HCl solution.

Atomic proportions have non-significate changes after experiments. Peaks of vanadium were observed after adsorption experiments. The cationic resin S 200 H showed the presence of Na, used to adjust the pH (NaOH).

Although iron was adsorbed, it was not identified in any of the resins studied by means of semi-quantitative EDS after the adsorption experiments due to the sensitivity of the technique. An important observation is that the quantification given by the EDS must be considered as a qualitative guide of the proportions of those elements, as this technique is not sufficiently accurate to serve as a chemical quantification.

5.3 Separation of cationic vanadium species from iron using chelating resins in continuous system to obtain high purity V_2O_5

Vinco, J. H.; Espinosa, D.C.R., Tenório, J.A.S.

Department of Chemical Engineering, Polytechnic School of the University of São Paulo (USP).

Abstract

Three ion exchange chelating resins – (i) Lewatit® MonoPlus TP 209 XL (iminodiacetic acid), (ii) Lewatit® TP 207 (iminodiacetic acid) and (iii) Dowex™ M4195 (bis-picolylamine) – were used to purify an acid solution of vanadium contaminated with iron (Fe^{2+}) in order to achieve a high purity V_2O_5 product. Column experiments were performed in two steps: loading (to recover vanadium from the solution) and elution with H_2SO_4 (to obtain a high purity solution of vanadium). Loading was accomplished testing two distinct flow rates and, for both of them, the breakthrough curves were similar. The three resins showed selectivity to adsorb vanadium. Iron was quickly adsorbed in the first bed volumes for all of them, but quickly desorbed by TP 209 XL and TP 207 resins. Desorption of iron during the loading was slower for M4195 resin, which caused the amount of adsorbed vanadium to be smaller compared to the other resins. Using five ion exchange columns in series resulted in the adsorption of 94% and 98% (TP 209 XL and TP 207 resins, respectively) of all the vanadium contained in the solution. Elution of the first columns generated vanadium solutions with 99.8% and 99.9% of purity, respectively. Precipitation of the purest solutions using $(NH_4)_2SO_4$ generated $(NH_4)_2V_6O_{16}$, which was later calcinated to form V_2O_5 (99.9% pure), as confirmed through XRD and thermogravimetric analysis.

Keywords: ion exchange; vanadium; purification; fixed-bed column; high purity vanadium.

5.3.1 Introduction

Vanadium is a metal whose physical (high tensile strength, hardness, fatigue resistance) and chemical (catalytic activity, multiple oxidation states) properties make it a strategic and essential resource in fields of application such as the aerospace industry, catalysts and in special ferrous and non-ferrous alloys [42,582,583]. Another use for vanadium is in the production of electrolyte for vanadium redox flow batteries (VRFB) [38]. VRFBs are among the most studied and promising redox flow batteries, gathering desirable characteristics such as fast charge-discharge cycle, elimination from cross-contamination of chemical constituents, flexible design, high efficiency, long life and safety [61]. These batteries are mainly used for large-scale energy storage, such as energy produced by renewable sources (wind and solar) which, given their inherently fluctuating production nature, require robust and efficient systems for storage and distribution [56]. Since global demand on new renewable energy sources are an increasing trend for the next years [55], the consumption of vanadium for this purpose is also expected to grow, mainly due to the increased visibility and improvements related to technology of these batteries [527].

Electrolytes in VRFBs represent one of the most important components [109], since its volume and its concentration in vanadium are directly related to the storage capacity of the battery [107]. In electrolytes, vanadium is present in its four oxidation states: the pair V^{2+}/V^{3+} in the negative electrolyte and the pair VO^{2+}/VO_2^{+} in the positive electrolyte [28]. By providing the best cost-benefit ratio, V_2O_5 currently represents the most demanded source of vanadium [30]. However, because the presence of impurities implies in several operational and performance problems [32], it is desirable a raw material at least 99.8% pure [31].

An impurity commonly associated with vanadium in its beneficiation process is iron, because, in addition to the ionic radius of vanadium and trivalent iron being close, V^{4+} can replace Ti^{+4} in ilmenite ($FeTiO_3$), causing vanadium to have a high affinity for iron oxides [196,584,585]. Over 90% of proven V_2O_5 reserves are related to titanomagnetite ores, so that approximately 80-85% of all vanadium produced globally is obtained from the direct extraction of deposits or from slag originating from the processing of vanadiferous titanomagnetite deposits [5,586,587].

Therefore, a purification technique must be used to selectively recover vanadium from contaminants such as iron. For this purpose, ion exchange appears as

an important alternative. In addition to the excellent selectivity in the adsorption of the target species, this technique provides high concentration enrichment rates with elution efficiency, operability over a wide pH range, simple mode of operation, durability and potential capital cost savings [588–590]. Within the ion exchange there are also exchangers that are chelators, which have donor groups in their functional groups that act by forming coordinated bonds with the metallic ions of interest in a Lewis acid-base system [483,484,591]. Through different functional groups, these resins demonstrate high specificity in the adsorption of a particular metal of interest.

Previous studies [39] were performed with an iron-contaminated vanadium solution through three chelating resins and a strong cation exchange resin. Batch studies were carried out in order to understand: (i) the adsorption mechanism, (ii) to adjust to an adsorption isotherm, (iii) obtain the thermodynamic parameters of the system and, also, (iv) to investigate the adsorption kinetics. Thus, because of the importance and significance that results in a continuous system have for practical applications [565], in this work, the authors bring the studies of adsorption in a column system for the three chelating resins, applied to the purification of the same solution. This new study reports data regarding loading and elution of resins in ion exchange columns, as well as obtaining high purity V_2O_5 after precipitation and calcination.

5.3.2 Methods

5.3.2.1 Chelating resins and synthetic solution

The ion exchange chelating resins used in this work were: (i) Lewatit® MonoPlus TP 209 XL (iminodiacetic acid), (ii) Lewatit® TP 207 (iminodiacetic acid) and (iii) Dowex™ M4195 (bis-picolylamine). First, they were subjected to alternating washings with hydrochloric acid solution (4 $mol.L^{-1}$ HCl) and ultrapure water three times each to eliminate any impurity and to charge their functional groups with exchangeable H^+ ions. The preparation procedure was carried out in Erlenmeyer flasks in an orbital shaker (200 rpm) throughout 4 hour intervals for each wash.

The synthetic solution was prepared according to the methodology described by Vinco et al. [39]. The concentrations of vanadium and iron in the final solution were respectively equal to 3.32 ± 0.41 $g.L^{-1}$ and 0.090 ± 0.002 $g.L^{-1}$. By using solutions of sodium hydroxide (NaOH) (10 $mol.L^{-1}$) and sodium dithionite ($Na_2S_2O_4$) (1 $mol.L^{-1}$) the

solution produced had its pH and redox potential (Eh) adjusted so that the vanadium species and iron were converted, respectively, to VO^{2+} and Fe^{2+}. Lastly, the pH of the solution was kept at 2.00, as this is the value at which these resins showed the highest adsorption of vanadium [39].

5.3.2.2 Column experiments

The ion exchange tests were carried out in fixed-bed glass columns with 50.0 cm in length, internal diameter equal to 1.0 cm and resin bed height of 30.0 cm, resulting in a bed volume (BV) of approximately 23.6 cm^3. The previously prepared wet resins were packed in the column. The synthetic solution percolated through the bed in a downstream flow, controlled by means of two peristaltic pumps installed upstream and downstream of the column (Figure 19). Two operating flows were evaluated: 2 BV/h (0.8 mL/min) and 3 BV/h (1.2 mL/min). Temperature was set at 25 ± 1 °C by flowing water through the column jacket. Effluent aliquots were periodically collected to determine the vanadium and iron content.

Figure 19. Apparatus used in the fixed bed column experiments.

After loading the resin to saturation, the column was then washed with water to remove all the solution still remaining in the column, leaving only the metal adsorbed

by the resin. Then, elution was performed using a sulfuric acid solution (H_2SO_4 1 mol.L^{-1}) at a fixed flow rate of 3 BV/h. Samples were collected at the outlet of the column at different times. Resin regeneration was performed by pumping 8 BV of a hydrochloric acid solution (4 mol.L^{-1} HCl) at a flow rate of 4 BV/h, followed by flowing ultrapure water through the column.

The resins that showed the best performance in vanadium adsorption were then subjected to a series column operation, in which the effluent from the first one fed the second column and so on, in order to increase the vanadium recovery at the end of the process.

5.3.2.3 Oxidation, precipitation and calcination

The purified vanadium solution eluted from the ion exchange column was then subjected to the precipitation procedure. The procedure was carried out in a 250 mL glass beaker placed in a bath with thermal fluid and the set placed on a hot plate with magnetic stirring.

First, the vanadium species was oxidized from VO^{2+} to VO_2^+ by using hydrogen peroxide (H_2O_2 29%), which reacts with VO^{2+} as in Eq. (36) [592]. The procedure was carried out at 50 °C for 30 minutes and the amount of H_2O_2 added was 10 times the stoichiometric one.

$$2VO^{2+} + H_2O_2 \rightarrow 2VO_2^+ + H_2O \quad (36)$$

After oxidation, the system was brought to a temperature of 90 °C and then a solution of ammonium sulfate ($(NH_4)_2SO_4$ 500 g.L^{-1}) was added until the pH of the solution reached 2.2, which was the best condition obtained in the studies of Li et al. [592]. The system was left stirring for 2 hours and, at the end, the precipitate was separated by vacuum filtration, washed with ultrapure water and dried in an oven at 60 °C for 24 hours.

The dried precipitate was then calcinated in a muffle furnace to obtain V_2O_5. The procedure was performed at 550 °C for 2 hours in a synthetic air atmosphere.

5.3.2.4 Analysis

Chemical analyzes for quantification of vanadium and iron in the solutions were performed using Atomic Absorption Spectrometry (AAS, SHIMADZU AA-7000). The precipitated was analyzed by X-Ray Diffractometry (XRD, Rigaku MiniFlex 300) with a copper radiation source, from 5° to 80° (2-Theta) - with 1.5°/min and steps of 0.02° - before and after calcination to identify their crystalline phases. A thermogravimetric analysis was performed on the precipitate using a thermogravimetric scale (Netzsch - STA 449 F1 Jupiter) under a synthetic air atmosphere (at a flow rate of 40 $mL.min^{-1}$) increasing the temperature up to 550°C (using a heating rate of 20 $°C.min^{-1}$) to correlate it with the phases identified through the XRD.

5.3.3 Results and discussion

5.3.3.1 Continuous system tests

5.3.3.1.1 Loading profiles (breakthrough curves)

Tests in a continuous system using fixed bed columns were carried out in order to selectively recover vanadium. Studying the adsorption as the solution percolates through the resin bed is important to define the breakthrough capacity (when the metal concentration in the effluent is 10% of the initial concentration). Also, it is important to determinate the moment when the resin has exhausted its ability to adsorb the metal of interest, i.e., when the concentration of the metal in the effluent is equal to the concentration of the feed (complete breakthrough) [46]. In Figure 20 are the vanadium and iron breakthrough curves obtained for the three chelating resins at the operating flow rates of 2 and 3 BV/h. In these, the ratios between the concentration of each of the metals in the effluent at a given moment and the initial concentration of these in the feed solution as a function of the number of bed volumes are presented.

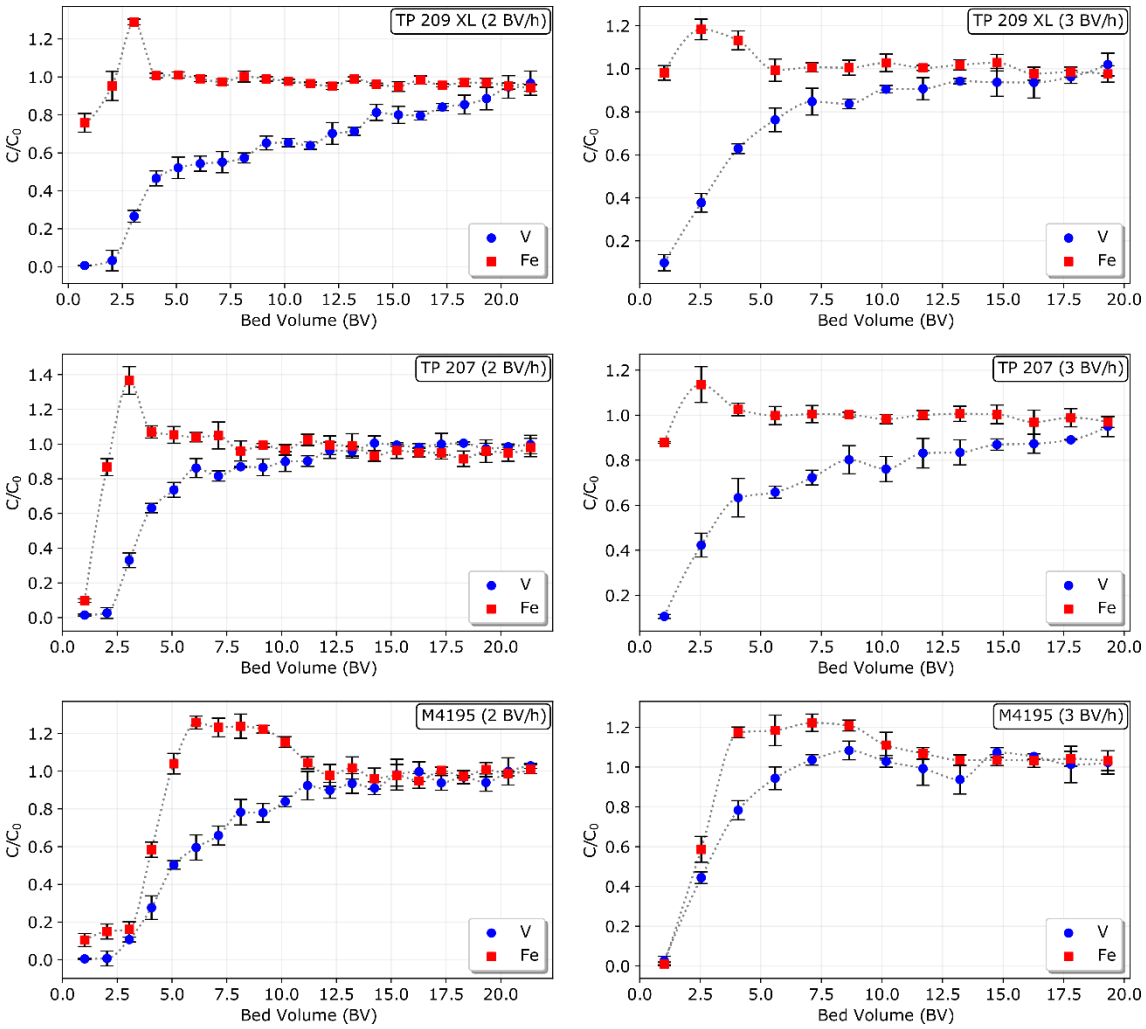

Figure 20. Breakthrough curves of vanadium and iron in two flow rates: 2 BV/h and 3 BV/h (pH = 2.0, T = 25 °C).

The curves reveal that vanadium was primarily adsorbed in relation to iron, even though iron was initially adsorbed. In all cases, the greater selectivity of the resins for vanadium implied a desorption and substitution of part of the adsorbed iron by the functional groups of the resins, releasing it in the effluent and causing some C/C_0 ratios to be greater than 1.

With the exception of the M4195 resin at a flow rate of 2 BV/h, the breakthrough of vanadium adsorption for the other cases occurred at values between 1 and 2.5 BV (between 23.6 and 58.9 mL of solution). The breakthrough for iron, on the other hand, except for TP 207 and M4195 resins at a flow rate of 2 BV/h, occurred right at the first BV of solution that ran through the column. For TP 209 XL and TP 207 resins, at both

flow rates, an equilibrium in iron adsorption was verified at least 15 BV before vanadium adsorption was exhausted.

Regarding the amount of adsorbed metal, the M4195 resin showed a higher iron adsorption (even in the first solution bed volumes) in relation to the other resins for both flow rates studied, which is evidenced by the greater volume of beds necessary to stabilize the C/C_0 ratio. Thus, the need to replace these ions by vanadium in the functional groups probably disfavored the adsorption of vanadium, leading to a lower recovery of vanadium for this resin. Although the final amount of iron adsorption for TP 209 XL and TP 207 resins was slightly higher at the end of the operation, these were more rapidly desorbed by the functional groups and, therefore, the greater exposure of vanadium ions to the free functional groups provided higher levels of recovery for vanadium at the end of the process.

In general, the increase in the operating flow from 2 to 3 BV/h showed little influence on the amount of vanadium adsorbed by the resins, both in terms of the breakthrough and in the final percentage of recovered metal. Some studies in which vanadium is adsorbed by ion exchange resins in a continuous system showed that the decrease in the feed flow resulted in an increase in vanadium adsorption, as well as in an increase in the breakthrough values [485,582,593]. Nevertheless, Zhu et al. [539] also reported that there was no significant increase in the percentage of adsorbed vanadium ions when the flow was decreased to values below 3.33 mL/min, so that it only had a negative effect on the amount of metal adsorbed at higher values. In addition to the small variation in flow, the concentration of metal in solution is also a factor that influences the breakthrough, as can be seen in the data by Gomes et al. [46]. In these, the decrease in the concentration of vanadium in solution from 5 to 3 $mg.L^{-1}$ was responsible for changing the breakthrough point, respectively, from 27 to 4000 BV. Therefore, this observation corroborates the fact that the high concentration of vanadium in the solution of the present work can explain the similarity of behavior between the curves obtained with different flows.

5.3.3.1.2 Elution profiles (elution curves)

The study of the elution of ion exchange columns was carried out using a solution of 1 mol.L^{-1} of H_2SO_4. Prior to elution, the resins were loaded by flowing the iron-contaminated vanadium solution at a flow rate of 3 BV/h, for a total of 20 BV. The elution profiles for the three resins are shown in Figure 21, where the concentration of vanadium and iron in the effluent is plotted as a function of the number of beds of eluted solution, at a flow rate of 3 BV/h.

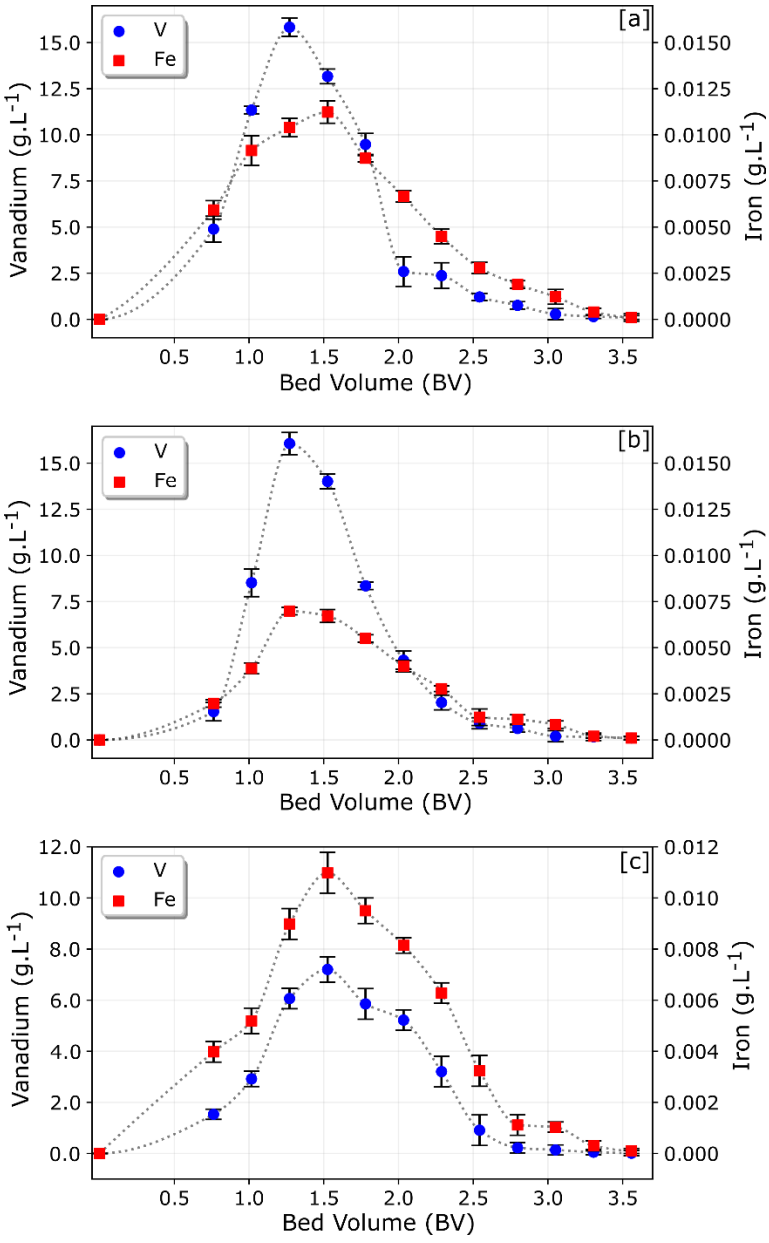

Figure 21. Vanadium and iron elution profiles from resins [a] TP 209 XL, [b] TP 207 and [c] M4195 using H_2SO_4 (1 mol.L^{-1}) at 3 BV/h.

TP 209 XL e TP 207 resins (Figure 21) are the ones that recovered the most vanadium, since their elution profiles showed vanadium concentration peaks at 1.3 BV, respectively equal to 15.8 and 16.1 $g.L^{-1}$. The M4195 resin showed a peak in the vanadium concentration eluted at 1.5 BV (of 7.2 $g.L^{-1}$), at least half of that observed in previous resins. It is also noted that iron was also eluted by the three resins, indicating that part of it remained adsorbed on the active sites of the resins until the end of the loading process. However, for the TP 209 XL and TP 207 resins, the concentration of vanadium in final eluate was almost twice as the concentration in the initial solution, as the concentration of iron decreased almost 10 times. This corroborates the fact that the adsorption of iron was very low and most of the adsorbed was desorbed and replaced by vanadium during the column loading process.

5.3.3.1.3 Mass balance of columns in series

As discussed in section 3.1.1, TP 209 XL and TP 207 resins showed higher adsorption of vanadium in the tests containing only one column. Thus, in order to increase the recovery of the metal present in the solution, ion exchange columns were used in a series operation, where the effluent of one was the solution that fed the next and so on. A 3 BV/h flow was used, considering that this flow resulted in loading profiles similar to those of a 2 BV/h flow, not causing damage to the efficiency of the process. Furthermore, from a practical point of view, it streamlines the operation. In Figure 22 are the mass balances performed for these systems. It was possible to obtain the percentage of recovery in each of the columns (as well as the purity of the solution eluted from each) based on the mass of vanadium and iron present in the stream of elution (Table 13).

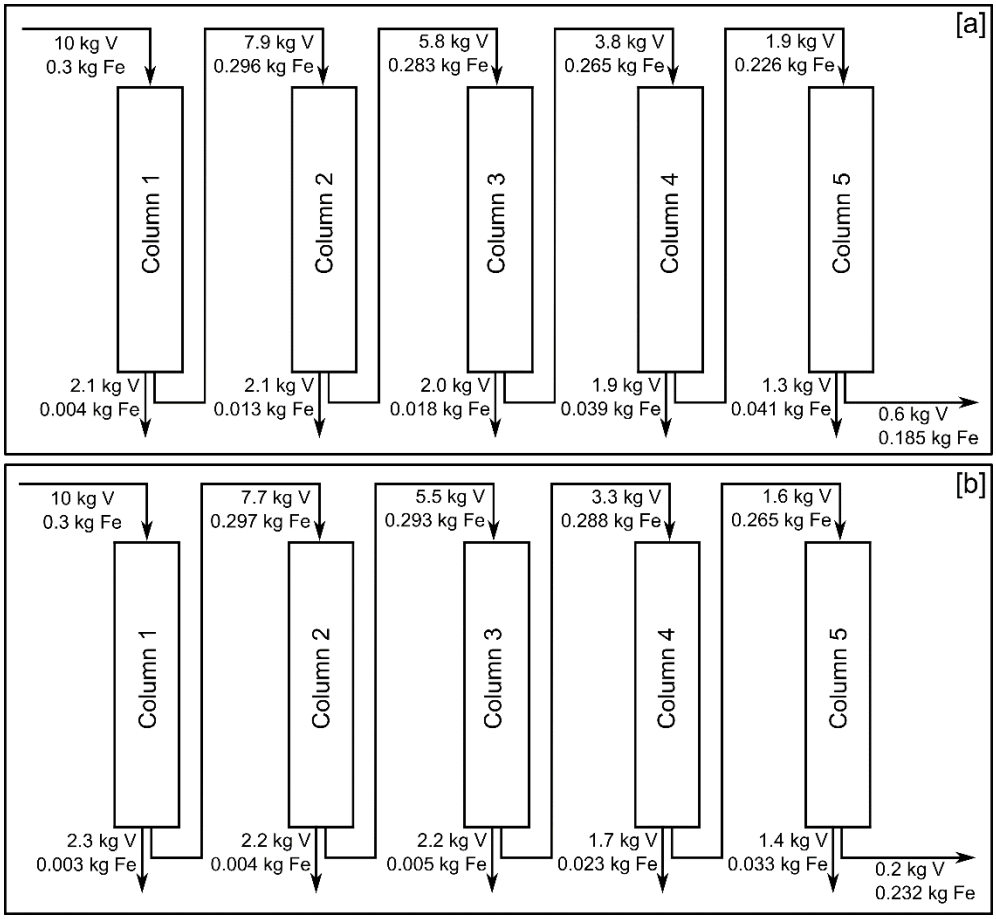

Figure 22. Mass balance for an ion exchange column system with resins [a] TP 209 XL and [b] TP 207 arranged in a series configuration.

Both resins (Figure 22) demonstrate similar behavior, probably because they are functionalized by the same functional group. Regarding the general performance, there is a decrease in the mass of vanadium eluted from column 1 to column 5, in contrast to iron, which presents an increase in the mass that is eluted from column 1 to 5. This behavior can be explained by the decrease in the concentration of vanadium in solution as it is adsorbed by the previous columns, causing less competition with iron for the active sites of the resins, thus increasing its adsorption.

Table 13. Percentage of vanadium and iron ions adsorbed on each column for the column in series and purity of the vanadium solution eluted from each column.

Column	TP 209 XL					TP 207				
	adsorbed (%) [a]		accumulated adsorbed (%) [b]		Vanadium purity (%)	adsorbed (%) [a]		accumulated adsorbed (%) [b]		Vanadium purity (%)
	V	Fe	V	Fe		V	Fe	V	Fe	
1	21.0	1.3	21.0	1.3	99.8	23.0	1.0	23.0	1.0	99.9
2	26.6	4.4	42.0	5.7	99.4	28.6	1.3	45.0	2.3	99.8
3	34.5	6.4	62.0	11.7	99.1	40.0	1.7	67.0	4.0	99.8
4	50.0	14.7	81.0	24.7	98.0	51.5	8.0	84.0	11.7	98.7
5	68.4	18.1	94.0	38.3	96.9	87.5	12.5	98.0	22.7	97.7

[a] Percentage of each metal adsorbed in relation to the own column feed.

[b] Percentage of each metal adsorbed relative to the starting solution that fed the first column

The global percentages of vanadium recovery by TP 209 XL and TP 207 resins were, respectively, equal to 94.0% and 98.0%, against 38.3% and 22.7% in the same order for iron. Thus, it is clear that the best resin for the purpose of selectively recovering vanadium was TP 207. However, it is important to highlight that the first column elution of both resins provides vanadium with a high purity: 99.9% for TP 207 and 99.8% for TP 209 XL. The vanadium purity in the second and third columns elution drops slightly for TP 207 resin (99.8%), but still meets the purity criteria required for VRFB electrolytes, while for TP 209 XL it has already becomes unsuitable for this application since the purity of second column elution is 99.4%.

5.3.3.2 Precipitation and obtaining of V_2O_5

The solution obtained from the elution of column 1 with TP 207 resin, which, as discussed in topic 3.1.3, showed a vanadium purity equal to 99.9%, was subjected to precipitation for vanadium recovery. After the addition of the H_2O_2 solution, the system was left under agitation for 30 minutes, the oxidation of the VO^{2+} to VO_2^+ was observed through the change in the color of the solution, from blue (Figure 23a) to yellow (Figure 23b). After oxidation, the increase of the temperature to 90ºC and adding $(NH_4)_2SO_4$ to adjust the pH up to 2.2, resulted in a solid phase after 2 hours of stirring (Figure 23c) and the solid separated through filtration. The vanadium precipitation efficiency was 80.1%, calculated from the mass variation of vanadium in solution before and after the precipitation process. The mass of iron in solution before and after precipitation did not change, indicating that the process took place without dragging the 0.1% of the metal that contaminated the purified solution. Vanadium when in its +5 oxidation state in solutions with a pH below 1 is practically entirely in the form of VO_2^+, which would possibly not react with NH_4^+. However, as the pH increases to higher values, which was the case with the condition used in the present work, the VO_2^+ species begin to be converted and different species start to coexist in solution, such as: $H_3V_{10}O_{28}^{3-}$, $H_2V_{10}O_{28}^{4-}$, $HV_{10}O_{28}^{5-}$, $V_{10}O_{28}^{6-}$ and $V_6O_{18}^{6-}$ [548,594,595]. Therefore, these species react differently with the NH^{4+} ion to precipitate vanadium, directly influencing the efficiency of the process [596].

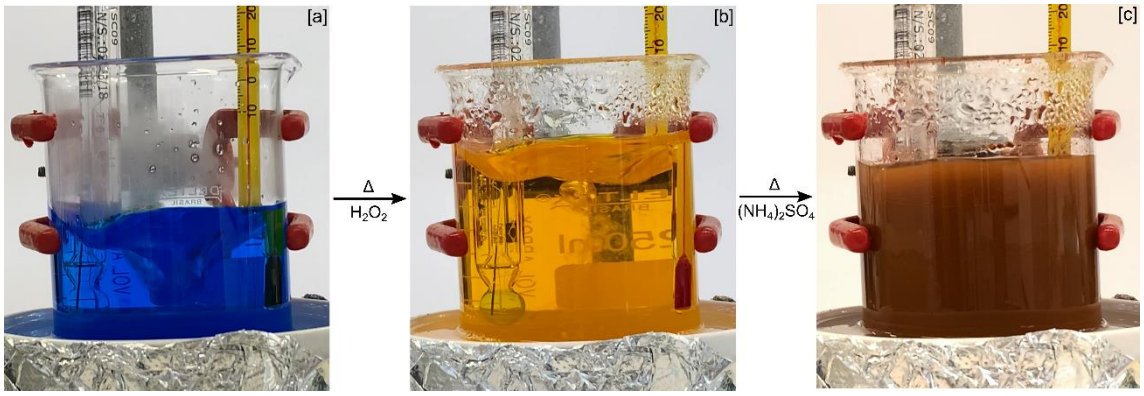

Figure 23. Solution containing vanadium [a] in its +4 oxidation state, [b] oxidized to +5 and then [c] precipitated.

The X-ray diffraction pattern confirms that vanadium precipitated in the crystalline phase of ammonium polyvanadate ($(NH_4)_2V_6O_{16}$) (Figure 24a). Peng et al. [536] used $CO(NH_2)_2$ in the precipitation of vanadium from a synthetic solution and obtained a precipitate with the same crystalline phase. The results of Wen et al. [596] also demonstrate the precipitation of vanadium obtained from the leaching of high chromium vanadium slag in the form of $(NH_4)_2V_6O_{16}$. In addition, these authors reached an efficiency of 99.75%, however, they used a pH equal to 8.0, which also allowed the precipitation of the iron that was in solution, reducing the purity of the product. The main application of ammonium polyvanadate is the production of vanadium pentoxide, produced when burned in the air [597].

$(NH_4)_2V_6O_{16}$ undergoes thermal decomposition in one stage, as shown in Eq. (37) [598], so that a theoretical mass loss after decomposition equal to 8.7% is expected.

$$(NH_4)_2V_6O_{16} \rightarrow 2NH_3 \uparrow + H_2O \uparrow + 3V_2O_5 \quad (37)$$

A thermal analysis (TG-DTG) was also used to characterize the crystalline phase formed in the precipitation. Its decomposition is seen in Figure 24b. The DTG curve has only a well-defined peak at 320 °C, indicating the occurrence of only one thermal event. The total mass loss observed was 10.7%, exactly 2.0% above the expected 8.7%. However, the change in mass that occurs before approximately 200°C should not be attributed exclusively to the decomposition of $(NH_4)_2V_6O_{16}$, since the beginning of this event is marked by the maximum positive value of the DTG that occurs at this temperature.

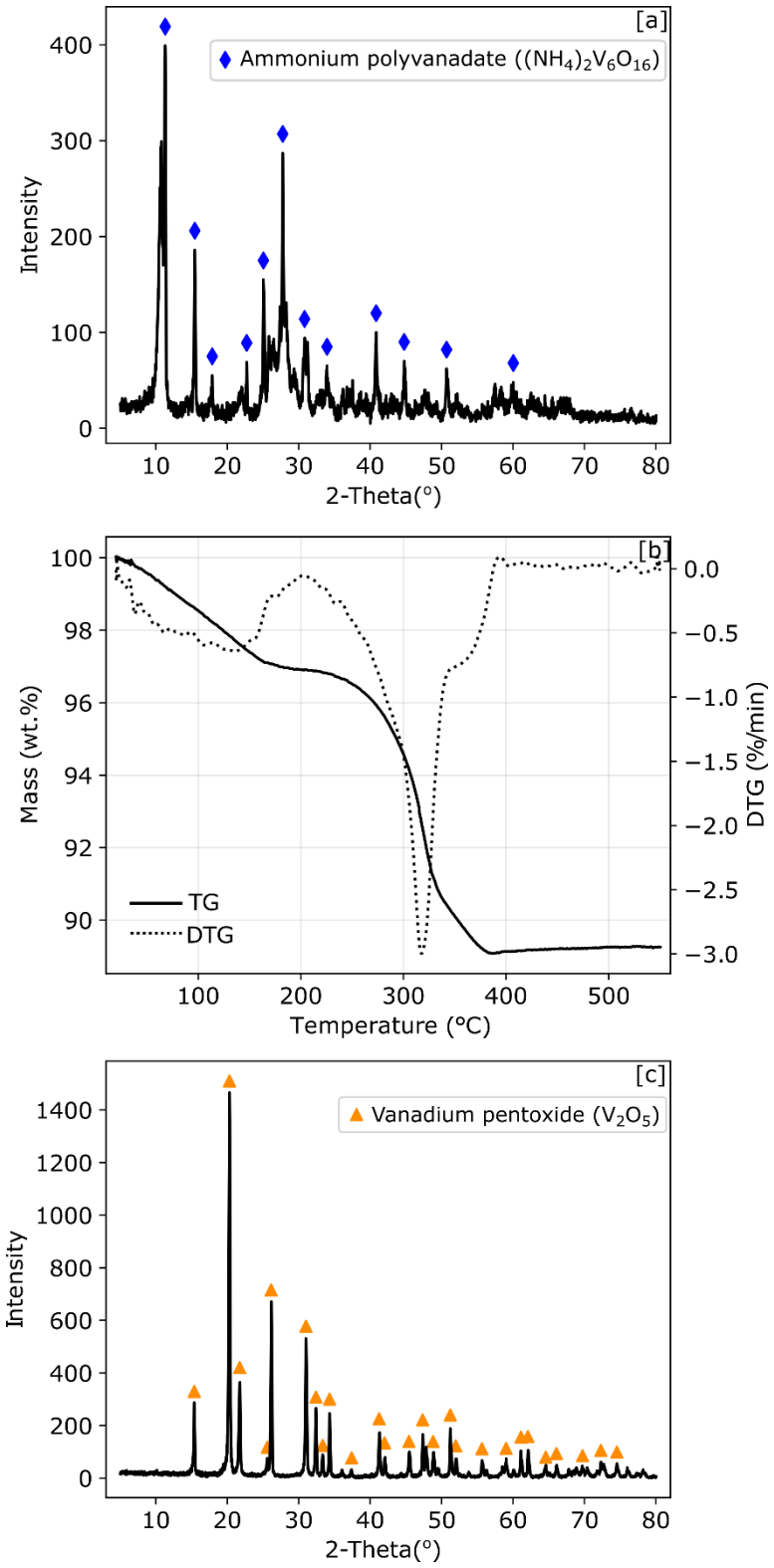

Figure 24. [a] XRD pattern and [b] TG-DTG curves of the formed precipitate. [c] XRD pattern of the calcinated precipitate.

The loss of mass verified in the initial steps can also be a result of the loss of moisture, volatilization of ammonia and, still, of remaining sulfates of the solution in the solid. Besides, as showed by Chithaiah et al. [599] and Han et al. [600], $(NH_4)_2V_6O_{16}$ can also precipitate in a hydrated form, having a mass loss close to 20% after decomposing to form V_2O_5. Therefore, if a very small fraction of the precipitated material (enough to be undetectable by XRD) was in the hydrated form, it would also contribute to the increase in the expected mass loss and would be related to this variation.

Figure 24c shows the XRD pattern of the material obtained with the muffle calcination of the precipitate. All of the detected peaks refer to the presence of the crystalline phase of vanadium pentoxide (V_2O_5). It is also noted that, in relation to the diffractogram of the precipitate, there was less noise generation, indicating that calcination provided greater crystallization of the material and the generation of high intensity peaks. Xiong et al. [601] precipitated vanadium from the leaching of vanadium-bearing shale also in the form of ammonium polyvanadate, which was later calcined to generate vanadium pentoxide. These authors haved used NH_4Cl as a precipitant, an acidic medium, pH equal to 2.0 at 90°C, so that at the end of the process the purity obtained for V_2O_5 was greater than 99%.

6. CONCLUSIONS

From the results presented in this study, the main conclusions were:

1. an increase in pH was associated with a greater adsorption of the vanadium and iron ions;
2. the chelating resins showed selectivity for vanadium adsorption in the tests varying the pH, for all of the values tested;
3. in batch experiments at pH 2.00, T = 298 K and t = 120 minutes, chelating resins showed the highest vanadium recoveries, respectively equal to 25.3, 24.8 and 29.8%, while, in the same order, adsorbed 7.4, 7.9 and 5.8% of the iron in solution;
4. the adsorption of vanadium by TP 209 XL, TP 207 and S 200 H resins was better adjusted to the Langmuir isotherm, while for M4195 resin better adjusted the experimental data to the Temkin isotherm;
5. iron adsorption process, in turn, was adjusted to the: (i) Langmuir isotherm for TP 209 XL resin; (ii) Freundlich isotherm for TP 207 and M4195 resins and (iii) Temkin isotherm for S 200 H resin;
6. the adsorption of vanadium and iron in the three chelating resins was favored by the increase in temperature and confirmed by the positive value obtained for the variation of positive enthalpy (endothermic process).
7. for the S 200 H resin, the adsorption of vanadium corresponds to an exothermic process, unlike iron, which is endothermic;
8. the negative values of ΔG^0 for both metals in all the four resins reveal the spontaneity of the adsorption reactions;
9. the resins TP 209 XL and TP 207 demonstrated different kinetic behavior and the resins M4195 and S 200 H tend to equilibrate the adsorption from the first 30 minutes of contact with the solution;
10. chelating resins, due to coordination interaction with metals, release less H^+ ions into the medium as the ions are adsorbed on their functional groups in relation to the cationic exchange resin;
11. the adsorption of both metals is better explained by the mechanism proposed by the pseudo-second order model, indicating that the adsorption rate of these metals by the four resins evaluated is controlled by a process of chemisorption;

12. the change in intensity and displacement of some peaks in the FT-IR spectra for the resins before and after the tests corroborated the understanding that complexation occurs in chelating resins;
13. TP 209 XL, TP 207 and M4195 ion exchange chelating resins demonstrated selectivity in the adsorption of vanadium over iron in the column studies, with the first two demonstrating greater efficiency in the amount of vanadium adsorbed with the same number of bed volumes of purified solution;
14. the variation in the flow rates studied (2 to 3 BV/h) did not influence the adsorption efficiency at the end of the process when the resins reached exhaustion;
15. for the elution process, vanadium was completely recovered using a 1 mol.L^{-1} de H_2SO_4 for the three chelating resins;
16. 94% and 98% of all the vanadium contained in the solution was adsorbed, respectively, by the TP 209 XL and TP 207 resins, when using 5 ion exchange columns in series. For the same system, however, in the same order, 38% and 23% of the iron was also adsorbed;
17. using columns in series, the mass of adsorbed vanadium decreases from the first to the fifth column, unlike iron, which begins to increase its adsorption as the vanadium decreases;
18. first column elution of TP 207 and TP 209 XL resins generated vanadium solutions with 99.9% and 99.8% of purity, respectively;
19. vanadium was precipitated from the solution with 99.9% purity (80% efficiency) by adding $(NH_4)_2SO_4$ at 90°C (stirred during 2 hours), as crystalline $(NH_4)_2V_6O_{16}$;
20. V_2O_5 (purity greater than 99.9%) was efficiently formed by calcinating the precipitate at 550°C for 2 hours;
21. TP 209 XL and TP 207 resins were shown to be a good alternative to purify acid solutions of vanadium contaminated with iron in continuous systems;
22. the high purity V_2O_5 obtained from the elution of the first column matches the standards to be further applied in VRFBs electrolytes.

REFERENCES

[1] M. Petranikova, A.H. Tkaczyk, A. Bartl, A. Amato, V. Lapkovskis, C. Tunsu, Vanadium sustainability in the context of innovative recycling and sourcing development, Waste Management. 113 (2020) 521–544. https://doi.org/10.1016/j.wasman.2020.04.007.

[2] G.A. Blengini, C.E.L. Latunussa, U. Eynard, C.T. de Matos, D. Wittme, K. Georgitzikis, C. Pavel, S. Carrara, L. Mancini, M. Unguru, D. Blagoeva, F. Mathieux, D. Pennington, Study on the EU's list of Critical Raw Materials, 2020. https://doi.org/10.2873/11619.

[3] A. Demas, Interior Releases 2018's Final List of 35 Minerals Deemed Critical to U.S. National Security and the Economy, USGS. (2018). https://www.usgs.gov/news/interior-releases-2018-s-final-list-35-minerals-deemed-critical-us-national-security-and (accessed July 8, 2021).

[4] BRASIL. Ministério de Minas e Energia. Secretaria de Geologia Mineração e Transformação Mineral, RESOLUÇÃO Nº 2, DE 18 DE JUNHO DE 2021, (2021) 103. https://www.in.gov.br/web/dou/-/resolucao-n-2-de-18-de-junho-de-2021-327352416.

[5] K.D. Kelley, C.T. Scott, D.E. Polyak, B.E. Kimball, Vanadium, in: K. Schulz, R. Seal, D. Bradley, J. Deyoung (Eds.), Critical Mineral Resources of the United States — Economic and Environmental Geology and Prospects for Future Supply, U.S. Geological Survey, Reston, Virginia, 2017: pp. U1–U36. https://doi.org/10.3133/pp1802U.

[6] D.E. Polyak, Vanadium, Mineral Commodity Summaries. (2021) 2. https://pubs.usgs.gov/periodicals/mcs2021/mcs2021-vanadium.pdf.

[7] D.E. Polyak, Vanadium, Mineral Commodity Summaries. (2016) 182–183. https://s3-us-west-2.amazonaws.com/prd-wret/assets/palladium/production/mineral-pubs/vanadium/mcs-2016-vanad.pdf.

[8] D.E. Polyak, Vanadium, Mineral Commodity Summaries. (2017) 182–183. https://s3-us-west-2.amazonaws.com/prd-wret/assets/palladium/production/mineral-pubs/vanadium/mcs-2017-vanad.pdf.

[9] D.E. Polyak, Vanadium, Mineral Commodity Summaries. (2018) 180–181. https://s3-us-west-2.amazonaws.com/prd-wret/assets/palladium/production/mineral-pubs/vanadium/mcs-2018-vanad.pdf.

[10] Vanadium Overview, Bushveld Minerals - About Vanadium. (2020). https://www.bushveldminerals.com/about-vanadium/ (accessed July 9, 2021).

[11] Brasil, Anuário Mineral Brasileiro: principais substâncias metálicas 2021, 2021.

[12] J.A.A.B. Teixeira, Vanádio, (2018) 2. https://www.gov.br/anm/pt-br/centrais-de-conteudo/publicacoes/serie-estatisticas-e-economia-mineral/sumario-mineral/sumario-mineral-brasileiro-2018.

[13] P.C. Rodriguez, L.A. da Silva, F. V Xavier, R.A. Campbell, G.G. Ferreira, An Updated Mine Plan, Mineral Reserve and Preliminary Economic Assessment of the Inferred Resources, 2017.

[14] E.M. Alcantara, T. Ogasawara, F.T. da Silva, E.F. Fontes, Extraction of vanadium from campo Alegre de Lourdes (BA, Brazil) Fe-Ti-V ore by partial reduction/magnetic concentration/salt roasting/hot water leaching, in: National Meeting on Mineral Treatment and Hydrometallurgy, 1988: pp. 836–851.

[15] J.C.S. Cassa, T. Ogasawara, F.T. da Silva, O.D. Cuéllar, Avaliação das alternativas de aproveitamento do minério de ferro-titânio-vanádio de Campo Alegre de Lourdes (Bahia-Brasil), in: Encontro Nacional de Mineração e Metalurgia Extrativa, Vol. 2, 1987: pp. 49–77.

[16] R.R. Moskalyk, A.M. Alfantazi, Processing of vanadium: A review, Minerals Engineering. 16 (2003) 793–805. https://doi.org/10.1016/S0892-6875(03)00213-9.

[17] Annexes to the report on Critical Raw Materials for the EU, (2014) 38. https://ec.europa.eu/growth/sectors/raw-materials/specific-interest/critical_en.

[18] R.L. Moss, E. Tzimas, H. Kara, P. Willis, J. Kooroshy, Critical Metals in Strategic Energy Technologies, 2011. https://doi.org/10.2790/35716.

[19] European Commission, Communication from the Commission to the European Parliament, the Council, the European Economic and Social Committee and the Committee of the Regions on the 2017 list of Critical Raw Materials for the EU, 2017.
[20] Largo announces qualification of its vanadium for use in production of titanium master alloys in the aerospace industry, Largo Resources. (2017). https://www.vanadiumcorp.com/news/industry/largo-announces-qualification-of-its-vanadium-for-use-in-production-of-titanium-master-alloys-in-the-aerospace-industry/.
[21] W. Wang, J.P. Kizewski, W. Duan, Introduction to Redox Flow Batteries, in: H. Zhang, X. Li, J. Zhang (Eds.), Redox Flow Batteries (Fundamentals and Applications), CRC Press, 2018: pp. 43–76. https://doi.org/10.1016/B978-0-444-62616-5.00017-6.
[22] W. Wang, X. Wei, D. Choi, X. Lu, G. Yang, C. Sun, Electrochemical cells for medium- and large-scale energy storage, in: C. Menictas, M. Skyllas-Kazacos, T.M. Lim (Eds.), Advances in Batteries for Medium and Large-Scale Energy Storage, Elsevier, United Kingdom, 2015: pp. 3–28. https://doi.org/10.1016/B978-1-78242-013-2.00001-7.
[23] H. Prifti, A. Parasuraman, S. Winardi, T.M. Lim, M. Skyllas-Kazacos, Membranes for redox flow battery applications, Membranes (Basel). 2 (2012) 275–306. https://doi.org/10.3390/membranes2020275.
[24] L.F. Arenas, C. Ponce de León, F.C. Walsh, Engineering aspects of the design, construction and performance of modular redox flow batteries for energy storage, Journal of Energy Storage. 11 (2017) 119–153. https://doi.org/10.1016/j.est.2017.02.007.
[25] M. Skyllas-Kazacos, R. Robins, All-vanadium redox battery, US 4786567, 1988.
[26] W. Wang, Q. Luo, B. Li, X. Wei, L. Li, Z. Yang, Recent progress in redox flow battery research and development, Advanced Functional Materials. 23 (2013) 970–986. https://doi.org/10.1002/adfm.201200694.
[27] M. Skyllas-Kazacos, M.H. Chakrabarti, S.A. Hajimolana, F.S. Mjalli, M. Saleem, Progress in Flow Battery Research and Development, Journal of The Electrochemical Society. 158 (2011) R55–R79. https://doi.org/10.1149/1.3599565.
[28] R. Gundlapalli, S. Kumar, S. Jayanti, Stack Design Considerations for Vanadium Redox Flow Battery, INAE Letters. 3 (2018) 149–157. https://doi.org/10.1007/s41403-018-0044-1.
[29] VANITEC, Vanadium Redox Flow Battery (VRFB) - technology is increasingly being tested or deployed across the globe, (2019). https://willigan.digital/pr/bold-editorial/vanitec/v3/ (accessed July 9, 2021).
[30] J. Heo, J.Y. Han, S. Kim, S. Yuk, C. Choi, R. Kim, J.H. Lee, A. Klassen, S.K. Ryi, H.T. Kim, Catalytic production of impurity-free V3.5+ electrolyte for vanadium redox flow batteries, Nature Communications. 10 (2019) 1–9. https://doi.org/10.1038/s41467-019-12363-7.
[31] C. Choi, S. Kim, R. Kim, Y. Choi, S. Kim, H. Jung, J.H. Yang, H.T. Kim, A review of vanadium electrolytes for vanadium redox flow batteries, Renewable and Sustainable Energy Reviews. 69 (2017) 263–274. https://doi.org/10.1016/j.rser.2016.11.188.
[32] L. Cao, M. Skyllas-Kazacos, C. Menictas, J. Noack, A review of electrolyte additives and impurities in vanadium redox flow batteries, Journal of Energy Chemistry. 27 (2018) 1269–1291. https://doi.org/10.1016/j.jechem.2018.04.007.
[33] J.S. John, Imergy Uses Recycled Vanadium to Cut Materials Costs for Flow Batteries, Greentech Media. (2014). https://www.greentechmedia.com/articles/read/imergys-slag-to-energy-storage-vanadium-recipe#gs.mZBWQtQ (accessed July 9, 2021).
[34] C.E. Harland, Discovery and structure of solid inorganic ion exchange materials, in: C.E. Harland (Ed.), Ion Exchange: Theory and Practice, 2nd ed., The Royal Society of Chemistry, 1994: pp. 1–20. https://doi.org/10.1039/9781847551184-00001.
[35] M.M. Nasef, Z. Ujang, Introduction to Ion Exchange Processes, in: Inamuddin, M. Luqman (Eds.), Ion Exchange Technology I, Springer Netherlands, Dordrecht, 2012: pp. 1–39. https://doi.org/10.1007/978-94-007-1700-8_1.

[36] A.A. Zagorodni, Ion Exchangers, their Structure and Major Properties, in: Ion Exchange Materials, 1st ed., Elsevier, 2007: pp. 9–54. https://doi.org/10.1016/B978-008044552-6/50003-4.
[37] J. Inczédy, Ion Exchangers, in: I. Buzás (Ed.), Analytical Applications of Ion Exchangers, Elsevier, 1966: pp. 6–39. https://doi.org/10.1016/B978-0-08-013545-8.50005-0.
[38] J.H. Vinco, A.E.E.C. Domingos, D.C.R. Espinosa, J.A.S. Tenório, M.P.G. Baltazar, Unfolding the Vanadium Redox Flow Batteries: An indeep perspective on its components and current operation challenges, Journal of Energy Storage. 43 (2021) 103180. https://doi.org/10.1016/j.est.2021.103180.
[39] J.H. Vinco, A.B. Botelho Junior, H.A. Duarte, D.C.R. Espinosa, J.A.S. Tenório, Purification of an iron contaminated vanadium solution through ion exchange resins, Minerals Engineering. 176 (2022) 107337. https://doi.org/10.1016/j.mineng.2021.107337.
[40] U. Schwertmann, G. Pfab, Structural vanadium and chromium in lateritic iron oxides: Genetic implications, Geochimica et Cosmochimica Acta. 60 (1996) 4279–4283. https://doi.org/10.1016/S0016-7037(96)00259-1.
[41] H.G. Dill, The “chessboard” classification scheme of mineral deposits: Mineralogy and geology from aluminum to zirconium, Earth-Science Reviews. 100 (2010) 1–420. https://doi.org/10.1016/j.earscirev.2009.10.011.
[42] W. Li, Y. Zhang, T. Liu, J. Huang, Y. Wang, Comparison of ion exchange and solvent extraction in recovering vanadium from sulfuric acid leach solutions of stone coal, Hydrometallurgy. 131–132 (2013) 1–7. https://doi.org/10.1016/j.hydromet.2012.09.009.
[43] A. Pidakhmet, E.E. Ergozhin, T.K. Chalov, A.I. Nikitina, Sorption of Vanadium (V) and Chromium (VI) Ions by Anion Exchanger Based on an Oligomers of Epichlorohydrin and 4-Vinylpyridine, International Journal of Chemical Sciences. 12 (2014) 855–862.
[44] H.I. Gomes, A. Jones, M. Rogerson, I.T. Burke, W.M. Mayes, Vanadium removal and recovery from bauxite residue leachates by ion exchange, Environmental Science and Pollution Research. 23 (2016) 23034–23042. https://doi.org/10.1007/s11356-016-7514-3.
[45] V.R. Gurjar, P.S. Koujalagi, H.N. Revankar, R.M. Kulkarni, Adsorptive removal of vanadium from aqueous media by ion exchange resin, Emergent Materials. (2021). https://doi.org/10.1007/s42247-021-00251-0.
[46] H.I. Gomes, A. Jones, M. Rogerson, G.M. Greenway, D.F. Lisbona, I.T. Burke, W.M. Mayes, Removal and recovery of vanadium from alkaline steel slag leachates with anion exchange resins, Journal of Environmental Management. 187 (2017) 384–392. https://doi.org/10.1016/j.jenvman.2016.10.063.
[47] K. Mazurek, P. Grzesiak, S. Druzyński, U. Kiełkowska, A. Wróbel, A. Szalla, Method of Utilization of the Spent Vanadium Catalyst, Polish Journal of Chemical Technology. 20 (2018) 1–7. https://doi.org/10.2478/pjct-2018-0031.
[48] X. Zhu, W. Li, S. Tang, M. Zeng, P. Bai, L. Chen, Selective recovery of vanadium and scandium by ion exchange with D201 and solvent extraction using P507 from hydrochloric acid leaching solution of red mud, Chemosphere. 175 (2017) 365–372. https://doi.org/10.1016/j.chemosphere.2017.02.083.
[49] M. Ding, T. Liu, Y. Zhang, Z. Cai, Y. Yang, Y. Yuan, Effect of Fe(III) on the positive electrolyte for vanadium redox flow battery, Royal Society Open Science. 6 (2019) 1–13. https://doi.org/10.1098/rsos.181309.
[50] S.D. Alexandratos, Ion-Exchange Resins: A Retrospective from Industrial and Engineering Chemistry, Industrial & Engineering Chemistry Research. 48 (2009) 388–398. https://doi.org/10.1021/ie801242v.
[51] M.M. Nasef, Z. Ujang, Introduction to Ion Exchange Processes, in: Inamuddin, M. Luqman (Eds.), Ion Exchange Technology I - Theory and Materials, 1st ed., Springer, 2013: pp. 1–39. https://doi.org/10.1007/978-94-007-1700-8.

[52] W.J. Ripple, C. Wolf, T.M. Newsome, P. Barnard, W.R. Moomaw, World Scientists' Warning of a Climate Emergency, BioScience. 70 (2020) 8–12. https://doi.org/10.1093/biosci/biz088.
[53] E. Papadis, G. Tsatsaronis, Challenges in the decarbonization of the energy sector, Energy. 205 (2020) 1–15. https://doi.org/10.1016/j.energy.2020.118025.
[54] BP, Statistical Review of World Energy, (Report ed. 68), (2019). https://www.bp.com/content/dam/bp/business-sites/en/global/corporate/pdfs/energy-economics/statistical-review/bp-stats-review-2019-full-report.pdf.
[55] International Energy Agency (IEA), World Energy Outlook 2019, 2019. https://www.iea.org/reports/world-energy-outlook-2019%0Ahttps://www.iea.org/reports/world-energy-outlook-2019%0Ahttps://webstore.iea.org/download/summary/2467?fileName=Japanese-Summary-WEO2019.pdf.
[56] H. Ibrahim, A. Ilinca, J. Perron, Energy storage systems-Characteristics and comparisons, Renewable and Sustainable Energy Reviews. 12 (2008) 1221–1250. https://doi.org/10.1016/j.rser.2007.01.023.
[57] H. Chen, T.N. Cong, W. Yang, C. Tan, Y. Li, Y. Ding, Progress in electrical energy storage system: A critical review, Progress in Natural Science. 19 (2009) 291–312. https://doi.org/10.1016/j.pnsc.2008.07.014.
[58] P. Leung, X. Li, C. Ponce De León, L. Berlouis, C.T.J. Low, F.C. Walsh, Progress in redox flow batteries, remaining challenges and their applications in energy storage, RSC Advances. 2 (2012) 10125–10156. https://doi.org/10.1039/c2ra21342g.
[59] M. Ulaganathan, V. Aravindan, Q. Yan, S. Madhavi, M. Skyllas-Kazacos, T.M. Lim, Recent Advancements in All-Vanadium Redox Flow Batteries, Advanced Materials Interfaces. 3 (2016) 1–22. https://doi.org/10.1002/admi.201500309.
[60] K. Lourenssen, J. Williams, F. Ahmadpour, R. Clemmer, S. Tasnim, Vanadium redox flow batteries: A comprehensive review, Journal of Energy Storage. 25 (2019) 2–17. https://doi.org/10.1016/j.est.2019.100844.
[61] M. Ding, T. Liu, Y. Zhang, Investigations of the influences of K+ impurity on the electrolyte for vanadium redox flow battery, Ionics (Kiel). 26 (2020) 3415–3423. https://doi.org/10.1007/s11581-019-03425-3.
[62] G. Kear, A.A. Shah, F.C. Walsh, Development of the all - vanadium redox flow battery for energy storage: a review of technological, financial and policy aspects, International Journal of Energy Research. 36 (2012) 1105–1120. https://doi.org/10.1002/er.1863.
[63] W. Wang, Q. Luo, B. Li, X. Wei, L. Li, Z. Yang, Recent progress in redox flow battery research and development, Advanced Functional Materials. 23 (2013) 970–986. https://doi.org/10.1002/adfm.201200694.
[64] M. Rychcik, M. Skyllas-Kazacos, Characteristics of a new all-vanadium redox flow battery, Journal of Power Sources. 22 (1988) 59–67. https://doi.org/10.1016/0378-7753(88)80005-3.
[65] R. Ye, D. Henkensmeier, S.J. Yoon, Z. Huang, D.K. Kim, Z. Chang, S. Kim, R. Chen, Redox Flow Batteries for Energy Storage: A Technology Review, Journal of Electrochemical Energy Conversion and Storage. 15 (2018) 1–21. https://doi.org/10.1115/1.4037248.
[66] X.Z. Yuan, C. Song, A. Platt, N. Zhao, H. Wang, H. Li, K. Fatih, D. Jang, A review of all-vanadium redox flow battery durability: Degradation mechanisms and mitigation strategies, International Journal of Energy Research. 43 (2019) 6599–6638. https://doi.org/10.1002/er.4607.
[67] W. Lu, X. Li, H. Zhang, The next generation vanadium flow batteries with high power density-A perspective, Physical Chemistry Chemical Physics. 20 (2017) 23–35. https://doi.org/10.1039/c7cp07456e.
[68] N. Roznyatovskaya, J. Noack, K. Pinkwart, J. Tübke, Aspects of electron transfer processes in vanadium redox-flow batteries, Current Opinion in Electrochemistry. 19 (2020) 42–48. https://doi.org/10.1016/j.coelec.2019.10.003.

[69] Y. Shi, C. Eze, B. Xiong, W. He, H. Zhang, T.M. Lim, A. Ukil, J. Zhao, Recent development of membrane for vanadium redox flow battery applications: A review, Applied Energy. 238 (2019) 202–224. https://doi.org/10.1016/j.apenergy.2018.12.087.
[70] T. Liu, X. Li, H. Zhang, J. Chen, Progress on the electrode materials towards vanadium flow batteries (VFBs) with improved power density, Journal of Energy Chemistry. 27 (2018) 1292–1303. https://doi.org/10.1016/j.jechem.2018.07.003.
[71] M. Skyllas-Kazacos, L. Cao, M. Kazacos, N. Kausar, A. Mousa, Vanadium Electrolyte Studies for the Vanadium Redox Battery—A Review, ChemSusChem. 9 (2016) 1521–1543. https://doi.org/10.1002/cssc.201600102.
[72] C. Blanc, A. Rufer, Understanding the Vanadium Redox Flow Batteries, in: J. Nathwani, A.W. Ng (Eds.), Paths to Sustainable Energy, INTECH, India, 2010: pp. 333–358. https://doi.org/10.5772/546.
[73] L. Li, S. Kim, W. Wang, M. Vijayakumar, Z. Nie, B. Chen, J. Zhang, G. Xia, J. Hu, G. Graff, J. Liu, Z. Yang, A stable vanadium redox-flow battery with high energy density for large-scale energy storage, Advanced Energy Materials. 1 (2011) 394–400. https://doi.org/10.1002/aenm.201100008.
[74] Á. Cunha, J. Martins, N. Rodrigues, F.P. Brito, Vanadium redox flow batteries: a technology review, International Journal of Energy Research. 39 (2015) 889–918. https://doi.org/10.1002/er.3260.
[75] M. Bartolozzi, Development of redox flow batteries. A historical bibliography, Journal of Power Sources. 27 (1989) 219–234. https://doi.org/10.1016/0378-7753(89)80037-0.
[76] S. Mehboob, G. Ali, H.J. Shin, J. Hwang, S. Abbas, K.Y. Chung, H.Y. Ha, Enhancing the performance of all-vanadium redox flow batteries by decorating carbon felt electrodes with SnO2 nanoparticles, Applied Energy. 229 (2018) 910–921. https://doi.org/10.1016/j.apenergy.2018.08.047.
[77] F.T. Bacon, Fuel-Cell Stack and System Design, in: T.F. Fuller, J.N. Harb (Eds.), Electrochemical Engineering, John Wiley & Sons, Hoboken, 2018: pp. 223 – 249.
[78] A.L. Dicks, D.A.J. Rand, Introducing Fuel Cells, in: Fuel Cell Systems Explained, John Wiley & Sons, Glasgow, 2018: pp. 1–26.
[79] A. Tang, J. Bao, M. Skyllas-Kazacos, Studies on pressure losses and flow rate optimization in vanadium redox flow battery, Journal of Power Sources. 248 (2014) 154–162. https://doi.org/10.1016/j.jpowsour.2013.09.071.
[80] L. Barelli, G. Bidini, P.A. Ottaviano, D. Pelosi, Vanadium redox flow batteries application to electric buses propulsion: Performance analysis of hybrid energy storage system, Journal of Energy Storage. 24 (2019) 1–9. https://doi.org/10.1016/j.est.2019.100770.
[81] L. Zeng, T.S. Zhao, L. Wei, H.R. Jiang, M.C. Wu, Anion exchange membranes for aqueous acid-based redox flow batteries: Current status and challenges, Applied Energy. 233–234 (2019) 622–643. https://doi.org/10.1016/j.apenergy.2018.10.063.
[82] T. Jirabovornwisut, S. Kheawhom, Y.S. Chen, A. Arpornwichanop, Optimal operational strategy for a vanadium redox flow battery, Computers and Chemical Engineering. 136 (2020) 1–12. https://doi.org/10.1016/j.compchemeng.2020.106805.
[83] W. Xiao, L. Tan, Control strategy optimization of electrolyte flow rate for all vanadium redox flow battery with consideration of pump, Renewable Energy. 133 (2019) 1445–1454. https://doi.org/10.1016/j.renene.2018.09.018.
[84] T. Wang, J. Fu, M. Zheng, Z. Yu, Dynamic control strategy for the electrolyte flow rate of vanadium redox flow batteries, Applied Energy. 227 (2018) 613–623. https://doi.org/10.1016/j.apenergy.2017.07.065.
[85] S. Mehboob, G. Ali, S. Abbas, K.Y. Chung, H.Y. Ha, Elucidating the performance-limiting electrode for all-vanadium redox flow batteries through in-depth physical and electrochemical analyses, Journal of Industrial and Engineering Chemistry. 80 (2019) 450–460. https://doi.org/10.1016/j.jiec.2019.05.045.
[86] M. Arbabzadeh, J.X. Johnson, R. De Kleine, G.A. Keoleian, Vanadium redox flow batteries to reach greenhouse gas emissions targets in an off-grid configuration, Applied Energy. 146 (2015) 397–408. https://doi.org/10.1016/j.apenergy.2015.02.005.

[87] S. Kim, E. Thomsen, G. Xia, Z. Nie, J. Bao, K. Recknagle, W. Wang, V. Viswanathan, Q. Luo, X. Wei, A. Crawford, G. Coffey, G. Maupin, V. Sprenkle, 1 kW/1 kWh advanced vanadium redox flow battery utilizing mixed acid electrolytes, Journal of Power Sources. 237 (2013) 300–309. https://doi.org/10.1016/j.jpowsour.2013.02.045.
[88] S. Han, L. Tan, Thermal and efficiency improvements of all vanadium redox flow battery with novel main-side-tank system and slow pump shutdown, Journal of Energy Storage. 28 (2020) 1–12. https://doi.org/10.1016/j.est.2020.101274.
[89] A.M. Pezeshki, R.L. Sacci, F.M. Delnick, D.S. Aaron, M.M. Mench, Elucidating effects of cell architecture, electrode material, and solution composition on overpotentials in redox flow batteries, Electrochimica Acta. 229 (2017) 261–270. https://doi.org/10.1016/j.electacta.2017.01.056.
[90] K. Geng, H. Tang, Y. Li, L. Liu, N. Li, A facile strategy for disentangling the conductivity and selectivity dilemma enables advanced composite membrane for vanadium flow batteries, Journal of Membrane Science. 607 (2020) 1–10. https://doi.org/10.1016/j.memsci.2020.118177.
[91] J. Balaji, M.G. Sethuraman, S.H. Roh, H.Y. Jung, Recent developments in sol-gel based polymer electrolyte membranes for vanadium redox flow batteries – A review, Polymer Testing. 89 (2020) 1–18. https://doi.org/10.1016/j.polymertesting.2020.106567.
[92] Z.W. Sun, Z.N. Duan, J.Q. Bai, Y. Wang, Numerical study of the performance of all vanadium redox flow battery by changing the cell structure, Journal of Energy Storage. 29 (2020) 1–9. https://doi.org/10.1016/j.est.2020.101370.
[93] F.F. Rivera, C. Ponce De León, F.C. Walsh, J.L. Nava, The reaction environment in a filter-press laboratory reactor: The FM01-LC flow cell, Electrochimica Acta. 161 (2015) 436–452. https://doi.org/10.1016/j.electacta.2015.02.161.
[94] S. Kumar, S. Jayanti, Effect of flow field on the performance of an all-vanadium redox flow battery, Journal of Power Sources. 307 (2016) 782–787. https://doi.org/10.1016/j.jpowsour.2016.01.048.
[95] J.W. Lim, D.G. Lee, Carbon fiber/polyethylene bipolar plate-carbon felt electrode assembly for vanadium redox flow batteries (VRFB), Composite Structures. 134 (2015) 483–492. https://doi.org/10.1016/j.compstruct.2015.08.057.
[96] B.W. Zhang, Y. Lei, B.F. Bai, T.S. Zhao, A two-dimensional model for the design of flow fields in vanadium redox flow batteries, International Journal of Heat and Mass Transfer. 135 (2019) 460–469. https://doi.org/10.1016/j.ijheatmasstransfer.2019.02.008.
[97] X. Ma, Vanadium Flow Batteries: Stacks and Systems, in: H. Zhang, X. Li, J. Zhang (Eds.), Redox Flow Batteries (Fundamentals and Applications), CRC Press, 2018: pp. 267–305.
[98] A. Pellegri, B.M. Broman, Redox Flow Battery System and Cell Stack, US 6,475,661 B1, 2002.
[99] C.R. Horne, K. Kinoshita, D.B. Hickley, Redox Flow Battery System for Distributed Energy Storage, US 7820,321 B2, 2010.
[100] S. Maeda, J. Sugawara, H. Hayami, Bipolar Plate for Redox Flow Battery, US 2013/0037760 A1, 2013.
[101] P. Lex, N. Coad, Battery Flow Frame Material Formulation, US 2014/0162096 A1, 2014.
[102] M. Al-Yasiri, J. Park, A novel cell design of vanadium redox flow batteries for enhancing energy and power performance, Applied Energy. 222 (2018) 530–539. https://doi.org/10.1016/j.apenergy.2018.04.025.
[103] J. Houser, A. Pezeshki, J.T. Clement, D. Aaron, M.M. Mench, Architecture for improved mass transport and system performance in redox flow batteries, Journal of Power Sources. 351 (2017) 96–105. https://doi.org/10.1016/j.jpowsour.2017.03.083.
[104] S. Maurya, P.T. Nguyen, Y.S. Kim, Q. Kang, R. Mukundan, Effect of flow field geometry on operating current density, capacity and performance of vanadium redox

flow battery, Journal of Power Sources. 404 (2018) 20–27. https://doi.org/10.1016/j.jpowsour.2018.09.093.
[105] Z. Liu, Y. Zou, Vanadium Flow Batteries (Principles, Characteristics, Structure, Evaluation), in: H. Zhang, X. Li, J. Zhang (Eds.), Redox Flow Batteries (Fundamentals and Applications), CRC Press, Boca Raton, 2018: pp. 77–125.
[106] M. Skyllas-Kazacos, C. Menictas, M. Kazacos, Thermal Stability of Concentrated V(V) Electrolytes in the Vanadium Redox Cell, Journal of The Electrochemical Society. 143 (1996) L86–L88. https://doi.org/10.1149/1.1836609.
[107] X. Wu, J. Liu, X. Xiang, J. Zhang, J. Hu, Y. Wu, Electrolytes for vanadium redox flow batteries, Pure and Applied Chemistry. 86 (2014) 661–669. https://doi.org/10.1515/pac-2013-1213.
[108] J.D. Milshtein, R.M. Darling, J. Drake, M.L. Perry, F.R. Brushett, The Critical Role of Supporting Electrolyte Selection on Flow Battery Cost, Journal of The Electrochemical Society. 164 (2017) A3883–A3895. https://doi.org/10.1149/2.1031714jes.
[109] S. Peng, N.F. Wang, X.J. Wu, S.Q. Liu, D. Fang, Y.N. Liu, K.L. Huang, Vanadium species in CH 3SO 3H and H 2SO 4 mixed acid as the supporting electrolyte for vanadium redox flow battery, International Journal of Electrochemical Science. 7 (2012) 643–649.
[110] M.H. Chakrabarti, R.A.W. Dryfe, E.P.L. Roberts, Evaluation of electrolytes for redox flow battery applications, Electrochimica Acta. 52 (2007) 2189–2195. https://doi.org/10.1016/j.electacta.2006.08.052.
[111] C. Ding, H. Zhang, X. Li, T. Liu, F. Xing, Vanadium flow battery for energy storage: Prospects and challenges, Journal of Physical Chemistry Letters. 4 (2013) 1281–1294. https://doi.org/10.1021/jz4001032.
[112] F. Rahman, M. Skyllas-Kazacos, Solubility of vanadyl sulfate in concentrated sulfuric acid solutions, Journal of Power Sources. 72 (1998) 105–110. https://doi.org/10.1016/S0378-7753(97)02692-X.
[113] S. Kim, M. Vijayakumar, W. Wang, J. Zhang, B. Chen, Z. Nie, F. Chen, J. Hu, L. Li, Z. Yang, Chloride supporting electrolytes for all-vanadium redox flow batteries, Physical Chemistry Chemical Physics. 13 (2011) 18186–18193. https://doi.org/10.1039/c1cp22638j.
[114] Q. Liu, A.E.S. Sleightholme, A.A. Shinkle, Y. Li, L.T. Thompson, Non-aqueous vanadium acetylacetonate electrolyte for redox flow batteries, Electrochemistry Communications. 11 (2009) 2312–2315. https://doi.org/10.1016/j.elecom.2009.10.006.
[115] D.N. Buckley, C. O'Dwyer, N. Quill, R.P. Lynch, Electrochemical Energy Storage, in: R.E. Hester, R.M. Harrison (Eds.), Energy Storage Options and Their Environmental Impact, The Royal Society of Chemistry, Croydon, 2018: pp. 115–149. https://doi.org/10.1039/9781788015530-00115.
[116] S. Kim, Vanadium Redox Flow Batteries: Electrochemical Engineering, in: M.T. Demirkan, A. Attia (Eds.), Energy Storage Devices, IntechOpen, 2019. https://doi.org/10.5772/intechopen.85166.
[117] Y. Wu, R. Holze, Electrocatalysis at electrodes for vanadium redox flow batteries, Batteries. 4 (2018) 1–62. https://doi.org/10.3390/batteries4030047.
[118] J. Friedl, U. Stimming, Determining Electron Transfer Kinetics at Porous Electrodes, Electrochimica Acta. 227 (2017) 235–245. https://doi.org/10.1016/j.electacta.2017.01.010.
[119] M.A. Goulet, M. Eikerling, E. Kjeang, Direct measurement of electrochemical reaction kinetics in flow-through porous electrodes, Electrochemistry Communications. 57 (2015) 14–17. https://doi.org/10.1016/j.elecom.2015.04.019.
[120] M. Skyllas-Kazacos, F. Grossmith, Efficient Vanadium Redox Flow Cell, Journal of The Electrochemical Society. 134 (1987) 2950–2953. https://doi.org/10.1149/1.2100321.
[121] G.L. Soloveichik, Flow Batteries: Current Status and Trends, Chemical Reviews. 115 (2015) 11533–11558. https://doi.org/10.1021/cr500720t.

[122] K.W. Knehr, E.C. Kumbur, Open circuit voltage of vanadium redox flow batteries: Discrepancy between models and experiments, Electrochemistry Communications. 13 (2011) 342–345. https://doi.org/10.1016/j.elecom.2011.01.020.
[123] M. Pavelka, F. Wandschneider, P. Mazur, Thermodynamic derivation of open circuit voltage in vanadium redox flow batteries, Journal of Power Sources. 293 (2015) 400–408. https://doi.org/10.1016/j.jpowsour.2015.05.049.
[124] N. Roznyatovskaya, J. Noack, M. Fühl, K. Pinkwart, J. Tübke, Towards an all-vanadium redox-flow battery electrolyte: electrooxidation of V(III) in V(IV)/V(III) redox couple, Electrochimica Acta. 211 (2016) 926–932. https://doi.org/10.1016/j.electacta.2016.06.073.
[125] K.E. Rodby, T.J. Carney, Y.A. Gandomi, J.L. Barton, R.M. Darling, F.R. Brushett, Assessing the levelized cost of vanadium redox flow batteries with capacity fade and rebalancing, Journal of Power Sources. 460 (2020) 227958. https://doi.org/10.1016/j.jpowsour.2020.227958.
[126] E. Agar, K.W. Knehr, D. Chen, M.A. Hickner, E.C. Kumbur, Species transport mechanisms governing capacity loss in vanadium flow batteries: Comparing Nafion® and sulfonated Radel membranes, Electrochimica Acta. 98 (2013) 66–74. https://doi.org/10.1016/j.electacta.2013.03.030.
[127] C. Sun, J. Chen, H. Zhang, X. Han, Q. Luo, Investigations on transfer of water and vanadium ions across Nafion membrane in an operating vanadium redox flow battery, Journal of Power Sources. 195 (2010) 890–897. https://doi.org/10.1016/j.jpowsour.2009.08.041.
[128] J. Sun, D. Shi, H. Zhong, X. Li, H. Zhang, Investigations on the self-discharge process in vanadium flow battery, Journal of Power Sources. 294 (2015) 562–568. https://doi.org/10.1016/j.jpowsour.2015.06.123.
[129] J. Sun, X. Li, X. Xi, Q. Lai, T. Liu, H. Zhang, The transfer behavior of different ions across anion and cation exchange membranes under vanadium flow battery medium, Journal of Power Sources. 271 (2014) 1–7. https://doi.org/10.1016/j.jpowsour.2014.07.111.
[130] L. Cao, A. Kronander, A. Tang, D.W. Wang, M. Skyllas-Kazacos, Membrane permeability rates of vanadium ions and their effects on temperature variation in vanadium redox batteries, Energies (Basel). 9 (2016) 1–15. https://doi.org/10.3390/en9121058.
[131] T.D. Nguyen, A. Whitehead, N. Wai, S.J.H. Ong, G.G. Scherer, Z.J. Xu, Equilibrium and Dynamic Absorption of Electrolyte Species in Cation/Anion Exchange Membranes of Vanadium Redox Flow Batteries, ChemSusChem. 12 (2019) 1076–1083. https://doi.org/10.1002/cssc.201802522.
[132] E. Wiedemann, A. Heintz, R.N. Lichtenthaler, Transport properties of vanadium ions in cation exchange membranes: Determination of diffusion coefficients using a dialysis cell, Journal of Membrane Science. 141 (1998) 215–221. https://doi.org/10.1016/S0376-7388(97)00308-6.
[133] J.Q. Chen, B.G. Wang, J.C. Yang, Adsorption and diffusion of VO2+ and VO2+ across cation membrane for all-vanadium redox flow battery, Solvent Extraction and Ion Exchange. 27 (2009) 312–327. https://doi.org/10.1080/07366290802674614.
[134] X.G. Yang, Q. Ye, P. Cheng, T.S. Zhao, Effects of the electric field on ion crossover in vanadium redox flow batteries, Applied Energy. 145 (2015) 306–319. https://doi.org/10.1016/j.apenergy.2015.02.038.
[135] M. Gattrell, J. Park, B. MacDougall, J. Apte, S. McCarthy, C.W. Wu, Study of the Mechanism of the Vanadium 4+/5+ Redox Reaction in Acidic Solutions, Journal of The Electrochemical Society. 151 (2004) A123–A130. https://doi.org/10.1149/1.1630594.
[136] L. Eifert, R. Banerjee, Z. Jusys, R. Zeis, Characterization of Carbon Felt Electrodes for Vanadium Redox Flow Batteries: Impact of Treatment Methods, Journal of The Electrochemical Society. 165 (2018) A2577–A2586. https://doi.org/10.1149/2.0531811jes.

[137] L. Eifert, Z. Jusys, R.J. Behm, R. Zeis, Side reactions and stability of pre-treated carbon felt electrodes for vanadium redox flow batteries: A DEMS study, Carbon N Y. 158 (2020) 580–587. https://doi.org/10.1016/j.carbon.2019.11.029.
[138] A. Fetyan, G.A. El-Nagar, I. Lauermann, M. Schnucklake, J. Schneider, C. Roth, Detrimental role of hydrogen evolution and its temperature-dependent impact on the performance of vanadium redox flow batteries, Journal of Energy Chemistry. 32 (2019) 57–62. https://doi.org/10.1016/j.jechem.2018.06.010.
[139] A.A. Shah, H. Al-Fetlawi, F.C. Walsh, Dynamic modelling of hydrogen evolution effects in the all-vanadium redox flow battery, Electrochimica Acta. 55 (2010) 1125–1139. https://doi.org/10.1016/j.electacta.2009.10.022.
[140] C.N. Sun, F.M. Delnick, L. Baggetto, G.M. Veith, T.A. Zawodzinski, Hydrogen evolution at the negative electrode of the all-vanadium redox flow batteries, Journal of Power Sources. 248 (2014) 560–564. https://doi.org/10.1016/j.jpowsour.2013.09.125.
[141] H. Kabir, I.O. Gyan, I.F. Cheng, Electrochemical modification of a pyrolytic graphite sheet for improved negative electrode performance in the vanadium redox flow battery, Journal of Power Sources. 342 (2017) 31–37. https://doi.org/10.1016/j.jpowsour.2016.12.045.
[142] R. Schweiss, A. Pritzl, C. Meiser, Parasitic Hydrogen Evolution at Different Carbon Fiber Electrodes in Vanadium Redox Flow Batteries, Journal of The Electrochemical Society. 163 (2016) A2089–A2094. https://doi.org/10.1149/2.1281609jes.
[143] A.H. Whitehead, M. Harrer, Investigation of a method to hinder charge imbalance in the vanadium redox flow battery, Journal of Power Sources. 230 (2013) 271–276. https://doi.org/10.1016/j.jpowsour.2012.11.148.
[144] L. Wei, T.S. Zhao, Q. Xu, X.L. Zhou, Z.H. Zhang, In-situ investigation of hydrogen evolution behavior in vanadium redox flow batteries, Applied Energy. 190 (2017) 1112–1118. https://doi.org/10.1016/j.apenergy.2017.01.039.
[145] E. Agar, C.R. Dennison, K.W. Knehr, E.C. Kumbur, Identification of performance limiting electrode using asymmetric cell configuration in vanadium redox flow batteries, Journal of Power Sources. 225 (2013) 89–94. https://doi.org/10.1016/j.jpowsour.2012.10.016.
[146] F. Chen, J. Liu, H. Chen, C. Yan, Study on hydrogen evolution reaction at a graphite electrode in the all-vanadium redox flow battery, International Journal of Electrochemical Science. 7 (2012) 3750–3764.
[147] D.J. Suárez, Z. González, C. Blanco, M. Granda, R. Menéndez, R. Santamaría, Graphite felt modified with bismuth nanoparticles as negative electrode in a vanadium redox flow battery, ChemSusChem. 7 (2014) 914–918. https://doi.org/10.1002/cssc.201301045.
[148] J. Piwek, C.R. Dennison, E. Frackowiak, H. Girault, A. Battistel, Vanadium-oxygen cell for positive electrolyte discharge in dual-circuit vanadium redox flow battery, Journal of Power Sources. 439 (2019) 227075. https://doi.org/10.1016/j.jpowsour.2019.227075.
[149] P. Peljo, H. Vrubel, V. Amstutz, J. Pandard, J. Morgado, A. Santasalo-Aarnio, D. Lloyd, F. Gumy, C.R. Dennison, K.E. Toghill, H.H. Girault, All-vanadium dual circuit redox flow battery for renewable hydrogen generation and desulfurisation, Green Chemistry. 18 (2016) 1785–1797. https://doi.org/10.1039/c5gc02196k.
[150] C.R. Dennison, H. Vrubel, V. Amstutz, P. Peljo, K.E. Toghill, H.H. Girault, Redox flow batteries, hydrogen and distributed storage, Chimia (Aarau). 69 (2015) 753–758. https://doi.org/10.2533/chimia.2015.753.
[151] V. Amstutz, K.E. Toghill, F. Powlesland, H. Vrubel, C. Comninellis, X. Hu, H.H. Girault, Renewable hydrogen generation from a dual-circuit redox flow battery, Energy and Environmental Science. 7 (2014) 2350–2358. https://doi.org/10.1039/c4ee00098f.
[152] H. Al-Fetlawi, A.A. Shah, F.C. Walsh, Modelling the effects of oxygen evolution in the all-vanadium redox flow battery, Electrochimica Acta. 55 (2010) 3192–3205. https://doi.org/10.1016/j.electacta.2009.12.085.

[153] F. Zhang, S. Huang, X. Wang, C. Jia, Y. Du, Q. Wang, Redox-targeted catalysis for vanadium redox-flow batteries, Nano Energy. 52 (2018) 292–299. https://doi.org/10.1016/j.nanoen.2018.07.058.
[154] S. Corcuera, M. Skyllas-Kazacos, State-of-Charge Monitoring and Electrolyte Rebalancing Methods for the Vanadium Redox Flow Battery, European Chemical Bulletin. 1 (2012) 511–519. https://doi.org/10.17628/ECB.2012.1.511.
[155] H. Liu, Q. Xu, C. Yan, Y. Qiao, Corrosion behavior of a positive graphite electrode in vanadium redox flow battery, Electrochimica Acta. 56 (2011) 8783–8790. https://doi.org/10.1016/j.electacta.2011.07.083.
[156] Z. Wei, A. Bhattarai, C. Zou, S. Meng, T.M. Lim, M. Skyllas-Kazacos, Real-time monitoring of capacity loss for vanadium redox flow battery, Journal of Power Sources. 390 (2018) 261–269. https://doi.org/10.1016/j.jpowsour.2018.04.063.
[157] N. Roznyatovskaya, T. Herr, M. Küttinger, M. Fühl, J. Noack, K. Pinkwart, J. Tübke, Detection of capacity imbalance in vanadium electrolyte and its electrochemical regeneration for all-vanadium redox-flow batteries, Journal of Power Sources. 302 (2016) 79–83. https://doi.org/10.1016/j.jpowsour.2015.10.021.
[158] T. Jirabovornwisut, A. Arpornwichanop, A review on the electrolyte imbalance in vanadium redox flow batteries, International Journal of Hydrogen Energy. 44 (2019) 24485–24509. https://doi.org/10.1016/j.ijhydene.2019.07.106.
[159] S. Tong, M.P. Klein, J.W. Park, On-line optimization of battery open circuit voltage for improved state-of-charge and state-of-health estimation, Journal of Power Sources. 293 (2015) 416–428. https://doi.org/10.1016/j.jpowsour.2015.03.157.
[160] K. Beyer, J. g Austing, B. Satola, T.D. Nardo, M. Zobel, C. Agert, Electrolyte Imbalance Determination of a Vanadium Redox Flow Battery by Potential-Step Analysis of the Initial Charging, ChemSusChem. 13 (2020) 2066–2071. https://doi.org/10.1002/cssc.201903485.
[161] D.N. Buckley, X. Gao, R.P. Lynch, N. Quill, M.J. Leahy, Towards Optical Monitoring of Vanadium Redox Flow Batteries (VRFBs): An Investigation of the Underlying Spectroscopy, Journal of The Electrochemical Society. 161 (2014) A524–A534. https://doi.org/10.1149/2.023404jes.
[162] Z. Tang, D.S. Aaron, A.B. Papandrew, T.A. Zawodzinski, Monitoring the State of Charge of Operating Vanadium Redox Flow Batteries, ECS Transactions. 41 (2019) 1–9. https://doi.org/10.1149/1.3697449.
[163] R.P. Brooker, C.J. Bell, L.J. Bonville, H.R. Kunz, J.M. Fenton, Determining Vanadium Concentrations Using the UV-Vis Response Method, Journal of The Electrochemical Society. 162 (2015) A608–A613. https://doi.org/10.1149/2.0371504jes.
[164] S. Rudolph, U. Schröder, I.M. Bayanov, On-line controlled state of charge rebalancing in vanadium redox flow battery, Journal of Electroanalytical Chemistry. 703 (2013) 29–37. https://doi.org/10.1016/j.jelechem.2013.05.011.
[165] A. Habekost, Vanadium Redox Flow Batteries with Different Electrodes and Membranes, World Journal of Chemical Education. 6 (2018) 8–13. https://doi.org/10.12691/wjce-6-1-2.
[166] Z. Yang, J. Zhang, M.C.W. Kintner-Meyer, X. Lu, D. Choi, J.P. Lemmon, J. Liu, Electrochemical energy storage for green grid, Chemical Reviews. 111 (2011) 3577–3613. https://doi.org/10.1021/cr100290v.
[167] M. Vijayakumar, L. Li, G. Graff, J. Liu, H. Zhang, Z. Yang, J.Z. Hu, Towards understanding the poor thermal stability of V5+ electrolyte solution in Vanadium Redox Flow Batteries, Journal of Power Sources. 196 (2011) 3669–3672. https://doi.org/10.1016/j.jpowsour.2010.11.126.
[168] F. Rahman, M. Skyllas-Kazacos, Vanadium redox battery: Positive half-cell electrolyte studies, Journal of Power Sources. 189 (2009) 1212–1219. https://doi.org/10.1016/j.jpowsour.2008.12.113.
[169] C. Ding, X. Ni, X. Li, X. Xi, X. Han, X. Bao, H. Zhang, Effects of phosphate additives on the stability of positive electrolytes for vanadium flow batteries, Electrochimica Acta. 164 (2015) 307–314. https://doi.org/10.1016/j.electacta.2015.02.187.

[170] M. Skyllas-Kazacos, J.F. McCann, Vanadium redox flow batteries (VRBs) for medium- and large-scale energy storage, in: C. Menictas, M. Skyllas-Kazacos, T.M. Lim (Eds.), Advances in Batteries for Medium and Large-Scale Energy Storage, Elsevier, United Kingdom, 2015: pp. 329–386. https://doi.org/10.1016/B978-1-78242-013-2.00010-8.
[171] S. Roe, C. Menictas, M. Skyllas-Kazacos, A High Energy Density Vanadium Redox Flow Battery with 3 M Vanadium Electrolyte, Journal of The Electrochemical Society. 163 (2016) A5023–A5028. https://doi.org/10.1149/2.0041601jes.
[172] A. Mousa, M. Skyllas-Kazacos, Kinetics of VIII and VII Sulfate Precipitation Processes in Negative Half-Cell Electrolyte of the Vanadium Redox Flow Battery, ChemElectroChem. 4 (2017) 130–142. https://doi.org/10.1002/celc.201600426.
[173] W. Chen, J. Kang, Optimization of electrolyte flow and vanadium ions conversion by utilizing variable porosity electrodes in vanadium redox flow batteries, Chemical Physics. 529 (2020) 1–14. https://doi.org/10.1016/j.chemphys.2019.110577.
[174] S.J. Yoon, S. Kim, D.K. Kim, Optimization of local porosity in the electrode as an advanced channel for all-vanadium redox flow battery, Energy. 172 (2019) 26–35. https://doi.org/10.1016/j.energy.2019.01.101.
[175] L. Wei, L. Zeng, M.C. Wu, X.Z. Fan, T.S. Zhao, Seawater as an alternative to deionized water for electrolyte preparations in vanadium redox flow batteries, Applied Energy. 251 (2019) 1–8. https://doi.org/10.1016/j.apenergy.2019.113344.
[176] X. Ma, H. Zhang, C. Sun, Y. Zou, T. Zhang, An optimal strategy of electrolyte flow rate for vanadium redox flow battery, Journal of Power Sources. 203 (2012) 153–158. https://doi.org/10.1016/j.jpowsour.2011.11.036.
[177] M. Skyllas-Kazacos, C. Menictas, T. Lim, Redox flow batteries for medium- to large-scale energy storage, in: Z. Melhem (Ed.), Electricity Transmission, Distribution and Storage Systems, Elsevier, 2013: pp. 398–441. https://doi.org/10.1533/9780857097378.3.398.
[178] A. Khazaeli, A. Vatani, N. Tahouni, M.H. Panjeshahi, Numerical investigation and thermodynamic analysis of the effect of electrolyte flow rate on performance of all vanadium redox flow batteries, Journal of Power Sources. 293 (2015) 599–612. https://doi.org/10.1016/j.jpowsour.2015.05.100.
[179] V. Murugesan, Key Materials of Vanadium Flow Batteries: Electrolytes, in: H. Zhang, X. Li, J. Zhang (Eds.), Redox Flow Batteries (Fundamentals and Applications), CRC Press, Boca Raton, 2018: pp. 217–238.
[180] W. Li, R. Zaffou, C.C. Sholvin, M.L. Perry, Y. She, Vanadium Redox-Flow-Battery Electrolyte Preparation with Reducing Agents, ECS Transactions. 53 (2013) 93–99. https://doi.org/10.1149/05307.0093ecst.
[181] M. Skyllas-Kazacos, Vanadium redox battery electrolyte, US 2004/0241552 A1, 2004.
[182] K. Ngamsai, A. Arpornwichanop, Analysis and measurement of the electrolyte imbalance in a vanadium redox flow battery, Journal of Power Sources. 282 (2015) 534–543. https://doi.org/10.1016/j.jpowsour.2015.01.188.
[183] M. Dassisti, G. Cozzolino, M. Chimienti, A. Rizzuti, P. Mastrorilli, P. L'Abbate, Sustainability of vanadium redox-flow batteries: Benchmarking electrolyte synthesis procedures, International Journal of Hydrogen Energy. 41 (2016) 16477–16488. https://doi.org/10.1016/j.ijhydene.2016.05.197.
[184] T. Sukkar, M. Skyllas-Kazacos, Water transfer behaviour across cation exchange membranes in the vanadium redox battery, Journal of Membrane Science. 222 (2003) 235–247. https://doi.org/10.1016/S0376-7388(03)00309-0.
[185] F. Chang, C. Hu, X. Liu, L. Liu, J. Zhang, Coulter dispersant as positive electrolyte additive for the vanadium redox flow battery, Electrochimica Acta. 60 (2012) 334–338. https://doi.org/10.1016/j.electacta.2011.11.065.
[186] M. Skyllas-Kazacos, M. Kazacos, Vanadium compound dissolution process, WO 89/05363, 1989.
[187] M. Skyllas-Kazacos, G. Kazacos, G. Poon, H. Verseema, Recent advances with UNSW vanadium-based redox flow batteries, International Journal of Energy Research. 34 (2010) 182–189. https://doi.org/10.1002/er.1658.

[188] K. Ngamsai, A. Arpornwichanop, Study on mechanism and kinetic of air oxidation of V(II) in electrolyte reservoir of a vanadium redox flow battery, Energy Procedia. 61 (2014) 1642–1645. https://doi.org/10.1016/j.egypro.2014.12.182.
[189] M. Skyllas-Kazacos, M. Kazacos, State of charge monitoring methods for vanadium redox flow battery control, Journal of Power Sources. 196 (2011) 8822–8827. https://doi.org/10.1016/j.jpowsour.2011.06.080.
[190] M. Jing, Z. Wei, W. Su, H. He, X. Fan, Y. Qin, J. Liu, C. Yan, Improved electrochemical performance for vanadium flow battery by optimizing the concentration of the electrolyte, Journal of Power Sources. 324 (2016) 215–223. https://doi.org/10.1016/j.jpowsour.2016.05.099.
[191] M.R. Mohamed, P.K. Leung, M.H. Sulaiman, Performance characterization of a vanadium redox flow battery at different operating parameters under a standardized test-bed system, Applied Energy. 137 (2015) 402–412. https://doi.org/10.1016/j.apenergy.2014.10.042.
[192] A.A. Shah, M.J. Watt-Smith, F.C. Walsh, A dynamic performance model for redox-flow batteries involving soluble species, Electrochimica Acta. 53 (2008) 8087–8100. https://doi.org/10.1016/j.electacta.2008.05.067.
[193] M. Kazacos, M. Cheng, M. Skyllas-Kazacos, Vanadium redox cell electrolyte optimization studies, Journal of Applied Electrochemistry. 20 (1990) 463–467. https://doi.org/10.1007/BF01076057.
[194] Y. Wen, Y. Xu, J. Cheng, G. Cao, Y. Yang, Investigation on the stability of electrolyte in vanadium flow batteries, Electrochimica Acta. 96 (2013) 268–273. https://doi.org/10.1016/j.electacta.2013.02.091.
[195] R. Islam, C. Nolen, K. Jeong, Effects of sulfuric acid concentration on volume transfer across ionexchange membrane in a single-cell vanadium redox flow battery, in: ASME International Mechanical Engineering Congress and Exposition, Proceedings (IMECE), Tampa, Florida - USA, 2017: pp. 1–8. https://doi.org/10.1115/IMECE2017-72359.
[196] R. Gilligan, A.N. Nikoloski, The extraction of vanadium from titanomagnetites and other sources, Minerals Engineering. 146 (2020) 1–18. https://doi.org/10.1016/j.mineng.2019.106106.
[197] M. Nakajima, T. Akahoshi, M. Sawahala, Y. Nomura, K. Sato, Method for producing high purity vanadium electrolytic solution, US 5,879,132, 1996.
[198] M. Kubata, O. Nakaishi, T. Nobuyuki, Electrolyte for redox flow battery, and redox flow battery, US 7,258,947 B2, 2007.
[199] A.W. Burch, Impurity Effects in All-Vanadium Redox Flow Batteries, University of Tennessee, 2015.
[200] F. Huang, Q. Zhao, C.H. Luo, G.X. Wang, K.P. Yan, D.M. Luo, Influence of Cr3+ concentration on the electrochemical behavior of the anolyte for vanadium redox flow batteries, Chinese Science Bulletin. 57 (2012) 4237–4243. https://doi.org/10.1007/s11434-012-5302-0.
[201] F. Huang, G. Wang, K.-P. Yan, D.-M. Luo, Influence of Mn2+ concentration on the electrochemical behavior of the anolyte for vanadium redox flow batteries., Chinese Journal of Inorganic Chemistry. 28 (2012) 898–904.
[202] Z. He, L. Chen, Y. He, C. Chen, Y. Jiang, Z. He, S. Liu, Effect of In3+ ions on the electrochemical performance of the positive electrolyte for vanadium redox flow batteries, Ionics (Kiel). 19 (2013) 1915–1920. https://doi.org/10.1007/s11581-013-0945-7.
[203] K.J. Kim, M.S. Park, Y.J. Kim, J.H. Kim, S.X. Dou, M. Skyllas-Kazacos, A technology review of electrodes and reaction mechanisms in vanadium redox flow batteries, Journal of Materials Chemistry A. 3 (2015) 16913–16933. https://doi.org/10.1039/c5ta02613j.
[204] C. Ponce de León, A. Frías-Ferrer, J. González-García, D.A. Szánto, F.C. Walsh, Redox flow cells for energy conversion, Journal of Power Sources. 160 (2006) 716–732. https://doi.org/10.1016/j.jpowsour.2006.02.095.

[205] J. Shen, S. Liu, Z. He, L. Shi, Influence of antimony ions in negative electrolyte on the electrochemical performance of vanadium redox flow batteries, Electrochimica Acta. 151 (2015) 297–305. https://doi.org/10.1016/j.electacta.2014.11.060.
[206] E. Sum, M. Skyllas-Kazacos, A study of the V(II)/V(III) redox couple for redox flow cell applications, Journal of Power Sources. 15 (1985) 179–190. https://doi.org/10.1016/0378-7753(85)80071-9.
[207] E. Sum, M. Rychcik, M. Skyllas-kazacos, Investigation of the V(V)/V(IV) system for use in the positive half-cell of a redox battery, Journal of Power Sources. 16 (1985) 85–95. https://doi.org/10.1016/0378-7753(85)80082-3.
[208] M. Skyllas-Kazacos, M. Rychcik, R.G. Robins, A.G. Fane, M.A. Green, New All − Vanadium Redox Flow Cell New All-Vanadium Redox Flow Cell, Journal of Electrochemical Society. 133 (1986) 1057–1058.
[209] M. Rychcik, M. Skyllas-Kazacos, Evaluation of electrode materials for vanadium redox cell, Journal of Power Sources. 19 (1987) 45–54. https://doi.org/10.1016/0378-7753(87)80006-X.
[210] S. Zhong, M. Skyllas-Kazacos, Electrochemical behaviour of vanadium(V)/vanadium(IV) redox couple at graphite electrodes, Journal of Power Sources. 39 (1992) 1–9. https://doi.org/10.1016/0378-7753(92)85001-Q.
[211] F. Mohammadi, P. Timbrell, S. Zhong, C. Padeste, M. Skyllas-Kazacos, Overcharge in the vanadium redox battery and changes in electrical resistivity and surface functionality of graphite-felt electrodes, Journal of Power Sources. 52 (1994) 61–68. https://doi.org/10.1016/0378-7753(94)01938-X.
[212] S. Zhong, C. Padeste, M. Kazacos, M. Skyllas-Kazacos, Comparison of the physical, chemical and electrochemical properties of rayon- and polyacrylonitrile-based graphite felt electrodes, Journal of Power Sources. 45 (1993) 29–41. https://doi.org/10.1016/0378-7753(93)80006-B.
[213] X. Li, K. Huang, S. Liu, N. Tan, L. Chen, Characteristics of graphite felt electrode electrochemically oxidized for vanadium redox battery application, Transactions of Nonferrous Metals Society of China (English Edition). 17 (2007) 195–199. https://doi.org/10.1016/S1003-6326(07)60071-5.
[214] T. Wu, K. Huang, S. Liu, S. Zhuang, D. Fang, S. Li, D. Lu, A. Su, Hydrothermal ammoniated treatment of PAN-graphite felt for vanadium redox flow battery, Journal of Solid State Electrochemistry. 16 (2012) 579–585. https://doi.org/10.1007/s10008-011-1383-y.
[215] P. Han, H. Wang, Z. Liu, X. Chen, W. Ma, J. Yao, Y. Zhu, G. Cui, Graphene oxide nanoplatelets as excellent electrochemical active materials for VO2+/VO2+ and V2+/V3+ redox couples for a vanadium redox flow battery, Carbon N Y. 49 (2011) 693–700. https://doi.org/10.1016/j.carbon.2010.10.022.
[216] B. Sun, M. Skyllas-Kazacos, Modification of graphite electrode materials for vanadium redox flow battery application-I. Thermal treatment, Electrochimica Acta. 37 (1992) 1253–1260. https://doi.org/10.1016/0013-4686(92)85064-R.
[217] J. Noack, J. Tübke, A Comparison of Materials and Treatment of Materials for Vanadium Redox Flow Battery, ECS Transactions. 25 (2019) 235–245. https://doi.org/10.1149/1.3414022.
[218] A.M. Pezeshki, J.T. Clement, G.M. Veith, T.A. Zawodzinski, M.M. Mench, High performance electrodes in vanadium redox flow batteries through oxygen-enriched thermal activation, Journal of Power Sources. 294 (2015) 333–338. https://doi.org/10.1016/j.jpowsour.2015.05.118.
[219] Z. He, L. Shi, J. Shen, Z. He, S. Liu, Effects of nitrogen doping on the electrochemical performance of graphite felts for vanadium redox flow batteries, International Journal of Energy Research. 39 (2015) 709–716. https://doi.org/10.1002/er.3291.
[220] H.J. Lee, D. Kil, H. Kim, Synthesis of Activated Graphite Felt Using Consecutive Post-Treatments for Vanadium Redox Flow Batteries, Journal of The Electrochemical Society. 163 (2016) A2586–A2591. https://doi.org/10.1149/2.0531613jes.

[221] A.M. Schwenke, T. Janoschka, C. Stolze, N. Martin, S. Hoeppener, U.S. Schubert, Microwave-assisted preparation of carbon nanofiber-functionalized graphite felts as electrodes for polymer-based redox-flow batteries, Journal of Power Sources. 335 (2016) 155–161. https://doi.org/10.1016/j.jpowsour.2016.09.121.
[222] D. Dixon, D.J. Babu, J. Langner, M. Bruns, L. Pfaffmann, A. Bhaskar, J.J. Schneider, F. Scheiba, H. Ehrenberg, Effect of oxygen plasma treatment on the electrochemical performance of the rayon and polyacrylonitrile based carbon felt for the vanadium redox flow battery application, Journal of Power Sources. 332 (2016) 240–248. https://doi.org/10.1016/j.jpowsour.2016.09.070.
[223] Z. He, Y. Jiang, Y. Li, L. Wang, L. Dai, Boosting the electrocatalytic performance of carbon nanotubes toward V(V)/V(IV) reaction by sulfonation treatment, International Journal of Energy Research. 42 (2018) 1625–1634. https://doi.org/10.1002/er.3958.
[224] J. Friedl, C.M. Bauer, A. Rinaldi, U. Stimming, Electron transfer kinetics of the VO 2 + / VO 2 + - Reaction on multi-walled carbon nanotubes, Carbon N Y. 63 (2013) 228–239. https://doi.org/10.1016/j.carbon.2013.06.076.
[225] A. Di Blasi, O. Di Blasi, N. Briguglio, A.S. Aricò, D. Sebastián, M.J. Lázaro, G. Monforte, V. Antonucci, Investigation of several graphite-based electrodes for vanadium redox flow cell, Journal of Power Sources. 227 (2013) 15–23. https://doi.org/10.1016/j.jpowsour.2012.10.098.
[226] L. Wei, T.S. Zhao, G. Zhao, L. An, L. Zeng, A high-performance carbon nanoparticle-decorated graphite felt electrode for vanadium redox flow batteries, Applied Energy. 176 (2016) 74–79. https://doi.org/10.1016/j.apenergy.2016.05.048.
[227] I. Mustafa, A. Al Shehhi, A. Al Hammadi, R. Susantyoko, G. Palmisano, S. Almheiri, Effects of carbonaceous impurities on the electrochemical activity of multiwalled carbon nanotube electrodes for vanadium redox flow batteries, Carbon N Y. 131 (2018) 47–59. https://doi.org/10.1016/j.carbon.2018.01.069.
[228] X. Fan, J. Liu, C. Yan, Key Materials of Vanadium Flow Batteries: Electrodes, in: H. Zhang, X. Li, J. Zhang (Eds.), Redox Flow Batteries (Fundamentals and Applications), CRC Press, Boca Raton, 2018: pp. 127–216.
[229] B. Sun, M. Skyllas-Kazacos, Chemical modification of graphite electrode materials for vanadium redox flow battery application-part II. Acid treatments, Electrochimica Acta. 37 (1992) 2459–2465. https://doi.org/10.1016/0013-4686(92)87084-D.
[230] M. Gattrell, J. Qian, C. Stewart, P. Graham, B. MacDougall, The electrochemical reduction of VO2+ in acidic solution at high overpotentials, Electrochimica Acta. 51 (2005) 395–407. https://doi.org/10.1016/j.electacta.2005.05.001.
[231] S. Zhong, M. Kazacos, R.P. Burford, M. Skyllas-Kazacos, Fabrication and activation studies of conducting plastic composite electrodes for redox cells, Journal of Power Sources. 36 (1991) 29–43. https://doi.org/10.1016/0378-7753(91)80042-V.
[232] D. Aaron, C.N. Sun, M. Bright, A.B. Papandrew, M.M. Mench, T.A. Zawodzinski, In situ kinetics studies in all-vanadium redox flow batteries, ECS Electrochemistry Letters. 2 (2013) 29–32. https://doi.org/10.1149/2.001303eel.
[233] C. Choi, Y. Choi, S. Kim, H. y Jung, H.T. Kim, Resistor Design for the Use of Dynamic Hydrogen Electrode in Vanadium Redox Flow Batteries, Electrochimica Acta. 213 (2016) 490–495. https://doi.org/10.1016/j.electacta.2016.07.152.
[234] C. Choi, H. Noh, S. Kim, R. Kim, J. Lee, J. Heo, H.T. Kim, Understanding the redox reaction mechanism of vanadium electrolytes in all-vanadium redox flow batteries, Journal of Energy Storage. 21 (2019) 321–327. https://doi.org/10.1016/j.est.2018.11.002.
[235] X.W. Wu, T. Yamamura, S. Ohta, Q.X. Zhang, F.C. Lv, C.M. Liu, K. Shirasaki, I. Satoh, T. Shikama, D. Lu, S.Q. Liu, Acceleration of the redox kinetics of VO2+/VO2+ and V3+/V2+ couples on carbon paper, Journal of Applied Electrochemistry. 41 (2011) 1183–1190. https://doi.org/10.1007/s10800-011-0343-7.
[236] L. Yue, W. Li, F. Sun, L. Zhao, L. Xing, Highly hydroxylated carbon fibres as electrode materials of all-vanadium redox flow battery, Carbon N Y. 48 (2010) 3079–3090. https://doi.org/10.1016/j.carbon.2010.04.044.

[237] J. Liang, Y. Jiao, M. Jaroniec, S.Z. Qiao, Sulfur and nitrogen dual-doped mesoporous graphene electrocatalyst for oxygen reduction with synergistically enhanced performance, Angewandte Chemie - International Edition. 51 (2012) 11496–11500. https://doi.org/10.1002/anie.201206720.
[238] D.S. Yang, D. Bhattacharjya, M.Y. Song, J.S. Yu, Highly efficient metal-free phosphorus-doped platelet ordered mesoporous carbon for electrocatalytic oxygen reduction, Carbon N Y. 67 (2014) 736–743. https://doi.org/10.1016/j.carbon.2013.10.065.
[239] K.J. Kim, H.S. Lee, J. Kim, M.S. Park, J.H. Kim, Y.J. Kim, M. Skyllas-Kazacos, Superior electrocatalytic activity of a robust carbon-felt electrode with oxygen-rich phosphate groups for all-vanadium redox flow batteries, ChemSusChem. 9 (2016) 1329–1338. https://doi.org/10.1002/cssc.201600106.
[240] X.L. Zhou, T.S. Zhao, Y.K. Zeng, L. An, L. Wei, A highly permeable and enhanced surface area carbon-cloth electrode for vanadium redox flow batteries, Journal of Power Sources. 329 (2016) 247–254. https://doi.org/10.1016/j.jpowsour.2016.08.085.
[241] W. Zhang, J. Xi, Z. Li, H. Zhou, L. Liu, Z. Wu, X. Qiu, Electrochemical activation of graphite felt electrode for VO 2+/VO2+ redox couple application, Electrochimica Acta. 89 (2013) 429–435. https://doi.org/10.1016/j.electacta.2012.11.072.
[242] W. Li, J. Liu, C. Yan, Graphite-graphite oxide composite electrode for vanadium redox flow battery, Electrochimica Acta. 56 (2011) 5290–5294. https://doi.org/10.1016/j.electacta.2011.02.083.
[243] X.L. Zhou, Y.K. Zeng, X.B. Zhu, L. Wei, T.S. Zhao, A high-performance dual-scale porous electrode for vanadium redox flow batteries, Journal of Power Sources. 325 (2016) 329–336. https://doi.org/10.1016/j.jpowsour.2016.06.048.
[244] Q. Wu, X. Zhang, Y. Lv, L. Lin, Y. Liu, X. Zhou, Bio-inspired multiscale-pore-network structured carbon felt with enhanced mass transfer and activity for vanadium redox flow batteries, Journal of Materials Chemistry A. 6 (2018) 20347–20355. https://doi.org/10.1039/c8ta06445h.
[245] X. Zhang, Q. Wu, Y. Lv, Y. Li, X. Zhou, Binder-free carbon nano-network wrapped carbon felt with optimized heteroatom doping for vanadium redox flow batteries, Journal of Materials Chemistry A. 7 (2019) 25132–25141. https://doi.org/10.1039/c9ta08859h.
[246] B. Schwenzer, J. Zhang, S. Kim, L. Li, J. Liu, Z. Yang, Membrane development for vanadium redox flow batteries, ChemSusChem. 4 (2011) 1388–1406. https://doi.org/10.1002/cssc.201100068.
[247] B.R. Chalamala, T. Soundappan, G.R. Fisher, M.R. Anstey, V. V Viswanathan, M.L. Perry, Redox flow batteries: An engineering perspective, Proceedings of the IEEE. 102 (2014) 976–999. https://doi.org/10.1109/JPROC.2014.2320317.
[248] X. Li, H. Zhang, Z. Mai, H. Zhang, I. Vankelecom, Ion exchange membranes for vanadium redox flow battery (VRB) applications, Energy and Environmental Science. 4 (2011) 1147–1160. https://doi.org/10.1039/c0ee00770f.
[249] Vanadium Redox Flow Batteries: An In-Depth Analysis, Palo Alto, CA, 2007.
[250] T.M. Gür, Review of electrical energy storage technologies, materials and systems: Challenges and prospects for large-scale grid storage, Energy and Environmental Science. 11 (2018) 2696–2767. https://doi.org/10.1039/c8ee01419a.
[251] K.W. Knehr, E. Agar, C.R. Dennison, A.R. Kalidindi, E.C. Kumbur, A Transient Vanadium Flow Battery Model Incorporating Vanadium Crossover and Water Transport through the Membrane, Journal of The Electrochemical Society. 159 (2012) A1446–A1459. https://doi.org/10.1149/2.017209jes.
[252] M. Pugach, M. Kondratenko, S. Briola, A. Bischi, Zero dimensional dynamic model of vanadium redox flow battery cell incorporating all modes of vanadium ions crossover, Applied Energy. 226 (2018) 560–569. https://doi.org/10.1016/j.apenergy.2018.05.124.
[253] Q. Luo, H. Zhang, J. Chen, P. Qian, Y. Zhai, Modification of Nafion membrane using interfacial polymerization for vanadium redox flow battery applications, Journal of

Membrane Science. 311 (2008) 98–103. https://doi.org/10.1016/j.memsci.2007.11.055.
[254] H. Zhang, H. Zhang, X. Li, Z. Mai, W. Wei, Y. Li, Crosslinkable sulfonated poly (diallyl-bisphenol ether ether ketone) membranes for vanadium redox flow battery application, Journal of Power Sources. 217 (2012) 309–315. https://doi.org/10.1016/j.jpowsour.2012.06.030.
[255] H. Zhang, H. Zhang, X. Li, Z. Mai, W. Wei, Silica modified nanofiltration membranes with improved selectivity for redox flow battery application, Energy and Environmental Science. 5 (2012) 6299–6303. https://doi.org/10.1039/c1ee02571f.
[256] Z. Li, J. Xi, H. Zhou, L. Liu, Z. Wu, X. Qiu, L. Chen, Preparation and characterization of sulfonated poly(ether ether ketone)/poly(vinylidene fluoride) blend membrane for vanadium redox flow battery application, Journal of Power Sources. 237 (2013) 132–140. https://doi.org/10.1016/j.jpowsour.2013.03.016.
[257] N. Wang, J. Yu, Z. Zhou, D. Fang, S. Liu, Y. Liu, SPPEK/TPA composite membrane as a separator of vanadium redox flow battery, Journal of Membrane Science. 437 (2013) 114–121. https://doi.org/10.1016/j.memsci.2013.02.053.
[258] F. Wang, J.M. Sylvia, M.M. Jacob, D. Peramunage, Amphiphilic block copolymer membrane for vanadium redox flow battery, Journal of Power Sources. 242 (2013) 575–580. https://doi.org/10.1016/j.jpowsour.2013.05.102.
[259] S. Maurya, S.H. Shin, K.W. Sung, S.H. Moon, Anion exchange membrane prepared from simultaneous polymerization and quaternization of 4-vinyl pyridine for non-aqueous vanadium redox flow battery applications, Journal of Power Sources. 255 (2014) 325–334. https://doi.org/10.1016/j.jpowsour.2014.01.047.
[260] Z. Li, W. Dai, L. Yu, J. Xi, X. Qiu, L. Chen, Sulfonated poly(ether ether ketone)/mesoporous silica hybrid membrane for high performance vanadium redox flow battery, Journal of Power Sources. 257 (2014) 221–229. https://doi.org/10.1016/j.jpowsour.2014.01.127.
[261] S. Winardi, S.C. Raghu, M.O. Oo, Q. Yan, N. Wai, T.M. Lim, M. Skyllas-Kazacos, Sulfonated poly (ether ether ketone)-based proton exchange membranes for vanadium redox battery applications, Journal of Membrane Science. 450 (2014) 313–322. https://doi.org/10.1016/j.memsci.2013.09.024.
[262] C.N. Sun, Z. Tang, C. Belcher, T.A. Zawodzinski, C. Fujimoto, Evaluation of Diels-Alder poly(phenylene) anion exchange membranes in all-vanadium redox flow batteries, Electrochemistry Communications. 43 (2014) 63–66. https://doi.org/10.1016/j.elecom.2014.03.010.
[263] S. Zhang, B. Zhang, G. Zhao, X. Jian, Anion exchange membranes from brominated poly(aryl ether ketone) containing 3,5-dimethyl phthalazinone moieties for vanadium redox flow batteries, Journal of Materials Chemistry A. 2 (2014) 3083–3091. https://doi.org/10.1039/c3ta14503d.
[264] J. Xi, Z. Li, L. Yu, B. Yin, L. Wang, L. Liu, X. Qiu, L. Chen, Effect of degree of sulfonation and casting solvent on sulfonated poly(ether ether ketone) membrane for vanadium redox flow battery, Journal of Power Sources. 285 (2015) 195–204. https://doi.org/10.1016/j.jpowsour.2015.03.104.
[265] B. Yin, Z. Li, W. Dai, L. Wang, L. Yu, J. Xi, Highly branched sulfonated poly(fluorenyl ether ketone sulfone)s membrane for energy efficient vanadium redox flow battery, Journal of Power Sources. 285 (2015) 109–118. https://doi.org/10.1016/j.jpowsour.2015.03.102.
[266] S. Yun, J. Parrondo, V. Ramani, Composite anion exchange membranes based on quaternized cardo-poly(etherketone) and quaternized inorganic fillers for vanadium redox flow battery applications, International Journal of Hydrogen Energy. 41 (2016) 10766–10775. https://doi.org/10.1016/j.ijhydene.2016.04.060.
[267] L. Chen, S. Zhang, Y. Chen, X. Jian, Low vanadium ion permeabilities of sulfonated poly(phthalazinone ether ketone)s provide high efficiency and stability for vanadium redox flow batteries, Journal of Power Sources. 355 (2017) 23–30. https://doi.org/10.1016/j.jpowsour.2017.04.045.

[268] J. Li, S. Liu, Z. He, Z. Zhou, A novel branched side-chain-type sulfonated polyimide membrane with flexible sulfoalkyl pendants and trifluoromethyl groups for vanadium redox flow batteries, Journal of Power Sources. 347 (2017) 114–126. https://doi.org/10.1016/j.jpowsour.2017.02.055.
[269] A. Rajput, H. Khan, S.K. Raj, R. Kothandaraman, V. Kulshrestha, Styrene- co -DVB grafted PVDF proton exchange membranes for vanadium redox flow battery applications, Materials Advances. 1 (2020) 1930–1938. https://doi.org/10.1039/d0ma00496k.
[270] L. Gubler, D. Vonlanthen, A. Schneider, F.J. Oldenburg, Composite Membranes Containing a Porous Separator and a Polybenzimidazole Thin Film for Vanadium Redox Flow Batteries, Journal of The Electrochemical Society. 167 (2020) 100502. https://doi.org/10.1149/1945-7111/ab945f.
[271] X. Zhou, R. Xue, Y. Zhong, Y. Zhang, F. Jiang, Asymmetric porous membranes with ultra-high ion selectivity for vanadium redox flow batteries, Journal of Membrane Science. 595 (2020) 117614. https://doi.org/10.1016/j.memsci.2019.117614.
[272] X. Teng, Y. Guo, D. Liu, G. Li, C. Yu, J. Dai, A polydopamine-coated polyamide thin film composite membrane with enhanced selectivity and stability for vanadium redox flow battery, Journal of Membrane Science. 601 (2020) 117906. https://doi.org/10.1016/j.memsci.2020.117906.
[273] H. Wei, Y. Liu, W. Xu, J. Liu, C. Yan, X. Che, J. Yang, J. Tong, W. Xiao, Communication—Polyethylene/PBI Pore-Filling Composite Membrane for High Performance Vanadium Redox Flow Battery, Journal of The Electrochemical Society. 166 (2019) A3207–A3209. https://doi.org/10.1149/2.0271914jes.
[274] Y. Quan, G. Wang, A. Li, X. Wei, F. Li, J. Zhang, J. Chen, R. Wang, Novel sulfonated poly(ether ether ketone)/triphenylamine hybrid membrane for vanadium redox flow battery applications, RSC Advances. 9 (2019) 3838–3846. https://doi.org/10.1039/c8ra09695c.
[275] Y. Zhang, L. Zheng, B. Liu, H. Wang, H. Shi, Sulfonated polysulfone proton exchange membrane influenced by a varied sulfonation degree for vanadium redox flow battery, Journal of Membrane Science. 584 (2019) 173–180. https://doi.org/10.1016/j.memsci.2019.04.073.
[276] Y. Zhang, H. Wang, B. Liu, J. Shi, J. Zhang, H. Shi, An ultra-high ion selective hybrid proton exchange membrane incorporated with zwitterion-decorated graphene oxide for vanadium redox flow batteries, Journal of Materials Chemistry A. 7 (2019) 12669–12680. https://doi.org/10.1039/c9ta01891c.
[277] M.A. Aziz, S. Shanmugam, Sulfonated graphene oxide-decorated block copolymer as a proton-exchange membrane: Improving the ion selectivity for all-vanadium redox flow batteries, Journal of Materials Chemistry A. 6 (2018) 17740–17750. https://doi.org/10.1039/c8ta06717a.
[278] S.I. Hossain, M.A. Aziz, D. Han, P. Selvam, S. Shanmugam, Fabrication of SPAEK-cerium zirconium oxide nanotube composite membrane with outstanding performance and durability for vanadium redox flow batteries, Journal of Materials Chemistry A. 6 (2018) 20205–20213. https://doi.org/10.1039/c8ta08349e.
[279] Y. Xing, L. Liu, C. Wang, N. Li, Side-chain-type anion exchange membranes for vanadium flow battery: Properties and degradation mechanism, Journal of Materials Chemistry A. 6 (2018) 22778–22789. https://doi.org/10.1039/c8ta08813f.
[280] P.T. Thong, T. Sadhasivam, H. Lim, C.-S. Jin, S.-K. Ryi, W. Park, H.T. Kim, S.-H. Roh, H.-Y. Jung, High Oxidizing Stability and Ion Selectivity of Hybrid Polymer Electrolyte Membrane for Improving Electrochemical Performance in Vanadium Redox Flow Battery, Journal of The Electrochemical Society. 165 (2018) A2321–A2329. https://doi.org/10.1149/2.1071810jes.
[281] T. Xu, Ion exchange membranes: State of their development and perspective, Journal of Membrane Science. 263 (2005) 1–29. https://doi.org/10.1016/j.memsci.2005.05.002.

[282] T. Mohammadi, S.C. Chieng, M. Skyllas-Kazacos, Water transport study across commercial ion exchange membranes in the vanadium redox flow battery, Journal of Membrane Science. 133 (1997) 151–159. https://doi.org/10.1016/S0376-7388(97)00092-6.
[283] Y. Zhang, J. Li, L. Ma, W. Cai, H. Cheng, Recent Developments on Alternative Proton Exchange Membranes: Strategies for Systematic Performance Improvement, Energy Technology. 3 (2015) 675–691. https://doi.org/10.1002/ente.201500028.
[284] K.A. Mauritz, R.B. Moore, State of understanding of Nafion, Chemical Reviews. 104 (2004) 4535–4585. https://doi.org/10.1021/cr0207123.
[285] J. Xi, Z. Wu, X. Qiu, L. Chen, Nafion/SiO2 hybrid membrane for vanadium redox flow battery, Journal of Power Sources. 166 (2007) 531–536. https://doi.org/10.1016/j.jpowsour.2007.01.069.
[286] B. Jiang, L. Wu, L. Yu, X. Qiu, J. Xi, A comparative study of Nafion series membranes for vanadium redox flow batteries, Journal of Membrane Science. 510 (2016) 18–26. https://doi.org/10.1016/j.memsci.2016.03.007.
[287] X. Luo, Z. Lu, J. Xi, Z. Wu, W. Zhu, L. Chen, X. Qiu, Influences of permeation of vanadium ions through PVDF-g-PSSA membranes on performances of vanadium redox flow batteries, Journal of Physical Chemistry B. 109 (2005) 20310–20314. https://doi.org/10.1021/jp054092w.
[288] X. Wei, Z. Nie, Q. Luo, B. Li, B. Chen, K. Simmons, V. Sprenkle, W. Wang, Nanoporous polytetrafl uoroethylene/silica composite separator as a high-performance all-vanadium redox flow battery membrane, Advanced Energy Materials. 3 (2013) 1215–1220. https://doi.org/10.1002/aenm.201201112.
[289] M. Amjadi, S. Rowshanzamir, S.J. Peighambardoust, S. Sedghi, Preparation, characterization and cell performance of durable nafion/SiO 2 hybrid membrane for high-temperature polymeric fuel cells, Journal of Power Sources. 210 (2012) 350–357. https://doi.org/10.1016/j.jpowsour.2012.03.011.
[290] X. Teng, J. Dai, J. Su, Y. Zhu, H. Liu, Z. Song, A high performance polytetrafluoroethene/Nafion composite membrane for vanadium redox flow battery application, Journal of Power Sources. 240 (2013) 131–139. https://doi.org/10.1016/j.jpowsour.2013.03.177.
[291] K.J. Lee, Y.H. Chu, Preparation of the graphene oxide (GO)/Nafion composite membrane for the vanadium redox flow battery (VRB) system, Vacuum. 107 (2014) 269–276. https://doi.org/10.1016/j.vacuum.2014.02.023.
[292] S. Jeong, L.H. Kim, Y. Kwon, S. Kim, Effect of nafion membrane thickness on performance of vanadium redox flow battery, Korean Journal of Chemical Engineering. 31 (2014) 2081–2087. https://doi.org/10.1007/s11814-014-0157-5.
[293] X. Teng, J. Dai, J. Su, G. Yin, Modification of Nafion membrane using fluorocarbon surfactant for all vanadium redox flow battery, Journal of Membrane Science. 476 (2015) 20–29. https://doi.org/10.1016/j.memsci.2014.11.014.
[294] D. Reed, E. Thomsen, W. Wang, Z. Nie, B. Li, X. Wei, B. Koeppel, V. Sprenkle, Performance of Nafion® N115, Nafion® NR-212, and Nafion® NR-211 in a 1 kW class all vanadium mixed acid redox flow battery, Journal of Power Sources. 285 (2015) 425–430. https://doi.org/10.1016/j.jpowsour.2015.03.099.
[295] D. Reed, E. Thomsen, B. Li, W. Wang, Z. Nie, B. Koeppel, J. Kizewski, V. Sprenkle, Stack Developments in a kW Class All Vanadium Mixed Acid Redox Flow Battery at the Pacific Northwest National Laboratory, Journal of The Electrochemical Society. 163 (2016) A5211–A5219. https://doi.org/10.1149/2.0281601jes.
[296] V.E. Sizov, V. V Zefirov, S.S. Abramchuk, A.A. Korlyukov, M.S. Kondratenko, V.G. Vasil'ev, M.O. Gallyamov, Composite Nafion-based membranes with nanosized tungsten oxides prepared in supercritical carbon dioxide, Journal of Membrane Science. 609 (2020) 118244. https://doi.org/10.1016/j.memsci.2020.118244.
[297] H.L. Yeager, A. Steck, Cation and Water Diffusion in Nafion Ion Exchange Membranes: Influence of Polymer Structure, Journal of The Electrochemical Society. 128 (1981) 1880–1884. https://doi.org/10.1149/1.2127757.

[298] A.C. Society, Perfluorinated Ionomer Membranes, ACS Symposium Series, Washington, DC, 1982. https://doi.org/10.1021/bk-1982-0180.fw001.
[299] E.J. Roche, M. Pineri, R. Duplessix, A.M. Levelut, Small-Angle Scattering Studies of Nafion Membranes., Journal of Polymer Science. Part A-2, Polymer Physics. 19 (1981) 1–11. https://doi.org/10.1002/pol.1981.180190101.
[300] M. Eikerling, A.A. Kornyshev, U. Stimming, Electrophysical properties of polymer electrolyte membranes: A random network model, Journal of Physical Chemistry B. 101 (1997) 10807–10820. https://doi.org/10.1021/jp972288t.
[301] T. Okada, G. Xie, O. Gorseth, S. Kjelstrup, N. Nakamura, T. Arimura, Ion and water transport characteristics of Nafion membranes as electrolytes, Electrochimica Acta. 43 (1998) 3741–3747. https://doi.org/10.1016/S0013-4686(98)00132-7.
[302] H.G. Haubold, T. Vad, H. Jungbluth, P. Hiller, Nano structure of NAFION: A SAXS study, Electrochimica Acta. 46 (2001) 1559–1563. https://doi.org/10.1016/S0013-4686(00)00753-2.
[303] L. Rubatat, A.L. Rollet, G. Gebel, O. Diat, Evidence of elongated polymeric aggregates in Nafion, Macromolecules. 35 (2002) 4050–4055. https://doi.org/10.1021/ma011578b.
[304] A.Z. Weber, J. Newman, Transport in Polymer-Electrolyte Membranes, Journal of The Electrochemical Society. 151 (2004) A326–A339. https://doi.org/10.1149/1.1639158.
[305] A. Vishnyakov, R. Mao, M.T. Lee, A. V Neimark, Coarse-grained model of nanoscale segregation, water diffusion, and proton transport in Nafion membranes, Journal of Chemical Physics. 148 (2018) 1–14. https://doi.org/10.1063/1.4997401.
[306] K. Schmidt-Rohr, Q. Chen, Parallel cylindrical water nanochannels in Nafion fuel-cell membranes, Nature Materials. 7 (2008) 75–83. https://doi.org/10.1038/nmat2074.
[307] T.D. Gierke, G.E. Munn, F.C. Wilson, Morphology in Nafion Perfluorinated Membrane Products, As Determined By Wide- and Small-Angle X-Ray Studies., Journal of Polymer Science. Part A-2, Polymer Physics. 19 (1981) 1687–1704. https://doi.org/10.1002/pol.1981.180191103.
[308] W.Y. Hsu, T.D. Gierke, Ion transport and clustering in nafion perfluorinated membranes, Journal of Membrane Science. 13 (1983) 307–326. https://doi.org/10.1016/S0376-7388(00)81563-X.
[309] Y. Tabuchi, R. Ito, S. Tsushima, S. Hirai, Analysis of in situ water transport in Nafion® by confocal micro-Raman spectroscopy, Journal of Power Sources. 196 (2011) 652–658. https://doi.org/10.1016/j.jpowsour.2010.07.078.
[310] R. Kuwertz, C. Kirstein, T. Turek, U. Kunz, Influence of acid pretreatment on ionic conductivity of Nafion® membranes, Journal of Membrane Science. 500 (2016) 225–235. https://doi.org/10.1016/j.memsci.2015.11.022.
[311] A. Kusoglu, A.Z. Weber, New Insights into Perfluorinated Sulfonic-Acid Ionomers, Chemical Reviews. 117 (2017) 987–1104. https://doi.org/10.1021/acs.chemrev.6b00159.
[312] M.B. Karimi, F. Mohammadi, K. Hooshyari, Recent approaches to improve Nafion performance for fuel cell applications: A review, International Journal of Hydrogen Energy. 44 (2019) 28919–28938. https://doi.org/10.1016/j.ijhydene.2019.09.096.
[313] S.P.F. Bordín, H.E. Andrada, A.C. Carreras, G.E. Castellano, R.G. Oliveira, V.M. Galván Josa, Nafion membrane channel structure studied by small-angle X-ray scattering and Monte Carlo simulations, Polymer (Guildf). 155 (2018) 58–63. https://doi.org/10.1016/j.polymer.2018.09.014.
[314] C. Yin, J. Li, Y. Zhou, H. Zhang, P. Fang, C. He, Phase Separation and Development of Proton Transport Pathways in Metal Oxide Nanoparticle/Nafion Composite Membranes during Water Uptake, Journal of Physical Chemistry C. 122 (2018) 9710–9717. https://doi.org/10.1021/acs.jpcc.8b02535.
[315] B. Gilois, F. Goujon, A. Fleury, A. Soldera, A. Ghoufi, Water nano-diffusion through the Nafion fuel cell membrane, Journal of Membrane Science. 602 (2020) 117958. https://doi.org/10.1016/j.memsci.2020.117958.
[316] S. Kim, J. Yan, B. Schwenzer, J. Zhang, L. Li, J. Liu, Z. Yang, M.A. Hickner, Cycling performance and efficiency of sulfonated poly(sulfone) membranes in vanadium redox

flow batteries, Electrochemistry Communications. 12 (2010) 1650–1653. https://doi.org/10.1016/j.elecom.2010.09.018.
[317] C. Jia, J. Liu, C. Yan, A multilayered membrane for vanadium redox flow battery, Journal of Power Sources. 203 (2012) 190–194. https://doi.org/10.1016/j.jpowsour.2011.10.102.
[318] X. Ling, C. Jia, J. Liu, C. Yan, Preparation and characterization of sulfonated poly(ether sulfone)/sulfonated poly(ether ether ketone) blend membrane for vanadium redox flow battery, Journal of Membrane Science. 415–416 (2012) 306–312. https://doi.org/10.1016/j.memsci.2012.05.014.
[319] D. Chen, S. Kim, L. Li, G. Yang, M.A. Hickner, Stable fluorinated sulfonated poly(arylene ether) membranes for vanadium redox flow batteries, RSC Advances. 2 (2012) 8087–8094. https://doi.org/10.1039/c2ra20834b.
[320] C. Fujimoto, S. Kim, R. Stains, X. Wei, L. Li, Z.G. Yang, Vanadium redox flow battery efficiency and durability studies of sulfonated Diels Alder poly(phenylene)s, Electrochemistry Communications. 20 (2012) 48–51. https://doi.org/10.1016/j.elecom.2012.03.037.
[321] S. MacKsasitorn, S. Changkhamchom, A. Sirivat, K. Siemanond, Sulfonated poly(ether ether ketone) and sulfonated poly(1,4-phenylene ether ether sulfone) membranes for vanadium redox flow batteries, High Performance Polymers. 24 (2012) 603–608. https://doi.org/10.1177/0954008312446762.
[322] K.D. Kreuer, Ion conducting membranes for fuel cells and other electrochemical devices, Chemistry of Materials. 26 (2014) 361–380. https://doi.org/10.1021/cm402742u.
[323] S. Maurya, S.H. Shin, Y. Kim, S.H. Moon, A review on recent developments of anion exchange membranes for fuel cells and redox flow batteries, RSC Advances. 5 (2015) 37206–37230. https://doi.org/10.1039/c5ra04741b.
[324] D. Chen, M.A. Hickner, E. Agar, E.C. Kumbur, Selective anion exchange membranes for high coulombic efficiency vanadium redox flow batteries, Electrochemistry Communications. 26 (2013) 37–40. https://doi.org/10.1016/j.elecom.2012.10.007.
[325] T. Mohammadi, M. Skyllas Kazacos, Modification of anion-exchange membranes for vanadium redox flow battery applications, Journal of Power Sources. 63 (1996) 179–186. https://doi.org/10.1016/S0378-7753(96)02463-9.
[326] G.J. Hwang, H. Ohya, Crosslinking of anion exchange membrane by accelerated electron radiation as a separator for the all-vanadium redox flow battery, Journal of Membrane Science. 132 (1997) 55–61. https://doi.org/10.1016/S0376-7388(97)00040-9.
[327] J. Qiu, M. Li, J. Ni, M. Zhai, J. Peng, L. Xu, H. Zhou, J. Li, G. Wei, Preparation of ETFE-based anion exchange membrane to reduce permeability of vanadium ions in vanadium redox battery, Journal of Membrane Science. 297 (2007) 174–180. https://doi.org/10.1016/j.memsci.2007.03.042.
[328] D. Xing, S. Zhang, C. Yin, B. Zhang, X. Jian, Effect of amination agent on the properties of quaternized poly(phthalazinone ether sulfone) anion exchange membrane for vanadium redox flow battery application, Journal of Membrane Science. 354 (2010) 68–73. https://doi.org/10.1016/j.memsci.2010.02.064.
[329] S. Zhang, C. Yin, D. Xing, D. Yang, X. Jian, Preparation of chloromethylated/quaternized poly(phthalazinone ether ketone) anion exchange membrane materials for vanadium redox flow battery applications, Journal of Membrane Science. 363 (2010) 243–249. https://doi.org/10.1016/j.memsci.2010.07.046.
[330] B. Tian, C.W. Yan, F.H. Wang, Modification and evaluation of membranes for vanadium redox battery applications, Journal of Applied Electrochemistry. 34 (2004) 1205–1210. https://doi.org/10.1007/s10800-004-1765-2.
[331] A. Tang, J. Bao, M. Skyllas-Kazacos, Dynamic modelling of the effects of ion diffusion and side reactions on the capacity loss for vanadium redox flow battery, Journal of

Power Sources. 196 (2011) 10737–10747. https://doi.org/10.1016/j.jpowsour.2011.09.003.
[332] T. Mohammadi, M. Skyllas-Kazacos, Evaluation of the chemical stability of some membranes in vanadium solution, Journal of Applied Electrochemistry. 27 (1997) 153–160. https://doi.org/10.1023/A:1018495722379.
[333] B. Zhang, S. Zhang, D. Xing, R. Han, C. Yin, X. Jian, Quaternized poly(phthalazinone ether ketone ketone) anion exchange membrane with low permeability of vanadium ions for vanadium redox flow battery application, Journal of Power Sources. 217 (2012) 296–302. https://doi.org/10.1016/j.jpowsour.2012.06.027.
[334] B. Zhang, S. Zhang, Z. Weng, G. Wang, E. Zhang, P. Yu, X. Chen, X. Wang, Quaternized adamantane-containing poly(aryl ether ketone) anion exchange membranes for vanadium redox flow battery applications, Journal of Power Sources. 325 (2016) 801–807. https://doi.org/10.1016/j.jpowsour.2016.06.101.
[335] B. Zhang, E. Zhang, G. Wang, P. Yu, Q. Zhao, F. Yao, Poly(phenyl sulfone) anion exchange membranes with pyridinium groups for vanadium redox flow battery applications, Journal of Power Sources. 282 (2015) 328–334. https://doi.org/10.1016/j.jpowsour.2015.02.070.
[336] L. Zeng, T.S. Zhao, L. Wei, Y.K. Zeng, Z.H. Zhang, Highly stable pyridinium-functionalized cross-linked anion exchange membranes for all vanadium redox flow batteries, Journal of Power Sources. 331 (2016) 452–461. https://doi.org/10.1016/j.jpowsour.2016.09.065.
[337] S.C. Chieng, M. Kazacos, M. Skyllas-Kazacos, Modification of Daramic, microporous separator, for redox flow battery applications, Journal of Membrane Science. 75 (1992) 81–91. https://doi.org/10.1016/0376-7388(92)80008-8.
[338] T. Mohammadi, M. Skyllas-Kazacos, Preparation of sulfonated composite membrane for vanadium redox flow battery applications, Journal of Membrane Science. 107 (1995) 35–45. https://doi.org/10.1016/0376-7388(95)00096-U.
[339] W.J. Koros, Y.H. Ma, T. Shimidzu, Terminology for membranes and membrane processes (IUPAC Recommendations 1996), Pure and Applied Chemistry. 68 (1996) 1479–1489. https://doi.org/10.1351/pac199668071479.
[340] P. Vandezande, L.E.M. Gevers, I.F.J. Vankelecom, Solvent resistant nanofiltration: Separating on a molecular level, Chemical Society Reviews. 37 (2008) 365–405. https://doi.org/10.1039/b610848m.
[341] H. Zhang, H. Zhang, X. Li, Z. Mai, J. Zhang, Nanofiltration (NF) membranes: The next generation separators for all vanadium redox flow batteries (VRBs)?, Energy and Environmental Science. 4 (2011) 1676–1679. https://doi.org/10.1039/c1ee01117k.
[342] G. Oriji, Y. Katayama, T. Miura, Investigations on V(IV)/V(V) and V(II)/V(III) redox reactions by various electrochemical methods, Journal of Power Sources. 139 (2005) 321–324. https://doi.org/10.1016/j.jpowsour.2004.03.008.
[343] X. Xi, C. Ding, H. Zhang, X. Li, Y. Cheng, H. Zhang, Solvent responsive silica composite nanofiltration membrane with controlled pores and improved ion selectivity for vanadium flow battery application, Journal of Power Sources. 274 (2015) 1126–1134. https://doi.org/10.1016/j.jpowsour.2014.10.160.
[344] X.L. Zhou, T.S. Zhao, L. An, L. Wei, C. Zhang, The use of polybenzimidazole membranes in vanadium redox flow batteries leading to increased coulombic efficiency and cycling performance, Electrochimica Acta. 153 (2015) 492–498. https://doi.org/10.1016/j.electacta.2014.11.185.
[345] Y. Li, H. Zhang, X. Li, H. Zhang, W. Wei, Porous poly(ether sulfone) membranes with tunable morphology: Fabrication and their application for vanadium flow battery, Journal of Power Sources. 233 (2013) 202–208. https://doi.org/10.1016/j.jpowsour.2013.01.088.
[346] J. Cao, H. Zhang, W. Xu, X. Li, Poly(vinylidene fluoride) porous membranes precipitated in water/ethanol dual-coagulation bath: The relationship between morphology and performance in vanadium flow battery, Journal of Power Sources. 249 (2014) 84–91. https://doi.org/10.1016/j.jpowsour.2013.10.069.

[347] J. Cao, Z. Yuan, X. Li, W. Xu, H. Zhang, Hydrophilic poly(vinylidene fluoride) porous membrane with well connected ion transport networks for vanadium flow battery, Journal of Power Sources. 298 (2015) 228–235. https://doi.org/10.1016/j.jpowsour.2015.08.067.
[348] Q. Zheng, X. Li, Y. Cheng, G. Ning, F. Xing, H. Zhang, Development and perspective in vanadium flow battery modeling, Applied Energy. 132 (2014) 254–266. https://doi.org/10.1016/j.apenergy.2014.06.077.
[349] D. You, H. Zhang, J. Chen, A simple model for the vanadium redox battery, Electrochimica Acta. 54 (2009) 6827–6836. https://doi.org/10.1016/j.electacta.2009.06.086.
[350] M. Zhang, M. Moore, J.S. Watson, T.A. Zawodzinski, R.M. Counce, Capital Cost Sensitivity Analysis of an All-Vanadium Redox-Flow Battery, Journal of The Electrochemical Society. 159 (2012) A1183–A1188. https://doi.org/10.1149/2.041208jes.
[351] J. Noack, L. Wietschel, N. Roznyatovskaya, K. Pinkwart, J. Tübke, Techno-economic modeling and analysis of redox flow battery systems, Energies (Basel). 9 (2016) 1–15. https://doi.org/10.3390/en9080627.
[352] Z. Wei, J. Zhao, B. Xiong, Dynamic electro-thermal modeling of all-vanadium redox flow battery with forced cooling strategies, Applied Energy. 135 (2014) 1–10. https://doi.org/10.1016/j.apenergy.2014.08.062.
[353] A. Tang, J. Bao, M. Skyllas-Kazacos, Thermal modelling of battery configuration and self-discharge reactions in vanadium redox flow battery, Journal of Power Sources. 216 (2012) 489–501. https://doi.org/10.1016/j.jpowsour.2012.06.052.
[354] B. Xiong, J. Zhao, K.J. Tseng, M. Skyllas-Kazacos, T.M. Lim, Y. Zhang, Thermal hydraulic behavior and efficiency analysis of an all-vanadium redox flow battery, Journal of Power Sources. 242 (2013) 314–324. https://doi.org/10.1016/j.jpowsour.2013.05.092.
[355] B. Turker, S. Arroyo Klein, E.M. Hammer, B. Lenz, L. Komsiyska, Modeling a vanadium redox flow battery system for large scale applications, Energy Conversion and Management. 66 (2013) 26–32. https://doi.org/10.1016/j.enconman.2012.09.009.
[356] F.C. Gu, H.C. Chen, K.Y. Li, Mathematic Modeling and Performance Analysis of Vanadium Redox Flow Battery, Energy and Fuels. 34 (2020) 10142–10147. https://doi.org/10.1021/acs.energyfuels.0c01536.
[357] A. Bhattacharjee, H. Saha, Design and experimental validation of a generalised electrical equivalent model of Vanadium Redox Flow Battery for interfacing with renewable energy sources, Journal of Energy Storage. 13 (2017) 220–232. https://doi.org/10.1016/j.est.2017.07.016.
[358] Z. Wei, T.M. Lim, M. Skyllas-Kazacos, N. Wai, K.J. Tseng, Online state of charge and model parameter co-estimation based on a novel multi-timescale estimator for vanadium redox flow battery, Applied Energy. 172 (2016) 169–179. https://doi.org/10.1016/j.apenergy.2016.03.103.
[359] Z. Wei, K.J. Tseng, N. Wai, T.M. Lim, M. Skyllas-Kazacos, Adaptive estimation of state of charge and capacity with online identified battery model for vanadium redox flow battery, Journal of Power Sources. 332 (2016) 389–398. https://doi.org/10.1016/j.jpowsour.2016.09.123.
[360] Z. Wei, J. Zhao, D. Ji, K.J. Tseng, A multi-timescale estimator for battery state of charge and capacity dual estimation based on an online identified model, Applied Energy. 204 (2017) 1264–1274. https://doi.org/10.1016/j.apenergy.2017.02.016.
[361] L.J. Ontiveros, G.O. Suvire, P.E. Mercado, Power conditioning system coupled with a flow battery for wind energy applications: Modelling and control design, IET Renewable Power Generation. 11 (2017) 987–995. https://doi.org/10.1049/iet-rpg.2016.0831.
[362] P. Jienkulsawad, T. Jirabovornwisut, Y.S. Chen, A. Arpornwichanop, Improving the Performance of an All-Vanadium Redox Flow Battery under Imbalance Conditions:

Online Dynamic Optimization Approach, ACS Sustainable Chemistry and Engineering. 8 (2020) 13610–13622. https://doi.org/10.1021/acssuschemeng.0c02973.
[363] S.T. Revankar, Chapter Six - Chemical Energy Storage, in: H. Bindra, S. Revankar (Eds.), Storage and Hybridization of Nuclear Energy, Academic Press, 2019: pp. 177–227. https://doi.org/https://doi.org/10.1016/B978-0-12-813975-2.00006-5.
[364] M.A. Miller, J. Petrasch, K. Randhir, N. Rahmatian, J. Klausner, Chemical energy storage, in: K. Brun, T. Allison, R. Dennis (Eds.), Thermal, Mechanical, and Hybrid Chemical Energy Storage Systems, Elsevier Inc., 2021: pp. 249–292. https://doi.org/10.1016/b978-0-12-819892-6.00005-8.
[365] I. Dincer, Y. Bicer, Electrochemical Energy Conversion, in: I. Dincer (Ed.), Comprehensive Energy Systems, 2018: pp. 856–894. https://doi.org/10.1016/B978-0-12-809597-3.00439-9.
[366] U. Koehler, General overview of non-lithium battery systems and their safety issues, in: J. Garche, K. Brandt (Eds.), Electrochemical Power Sources: Fundamentals, Systems, and Applications Li-Battery Safety, Elsevier B.V., 2018: pp. 21–46. https://doi.org/10.1016/B978-0-444-63777-2.00002-5.
[367] G.J. May, A. Davidson, B. Monahov, Lead batteries for utility energy storage: A review, Journal of Energy Storage. 15 (2018) 145–157. https://doi.org/10.1016/j.est.2017.11.008.
[368] N.M. Johnson, Battery technology for CO2 reduction, in: R. Folkson (Ed.), Alternative Fuels and Advanced Vehicle Technologies for Improved Environmental Performance: Towards Zero Carbon Transportation, 2014: pp. 582–631. https://doi.org/10.1533/9780857097422.3.582.
[369] K.S. Boparai, R. Singh, Electrochemical Energy Storage Using Batteries, Superconductors and Hybrid Technologies, in: S. Hashmi, I.A. Choudhury (Eds.), Encyclopedia of Renewable and Sustainable Materials, Elsevier Ltd., 2020: pp. 248–254. https://doi.org/10.1016/b978-0-12-803581-8.11277-9.
[370] D. Pavlov, H2SO4 Electrolyte—An Active Material in the Lead–Acid Cell, in: D. Pavlov (Ed.), Lead-Acid Batteries: Science and Technology, 2017: pp. 133–167. https://doi.org/10.1016/b978-0-444-59552-2.00003-1.
[371] B. Pinnangudi, M. Kuykendal, S. Bhadra, Smart Grid Energy Storage, in: B.W. D'Andrade (Ed.), The Power Grid: Smart, Secure, Green and Reliable, Elsevier Ltd, 2017: pp. 93–135. https://doi.org/10.1016/B978-0-12-805321-8.00004-5.
[372] T. Wilberforce, J. Thompson, A.G. Olabi, Classification of Energy Storage Materials, Reference Module in Materials Science and Materials Engineering. (2020) 1–7. https://doi.org/10.1016/b978-0-12-803581-8.11762-x.
[373] D.C.R. Espinosa, J.A.S. Tenório, Recycling of nickel-cadmium batteries using coal as reducing agent, Journal of Power Sources. 157 (2006) 600–604. https://doi.org/10.1016/j.jpowsour.2005.07.061.
[374] D.D. Macdonald, M.L. Challingsworth, Thermodynamics of Nickel-Cadmium and Nickel-Hydrogen Batteries, Journal of The Electrochemical Society. 140 (1993) 606–609. https://doi.org/10.1149/1.2056129.
[375] Y. Morioka, S. Narukawa, T. Itou, State-of-the-art of alkaline rechargeable batteries, Journal of Power Sources. 100 (2001) 107–116. https://doi.org/10.1016/S0378-7753(01)00888-6.
[376] A.K. Shukla, S. Venugopalan, B. Hariprakash, Secondary Batteries – Nickel Systems | Nickel–Cadmium: Overview, in: J. Garche (Ed.), Encyclopedia of Electrochemical Power Sources, Elsevier, 2009: pp. 452–458. https://doi.org/10.1016/B978-044452745-5.00153-2.
[377] M.B. Tahir, M. Abrar, A. Tehseen, T.I. Awan, A. Bashir, G. Nabi, Nanotechnology: the road ahead, in: T.I. Awan, A. Bashir, A. Tehseen (Eds.), Chemistry of Nanomaterials, Elsevier, 2020: pp. 289–308. https://doi.org/10.1016/b978-0-12-818908-5.00011-1.
[378] E. Lemaire-Potteau, M. Perrin, S. Genies, Batteries | Charging Methods, Encyclopedia of Electrochemical Power Sources. (2009) 413–423. https://doi.org/10.1016/B978-044452745-5.00885-6.

[379] S. Qazi, Fundamentals of Standalone Photovoltaic Systems, in: S. Qazi (Ed.), Standalone Photovoltaic (PV) Systems for Disaster Relief and Remote Areas, Elsevier, 2017: pp. 31–82. https://doi.org/10.1016/b978-0-12-803022-6.00002-2.
[380] Z. Abdin, K.R. Khalilpour, Single and polystorage technologies for renewable-based hybrid energy systems, in: K.R. Khalilpour (Ed.), Polygeneration with Polystorage: For Chemical and Energy Hubs, Elsevier Inc., 2019: pp. 77–131. https://doi.org/10.1016/B978-0-12-813306-4.00004-5.
[381] F. Hussain, M.Z. Rahman, A.N. Sivasengaran, M. Hasanuzzaman, Energy storage technologies, in: M.D. Hasanuzzaman, N.A. Rahim (Eds.), Energy for Sustainable Development: Demand, Supply, Conversion and Management, Elsevier Inc., 2020: pp. 125–165. https://doi.org/10.1016/B978-0-12-814645-3.00006-7.
[382] T. Kim, W. Song, D.Y. Son, L.K. Ono, Y. Qi, Lithium-ion batteries: outlook on present, future, and hybridized technologies, Journal of Materials Chemistry A. 7 (2019) 2942–2964. https://doi.org/10.1039/C8TA10513H.
[383] C. Semeraro, A.-G. Olabi, M. Dassisti, Sustainability Issues in Manufacturing and Operation of Second-Generation Flow Batteries, in: Reference Module in Materials Science and Materials Engineering, Elsevier, 2021: pp. 1–8. https://doi.org/10.1016/B978-0-12-815732-9.00076-0.
[384] G. Zubi, R. Dufo-López, M. Carvalho, G. Pasaoglu, The lithium-ion battery: State of the art and future perspectives, Renewable and Sustainable Energy Reviews. 89 (2018) 292–308. https://doi.org/10.1016/j.rser.2018.03.002.
[385] P.K.D. Pramanik, N. Sinhababu, B. Mukherjee, S. Padmanaban, A. Maity, B.K. Upadhyaya, J.B. Holm-Nielsen, P. Choudhury, Power Consumption Analysis, Measurement, Management, and Issues: A State-of-the-Art Review of Smartphone Battery and Energy Usage, IEEE Access. 7 (2019) 182113–182172. https://doi.org/10.1109/ACCESS.2019.2958684.
[386] M. Dalal, J. Ma, D. He, Lithium-ion battery life prognostic health management system using particle filtering framework, Proceedings of the Institution of Mechanical Engineers, Part O: Journal of Risk and Reliability. 225 (2011) 81–90. https://doi.org/10.1177/1748006XJRR342.
[387] P. Breeze, Power System Energy Storage Technologies, in: Power Generation Technologies, Elsevier, 2019: pp. 219–249. https://doi.org/10.1016/b978-0-08-102631-1.00010-9.
[388] B. Dunn, H. Kamath, J.M. Tarascon, Electrical energy storage for the grid: A battery of choices, Science (1979). 334 (2011) 928–935. https://doi.org/10.1126/science.1212741.
[389] H. Chen, Y. Xu, C. Liu, F. He, S. Hu, Storing Energy in China-An Overview, in: T.M. Letcher (Ed.), Storing Energy: With Special Reference to Renewable Energy Sources, Elsevier Inc., 2016: pp. 509–527. https://doi.org/10.1016/B978-0-12-803440-8.00024-5.
[390] D.W. Gao, Basic Concepts and Control Architecture of Microgrids, in: D.W. Gao (Ed.), Energy Storage for Sustainable Microgrid, Elsevier, 2015: pp. 1–34. https://doi.org/10.1016/b978-0-12-803374-6.00001-9.
[391] C. Doetsch, J. Burfeind, Vanadium Redox Flow Batteries, in: T.M. Letcher (Ed.), Storing Energy, Elsevier, 2016: pp. 227–246. https://doi.org/10.1016/B978-0-12-803440-8.00012-9.
[392] M.J. Watt-Smith, R.G.A. Wills, F.C. Walsh, Secondary Batteries – Flow Systems | Overview, in: J. Garche (Ed.), Encyclopedia of Electrochemical Power Sources, Elsevier, 2009: pp. 438–443. https://doi.org/10.1016/B978-044452745-5.00176-3.
[393] C. Doetsch, A. Pohlig, The use of flow batteries in storing electricity for national grids, in: T.M. Letcher (Ed.), Future Energy: Improved, Sustainable and Clean Options for Our Planet, Elsevier Ltd, 2020: pp. 263–277. https://doi.org/10.1016/B978-0-08-102886-5.00013-X.
[394] E. Sánchez-Díez, E. Ventosa, M. Guarnieri, A. Trovò, C. Flox, R. Marcilla, F. Soavi, P. Mazur, E. Aranzabe, R. Ferret, Redox flow batteries: Status and perspective towards

sustainable stationary energy storage, Journal of Power Sources. 481 (2021) 228804. https://doi.org/10.1016/j.jpowsour.2020.228804.
[395] A.Z. Weber, M.M. Mench, J.P. Meyers, P.N. Ross, J.T. Gostick, Q. Liu, Redox flow batteries: A review, Journal of Applied Electrochemistry. 41 (2011) 1137–1164. https://doi.org/10.1007/s10800-011-0348-2.
[396] A. Dinesh, S. Olivera, K. Venkatesh, M.S. Santosh, M.G. Priya, Inamuddin, A.M. Asiri, H.B. Muralidhara, Iron-based flow batteries to store renewable energies, Environmental Chemistry Letters. 16 (2018) 683–694. https://doi.org/10.1007/s10311-018-0709-8.
[397] H. Zhang, C. Sun, Cost-effective iron-based aqueous redox flow batteries for large-scale energy storage application: A review, Journal of Power Sources. 493 (2021) 229445. https://doi.org/10.1016/j.jpowsour.2020.229445.
[398] X. Luo, J. Wang, M. Dooner, J. Clarke, Overview of current development in electrical energy storage technologies and the application potential in power system operation, Applied Energy. 137 (2015) 511–536. https://doi.org/10.1016/j.apenergy.2014.09.081.
[399] M.H. Chakrabarti, S.A. Hajimolana, F.S. Mjalli, M. Saleem, I. Mustafa, Redox Flow Battery for Energy Storage, Arabian Journal for Science and Engineering. 38 (2013) 723–739. https://doi.org/10.1007/s13369-012-0356-5.
[400] H. Zhang, Polysulfide-bromine flow batteries (PBBs) for medium- and large-scale energy storage, in: C. Menictas, M. Skyllas-Kazacos, T.M. Lim (Eds.), Advances in Batteries for Medium and Large-Scale Energy Storage: Types and Applications, Elsevier Ltd., 2015: pp. 317–327. https://doi.org/10.1016/B978-1-78242-013-2.00009-1.
[401] Z. Xie, Q. Liu, Z. Chang, X. Zhang, The developments and challenges of cerium half-cell in zinc-cerium redox flow battery for energy storage, Electrochimica Acta. 90 (2013) 695–704. https://doi.org/10.1016/j.electacta.2012.12.066.
[402] K. Amini, M.D. Pritzker, Life-cycle analysis of zinc-cerium redox flow batteries, Electrochimica Acta. 356 (2020) 1–14. https://doi.org/10.1016/j.electacta.2020.136785.
[403] R.K. Emmett, M.E. Roberts, Recent developments in alternative aqueous redox flow batteries for grid-scale energy storage, Journal of Power Sources. 506 (2021) 230087. https://doi.org/10.1016/j.jpowsour.2021.230087.
[404] T. Allison, N.R. Smith, Z. Ma, Introduction to energy storage, Elsevier Inc., 2021. https://doi.org/10.1016/b978-0-12-819892-6.00001-0.
[405] D.D. Macdonald, M.L. Challingsworth, Thermodynamics of Nickel-Cadmium and Nickel-Hydrogen Batteries, Journal of The Electrochemical Society. 140 (1993) 606–609. https://doi.org/10.1149/1.2056129.
[406] EASE, Nickel Metal Hydride Batteries, Brussels, 2016. https://doi.org/10.3390/books978-3-03842-303-4.
[407] B. Dunn, H. Kamath, J.M. Tarascon, Electrical energy storage for the grid: A battery of choices, Science (1979). 334 (2011) 928–935. https://doi.org/10.1126/science.1212741.
[408] E. Sánchez-Díez, E. Ventosa, M. Guarnieri, A. Trovò, C. Flox, R. Marcilla, F. Soavi, P. Mazur, E. Aranzabe, R. Ferret, Redox flow batteries: Status and perspective towards sustainable stationary energy storage, Journal of Power Sources. 481 (2021) 228804. https://doi.org/10.1016/j.jpowsour.2020.228804.
[409] C. Doetsch, J. Burfeind, Vanadium Redox Flow Batteries, in: Storing Energy: With Special Reference to Renewable Energy Sources, Elsevier Inc., 2016: pp. 227–246. https://doi.org/10.1016/B978-0-12-803440-8.00012-9.
[410] C. Fabjan, J. Garche, B. Harrer, L. Jörissen, C. Kolbeck, F. Philippi, G. Tomazic, F. Wagner, The vanadium redox-battery: An efficient storage unit for photovoltaic systems, Electrochimica Acta. 47 (2001) 825–831. https://doi.org/10.1016/S0013-4686(01)00763-0.
[411] L. Joerissen, J. Garche, C. Fabjan, G. Tomazic, Possible use of vanadium redox-flow batteries for energy storage in small grids and stand-alone photovoltaic systems,

Journal of Power Sources. 127 (2004) 98–104. https://doi.org/10.1016/j.jpowsour.2003.09.066.
[412] C.J. Rydh, B.A. Sandén, Energy analysis of batteries in photovoltaic systems. Part I: Performance and energy requirements, Energy Conversion and Management. 46 (2005) 1957–1979. https://doi.org/10.1016/j.enconman.2004.10.003.
[413] C.J. Rydh, B.A. Sandén, Energy analysis of batteries in photovoltaic systems. Part II: Energy return factors and overall battery efficiencies, Energy Conversion and Management. 46 (2005) 1980–2000. https://doi.org/10.1016/j.enconman.2004.10.004.
[414] E. Mena, R. López-Vizcaíno, M. Millán, P. Cañizares, J. Lobato, M.A. Rodrigo, Vanadium redox flow batteries for the storage of electricity produced in wind turbines, International Journal of Energy Research. 42 (2018) 720–730. https://doi.org/10.1002/er.3858.
[415] M. Stone, Redox flow batteries for energy storage, Energy Storage Report. (2014). http://energystoragereport.info/redox-flow-batteries-for-energy-storage/.
[416] T. Shigematsu, T. Kumamoto, H. Deguchi, T. Hara, Applications of a vanadium redox-flow battery to maintain power quality, Proceedings of the IEEE Power Engineering Society Transmission and Distribution Conference. 2 (2002) 1065–1070. https://doi.org/10.1109/TDC.2002.1177625.
[417] A. Shibata, K. Sato, Development of vanadium redox flow battery for electricity storage, Power Engineering Journal. 13 (1999) 130–135. https://doi.org/10.1049/pe:19990305.
[418] M.P. Johnson, A. Bar-Noy, O. Liu, Y. Feng, Energy peak shaving with local storage, Sustainable Computing: Informatics and Systems. 1 (2011) 177–188. https://doi.org/10.1016/j.suscom.2011.05.001.
[419] I. Aramendia, U. Fernandez-Gamiz, A. Martinez-San-vicente, E. Zulueta, J.M. Lopez-Guede, Vanadium redox flow batteries: A review oriented to fluid-dynamic optimization, Energies (Basel). 14 (2021). https://doi.org/10.3390/en14010176.
[420] C. Minke, U. Kunz, T. Turek, Techno-economic assessment of novel vanadium redox flow batteries with large-area cells, Journal of Power Sources. 361 (2017) 105–114. https://doi.org/10.1016/j.jpowsour.2017.06.066.
[421] C. Minke, T. Turek, Materials, system designs and modelling approaches in techno-economic assessment of all-vanadium redox flow batteries – A review, Journal of Power Sources. 376 (2018) 66–81. https://doi.org/10.1016/j.jpowsour.2017.11.058.
[422] IRENA, Electricity storage and renewables: Costs and markets to 2030, (2017) 132. http://irena.org/publications/2017/Oct/Electricity-storage-and-renewables-costs-and-markets%0Ahttps://www.irena.org/-/media/Files/IRENA/Agency/Publication/2017/Oct/IRENA_Electricity_Storage_Costs_2017.pdf.
[423] V. Viswanathan, A. Crawford, D. Stephenson, S. Kim, W. Wang, B. Li, G. Coffey, E. Thomsen, G. Graff, P. Balducci, M. Kintner-Meyer, V. Sprenkle, Cost and performance model for redox flow batteries, Journal of Power Sources. 247 (2014) 1040–1051. https://doi.org/10.1016/j.jpowsour.2012.12.023.
[424] C. Minke, U. Kunz, T. Turek, Carbon felt and carbon fiber - A techno-economic assessment of felt electrodes for redox flow battery applications, Journal of Power Sources. 342 (2017) 116–124. https://doi.org/10.1016/j.jpowsour.2016.12.039.
[425] C. Minke, T. Turek, Economics of vanadium redox flow battery membranes, Journal of Power Sources. 286 (2015) 247–257. https://doi.org/10.1016/j.jpowsour.2015.03.144.
[426] A. Crawford, V. Viswanathan, D. Stephenson, W. Wang, E. Thomsen, D. Reed, B. Li, P. Balducci, M. Kintner-Meyer, V. Sprenkle, Comparative analysis for various redox flow batteries chemistries using a cost performance model, Journal of Power Sources. 293 (2015) 388–399. https://doi.org/10.1016/j.jpowsour.2015.05.066.
[427] Y.K. Zeng, T.S. Zhao, L. An, X.L. Zhou, L. Wei, A comparative study of all-vanadium and iron-chromium redox flow batteries for large-scale energy storage, Journal of Power Sources. 300 (2015) 438–443. https://doi.org/10.1016/j.jpowsour.2015.09.100.

[428] M. Zheng, J. Sun, C.J. Meinrenken, T. Wang, Pathways toward enhanced techno-economic performance of flow battery systems in energy system applications, Journal of Electrochemical Energy Conversion and Storage. 16 (2019) 1–11. https://doi.org/10.1115/1.4040921.
[429] C.S. Jin, J.Y. So, K.H. Shin, E.B. Ha, M.J. Choi, S.K. Park, Y.J. Lee, S.H. Yeon, Effect of organophosphorus compound additives for thermal stability on the positive electrolyte of a vanadium redox flow battery, Journal of Applied Electrochemistry. 48 (2018) 1019–1030. https://doi.org/10.1007/s10800-018-1227-x.
[430] S. Li, K. Huang, S. Liu, D. Fang, X. Wu, D. Lu, T. Wu, Effect of organic additives on positive electrolyte for vanadium redox battery, Electrochimica Acta. 56 (2011) 5483–5487. https://doi.org/10.1016/j.electacta.2011.03.048.
[431] Y. Lei, S. Liu, C. Gao, X. Liang, Z. He, Y. Deng, Z. He, Effect of Amino Acid Additives on the Positive Electrolyte of Vanadium Redox Flow Batteries, Journal of The Electrochemical Society. 160 (2013) A722–A727. https://doi.org/10.1149/2.006306jes.
[432] X. Wu, S. Liu, N. Wang, S. Peng, Z. He, Influence of organic additives on electrochemical properties of the positive electrolyte for all-vanadium redox flow battery, Electrochimica Acta. 78 (2012) 475–482. https://doi.org/10.1016/j.electacta.2012.06.065.
[433] J. Zhang, L. Li, Z. Nie, B. Chen, M. Vijayakumar, S. Kim, W. Wang, B. Schwenzer, J. Liu, Z. Yang, Effects of additives on the stability of electrolytes for all-vanadium redox flow batteries, Journal of Applied Electrochemistry. 41 (2011) 1215–1221. https://doi.org/10.1007/s10800-011-0312-1.
[434] T.D. Nguyen, A. Whitehead, G.G. Scherer, N. Wai, M.O. Oo, A. Bhattarai, G.P. Chandra, Z.J. Xu, The oxidation of organic additives in the positive vanadium electrolyte and its effect on the performance of vanadium redox flow battery, Journal of Power Sources. 334 (2016) 94–103. https://doi.org/10.1016/j.jpowsour.2016.10.017.
[435] F. Rahman, M. Skyllas-Kazacos, Evaluation of additive formulations to inhibit precipitation of positive electrolyte in vanadium battery, Journal of Power Sources. 340 (2017) 139–149. https://doi.org/10.1016/j.jpowsour.2016.11.071.
[436] S.-K. Park, J. Shim, J.H. Yang, C.-S. Jin, B.S. Lee, Y.-S. Lee, K.-H. Shin, J.-D. Jeon, Effect of inorganic additive sodium pyrophosphate tetrabasic on positive electrolytes for a vanadium redox flow battery, Electrochimica Acta. 121 (2014) 321–327. https://doi.org/10.1016/j.electacta.2014.01.008.
[437] F. Tian, L. Wang, C.-S. Wang, The effect of phosphate additive on the positive electrolyte stability of vanadium redox flow battery, Journal of Energy Chemistry. 27 (2018) 1376–1380. https://doi.org/10.1016/j.jechem.2018.05.018.
[438] N. V Roznyatovskaya, V.A. Roznyatovsky, C.-C. Höhne, M. Fühl, T. Gerber, M. Küttinger, J. Noack, P. Fischer, K. Pinkwart, J. Tübke, The role of phosphate additive in stabilization of sulphuric-acid-based vanadium(V) electrolyte for all-vanadium redox-flow batteries, Journal of Power Sources. 363 (2017) 234–243. https://doi.org/10.1016/j.jpowsour.2017.07.100.
[439] T.D. Nguyen, L.P. Wang, A. Whitehead, N. Wai, G.G. Scherer, Z.J. Xu, Insights into the synergistic effect of ammonium and phosphate-containing additives for a thermally stable vanadium redox flow battery electrolyte, Journal of Power Sources. 402 (2018) 75–81. https://doi.org/10.1016/j.jpowsour.2018.09.024.
[440] Y. Yang, Y. Zhang, T. Liu, J. Huang, Improved broad temperature adaptability and energy density of vanadium redox flow battery based on sulfate-chloride mixed acid by optimizing the concentration of electrolyte, Journal of Power Sources. 415 (2019) 62–68. https://doi.org/10.1016/j.jpowsour.2019.01.049.
[441] Y. Yang, Y. Zhang, L. Tang, T. Liu, J. Huang, S. Peng, X. Yang, Investigations on physicochemical properties and electrochemical performance of sulfate-chloride mixed acid electrolyte for vanadium redox flow battery, Journal of Power Sources. 434 (2019) 1–10. https://doi.org/10.1016/j.jpowsour.2019.226719.
[442] Y. Yang, Y. Zhang, L. Tang, T. Liu, S. Peng, X. Yang, Improved energy density and temperature range of vanadium redox flow battery by controlling the state of charge of

positive electrolyte, Journal of Power Sources. 450 (2020) 1–9. https://doi.org/10.1016/j.jpowsour.2019.227675.
[443] K. Wang, Y. Zhang, L. Liu, J. Xi, Z. Wu, X. Qiu, Broad temperature adaptability of vanadium redox flow battery-Part 3: The effects of total vanadium concentration and sulfuric acid concentration, Electrochimica Acta. 259 (2018) 11–19. https://doi.org/10.1016/j.electacta.2017.10.148.
[444] W. Duan, B. Li, D. Lu, X. Wei, Z. Nie, V. Murugesan, J.P. Kizewski, A. Hollas, D. Reed, V. Sprenkle, W. Wang, Towards an all-vanadium redox flow battery with higher theoretical volumetric capacities by utilizing the VO2+/V3+ couple, Journal of Energy Chemistry. 27 (2018) 1381–1385. https://doi.org/10.1016/j.jechem.2018.05.020.
[445] S. Park, H.J. Lee, H. Lee, H. Kim, Development of a Redox Flow Battery with Multiple Redox Couples at Both Positive and Negative Electrolytes for High Energy Density, Journal of The Electrochemical Society. 165 (2018) A3215–A3220. https://doi.org/10.1149/2.0301814jes.
[446] D.O. Opar, R. Nankya, J. Lee, H. Jung, Three-dimensional mesoporous graphene-modified carbon felt for high-performance vanadium redox flow batteries, Electrochimica Acta. 330 (2020) 1–14. https://doi.org/10.1016/j.electacta.2019.135276.
[447] A. Bhattarai, N. Wai, R. Schweiss, A. Whitehead, T.M. Lim, H.H. Hng, Advanced porous electrodes with flow channels for vanadium redox flow battery, Journal of Power Sources. 341 (2017) 83–90. https://doi.org/10.1016/j.jpowsour.2016.11.113.
[448] R.K. Gautam, A. Verma, Uniquely designed surface nanocracks for highly efficient and ultra-stable graphite felt electrode for vanadium redox flow battery, Materials Chemistry and Physics. 251 (2020) 1–12. https://doi.org/10.1016/j.matchemphys.2020.123178.
[449] N. Yun, J.J. Park, O.O. Park, K.B. Lee, J.H. Yang, Electrocatalytic effect of NiO nanoparticles evenly distributed on a graphite felt electrode for vanadium redox flow batteries, Electrochimica Acta. 278 (2018) 226–235. https://doi.org/10.1016/j.electacta.2018.05.039.
[450] Q. Wu, Y. Lv, L. Lin, X. Zhang, Y. Liu, X. Zhou, An improved thin-film electrode for vanadium redox flow batteries enabled by a dual layered structure, Journal of Power Sources. 410–411 (2019) 152–161. https://doi.org/10.1016/j.jpowsour.2018.11.020.
[451] Z. He, M. Li, Y. Li, J. Zhu, Y. Jiang, W. Meng, H. Zhou, L. Wang, L. Dai, Flexible electrospun carbon nanofiber embedded with TiO2 as excellent negative electrode for vanadium redox flow battery, Electrochimica Acta. 281 (2018) 601–610. https://doi.org/10.1016/j.electacta.2018.06.011.
[452] J. Vázquez-Galván, C. Flox, J.R. Jervis, A.B. Jorge, P.R. Shearing, J.R. Morante, High-power nitrided TiO2 carbon felt as the negative electrode for all-vanadium redox flow batteries, Carbon N Y. 148 (2019) 91–104. https://doi.org/10.1016/j.carbon.2019.01.067.
[453] Y. Xiang, W.A. Daoud, Investigation of an advanced catalytic effect of cobalt oxide modification on graphite felt as the positive electrode of the vanadium redox flow battery, Journal of Power Sources. 416 (2019) 175–183. https://doi.org/10.1016/j.jpowsour.2019.01.079.
[454] A.B. Shah, Y. Wu, Y.L. Joo, Direct addition of sulfur and nitrogen functional groups to graphite felt electrodes for improving all-vanadium redox flow battery performance, Electrochimica Acta. 297 (2019) 905–915. https://doi.org/10.1016/j.electacta.2018.12.052.
[455] S.-C. Kim, H. Lim, H. Kim, J.S. Yi, D. Lee, Nitrogen and oxygen dual-doping on carbon electrodes by urea thermolysis and its electrocatalytic significance for vanadium redox flow battery, Electrochimica Acta. 348 (2020) 1–13. https://doi.org/10.1016/j.electacta.2020.136286.
[456] C. Sun, E. Negro, K. Vezzù, G. Pagot, G. Cavinato, A. Nale, Y.H. Bang, V.D. Noto, Hybrid inorganic-organic proton-conducting membranes based on SPEEK doped with

WO3 nanoparticles for application in vanadium redox flow batteries, Electrochimica Acta. 309 (2019) 311–325. https://doi.org/10.1016/j.electacta.2019.03.056.
[457] S.-H. Roh, M.-H. Lim, T. Sadhasivam, H.-Y. Jung, Investigation on physico-chemical and electrochemical performance of poly(phenylene oxide)-based anion exchange membrane for vanadium redox flow battery systems, Electrochimica Acta. 325 (2019) 1–9. https://doi.org/10.1016/j.electacta.2019.134944.
[458] T. Wang, J.Y. Jeon, J. Han, J.H. Kim, C. Bae, S. Kim, Poly(terphenylene) anion exchange membranes with high conductivity and low vanadium permeability for vanadium redox flow batteries (VRFBs), Journal of Membrane Science. 598 (2020) 1–7. https://doi.org/10.1016/j.memsci.2019.117665.
[459] S.S. Sha'rani, E. Abouzari-Lotf, M.M. Nasef, A. Ahmad, T.M. Ting, R.R. Ali, Improving the redox flow battery performance of low-cost thin polyelectrolyte membranes by layer-by-Layer Surface assembly, Journal of Power Sources. 413 (2019) 182–190. https://doi.org/10.1016/j.jpowsour.2018.12.037.
[460] T. Wang, S.J. Moon, D.-S. Hwang, H. Park, J. Lee, S. Kim, Y.M. Lee, S. Kim, Selective ion transport for a vanadium redox flow battery (VRFB) in nano-crack regulated proton exchange membranes, Journal of Membrane Science. 583 (2019) 16–22. https://doi.org/10.1016/j.memsci.2019.04.017.
[461] X. Che, H. Zhao, X. Ren, D. Zhang, H. Wei, J. Liu, X. Zhang, J. Yang, Porous polybenzimidazole membranes with high ion selectivity for the vanadium redox flow battery, Journal of Membrane Science. 611 (2020) 1–10. https://doi.org/10.1016/j.memsci.2020.118359.
[462] Y. Zhang, X. Zhou, R. Xue, Q. Yu, F. Jiang, Y. Zhong, Proton exchange membranes with ultra-low vanadium ions permeability improved by sulfated zirconia for all vanadium redox flow battery, International Journal of Hydrogen Energy. 44 (2019) 5997–6006. https://doi.org/10.1016/j.ijhydene.2019.01.043.
[463] H.-Y. Jung, M.-S. Cho, T. Sadhasivam, J.-Y. Kim, S.-H. Roh, Y. Kwon, High ionic selectivity of low permeable organic composite membrane with amphiphilic polymer for vanadium redox flow batteries, Solid State Ionics. 324 (2018) 69–76. https://doi.org/10.1016/j.ssi.2018.06.009.
[464] R.B. Vignesh, J. Balaji, M.G. Sethuraman, Surface modification, characterization and corrosion protection of 1,3-diphenylthiourea doped sol-gel coating on aluminium, Progress in Organic Coatings. 111 (2017) 112–123. https://doi.org/10.1016/j.porgcoat.2017.05.013.
[465] S.M. Ali, K.M. Emran, M. Messali, Improved protection performance of modified sol-gel coatings with pyridinium-based ionic liquid for cast iron corrosion in 0.5 M HCl solution, Progress in Organic Coatings. 130 (2019) 226–234. https://doi.org/10.1016/j.porgcoat.2019.02.002.
[466] European Comission, Study on the review of the list of Critical Raw Materials, 2017. https://doi.org/10.2873/876644.
[467] D.R. Swinbourne, T. Richardson, F. Cabalteja, Understanding ferrovanadium smelting through computational thermodynamics modelling, Transactions of the Institutions of Mining and Metallurgy. 125 (2016) 45–55. https://doi.org/10.1179/1743285515Y.0000000019.
[468] X.Y. Chen, X.Z. Lan, Q.L. Zhang, H.Z. Ma, J. Zhou, Leaching vanadium by high concentration sulfuric acid from stone coal, Transactions of Nonferrous Metals Society of China (English Edition). 20 (2010) s123–s126. https://doi.org/10.1016/S1003-6326(10)60025-8.
[469] B. Zhang, Z. Gao, H. Liu, W. Wang, Y. Cao, Direct Acid Leaching of Vanadium from Stone Coal, High Temperature Materials and Processes. 36 (2017) 877–883. https://doi.org/10.1515/htmp-2016-0055.
[470] Z. Cai, Y. Zhang, T. Liu, J. Huang, Mechanisms of vanadium recovery from stone coal by novel BaCO3/CaO composite additive roasting and acid leaching technology, Minerals. 6 (2016) 1–14. https://doi.org/10.3390/min6020026.

[471] J. Dunlop, O. Özdemir, Rock Magnetism: Fundamentals and frontiers, 1st ed., Cambridge University Press, Cambridge, 1997.
[472] X. Zhu, W. Li, X. Guan, Vanadium extraction from titano-magnetite by hydrofluoric acid, International Journal of Mineral Processing. 157 (2016) 55–59. https://doi.org/10.1016/j.minpro.2016.09.012.
[473] Y. Luo, X. Che, X. Cui, Q. Zheng, L. Wang, Selective leaching of vanadium from V-Ti magnetite concentrates by pellet calcification roasting-H2SO4 leaching process, International Journal of Mining Science and Technology. 31 (2021) 507–513. https://doi.org/10.1016/j.ijmst.2021.02.002.
[474] Y. Li, S. Chen, H. Duan, A new process of extracting titanium from vanadium- titanium magnetite, Crystals (Basel). 11 (2021). https://doi.org/10.3390/cryst11040327.
[475] D.G. Nejad, A.R. Khanchi, M. Taghizadeh, Recovery of Vanadium from Magnetite Ore Using Direct Acid Leaching: Optimization of Parameters by Plackett–Burman and Response Surface Methodologies, Jom. 70 (2018) 1024–1030. https://doi.org/10.1007/s11837-018-2821-4.
[476] T.A. Sedneva, E.P. Lokshin, P.B. Gromov, E.K. Kopkova, E.A. Shchelokova, Decomposing the Titaniferous Magnetite Concentrate with Hydrochloric Acid, Theoretical Foundations of Chemical Engineering. 45 (2011) 753–763. https://doi.org/10.1134/S0040579511050125.
[477] J.C. Lee, Kurniawan, E.Y. Kim, K.W. Chung, R. Kim, H.S. Jeon, A review on the metallurgical recycling of vanadium from slags: Towards a sustainable vanadium production, Journal of Materials Research and Technology. 12 (2021) 343–364. https://doi.org/10.1016/j.jmrt.2021.02.065.
[478] S. Liu, E. Ding, P. Ning, G. Xie, N. Yang, Vanadium extraction from roasted vanadium-bearing steel slag via pressure acid leaching, Journal of Environmental Chemical Engineering. 9 (2021) 105195. https://doi.org/10.1016/j.jece.2021.105195.
[479] W. Li, C. Ma, W. Gong, X. Zhu, Clean production technology for effective recovery of vanadium from shale: Interaction between activators and vanadium-loaded minerals, Journal of Cleaner Production. 315 (2021) 128170. https://doi.org/10.1016/j.jclepro.2021.128170.
[480] M. Wang, B. Chen, S. Huang, X. Wang, B. Liu, Q. Ge, S. Xie, A novel technology for vanadium and chromium recovery from V-Cr-bearing reducing slag, Hydrometallurgy. 171 (2017) 116–122. https://doi.org/10.1016/j.hydromet.2017.05.007.
[481] L. Wu, C. Dai, H. Wang, J. Wang, Y. Dong, Leaching of vanadium, potassium, and iron from spent catalyst of the manufacture of sulfuric acid, Journal of Materials Research and Technology. 11 (2021) 905–913. https://doi.org/10.1016/j.jmrt.2021.01.072.
[482] S. Kagaya, M. Gemmei-Ide, Y. Inoue, Chelating Resins, in: S. Kobayashi, K. Müllen (Eds.), Encyclopedia of Polymeric Nanomaterials, Springer Berlin Heidelberg, London, 2015: pp. 369–378. https://doi.org/10.1007/978-3-642-29648-2.
[483] K. Sirola, M. Laatikainen, M. Lahtinen, E. Paatero, Removal of copper and nickel from concentrated ZnSO4 solutions with silica-supported chelating adsorbents, Separation and Purification Technology. 64 (2008) 88–100. https://doi.org/10.1016/j.seppur.2008.08.001.
[484] L. Ulloa, M. Martínez-Minchero, E. Bringas, A. Cobo, M.F. San-Román, Split regeneration of chelating resins for the selective recovery of nickel and copper, Separation and Purification Technology. 253 (2020) 117516. https://doi.org/10.1016/j.seppur.2020.117516.
[485] L. Zeng, Q. Li, L. Xiao, Extraction of vanadium from the leach solution of stone coal using ion exchange resin, Hydrometallurgy. 97 (2009) 194–197. https://doi.org/10.1016/j.hydromet.2009.03.005.
[486] T. Soldi, M. Pesavento, G. Alberti, Separation of vanadium(V) and -(IV) by sorption on an iminodiacetic chelating resin, Analytica Chimica Acta. 323 (1996) 27–37. https://doi.org/10.1016/0003-2670(95)00612-5.

[487] X. Zhu, G. Huo, J. Ni, Q. Song, Removal of tungsten and vanadium from molybdate solutions using ion exchange resin, Transactions of Nonferrous Metals Society of China (English Edition). 27 (2017) 2727–2732. https://doi.org/10.1016/S1003-6326(17)60301-7.
[488] T.H. Nguyen, M.S. Lee, Separation of molybdenum and vanadium from acid solutions by ion exchange, Hydrometallurgy. 136 (2013) 65–70. https://doi.org/10.1016/j.hydromet.2013.03.007.
[489] Lewatit® MonoPlus TP 209 XL, (2017) 1–4. https://www.lenntech.com/Data-sheets/Lewatit-MonoPlus-TP-209-XL-EN-L.pdf.
[490] Lewatit® TP 207, (2015) 1–5. https://www.lenntech.com/Data-sheets/Lewatit-TP-207-L.pdf.
[491] Dowex™ M4195, (n.d.) 1–4. http://www.lenntech.com/Data-sheets/Dowex-M-4195-L.pdf.
[492] Lewatit® MonoPlus S 200 H, Opadry. (2020) 1–5. https://lanxess.com/en/Products-and-Solutions/Products/l/LEWATIT--MonoPlus-S-200-H.
[493] A.B. Botelho Junior, M.M. Jiménez Correa, D.C.R. Espinosa, D. Dreisinger, J.A.S. Tenório, Recovery of Cu(II) from nickel laterite leach using prereduction and chelating resin extraction: Batch and continuous experiments, Canadian Journal of Chemical Engineering. 97 (2019) 924–929. https://doi.org/10.1002/cjce.23306.
[494] M.J. Slater, Hydrometallurgical Extraction and Reclamation, Elsevier BV, 1987. https://doi.org/10.1016/0304-386x(87)90057-0.
[495] A.B. Botelho Junior, A.D.A. Vicente, D.C.R. Espinosa, J.A.S. Tenório, Recovery of metals by ion exchange process using chelating resin and sodium dithionite, Journal of Materials Research and Technology. 8 (2019) 4464–4469. https://doi.org/10.1016/j.jmrt.2019.07.059.
[496] N. Mbedzi, D. Ibana, L. Dyer, R. Browner, The effect of oxidant addition on ferrous iron removal from multi-element acidic sulphate solutions, in: AIP Conference Proceedings, 2017: pp. 1–8. https://doi.org/10.1063/1.4974413.
[497] M.C.B. Fortes, A.H. Martins, J.S. Benedetto, Indium absorption onto ion exchange polymeric resins, Minerals Engineering. 16 (2003) 659–663. https://doi.org/10.1016/S0892-6875(03)00130-4.
[498] Z. Abbasi, L. Cseri, X. Zhang, B.P. Ladewig, H. Wang, Metal-organic frameworks (MOFs) and MOF-derived porous carbon materials for sustainable adsorptive wastewater treatment, in: Sustainable Nanoscale Engineering: From Materials Design to Chemical Processing, Elsevier, 2019: pp. 163–194. https://doi.org/10.1016/B978-0-12-814681-1.00007-2.
[499] I. Anastopoulos, A. Bhatnagar, E.C. Lima, Adsorption of rare earth metals: A review of recent literature, Journal of Molecular Liquids. 221 (2016) 954–962. https://doi.org/10.1016/j.molliq.2016.06.076.
[500] I. Langmuir, The adsorption of gases on plane surfaces of glass, mica and platinum, J Am Chem Soc. 40 (1918) 1361–1403. https://doi.org/10.1021/ja02242a004.
[501] P.S. Kumar, S. Ramalingam, C. Senthamarai, M. Niranjanaa, P. Vijayalakshmi, S. Sivanesan, Adsorption of dye from aqueous solution by cashew nut shell: Studies on equilibrium isotherm, kinetics and thermodynamics of interactions, Desalination. 261 (2010) 52–60. https://doi.org/10.1016/j.desal.2010.05.032.
[502] E. Wibowo, M. Rokhmat, Sutisna, Khairurrijal, M. Abdullah, Reduction of seawater salinity by natural zeolite (Clinoptilolite): Adsorption isotherms, thermodynamics and kinetics, Desalination. 409 (2017) 146–156. https://doi.org/10.1016/j.desal.2017.01.026.
[503] A. Günay, E. Arslankaya, I. Tosun, Lead removal from aqueous solution by natural and pretreated clinoptilolite: Adsorption equilibrium and kinetics, Journal of Hazardous Materials. 146 (2007) 362–371. https://doi.org/10.1016/j.jhazmat.2006.12.034.
[504] N.B. Singh, G. Nagpal, S. Agrawal, Rachna, Water purification by using Adsorbents: A Review, Environmental Technology and Innovation. 11 (2018) 187–240. https://doi.org/10.1016/j.eti.2018.05.006.

[505] G. Moussavi, R. Khosravi, The removal of cationic dyes from aqueous solutions by adsorption onto pistachio hull waste, Chemical Engineering Research and Design. 89 (2011) 2182–2189. https://doi.org/10.1016/j.cherd.2010.11.024.
[506] W.T. Tsai, Y.M. Chang, C.W. Lai, C.C. Lo, Adsorption of ethyl violet dye in aqueous solution by regenerated spent bleaching earth, Journal of Colloid and Interface Science. 289 (2005) 333–338. https://doi.org/10.1016/j.jcis.2005.03.087.
[507] E.C. Lima, A. Hosseini-Bandegharaei, J.C. Moreno-Piraján, I. Anastopoulos, A critical review of the estimation of the thermodynamic parameters on adsorption equilibria. Wrong use of equilibrium constant in the Van't Hoof equation for calculation of thermodynamic parameters of adsorption, Journal of Molecular Liquids. 273 (2019) 425–434. https://doi.org/10.1016/j.molliq.2018.10.048.
[508] C.C. Nnaji, A.E. Agim, C.N. Mama, P.G.C. Emenike, N.M. Ogarekpe, Equilibrium and thermodynamic investigation of biosorption of nickel from water by activated carbon made from palm kernel chaff, Scientific Reports. 11 (2021) 1–20. https://doi.org/10.1038/s41598-021-86932-6.
[509] S.K. Milonjić, A consideration of the correct calculation of thermodynamic parameters of adsorption, Journal of the Serbian Chemical Society. 72 (2007) 1363–1367. https://doi.org/10.2298/JSC0712363M.
[510] S.R. Taffarel, J. Rubio, Removal of Mn2+ from aqueous solution by manganese oxide coated zeolite, Minerals Engineering. 23 (2010) 1131–1138. https://doi.org/10.1016/j.mineng.2010.07.007.
[511] R.R. Bhatt, B.A. Shah, Sorption studies of heavy metal ions by salicylic acid-formaldehyde-catechol terpolymeric resin: Isotherm, kinetic and thermodynamics, Arabian Journal of Chemistry. 8 (2015) 414–426. https://doi.org/10.1016/j.arabjc.2013.03.012.
[512] I. Tsuboi, S. Kasai, E. Kunugita, I. Komasawa, Recovery of gallium and vanadium from coal fly Ash, Journal of Chemical Engineering of Japan. 24 (1991) 15–20. https://doi.org/10.1252/jcej.24.15.
[513] Y. Fan, X. Wang, M. Wang, Separation and recovery of chromium and vanadium from vanadium-containing chromate solution by ion exchange, Hydrometallurgy. 136 (2013) 31–35. https://doi.org/10.1016/j.hydromet.2013.03.008.
[514] H.I. Gomes, A. Jones, M. Rogerson, G.M. Greenway, D.F. Lisbona, I.T. Burke, W.M. Mayes, Removal and recovery of vanadium from alkaline steel slag leachates with anion exchange resins, Journal of Environmental Management. 187 (2017) 384–392. https://doi.org/10.1016/j.jenvman.2016.10.063.
[515] J. Ghogomu, T.D. Noufame, M.J. Ketcha, N.J. Ndi, Removal of Pb(II) Ions from Aqueous Solutions by Kaolinite and Metakaolinite Materials, British Journal of Applied Science & Technology. 3 (2013) 942–961. https://doi.org/10.9734/bjast/2014/4384.
[516] O. Hamdaoui, E. Naffrechoux, Modeling of adsorption isotherms of phenol and chlorophenols onto granular activated carbon. Part I. Two-parameter models and equations allowing determination of thermodynamic parameters, Journal of Hazardous Materials. 147 (2007) 381–394. https://doi.org/10.1016/j.jhazmat.2007.01.021.
[517] M.A. Al-Ghouti, D.A. Da'ana, Guidelines for the use and interpretation of adsorption isotherm models: A review, Journal of Hazardous Materials. 393 (2020) 122383. https://doi.org/10.1016/j.jhazmat.2020.122383.
[518] P. Palanivell, O.H. Ahmed, O. Latifah, N.M.A. Majid, Adsorption and desorption of nitrogen, phosphorus, potassium, and soil buffering capacity following application of chicken litter biochar to an acid soil, Applied Sciences (Switzerland). 10 (2020) 1–18. https://doi.org/10.3390/app10010295.
[519] J. Kiurski, S. Adamović, I. Oros, J. Krstić, I. Kovačević, Adsorption feasibility in the Cr(total) ions removal from waste printing developer, Global Nest Journal. 14 (2012) 18–23. https://doi.org/10.30955/gnj.000810.
[520] W. Guan, J. Pan, H. Ou, X. Wang, X. Zou, W. Hu, C. Li, X. Wu, Removal of strontium (II) ions by potassium tetratitanate whisker and sodium trititanate whisker from

aqueous solution : Equilibrium , kinetics and thermodynamics, Chemical Engineering Journal. 167 (2011) 215–222. https://doi.org/10.1016/j.cej.2010.12.025.
[521] G. Crini, Kinetic and equilibrium studies on the removal of cationic dyes from aqueous solution by adsorption onto a cyclodextrin polymer, Dyes and Pigments. 77 (2008) 415–426. https://doi.org/10.1016/j.dyepig.2007.07.001.
[522] D. V Morales, B.L. Rivas, M. González, Poly(4-vinylbenzyl)trimethylammonium chloride) resin with removal properties for vanadium(v) and molybdenum(vi). A thermodynamic and kinetic study, Journal of the Chilean Chemical Society. 66 (2021) 5118–5124. https://doi.org/10.4067/S0717-97072021000105118.
[523] I. Polowczyk, P. Cyganowski, B.F. Urbano, B.L. Rivas, M. Bryjak, N. Kabay, Hydrometallurgy Amberlite IRA-400 and IRA-743 chelating resins for the sorption and recovery of molybdenum (VI) and vanadium (V): Equilibrium and kinetic studies, Hydrometallurgy. 169 (2017) 496–507. https://doi.org/10.1016/j.hydromet.2017.02.017.
[524] X. Huang, Z. Ye, L. Chen, X. Chen, C. Liu, Y. Yin, X. Wang, Y. Wei, Removal of V(V) From Solution Using a Silica-Supported Primary Amine Resin: Batch Studies, Experimental Analysis, and Mathematical Modeling, Molecules. 25 (2020) 1448. https://doi.org/10.3390/molecules25061448.
[525] F. Gode, E. Pehlivan, A comparative study of two chelating ion-exchange resins the removal of chromium (III) from aqueous solution, Journal of Hazardous Materials. 100 (2003) 231–243. https://doi.org/10.1016/S0304-3894(03)00110-9.
[526] V. Algar, Investing in the energy storage future Resources Rising Stars 2017, 2017.
[527] Bushveld Minerals, Bushveld Minerals – Corporate Presentation 2021, 2021.
[528] H. Mahandra, R. Singh, B. Gupta, Recovery of vanadium(V) from synthetic and real leach solutions of spent catalyst by solvent extraction using Cyphos IL 104, Hydrometallurgy. 196 (2020) 105405. https://doi.org/10.1016/j.hydromet.2020.105405.
[529] M. Wang, G. Zhang, X. Wang, J. Zhang, Solvent extraction of vanadium from sulfuric acid solution, Rare Metals. 28 (2009) 209–211. https://doi.org/10.1007/s12598-009-0041-3.
[530] M. Tavakolikhaledi, Vanadium: leaching and solvent extraction, University of British Columbia, 2014. https://doi.org/10.14288/1.0167467.
[531] X. Li, C. Wei, Z. Deng, C. Li, G. Fan, M. Li, H. Huang, Recovery of Vanadium from H2SO4-HF Acidic Leaching Solution of Black Shale by Solvent Extraction and Precipitation, Metals (Basel). 6 (2016) 63. https://doi.org/10.3390/met6030063.
[532] Z.G. Deng, C. Wei, G. Fan, M.T. Li, C.X. Li, X.B. Li, Extracting vanadium from stone-coal by oxygen pressure acid leaching and solvent extraction, Transactions of Nonferrous Metals Society of China. 20 (2010) s118–s122. https://doi.org/10.1016/S1003-6326(10)60024-6.
[533] X.B. Li, C. Wei, J. Wu, C.X. Li, M.T. Li, Z.G. Deng, H.S. Xu, Thermodynamics and mechanism of vanadium(IV) extraction from sulphate medium with D2EHPA, EHEHPA and CYANEX 272 in kerosene, Transactions of Nonferrous Metals Society of China. 22 (2012) 461–466. https://doi.org/10.1016/S1003-6326(11)61199-0.
[534] R. Navarro, J. Guzman, I. Saucedo, J. Revilla, E. Guibal, Vanadium recovery from oil fly ash by leaching, precipitation and solvent extraction processes, Waste Management. 27 (2007) 425–438. https://doi.org/10.1016/j.wasman.2006.02.002.
[535] B. Hu, B. Chen, C. Zhang, Y. Dai, M. Wang, X. Wang, Separation and Recovery of Chromium from Solution After Vanadium Precipitation, Mining, Metallurgy & Exploration. 38 (2021) 289–297. https://doi.org/10.1007/s42461-020-00342-2.
[536] H. Peng, L. Yang, L. Wang, J. Guo, B. Li, Recovery of vanadium with urea in acidic medium, Environmental Chemistry Letters. 17 (2019) 1867–1871. https://doi.org/10.1007/s10311-019-00902-z.
[537] S. Drużyński, K. Mazurek, K. Białowicz, The Use of Ion Exchange in the Recovery of Vanadium from the Mass of a Spent Catalyst Used in the Oxidation of SO 2 to SO 3, Polish Journal of Chemical Technology. 16 (2014) 69–73. https://doi.org/10.2478/pjct-2014-0032.

[538] Q. Li, L. Zeng, L. Xiao, Y. Yang, Q. Zhang, Completely removing vanadium from ammonium molybdate solution using chelating ion exchange resins, Hydrometallurgy. 98 (2009) 287–290. https://doi.org/10.1016/j.hydromet.2009.05.014.
[539] X. Zhu, W. Li, S. Tang, M. Zeng, P. Bai, L. Chen, Selective recovery of vanadium and scandium by ion exchange with D201 and solvent extraction using P507 from hydrochloric acid leaching solution of red mud, Chemosphere. 175 (2017) 365–372. https://doi.org/10.1016/j.chemosphere.2017.02.083.
[540] M. Li, B. Zhang, S. Zou, Q. Liu, M. Yang, Highly selective adsorption of vanadium (V) by nano-hydrous zirconium oxide-modified anion exchange resin, Journal of Hazardous Materials. 384 (2020) 121386. https://doi.org/10.1016/j.jhazmat.2019.121386.
[541] X. Zhu, G. Huo, J. Ni, Q. Song, Removal of tungsten and vanadium from molybdate solutions using ion exchange resin, Transactions of Nonferrous Metals Society of China (English Edition). 27 (2017) 2727–2732. https://doi.org/10.1016/S1003-6326(17)60301-7.
[542] J. Zhang, W. Zhang, L. Zhang, S. Gu, A Critical Review of Technology for Selective Recovery of Vanadium from Leaching Solution in V2O5 Production, Solvent Extraction and Ion Exchange. 32 (2014) 221–248. https://doi.org/10.1080/07366299.2013.877753.
[543] D.S. Sholl, R.P. Lively, Seven chemical separations to change the world, Nature. 532 (2016) 435–437. https://doi.org/10.1038/532435a.
[544] P. Cyganowski, A. Dzimitrowicz, A mini-review on anion exchange and chelating polymers for applications in hydrometallurgy, environmental protection, and biomedicine, Polymers (Basel). 12 (2020). https://doi.org/10.3390/POLYM12040784.
[545] F. Batool, J. Akbar, S. Iqbal, S. Noreen, S.N.A. Bukhari, Study of Isothermal, Kinetic, and Thermodynamic Parameters for Adsorption of Cadmium: An Overview of Linear and Nonlinear Approach and Error Analysis, Bioinorganic Chemistry and Applications. 2018 (2018). https://doi.org/10.1155/2018/3463724.
[546] R.K. Gautam, M.C. Chattopadhyaya, Kinetics and Equilibrium Isotherm Modeling: Graphene-Based Nanomaterials for the Removal of Heavy Metals From Water, in: Nanomaterials for Wastewater Remediation, Elsevier, 2016: pp. 79–109. https://doi.org/10.1016/B978-0-12-804609-8.00005-4.
[547] J. Febrianto, A.N. Kosasih, J. Sunarso, Y.H. Ju, N. Indraswati, S. Ismadji, Equilibrium and kinetic studies in adsorption of heavy metals using biosorbent: A summary of recent studies, Journal of Hazardous Materials. 162 (2009) 616–645. https://doi.org/10.1016/j.jhazmat.2008.06.042.
[548] Y. Zhang, T.A. Zhang, D. Dreisinger, W. Zhou, F. Xie, G. Lv, W. Zhang, Chelating extraction of vanadium(V) from low pH sulfuric acid solution by Mextral 973H, Separation and Purification Technology. 190 (2018) 123–135. https://doi.org/10.1016/j.seppur.2017.07.016.
[549] H. Tokuyama, S. Nii, F. Kawaizumi, K. Takahashi, Process development for recovery of vanadium and nickel from heavy oil fly ash by leaching and ion exchange, Separation Science and Technology. 38 (2003) 1329–1344. https://doi.org/10.1081/SS-120018812.
[550] H. Moussout, H. Ahlafi, M. Aazza, H. Maghat, Critical of linear and nonlinear equations of pseudo-first order and pseudo-second order kinetic models, Karbala International Journal of Modern Science. 4 (2018) 244–254. https://doi.org/10.1016/j.kijoms.2018.04.001.
[551] S. Lagergreen, Zur Theorie der sogenannten Adsorption gelöster Stoffe, Zeitschrift Für Chemie Und Industrie Der Kolloide. 2 (1907) 15. https://doi.org/10.1007/BF01501332.
[552] F. Arroyo, J. Morillo, J. Usero, D. Rosado, H.E. Bakouri, Lithium recovery from desalination brines using specific ion-exchange resins, Desalination. 468 (2019) 114073. https://doi.org/10.1016/j.desal.2019.114073.

[553] T.H. Shek, A. Ma, V.K.C. Lee, G. McKay, Kinetics of zinc ions removal from effluents using ion exchange resin, Chemical Engineering Journal. 146 (2009) 63–70. https://doi.org/10.1016/j.cej.2008.05.019.
[554] O. Abdelwahab, N.K. Amin, E.S.Z. El-Ashtoukhy, Removal of zinc ions from aqueous solution using a cation exchange resin, Chemical Engineering Research and Design. 91 (2013) 165–173. https://doi.org/10.1016/j.cherd.2012.07.005.
[555] Y.S. Ho, G. McKay, Pseudo-second order model for sorption processes, Process Biochemistry. 34 (1999) 451–465. https://doi.org/10.1016/S0032-9592(98)00112-5.
[556] Y. Khambhaty, K. Mody, S. Basha, B. Jha, Kinetics, equilibrium and thermodynamic studies on biosorption of hexavalent chromium by dead fungal biomass of marine Aspergillus niger, Chemical Engineering Journal. 145 (2009) 489–495. https://doi.org/10.1016/j.cej.2008.05.002.
[557] G. Crini, P.M. Badot, Application of chitosan, a natural aminopolysaccharide, for dye removal from aqueous solutions by adsorption processes using batch studies: A review of recent literature, Progress in Polymer Science (Oxford). 33 (2008) 399–447. https://doi.org/10.1016/j.progpolymsci.2007.11.001.
[558] P.C.C. Siu, L.F. Koong, J. Saleem, J. Barford, G. McKay, Equilibrium and kinetics of copper ions removal from wastewater by ion exchange, Chinese Journal of Chemical Engineering. 24 (2016) 94–100. https://doi.org/10.1016/j.cjche.2015.06.017.
[559] S.H. Chien, W.R. Clayton, Application of Elovich Equation to the Kinetics of Phosphate Release and Sorption in Soils, Soil Science Society of America Journal. 44 (1980) 265–268. https://doi.org/10.2136/sssaj1980.03615995004400020013x.
[560] A. Pholosi, E.B. Naidoo, A.E. Ofomaja, Intraparticle diffusion of Cr(VI) through biomass and magnetite coated biomass: A comparative kinetic and diffusion study, South African Journal of Chemical Engineering. 32 (2020) 39–55. https://doi.org/10.1016/j.sajce.2020.01.005.
[561] W.J. Weber, J.C. Morris, Kinetics of Adsorption on Carbon from Solution, Journal of the Sanitary Engineering Division. 89 (1963) 31–59. https://doi.org/10.1061/JSEDAI.0000430.
[562] Z. Zainol, M.J. Nicol, Comparative study of chelating ion exchange resins for the recovery of nickel and cobalt from laterite leach tailings, Hydrometallurgy. 96 (2009) 283–287. https://doi.org/10.1016/j.hydromet.2008.11.005.
[563] S.-Y. Pan, W.-J. Syu, T.-K. Chang, C.-H. Lee, A multiple model approach for evaluating the performance of time-lapse capsules in trapping heavy metals from water bodies, RSC Advances. 10 (2020) 16490–16501. https://doi.org/10.1039/D0RA03017A.
[564] N. Fatima, Q. Zhang, R. Chen, D. Yan, Q. Zhou, X. Lu, J. Xin, Adsorption thermodynamics and kinetics of resin for metal impurities in bis(2-hydroxyethyl) terephthalate, Polymers (Basel). 12 (2020) 1–12. https://doi.org/10.3390/polym12122866.
[565] C. Xiong, Y. Li, G. Wang, L. Fang, S. Zhou, C. Yao, Q. Chen, X. Zheng, D. Qi, Y. Fu, Y. Zhu, Selective removal of Hg(II) with polyacrylonitrile-2-amino-1,3,4-thiadiazole chelating resin: Batch and column study, Chemical Engineering Journal. 259 (2015) 257–265. https://doi.org/10.1016/j.cej.2014.07.114.
[566] D. Kołodyńska, Z. Hubicki, S. Pasieczna-Patkowska, FT-IR/PAS studies of Cu(II)-EDTA complexes sorption on the chelating ion exchangers, Acta Physica Polonica A. 116 (2009) 340–343. https://doi.org/10.12693/APhysPolA.116.340.
[567] W. Garcia-Vasquez, L. Dammak, C. Larchet, V. Nikonenko, N. Pismenskaya, D. Grande, Evolution of anion-exchange membrane properties in a full scale electrodialysis stack, Journal of Membrane Science. 446 (2013) 255–265. https://doi.org/10.1016/j.memsci.2013.06.042.
[568] M. Kuć, K. Cieślik-Boczula, P. Świątek, A. Jaszczyszyn, K. Gąsiorowski, W. Malinka, FTIR-ATR study of the influence of the pyrimidine analog of fluphenazine on the chain-melting phase transition of sphingomyelin membranes, Chemical Physics. 458 (2015) 9–17. https://doi.org/10.1016/j.chemphys.2015.06.010.

[569] D. Kołodyńska, W. Sofińska-Chmiel, E. Mendyk, Z. Hubicki, DOWEX M 4195 and LEWATIT®MonoPlus TP 220 in Heavy Metal Ions Removal from Acidic Streams, Separation Science and Technology (Philadelphia). 49 (2014) 2003–2015. https://doi.org/10.1080/01496395.2014.908920.
[570] P. Wiercik, B. Frączek, P. Chrobot, Fouling of anion exchanger by image and FTIR analyses, Journal of Environmental Chemical Engineering. 8 (2020). https://doi.org/10.1016/j.jece.2020.103761.
[571] J. Tarchitzky, O. Lerner, U. Shani, G. Arye, A. Lowengart-Aycicegi, A. Brener, Y. Chen, Water distribution pattern in treated wastewater irrigated soils: Hydrophobicity effect, European Journal of Soil Science. 58 (2007) 573–588. https://doi.org/10.1111/j.1365-2389.2006.00845.x.
[572] G. Granados-Oliveros, F.M. Ortega, E. Páez-Mozo, C. Ferronato, J.M. Chovelon, Photoactivity of metal-phenylporphyrins adsorbed on TiO2 under visible light radiation: Influence of central metal, Open Materials Science Journal. 4 (2010) 15–22. https://doi.org/10.2174/1874088X01004020015.
[573] Q. Xu, J.C.C. Lo, S.W.R. Lee, Directly printed hollow connectors for microfluidic interconnection with UV-assisted coaxial 3D printing, Applied Sciences (Switzerland). 10 (2020). https://doi.org/10.3390/APP10103384.
[574] S. Ghosh, K. Dhole, M.K. Tripathy, R. Kumar, R.S. Sharma, FTIR spectroscopy in the characterization of the mixture of nuclear grade cation and anion exchange resins, Journal of Radioanalytical and Nuclear Chemistry. 304 (2015) 917–923. https://doi.org/10.1007/s10967-014-3906-3.
[575] S. Caprarescu, M.C. Corobea, V. Purcar, C.I. Spataru, R. Ianchis, G. Vasilievici, Z. Vuluga, San copolymer membranes with ion exchangers for Cu(II) removal from synthetic wastewater by electrodialysis, Journal of Environmental Sciences (China). 35 (2015) 27–37. https://doi.org/10.1016/j.jes.2015.02.005.
[576] S. Morsch, Y. Liu, S.B. Lyon, S.R. Gibbon, B. Gabriele, M. Malanin, K.J. Eichhorn, Examining the early stages of thermal oxidative degradation in epoxy-amine resins, Polymer Degradation and Stability. 176 (2020) 109147. https://doi.org/10.1016/j.polymdegradstab.2020.109147.
[577] L. Yang, P.W. May, L. Yin, J.A. Smith, K.N. Rosser, Ultra fine carbon nitride nanocrystals synthesized by laser ablation in liquid solution, Journal of Nanoparticle Research. 9 (2007) 1181–1185. https://doi.org/10.1007/s11051-006-9192-4.
[578] A.B. Botelho Junior, A.A. Vicente, D.C.R. Espinosa, J.A.S. Tenório, Effect of iron oxidation state for copper recovery from nickel laterite leach solution using chelating resin, Separation Science and Technology (Philadelphia). 55 (2019) 788–798. https://doi.org/10.1080/01496395.2019.1574828.
[579] W. Sofińska-Chmiel, D. Kołodyńska, Application of ion exchangers for the purification of galvanic wastewater from heavy metals, Separation Science and Technology (Philadelphia). 53 (2017) 1097–1106. https://doi.org/10.1080/01496395.2017.1330350.
[580] A. Wołowicz, Z. Hubicki, The use of the chelating resin of a new generation Lewatit MonoPlus TP-220 with the bis-picolylamine functional groups in the removal of selected metal ions from acidic solutions, Chemical Engineering Journal. 197 (2012) 493–508. https://doi.org/10.1016/j.cej.2012.05.047.
[581] Lewatit® MonoPlus TP 209 XL, (2019) 1–2. https://lanxess.com/en/Products-and-Solutions/Products/l/LEWATIT--MonoPlus-TP-209-XL.
[582] X. Zhu, W. Li, Q. Zhang, C. Zhang, L. Chen, Separation characteristics of vanadium from leach liquor of red mud by ion exchange with different resins, Hydrometallurgy. 176 (2018) 42–48. https://doi.org/10.1016/j.hydromet.2018.01.009.
[583] Y. Liu, Q. Li, T. Zhang, X. Wu, J. Du, G. Zhang, L. Zeng, New process consisting of oxidative stripping of vanadium from loaded D2EHPA organic solution with H2O2 and direct precipitation with sulfuric acid, Hydrometallurgy. 203 (2021) 105611. https://doi.org/10.1016/j.hydromet.2021.105611.

[584] B. Yang, J. He, G. Zhang, J. Guo, eds., Chapter 3 - Vanadium mineral resources, in: Vanadium - Extraction, Manufacturing and Applications, Elsevier, 2021: pp. 33–58. https://doi.org/10.1016/b978-0-12-818898-9.00003-6.
[585] T. Leiviskä, J. Matusik, B. Muir, J. Tanskanen, Vanadium removal by organo-zeolites and iron-based products from contaminated natural water, Journal of Cleaner Production. 167 (2017) 589–600. https://doi.org/10.1016/j.jclepro.2017.08.209.
[586] R.L. Langford, T.J. Ivanic, R.J. Arculus, K.J.A. Wills, Ti–V magnetite stratigraphy of the Upper Zone of the Windimurra Igneous Complex, Western Australia, Ore Geology Reviews. 128 (2021) 103922. https://doi.org/10.1016/j.oregeorev.2020.103922.
[587] V.I. Sachkov, R.A. Nefedov, V. V Orlov, R.O. Medvedev, A.S. Sachkova, Hydrometallurgical processing technology of titanomagnetite ores, Minerals. 8 (2018) 1–12. https://doi.org/10.3390/min8010002.
[588] J. van Deventer, Selected Ion exchange applications in the hydrometallurgical industry, Solvent Extraction and Ion Exchange. 29 (2011) 695–718. https://doi.org/10.1080/07366299.2011.595626.
[589] M.L. Strauss, L.A. Diaz, J. McNally, J. Klaehn, T.E. Lister, Separation of cobalt, nickel, and manganese in leach solutions of waste lithium-ion batteries using Dowex M4195 ion exchange resin, Hydrometallurgy. 206 (2021) 105757. https://doi.org/10.1016/j.hydromet.2021.105757.
[590] X. Yi, G. Huo, H. Pu, Z. Zhang, P. Chen, J. Liu, Improving the washing and desorption of tungsten-adsorbed weak base resin, Hydrometallurgy. 192 (2020) 105258. https://doi.org/10.1016/j.hydromet.2020.105258.
[591] A.K. Sengupta, Y. Zhu, D. Hauze, Metal(II) Ion Binding onto Chelating Exchangers with Nitrogen Donor Atoms: Some New Observations and Related Implications, Environmental Science and Technology. 25 (1991) 481–488. https://doi.org/10.1021/es00015a016.
[592] X. Li, C. Wei, Z. Deng, C. Li, G. Fan, M. Li, H. Huang, Recovery of vanadium from H2SO4-HF acidic leaching solution of black shale by solvent extraction and precipitation, Metals (Basel). 6 (2016) 1–13. https://doi.org/10.3390/met6030063.
[593] H.Y. Li, Y. Yang, M. Zhang, W. Wei, B. Xie, A novel anion exchange method based on in situ selectively reductive desorption of Cr(VI) for its separation from V(V): Toward the comprehensive use of hazardous wastewater, Journal of Hazardous Materials. 368 (2019) 670–679. https://doi.org/10.1016/j.jhazmat.2019.01.099.
[594] H. Peng, H. Qiu, C. Wang, B. Yuan, H. Huang, B. Li, Thermodynamic and Kinetic Studies on Adsorption of Vanadium with Glutamic Acid, ACS Omega. 6 (2021) 21563–21570. https://doi.org/10.1021/acsomega.1c02590.
[595] J. Wen, T. Jiang, Y. Xu, J. Cao, X. Xue, Efficient extraction and separation of vanadium and chromium in high chromium vanadium slag by sodium salt roasting-(NH4)2SO4 leaching, Journal of Industrial and Engineering Chemistry. 71 (2019) 327–335. https://doi.org/10.1016/j.jiec.2018.11.043.
[596] J. Wen, T. Jiang, W. Zhou, H. Gao, X. Xue, A cleaner and efficient process for extraction of vanadium from high chromium vanadium slag: Leaching in (NH4)2SO4-H2SO4 synergistic system and NH4+ recycle, Separation and Purification Technology. 216 (2019) 126–135. https://doi.org/10.1016/j.seppur.2019.01.078.
[597] B. Yang, J. He, G. Zhang, J. Guo, eds., Chapter 14 - Vanadium series products and functional materials, in: Vanadium - Extraction, Manufacturing and Applications, Elsevier, 2021: pp. 395–413. https://doi.org/10.1016/b978-0-12-818898-9.00014-0.
[598] M.A. Teplonogova, A.D. Yapryntsev, A.E. Baranchikov, V.K. Ivanov, Selective hydrothermal synthesis of ammonium vanadates(V) and (IV,V), Transition Metal Chemistry. 44 (2019) 25–30. https://doi.org/10.1007/s11243-018-0265-x.
[599] P. Chithaiah, G. V Vijaya, G.P. Nagabhushana, G. Nagaraju, G.T. Chandrappa, Synthesis of single crystalline (NH4)2V 6O16·1.5H2O nest-like structures, Physica E: Low-Dimensional Systems and Nanostructures. 59 (2014) 218–222. https://doi.org/10.1016/j.physe.2013.12.022.

[600] J. Han, Y. Zhang, T. Liu, J. Huang, N. Xue, P. Hu, Preparation of vanadium nitride using a thermally processed precursor with coating structure, Metals (Basel). 7 (2017) 1–12. https://doi.org/10.3390/met7090360.
[601] P. Xiong, Y. Zhang, S. Bao, J. Huang, Precipitation of vanadium using ammonium salt in alkaline and acidic media and the effect of sodium and phosphorus, Hydrometallurgy. 180 (2018) 113–120. https://doi.org/10.1016/j.hydromet.2018.07.014.